

Investigation of the effects of prediabetes and non - obese type 2 diabetes mellitus on the heart in experimental models

Ph.D. Thesis

Andrea Sója

Supervisor: Tamás Csont MD Ph.D.

Doctoral School of Multidisciplinary Medical Sciences

Department of Biochemistry

Albert Szent-Györgyi Medical School

University of Szeged



Szeged

2021

Publications related to the thesis

- I. Sárközy M, Szűcs G, Fekete V, Pipicz M, Éder K, Gáspár R, **Sója A**, Pipis J, Ferdinandy P, Csonka C, Csont T.
Transcriptomic alterations in the heart of non-obese type 2 diabetic Goto-Kakizaki rats
Cardiovascular Diabetology (2016) 15:110
IF: 4.752

- II. Szűcs G¹, **Sója A**¹, Péter M¹, Sárközy M, Bruszel B, Siska A, Földesi I, Szabó Z, Janáky T, Víggh L, Balogh G, Csont T.
Prediabetes Induced by Fructose-Enriched Diet Influences Cardiac Lipidome and Proteome and Leads to Deterioration of Cardiac Function prior to the Development of Excessive Oxidative Stress and Cell Damage
Oxidative Medicine and Cellular Longevity 2019:3218275
¹ Equal contributors
IF: 4.868

- Cumulate IF: 9.62

Conference presentation related to the thesis

- I. Andrea, Sója; Gergő, Szűcs; Márta, Sárközy; Flóra, Diána Gausz; Alexandra, Fejes; Tamás, Csont
Effect of fructose-enriched diet on cardiac function in rats
CARDIOLOGIA HUNGARICA 49: Supplementum B pp. B33-B33. (2019)

TABLE OF CONTENTS

1. INTRODUCTION	7
1.1. CHARACTERIZATION OF PREDIABETES: EPIDEMIOLOGY, PATHOMECHANISM, CARDIAC EFFECTS.....	8
1.2. CHARACTERIZATION OF DIABETES MELLITUS: TYPES, EPIDEMIOLOGY, PATHOMECHANISM, CARDIAC EFFECTS	10
1.3. PRECLINICAL MODELS OF DIABETES MELLITUS AND PREDIABETES.....	12
2. AIMS.....	15
3. METHODS.....	16
3.1. DIET-INDUCED PREDIABETES MODEL	16
3.1.1. <i>Experimental design</i>	16
3.1.2. <i>Measurement of serum glucose levels and OGTT</i>	16
3.1.3. <i>Measurement of serum and pancreatic insulin levels</i>	17
3.1.4. <i>Homeostatic model assessment for insulin resistance (HOMA-IR index)</i>	17
3.1.5. <i>Measurement of serum lipid levels</i>	17
3.1.6. <i>Measurement of serum markers of liver and heart damage</i>	18
3.1.7. <i>Transthoracic echocardiography</i>	18
3.1.8. <i>Working heart perfusion</i>	19
3.1.9. <i>mRNA expression profiling by qRT-PCR</i>	19
3.1.10. <i>Lipidomics</i>	20
3.1.11. <i>Determination of oxidative stress: measurement of MDA and 3-NT levels</i>	20
3.1.12. <i>Western blot</i>	21
3.1.13. <i>Statistical analysis</i>	21
3.2. NON-OBESE GENETIC MODEL OF TYPE 2 DIABETES	22
3.2.1. <i>Experimental design</i>	22
3.2.2. <i>Measurement of serum glucose levels and OGTT</i>	22
3.2.3. <i>Measurement of serum and pancreatic insulin levels, HOMA-IR index</i>	23
3.2.4. <i>Measurement of serum cholesterol levels</i>	23
3.2.5. <i>RNA preparation and DNA microarray analysis</i>	23
3.2.6. <i>mRNA expression profiling by qRT-PCR</i>	23
3.2.7. <i>GO analysis</i>	24
3.2.8. <i>Statistical analysis</i>	24
4. RESULTS	26
4.1. DIET-INDUCED PREDIABETES MODEL	26
4.1.1. <i>Characterization of the animal model</i>	26
4.1.2. <i>Heart function and morphology</i>	28
4.1.3. <i>Lipidomics</i>	30
4.1.4. <i>Oxidative stress</i>	34
4.1.5. <i>Apoptosis</i>	34
4.2. NON-OBESE GENETIC MODEL OF TYPE 2 DIABETES	35
4.2.1. <i>Metabolic characterization of the GK rats</i>	35
4.2.2. <i>Body weight, heart weight and CF</i>	37
4.2.3. <i>Cardiac gene expression profile and qRT-PCR in non-obese T2DM</i>	38
4.2.4. <i>Gene ontology analysis</i>	40
5. DISCUSSION.....	42
5.1. DIET-INDUCED PREDIABETES MODEL	42
5.2. NON-OBESE GENETIC MODEL OF TYPE 2 DIABETES	47
5.3. CONCLUSION	51

ABBREVIATIONS

3-NT: 3-nitrotyrosine

4CH: 4 chamber view

A

A: Atrial (flow velocity)

Acaca: Acetyl-CoA carboxylase 1

Adam33: ADAM metalloproteinase domain 33

Adra1d: Adrenoceptor alpha 1d

ALAT: Alanine aminotransferase

ASAT: Aspartate aminotransferase

AUC: Area under the curve

B

BAX: Bcl-2-associated X

BCA: Bicinchoninic acid

BCL-2: B-cell lymphoma 2

BCL-XL: B-cell lymphoma-extra large

BSA: Bovine serum albumin

C

C3: Complement component 3

C4a: Complement component 4a

CAD: Coronary artery disease

Ccl12: Chemokine (C-C motif) ligand 12

Cer: Ceramide

CF: Coronary flow

Chrna1: Cholinergic receptor, nicotinic, alpha 1 (muscle)

Chrng: Cholinergic receptor, nicotinic, gamma (muscle)

CK: Creatine kinase

CL: Cardiolipin

Cma1: Chymase 1, mast cell

Col5a3: collagen, type V, alpha 3

CV: Coefficient of variance

CVD: Cardiovascular diseases

Cxcl13: Chemokine (C-X-C motif) ligand 13

Cxcl14: Chemokine (C-X-C motif) ligand 14

Cxcr6: Chemokine (C-X-C motif) receptor 6

D

db: double bond

DBI: Double bond index

DCM: Diabetic cardiomyopathy

DM: Diabetes Mellitus

DNL: de novo lipogenesis

Dpp4: Dipeptidyl peptidase 4

E

E: Early (flow velocity)

EDTA: Ethylenediamine tetra-acetic acid

EF: Ejection fraction

ELISA: Enzyme-linked immunosorbent assay

Elovl6: Elongation of very-long-chain fatty acids protein 6

Epn3: Epsin 3

F

FA: Fatty acid

Fads1: Fatty acid desaturase 1

Fads2: Fatty acid desaturase 2

Fasn: Fatty acid synthase

FBG: Fasting blood glucose

FFAs: Free fatty acids

FPG: Fasting plasma glucose

FS: Fractional shortening

G

GAPDH: Glyceraldehyde-3-phosphate dehydrogenase

GDM: Gestational diabetes mellitus

GK: Goto-Kakizaki

GO: Gene ontology

H

HDL: High-density lipoprotein

HOMA-IR: Homeostatic Model Assessment for Insulin Resistance

HPRT1: Hypoxanthine phosphoribosyltransferase 1

HW/BW: heart weight to body weight ratio

I

IDF: International Diabetes Federation

J

Jund: Jun D proto-oncogene

K

Klk1c3: Kallikrein 1-related peptidase C3

Klre1: Killer cell lectin-like receptor, family E, member 1

L

LA: long axis

LCMS: Liquid chromatography-Mass spectrometry

LDH: Lactate dehydrogenase

LDL: Low-density lipoprotein

Lrp8: Low density lipoprotein receptor-related protein 8, apolipoprotein E receptor

LV: Left ventricular

LVDP: Left ventricular developed pressure

LVEDD: Left ventricular end-diastolic diameter

LVEDP: Left ventricular end-diastolic pressure

LVEDV: Left ventricular end-diastolic volume

LVESD: Left ventricular end-systolic diameter

LVESV: Left ventricular end-systolic volume

M

MCF-7: Michigan Cancer Foundation-7

MDA: Malondialdehyde

MLCL: Monolysocardiolipin

***Mlxip1*:** Carbohydrate-responsive element-binding protein

MM: Motion mode

MS: Mass spectrometry

***Msln*:** Mesothelin

***Myh6*:** Myosin heavy chain α isoform

***Myh7*:** Myosin heavy chain β isoform

***Myl7*:** myosin, light chain 7, regulatory

***Mylk2*:** myosin light chain kinase 2

N

NAFLD: Nonalcoholic fatty liver disease

***Ntrk2*:** Neurotrophic tyrosine kinase, receptor, type 2

***Ntrk3*:** Neurotrophic tyrosine kinase, receptor, type 3

O

OD: Optical density

OGTT: Oral glucose tolerance test

P

PBS: Phosphate buffered saline

PCA: Principal component analysis

PL: Phospholipid

PMSF: Phenylmethanesulfonyl fluoride

Q

qRT-PCR: Quantitative real-time - Polymerase chain reaction

R

***Ret*:** Ret proto-oncogene transcript variant 1

RIN: RNA integrity number

RIPA: Radio-immunoprecipitation assay

RPS18: Ribosomal protein S18

S

SA: short axis

***Sln*:** Sarcolipin

***Scd1*:** Stearoyl-CoA desaturase 1

***Sdc1*:** Syndecan 1

SDS: Sodium dodecyl sulfate

SDS-PAGE: Sodium dodecyl-sulfate polyacrylamide gel electrophoresis

SEM: Standard error of the mean

SERCA: Sarcoplasmic reticulum Ca^{2+} -ATPase

SL: Sphingolipid

SM: Sphingomyelin

***Srebfl1*:** Sterol regulatory element-binding transcription factor 1

***Stat3*:** Signal transducer and activator of transcription 3

STZ: Streptozotocin

T

T1DM: Type 1 diabetes mellitus

T2DM: Type 2 diabetes mellitus

TBA: Thiobarbituric acid

***Tef*:** Thyrotroph embryonic factor

TG: Triglyceride

***Tnni1*:** troponin I type 1 (skeletal, slow)

U

UV: Ultraviolet

V

VEGF: Vascular endothelial growth factor

SUMMARY

Background and goals: Nowadays sedentary lifestyle and carbohydrate- and lipid-rich diet are huge problems worldwide. These habits can lead to the development of many pathological conditions, primarily obesity and diabetes mellitus (DM). DM is in fact a group of metabolic disorders and the main cause of the pathological changes here is hyperglycemia. This elevated blood glucose level can damage several organs, such as the heart, blood vessels, kidneys and eyes. Since cardiovascular diseases (CVD) are responsible for a significantly high proportion of death cases in the world, our research was focusing on the cardiac effects of DM. Although it is common knowledge that the most frequent type of DM is type two DM (T2DM) and this type has the most prominent role in death due to diabetes, it is to be known that the prediabetic state - which precedes overt diabetes - also poses a high risk to the heart. Besides, considering cardiovascular risk, a less known but notable type of DM, non-obese T2DM should be mentioned as well. Unlike the traditional, obese type of T2DM, our knowledge on the molecular mechanisms leading to cardiac dysfunctions in non-obese T2DM and prediabetes is quite limited. Thus, our main goal was to investigate the possible causes of prediabetes- and non-obese T2DM-induced cardiac complications.

Methods: To induce prediabetes, male Wistar rats were fed with a high-fructose (60% w/w) diet for 24 weeks, while the control group was given a standard laboratory chow. Fasting blood glucose (FBG) was measured every 4 weeks, while at weeks 12, 16, 20 and 24 oral glucose tolerance test (OGTT) was performed. At week 20 and 24, blood samples were taken to measure serum parameters such as insulin, triglyceride (TG), cholesterol, markers of heart and liver damage and oxidative stress. At the end of the 24 weeks feeding period, cardiac function was assessed by *in vivo* echocardiography and *ex vivo* isolated working heart perfusions. Following the perfusions, myocardial tissue, liver and pancreata were harvested for biochemical and/or molecular biological analyses.

As for non-obese T2DM, we used a well-known genetic animal model of the disease, i.e. the Goto-Kakizaki (GK) rat. 6 weeks old male GK rats and their aged-matched male Wistar controls were investigated for 9 weeks. Body weight, FBG, insulin and cholesterol levels were measured at week 7, 11 and 15, while at week 15, OGTTs were performed. Following anaesthesia at 15 weeks of age, the animals' hearts and pancreata were isolated and the hearts were perfused according to Langendorff. After perfusion, ventricular tissue was frozen for gene expression analyses. Finally, gene ontology (GO) analysis was used for integration genes with pathways and biological interaction networks to detect coordinated changes in functionally related genes.

Main results: Due to chronic fructose feeding, FBG measurement and OGTT showed slightly but significantly elevated values indicating the development of prediabetic condition. Besides, the significantly increased homeostatic model assessment for insulin resistance (HOMA-IR index) and pancreatic insulin levels, along with the unaltered serum insulin levels demonstrated the emergence of a mild insulin resistance in the fructose-fed group. As for the liver, there were macroscopic signs of fatty degeneration possibly caused by de novo lipogenesis (DNL) initiated by fructose feeding. Both echocardiographic and isolated working heart perfusion data demonstrated diastolic dysfunction in the fructose-fed group. Lipidomic analysis revealed complex rearrangement of the whole lipidome with special emphasis on the defects in cardiolipin (CL) remodeling. Serum lipid parameters, markers of heart and liver damage and oxidative stress did not show significant alterations.

In GK rats, FBG, serum insulin and cholesterol levels were significantly increased, while glucose tolerance and insulin sensitivity were significantly impaired as compared to the controls. In the hearts of the GK rats, 138 genes showed more than threefold change of expression as compared to the levels of control rats. Among these genes, 50 were significantly upregulated and 88 were significantly downregulated. The genes influenced by non-obese T2DM include functional clusters of metabolism, signal transduction, receptors and ion channels, membrane and structural proteins, cell growth and differentiation, immune response and others. GO analysis revealed numerous significantly enriched functional interrelationships between genes affected by non-obese T2DM.

Conclusions: Our findings demonstrate that even very early stages of prediabetes can impair cardiac function and can lead to significant changes in the lipidome of the heart prior to the development of excessive oxidative stress and cellular damage.

In our other study, we have presented for the first time that non-obese T2DM is associated with a profound modification of the cardiac transcriptome. The altered genes might be involved in the development of diabetic cardiomyopathy (DCM) and could be potential therapeutic targets in non-obese T2DM.

1. INTRODUCTION

Unfortunately, nowadays a significant proportion of people consume too much, especially carbohydrate-rich food and drinks, and/or spend too little time exercising. These and many other factors can result in obesity and DM. DM is a group of metabolic diseases with one common manifestation, i.e. hyperglycemia. Chronic hyperglycemia can lead to impairment of the heart, blood vessels, nerves, eyes, kidneys etc. In the background of this pathologically elevated blood glucose level, however, there is greatly different etiology and pathophysiology, meaning that diabetic patients need diverse prevention strategies, diagnostic screening techniques and treatments [1].

The vast majority of cases of DM falls into two broad categories: type one- and type two DM (T1DM and T2DM). In the background of T1DM - which is the less common form - there is an absolute deficiency of insulin secretion [2]. These patients are usually young and thin. As for the much more prevalent T2DM, the causes are resistance to insulin action and consequently an insufficient insulin secretory response [2]. People struggling with this type of DM are primarily adults and obese. In addition to the two main types of DM, the significance of prediabetes also should be emphasized, since this hyperglycemic, pathological state preceding overt diabetes may strongly be associated with an elevated risk of heart diseases [3].

The number of people struggling with diabetes increased from 108 million in 1980 to 422 million in 2014, and this growth can be observed mainly in the low- and middle-income countries. In 2019, approximately 1.5 million deaths could directly be connected to DM [4].

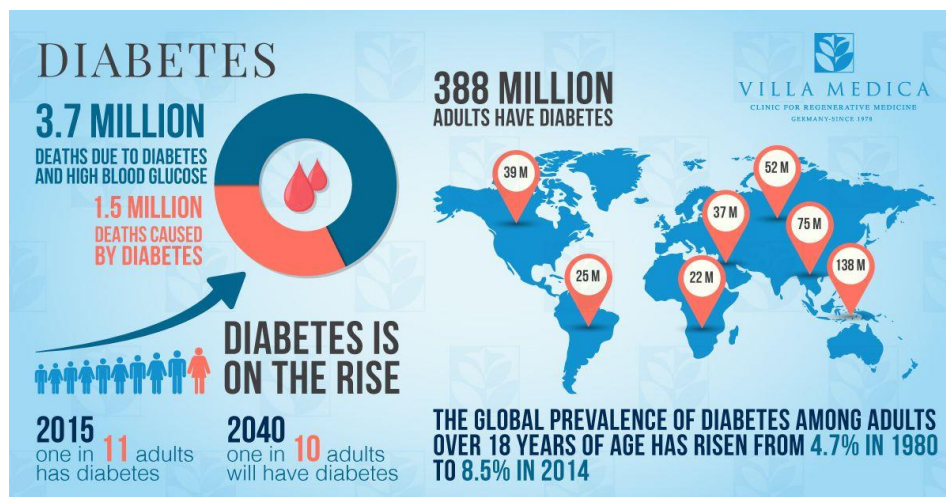


Figure 1. General statistical data on diabetes mellitus according to WHO. Source: [5]

T2DM is the most common form of diabetes - it accounts for 90-95% of all DM cases [6]. One of the most important complications of the disease is heart failure and it is known that diabetic patients have over twice the risk of developing this disorder than patients without T2DM [7,8]. Although researchers published a lot of data about DM and its effects on the cardiovascular system, there are still several uncertain and lacking information that would serve the better understanding of the pathomechanism in the background of the disease and would help to develop better therapeutic methods. Thus, further research on diabetes and its complications have great relevance. In the following paragraphs of the introduction, I will focus on and briefly demonstrate prediabetes and a less known but significant form of T2DM, i.e. non-obese T2DM, concentrating on their connection with heart diseases. Besides, preclinical models that used for investigating these pathological states will also be discussed in this part of my thesis.

1.1. Characterization of prediabetes: epidemiology, pathomechanism, cardiac effects

By definition prediabetes is a metabolic state when fasting plasma glucose (FPG) level is between 5.6 and 7 mmol/L, or blood glucose value measured at the second hour of an OGTT is between 7.8 and 11.1 mmol/L or hemoglobin A1c (HbA1c) level is between 5.7 and 6.5%. Thus we can say that though the glucose parameters are too high to be considered normal, they do not meet the criteria for diabetes. Prediabetes - which usually precedes DM - affects approximately 35% of the population and unfortunately may remain symptomless for many years [9], consequently only every third patient suffering from prediabetes is aware of his or her disease.

Although currently we have much less data about prediabetes than DM, plenty of research focus on it due to its high prevalence and severe consequences [10]. The most important risk factors for prediabetes include obesity, age, familiar appearance of T2DM and decreased physical activity. Recognizing the disease can be problematic, since it has only a few silent symptoms such as impaired glucose tolerance, hyperinsulinemia, insulin resistance and mild hyperglycemia. Another reason why it is complicated to recognize prediabetic state is that the early symptoms can not be detected by simple clinical tests; complex measurements like OGTT are needed that are used less frequently in the clinical routine. As a result of the above, unfortunately, a significant proportion of prediabetic patients notices their illness when it has already turned to T2DM.

The transition from a metabolically healthy state to prediabetes commonly includes an obese state characterized by hyperinsulinemia, insulin resistance and dyslipidemia [11,12]. However, it is important to emphasize that both metabolically healthy obese individuals and metabolically unhealthy lean individuals can be found in the general population [13]. This fact indicates that obesity might not automatically result in the development of prediabetes and subsequent T2DM [14].

It should be stressed that even the previously mentioned slightly elevated but nondiabetic levels of hyperglycemia and impaired glucose tolerance can have a cause-effect relationship to CVD [3,15]. As prediabetes is difficult to recognize, this condition is associated with a latent cardiovascular risk, which can lead to heart damage and later severe complications. Even though some of the risk might be due to the progression to overt diabetes, there is still an independent risk in individuals who have not yet progressed to DM [16].

Although only a limited amount of data is available about the effect of prediabetes on the heart, we know that the main macrovascular complications associated with this pathological condition are coronary artery disease (CAD) and heart failure. Developing atherosclerosis and then CAD has a high risk in these patients, as prediabetes and metabolic syndrome often coexist [17]. In addition to this, according to the literature prediabetic people have an increase in fibrinogen and high-sensitivity C-reactive protein (hs-CRP) - both considered as proatherogenic factors- compared with normoglycemic patients [18,19].

It was reported that prediabetes can cause heart failure with preserved ejection fraction (HFpEF) in rats [10] and patients [20,21], characterized by diastolic dysfunction. Although the exact molecular mechanisms in the background of diastolic dysfunction in prediabetes and DM are not clarified, some processes can be supposed, such as cardiac mitochondrial disorders, cardiac lipid accumulation, decreased β -myosin heavy chain (β -MHC) expression and decreased Sarcoplasmic/Endoplasmic reticulum calcium ATP-ase 2a (SERCA2a) activity [10,22–24]. As for T2DM, it is indicated that its pathology is associated with myocardial lipotoxicity [25], which can lead to defective mitochondrial function [26]. Due to the impairment of mitochondrial function enhanced oxidative stress and activated apoptosis occur, and these processes contribute to cardiac dysfunction [27]. Although the role of lipotoxicity, oxidative stress and apoptosis has been well studied in DM, the function of these mechanisms in prediabetes has not been well characterized yet.

Schlame and Ren reported that the proper lipid composition in the heart is strongly correlated with cardiac function and greatly relies on proper CL content and species profile [28]. CL is a crucial phospholipid (PL) of the mitochondria that takes part in essential processes

like respiration and energy conversion [29]. As the heart is full of mitochondria and CL accounts for approximately 15% of all membrane lipids, alterations in CL content and/or species profile, i. e. the proper cardiac lipid composition can cause mitochondrial dysfunction which can lead to cardiac diseases including prediabetes and diabetes [30]. Alteration of the lipid composition can be reached by the induction of DNL, as it has the capacity to modify the circulating nonesterified fatty acid (FA) profile [31]. High-fructose diet is often used to induce prediabetes in rats, and since the metabolism of fructose leads to enhanced DNL in the liver, this model could be suitable to investigate the possible cardiac effects of the modified lipid pool in prediabetic state.

1.2. Characterization of diabetes mellitus: types, epidemiology, pathomechanism, cardiac effects

DM is a heterogenous chronic metabolic disorder characterized by hyperglycemia resulting from impaired insulin secretion, insulin resistance, or both [32]. The disease can be described by FPG level higher than 7 mmol/L, or blood glucose value measured at the second hour of an OGTT higher than 11.1 mmol/L or HbA1c level more than 6.5%.

It was reported by the International Diabetes Federation (IDF) that in 2019, circa 463 million adults were suffering from DM and this huge number was estimated to reach 700 million by 2045. As stated also by the IDF, in 2019, 1 in 5 people above 65 years had diabetes [33]. Clearly, T2DM is the most common form of diabetes - it accounts for 90-95% of all DM cases [6].

DM is classified by etiology and pathology as T1DM, T2DM and gestational DM (GDM). GDM affects about 5% of pregnant women and in most cases is an early form of T2DM. T1DM accounts for 5% to 10% of people with diabetes and the remainder, about 90% is affected by T2DM [34].

T1DM is primarily a genetic disease of the immune system and the genes responsible for this disease are carried on chromosome 6. When some of these genes are abnormal, autoimmune diseases such as T1DM can be developed. However, genetics is not the only reason - there are some environmental factors involved that trigger the immune system to attack and destroy the β cells of the pancreas, causing insulin deficiency and diabetes. These environmental factors can be certain viruses, such as coxsackie viruses. The death of the β cells by the T lymphocytes of the immune system manifests as the total loss of insulin production. As the insulin deficit is absolute and lifelong, treatment in all persons with T1DM must be with insulin - for life.

Absolute insulin deficiency results in an impairment of some metabolic processes: glucose cannot enter the cells and accumulates in the blood leading to hyperglycemia, which causes polyuria, then polydipsia and polyphagia. In spite of polyphagia, there is cell death and loss, so there is weight loss. Fat breakdown results in free fatty acids (FFAs) being released from fat cells. FFAs are changed into ketone bodies and can cause ketoacidosis, which can result in coma and death without treatment [34]. According to the reports of the IDF, in 2019 more than 1.1 million children and adolescents were suffering from T1DM [33].

T2DM is in fact a group of diseases, i.e. a syndrome with different genetics and pathophysiology but similar symptoms and outcome [35]. T2DM is increasing in prevalence worldwide [36], and it is strongly associated with obesity and insulin resistance [37]. Insulin resistance is probably the first defect in T2DM, which is caused by genetic factors in the peripheral cells and liver cells as well as environmental factors like aging, sedentary lifestyle and obesity. All obese people have a degree of insulin resistance and compensatory hyperinsulinemia, but not all of these people will get diabetes. Progressive insulin deficiency is the other defect of T2DM. It is different from the insulin deficiency of T1DM in that it is not mediated by the immune system. In case of T2DM, the phenomenon may be due to β cell exhaustion from the hypersecretion of insulin, glucose or lipid toxicity to the β cells, or genetic factors [34].

The pathophysiology of diabetic complications can be differentiated into three kinds: macrovascular, microvascular and neurologic. The common denominator of these complications is elevated blood glucose level. Microvascular disease affects capillaries all over the body; the eyes and the kidneys are the organs most obviously involved. Diabetic retinopathy is the most common cause of adult blindness, as well as diabetic nephropathy accounts for over half of the people on dialysis or receiving kidney transplants [34].

Neuropathy resulting from diabetes is estimated to affect 60% – 70% of people with diabetes depending on age, duration of diabetes, presence or absence of pain, and whether or not other causes of neuropathy are excluded. Neuropathies are characterized by a progressive loss of nerve fibers affecting both the autonomic and somatic divisions of the nervous system [38]. Epidemiologic studies have identified duration and severity of hyperglycemia as the major risk factors for the development of diabetic neuropathy in patients with both T1DM and T2DM [39].

In case of the macrovascular complications mainly the large blood vessels of the heart, brain and legs are affected. The commonest manifestation of macrovascular disease is the atherosclerosis of the coronary arteries, which is the major cause of death in people with

diabetes [34]. Among the risk factors of atherosclerosis, not only T2DM, but also cholesterol, smoking, sedentary lifestyle, obesity and hypertension are to be mentioned. [34].

Furthermore, it is common knowledge that besides atherosclerosis, diabetic patients also have an increased risk of developing other CVD, such as DCM. DCM is considered as left ventricular (LV) diastolic and/or systolic dysfunction with hypertrophy and fibrosis without preceding hypertension, coronary artery disease and valvular or congenital heart disease [40].

T2DM patients are generally obese, however, we should not forget that around 20% of people suffering from the disease are non-obese in Europe and Asia [41–44]. In the background of the non-obese T2DM there is a more pronounced reduction in insulin secretion and less severe insulin resistance when compared with the more characteristic obese phenotype [41]. The risk of T2DM in these non-obese individuals is said to be primarily affected by polygenic inheritance and prenatal environment [41]. Similarly to obese T2DM patients, non-obese ones also have an elevated risk of CVD, as it has been described several times in the relevant literature [41,45,46]. These cardiovascular complications include LV hypertrophy, fibrosis and diastolic and/or systolic dysfunction [32,47–49]. Nonetheless, the exact molecular mechanisms leading to these pathological alterations are not well-known. In the background of systolic dysfunction, a possible key factor might be an antioxidative derangement, indicated by the significantly inhibited nuclear erythroid 2-related factor 2 (Nrf2) pathway observed in a non-obese T2DM mouse model [50]. As for the potential causes behind cardiac hypertrophy, Apaijai et al. postulated that estrogen deprivation increased the severity of hypertrophy by provoking inflammation and oxidative stress in the heart of GK rats [51]. Despite we have the above mentioned experimental findings about the cardiac effects of non-obese T2DM, we still need to expand our knowledge about the causes of myocardial injuries. One possible way to do so is the analysis of cardiac gene expression profile, since the up-or downregulation of certain genes can induce pathological processes and result in deteriorations in the heart. The analysis of the transcriptome is a frequently used method in different DM models [52,53], but as for non-obese T2DM, very little data is available.

1.3. Preclinical models of diabetes mellitus and prediabetes

Animal models play a crucial role in the research and characterization of disease pathophysiology, target identification, and in the evaluation of novel therapeutic agents and treatments *in vivo* [54]. Basically, we can distinguish the following types of animal models: [i] genetic - or spontaneously ill - models, [ii] genetically modified models, [iii] diet-induced

models, [iv] surgically created models and [v] chemically-induced models. Focusing on DM, the most common animal models are, on the one hand, chemically-induced models, on the other hand, genetic models [54]. In case of chemically-induced diabetes, streptozotocin (STZ) and alloxan are the main drugs to be applied [55]. Both chemicals are employed as cytotoxic glucose analogues that are prone to accumulate in pancreatic beta cells using glucose transporter 2 [55]. As for the genetic models of T2DM, Zucker Diabetic Fatty (ZDF) rats, GK rats [54] and db/db mice are used most commonly.

For the investigation of the cardiac effects of non-obese T2DM, we decided to use a genetic model animal, the GK rat. GK rat is a widely known and used model animal of inherited T2DM [56,57]. This special strain was developed by selective breeding of ordinary Wistar rats with the highest normal blood glucose levels after applying OGTT [58]. By week 4-5, GK rats can be characterized with a non-obese and slight hyperglycemic phenotype along with glucose intolerance and subsequently peripheral insulin resistance [56], which turns to a hyperglycemic insulin-deficient condition as they getting older [59,60].

GK rats show valuable characteristics that are more or less common and functionally present in human diabetic patients [57]. However, hyperglycemia and glucose intolerance developed in these animals are not connected with the development of obesity or hypertension [32]. Another characteristic features of this non-obese rat strain are impaired insulin secretion in response to glucose not only *in vivo* but in isolated pancreata, elevated glycosylated hemoglobin, altered heart and body weight, and various late complications, including neuropathy, nephropathy [57] and cardiovascular disorders [32,47–49]. Since these cardiovascular disorders include hypertrophy, fibrosis and systolic and/or diastolic dysfunction, which can be found in the background of DCM [40], the development of DCM is very likely in GK rats.

As mentioned above, in adult GK rats several cardiovascular complications has been shown to develop, and considering that the pathogenesis of T2DM present in humans is quite well mimicked in this rodent, we can state that GK rat is an applicable model animal for the examination of the consequences of non-obese T2 diabetes in the heart. Another reason we chose this genetic model to study non-obese T2DM was that in GK rats the development of the disease is spontaneous, as opposed to the other frequently applied models of DM, the chemically-induced models. The latter methods are rather used to induce T1DM, since the previously mentioned chemical agents, STZ and alloxan cause the degradation of pancreatic beta cells and thus significantly reduce the number of insulin producing cells. Another argument against chemically-induced models is that the intraperitoneal or intravenous administration of

the drugs (mainly when applied repeatedly) makes the animals stressed and this may induce adverse metabolic processes.

In addition to genetic and chemical animal models, the mostly high carbohydrate and/or high fat containing, diet-induced models are also used quite often to achieve experimental diabetic or prediabetic condition. As people nowadays consume more and more food containing a high amount of carbohydrates and/or fats, applying especially chronic, diet-induced models seems to be an appropriate way to induce and examine the developed prediabetic or diabetic states.

As previously mentioned, high-fat diet, high-carbohydrate diet and mostly their combination [61–63] are also applied to mimic the pathological effects of prediabetes and DM in humans, and it has a notably rich literature. As a source of sugar in the chow and/or drinking water of the experimental animals, fructose [64,65], sucrose [66,67], and glucose [68] are most commonly used. Regarding high-fat diet, the use of lard [69,70] and vegetable oils [71] is usual. It is also common to supplement these special diets with STZ injection [72–75]. In our study, we used fructose-enriched diet for two reasons. On the one hand, high-fructose corn syrup is often used as a sweetener in foods and drinks, and consuming these fructose-rich foods or beverages results in adverse effects on animals [76] and humans [77]. On the other hand, as mentioned earlier, high-fructose diet is often applied to induce prediabetes in rats, and since the metabolism of fructose gives rise to enhanced DNL in the liver, it might be a proper method to investigate the effects of the modified lipid pool in the heart as well.

Due to the continuous increase in the prevalence of DM in the world, diabetic animal models are admittedly play a crucial role in clarifying the pathogenesis of human diabetes and its complications. Moreover, these models are also important for investigating and developing novel drugs for the disease along with the complications of it [54]. The better understanding of refined animal models will hopefully lead to more appropriate preclinical studies and improvement of therapeutics for DM [78].

2. AIMS

Our main goal was to investigate the cardiac effects of prediabetes and non-obese T2DM. For the prediabetic study, we used a chronic, high-fructose diet-induced non-genetic rat model. Unlike in diabetes, not much is known about the molecular mechanisms causing diastolic dysfunction in prediabetes. It is common knowledge, however, that the metabolism of fructose leads to DNL in the liver. Thus, we were curious whether the altered lipidome has adverse effects on the heart, playing a role in cardiac dysfunction. Moreover, since increased apoptosis and oxidative stress - possibly caused by myocardial lipotoxicity - often contribute to cardiac dysfunction (which is known to be developed already in this early, mild prediabetic stage), in our present study, we also aimed to explore the effects of prediabetes on apoptosis and oxidative stress in the heart.

To investigate the cardiac effects of non-obese T2DM, GK rat, a well-known genetic model of the disease was chosen. The molecular mechanisms in the background of cardiac complications in non-obese T2DM are not known exactly. Though there are some literature data on the cardiovascular complications of non-obese T2DM, alterations in the heart of GK rats at the transcript level has never been studied before. There are a few data about the effects of non-obese T2DM on gene expression pattern in various tissue types (pancreatic islets [79,80], liver [81], skeletal muscle [82], adipose tissue [83], hippocampus and prefrontal cortex [84]), but not in the heart. So our goal was to examine the influence of non-obese T2 diabetes on cardiac alterations of the transcriptome in GK rats.

3. METHODS

3.1. Diet-induced prediabetes model

3.1.1. Experimental design

Male Wistar rats (310–450 g, $n=16$ in the entire study) were kept under controlled temperature with 12/12 h light/dark cycles. Animals were divided into two groups and were fed with the following diets for 24 weeks: the control group ($n=8$) was fed with a standard laboratory chow, while the fructose-fed group ($n=8$) received a chow containing 60% w/w fructose. FBG was measured every 4 weeks, while at weeks 12, 16, 20 and 24 OGTTs were performed. At week 20 and week 24, blood samples were taken to measure serum parameters such as insulin, TG, cholesterol, markers of heart and liver damage (e. g. creatine kinase (CK), alanine- and aspartate aminotransferase (ALAT, ASAT)) and oxidative stress (malondialdehyde (MDA), 3-nitrotyrosine (3-NT)). At the end of the feeding protocol, cardiac function was assessed by both *in vivo* echocardiography and *ex vivo* isolated working heart perfusions (Figure 2). Following the perfusions, myocardial tissue was harvested for biochemical analysis.

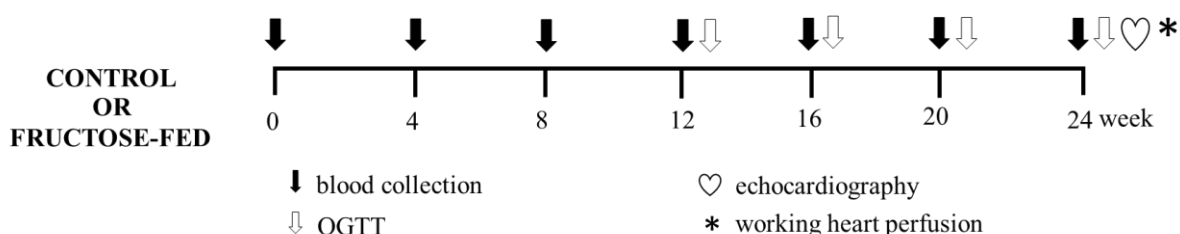


Figure 2. Experimental protocol. Male Wistar rats were divided into control ($n=8$) and fructose-fed ($n=8$) groups receiving either a standard chow or a chow supplemented with 60% w/w fructose, respectively, for 24 weeks. Fasting blood glucose measurement or oral glucose tolerance test (OGTT) was performed every four weeks to monitor the development of prediabetic condition. At week 24, transthoracic echocardiography was performed to monitor cardiac function and morphology. Then, the hearts of the animals were isolated and mounted on a working heart perfusion system to measure hemodynamic and left ventricular pressure parameters. After the perfusions, hearts were frozen for measurement of biochemical parameters.

3.1.2. Measurement of serum glucose levels and OGTT

As described previously, rats were fasted overnight prior to serum glucose level measurements (weeks 0, 4 and 8) and OGTTs (weeks 12, 16, 20 and 24) to verify the development of hyperglycemia and glucose-intolerance as diagnostic criteria of diabetes

mellitus [49,52,53]. Blood samples were collected from the saphenous vein. Blood glucose levels were measured using Accu-Chek blood glucose monitoring systems (Roche Diagnostics Corporation, USA, Indianapolis) [52,53,85]. In case of OGTT, after the measurement of baseline glucose concentrations, 1.5 g/kg body weight glucose was administered *per os* via gavage and blood glucose levels were checked 30, 60 and 120 min later [52,53,85]. Area under the curve (AUC) values for OGTT was also calculated.

3.1.3. Measurement of serum and pancreatic insulin levels

Serum and pancreatic insulin levels were measured by enzyme-linked immunosorbent assay (ELISA) (Mercodia, Ultrasensitive Rat Insulin ELISA). Insulin ELISA was carried out according to the instructions of the manufacturer from either sera or homogenized pancreatic tissue samples of fructose-fed and control rats. At week 20 sera were centrifuged (2000 g for 10 min at 4 °C) and kept at -20 °C until further investigation. At week 24 pancreata were removed, trimmed free of adipose tissue and weighed. Pancreata were homogenized in 6 mL cold acidified ethanol (0.7 M HCl: ethanol (1: 3 v/v)) with an Ultra Turrax homogenizer and were kept at 4 °C for 24 h. Then, pancreas homogenates were centrifuged (900 g for 15 min at 4 °C) and the supernatants were stored at 4 °C. The pellet was extracted again with 3 mL acidified ethanol for 24 h at 4 °C. The supernatant obtained after centrifugation was pooled with the previous one and kept at -20 °C until assayed [52,86].

3.1.4. Homeostatic model assessment for insulin resistance (HOMA-IR index)

To estimate insulin resistance in fructose-fed or control rats, the widely used HOMA-IR index was calculated [52,87,88] by multiplying fasting serum insulin ($\mu\text{U/mL}$) with fasting serum glucose (mmol/L) then dividing by the constant 22.5, i.e., $\text{HOMA-IR} = (\text{fasting serum insulin concentration} \times \text{fasting serum glucose concentration}) / 22.5$.

3.1.5. Measurement of serum lipid levels

Serum total cholesterol (TC), TG, and LDL and HDL (low-density and high-density lipoprotein) cholesterol levels were measured at week 24 in triplicate, using commercially available colorimetric assay kits applying enzymatic determinations (Diagnosticum Ltd., Budapest, Hungary) adapted to 96-well plates. Accuracy of the assays was monitored by using Standard Lipid Controls (Sentinel, Milan, Italy). Results are expressed as mmol/L of serum [89].

3.1.6. Measurement of serum markers of liver and heart damage

ALAT, ASAT, CK and lactate dehydrogenase (LDH) enzyme activities were measured with UV assays standardized according to the recommendations of the International Federation of Clinical Chemistry (IFCC). CK-MB enzyme activities were determined using an immunological UV assay. All reagents and instruments were purchased from Roche Diagnostics.

3.1.7. Transthoracic echocardiography

Cardiac morphology and function were assessed by transthoracic echocardiography at week 24 as described previously [90–92]. Briefly, rats were anesthetized with sodium pentobarbital (Euthasol, 40 mg/kg body weight i.p.). Then, the chest was shaved, and the rat was placed in a supine position onto a heating pad. Two-dimensional, motion-mode (MM) and Doppler echocardiographic examinations were performed by the criteria of the American Society of Echocardiography with a Vivid IQ ultrasound system (General Electric Medical Systems), using a phased array 5.0–11 MHz transducer (GE 12S-RS probe). Data of three consecutive heart cycles were analyzed (EchoPac Dimension software; General Electric Medical Systems) by an experienced investigator in a blinded manner. Systolic and diastolic wall thickness parameters were obtained from parasternal short-axis (SA) view at the level of the papillary muscles (anterior and inferior walls) and long-axis (LA) view at the level of the mitral valve (septal and posterior walls). The LV diameters were measured by means of MM echocardiography from LA views between the endocardial borders. Fractional shortening (FS) was used as a measure of cardiac contractility ($FS = (LV \text{ end-diastolic diameter (LVEDD)} - LV \text{ end-systolic diameter (LVESD)}) / LVEDD \times 100$). Functional parameters including LV end-diastolic volume (LVEDV) and LV end-systolic volume (LVESV) were calculated on four-chamber (4CH) view images delineating the endocardial borders in diastole and systole. Stroke volume was calculated as the difference of LVEDV and LVESV. Ejection fraction (EF) was calculated according to the formula $(LVEDV - LVESV) / LVEDV \times 100$. Diastolic function was assessed using pulse-wave Doppler across the mitral valve from the apical 4CH view. Early (E) and atrial (A) flow velocities provide an indication of diastolic function. Heart rate was also calculated using pulse-wave Doppler images during the measurement of transvalvular flow velocity profiles according to the length of 3 consecutive heart cycles measured between the start points of the E waves. The mean values of three measurements were calculated and used for statistical evaluation.

3.1.8. Working heart perfusion

Immediately after the echocardiography, cardiac performance was assessed in isolated working rat hearts, as described earlier [89,93,94]. Anesthetized rats were given 500 U/kg heparin intravenously. Hearts were then isolated, and the aorta was cannulated and initially perfused in Langendorff mode (at a constant pressure of 73 mmHg, 37 °C) with Krebs-Henseleit buffer containing NaCl 118 mM, NaHCO₃ 25 mM, KCl 4.3 mM, CaCl₂ 2.4 mM, KH₂PO₄ 1.2 mM, MgSO₄ 1.2 mM and glucose 11 mM, gassed with 95% O₂ and 5% CO₂ [90,95]. Then, the perfusion system was switched to working mode according to Neely with recirculating buffer [95,96]. Hydrostatic preload and afterload were kept constant at 13 mmHg and 73 mmHg, respectively, throughout the experiments. Hearts were subjected to 10 min equilibration period before measurement. Cardiac functional parameters including heart rate, coronary flow (CF), aortic flow, cardiac output, LV developed pressure (LVDP) and its first derivatives (dp/dt max and dp/dt min) and LV end-diastolic pressure (LVEDP) were measured. CF was collected in a beaker for one minute, then measured by a measuring cylinder. Aortic flow was measured by a flowmeter. LV pressure parameters were registered by a cannula placed into the left ventricle through the left atrium. ISOSYS software was used to evaluate aortic flow and LV pressure values. At the end of the perfusion, the hearts were weighed, and the left and right ventricles were separated. The left ventricles were snap frozen in liquid nitrogen and stored at -80 °C until they were used for biochemical assays.

3.1.9. mRNA expression profiling by qRT-PCR

Quantitative real-time - Polymerase chain reaction (qRT-PCR) was performed with gene-specific primers to monitor mRNA expression as described previously [92]. To assess DNL, expression of sterol regulatory element-binding transcription factor 1 (*Srebf1*), stearoyl-CoA desaturase 1 (*Scd1*), fatty acid synthase (*Fasn*), acetyl-CoA carboxylase 1 (*Acaca*), carbohydrate-responsive element-binding protein (*Mlxipl*), elongation of very-long-chain fatty acids protein 6 (*Elovl6*), fatty acid desaturase 1 (*Fads1*) and fatty acid desaturase 2 (*Fads2*) were measured from liver samples. To assess cardiac hypertrophy, expression of myosin heavy chain α isoform (*Myh6*) and myosin heavy chain β isoform (*Myh7*) was measured. RNA was isolated using Qiagen RNeasy Fibrous Tissue Mini Kit (Qiagen, #74704) from the liver and heart tissues. Briefly, 4 μ g and 2.2 μ g of total RNA from liver and heart samples, respectively, were reverse transcribed using iScript™ Advanced cDNA Synthesis kit (Bio-Rad, 1725038), and specific primers and SsoAdvanced™ Universal SYBR® Green Supermix (Bio-Rad) were

used according to the manufacturer's instructions. Hypoxanthine phosphoribosyltransferase 1 (*Hprt1*) was used as control for normalization.

3.1.10. Lipidomics

Approximately 20 mg of the powdered left ventricle was directly extracted by adding 1 mL of methanol containing 0.001% butylated hydroxytoluene as an antioxidant and 60 μ g di20:0 phosphatidylcholine as extraction standard. After a 5 min sonication in a water bath sonicator, the mixture was shaken for 5 min and centrifuged at $10000 \times g$ for 5 min. The supernatant was transferred into a new Eppendorf tube and stored at -20°C until mass spectrometry (MS) analysis. The solvents used for extraction and MS analyses were of Optima Liquid chromatography-Mass spectrometry (LCMS) grade from Thermo Fisher Scientific (Bremen, Germany) and liquid chromatographic grade from Merck (Darmstadt, Germany). Lipid standards were purchased from Avanti Polar Lipids (Alabaster, AL). All other chemicals were from Sigma-Aldrich (Steinheim, Germany) and were of the best available grade. MS analyses were performed on an LTQ-Orbitrap Elite instrument (Thermo Fisher Scientific, Bremen, Germany) equipped with a robotic nanoflow ion source (TriVersa NanoMate; Advion BioSciences; Ithaca, NY, USA) as described in [97].

3.1.11. Determination of oxidative stress: measurement of MDA and 3-NT levels

In order to determine the level of systemic and cardiac lipid peroxidation, serum MDA and cardiac tissue MDA were measured by the following manner. Serum samples were mixed thoroughly with 1.2 volumes of a stock solution of 15% w/v trichloroacetic acid, 0.375% w/v thiobarbituric acid (TBA) and 0.25 N HCl, and heated for 30 min at 95°C . After cooling and centrifugation at $1000 \times g$ for 10 min, the supernatant containing TBA were extracted in butanol and assayed spectrophotometrically at 535 nm. Freshly diluted tetramethoxypropane which yields MDA was used as the external standard [98]. Results are expressed as nmol/mL serum or nmol/mg protein.

For the measurement of 3-NT, a double-antibody sandwich ELISA kit was purchased from Genasiabio (Shanghai, China). Left ventricles were homogenized (Heilscher UP100H Ultrasonic Processor) in Phosphate Buffer Saline (PBS) (pH 7.2–7.4) and then centrifuged at 3000 rpm for 20 min at 4°C . 3-NT was measured according to the manufacturer's instructions and protocols, and optical densities (OD) were determined at 450 nm. Results were expressed as nmol/mg protein.

3.1.12. Western blot

The standard western blot technique was used to investigate changes of B-cell lymphoma 2 (BCL-2), Bcl-2-associated X (BAX), B-cell lymphoma-extra large (BCL-XL), caspase-7 and caspase-3 apoptotic proteins in the cardiac tissue, with actin or tubulin loading background. LV samples ($n=8$ per group) were homogenized with an ultrasonicator (UP100H Hielscher, Teltow, Germany) in Radio-Immunoprecipitation Assay (RIPA) buffer (50 mM Tris-HCl (pH 8.0)), 150 mM NaCl, 0.5% sodium deoxycholate, 5 mM ethylenediamine tetra-acetic acid (EDTA), 0.1% sodium dodecyl sulfate (SDS), 1% NP-40 (Cell Signaling, Carlsbad, CA, USA) supplemented with phenylmethanesulfonyl fluoride (PMSF). The crude homogenates were centrifuged at $15000 \times g$ for 30 min at 4 °C. After quantification of protein concentrations of the supernatants using the BCA Protein Assay Kit (Pierce, Rockford, IL, USA), 25 μ g of reduced and denatured protein was loaded. Then, SDS - polyacrylamide gel electrophoresis (SDS-PAGE) was performed (10% gel, 50 V, 4 h) followed by the transfer of proteins onto a nitrocellulose membrane (20% methanol, 35 V, 1.5 h). The efficacy of transfer was checked using Ponceau staining. The membranes were cut horizontally into parts corresponding to the molecular weights of BAX, BCL-2, BCL-XL, caspase-7, caspase-3, actin and tubulin. Membranes were blocked for 1 h in 5% w/v bovine serum albumin (BSA) and were incubated with primary antibodies in the concentrations of 1:1000 against BAX (#2772), BCL-2 (#3498), BCL-XL (#2764), caspase-7 (#12827), caspase-3 (#14220), α -tubulin (#2144) and β -actin (#4970) overnight at 4 °C in 5% BSA. Then, the membranes were incubated with IRDye® 800CW Goat Anti-Rabbit secondary antibody (Li-Cor) for 1 h at room temperature in 5% BSA. Fluorescent signals were detected by Odyssey CLx (LI-COR Biotechnology, Lincoln, Nebraska USA), and digital images were analyzed and evaluated by Quantity One Software.

3.1.13. Statistical analysis

Lipidomic data are presented as mean \pm SEM; statistical significance was determined according to Storey and Tibshirani [99] and was accepted for $p < 0.05$ corresponding to a false discovery rate < 0.05 . Principal component analysis (PCA) was performed using MetaboAnalyst [100]. All other parameters are presented as mean \pm SEM, and significance between groups was determined with two sample t -test or Mann-Whitney Rank Sum Test.

3.2. Non-obese genetic model of type 2 diabetes

3.2.1. Experimental design

Male GK rats and their age-matched male Wistar controls were obtained from Charles River Laboratories at the age of 6 weeks and were housed at 22 ± 2 °C with a 12:12-h light–dark cycle. The rats received standard rat chow and water ad libitum for 9 weeks after their arrival.

Body weight, serum glucose, insulin, cholesterol levels and HOMA-IR were determined at 7, 11 and 15 weeks of age in order to monitor the basic parameters of glucose and lipid metabolism and insulin resistance in GK and control rats. OGTT was performed at week 15 to further characterize glucose homeostasis of GK and control rats. At 15 weeks of age, rats were anaesthetized using pentobarbital sodium (Euthasol, 50 mg/kg, Produlab Pharma b.v., Raamsdonksveer, The Netherlands). Hearts and pancreata were isolated, and then hearts were perfused according to Langendorff as described earlier in 4.1.8. (Figure 3). After 5 min perfusion ventricular tissue was frozen and stored at -80 °C until gene expression analysis by DNA microarray and qRT-PCR techniques.

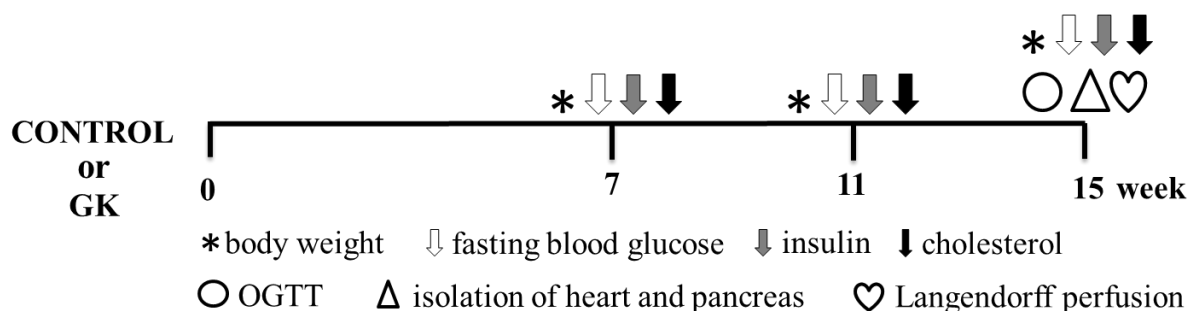


Figure 3. Experimental protocol. Male Goto-Kakizaki (GK) rats and their age-matched male Wistar controls received standard rat chow and water for 9 weeks after their arrival (6 weeks of age). Body weight, fasting blood glucose, insulin and cholesterol levels were measured at week 7, 11 and 15 to monitor the basic parameters of glucose and lipid metabolism. At week 15, oral glucose tolerance test (OGTT) was performed to further characterize glucose homeostasis. Following anaesthesia at 15 weeks of age, the animals' hearts and pancreata were isolated and the hearts were perfused according to Langendorff. After perfusion, ventricular tissue was frozen for gene expression analyses.

3.2.2. Measurement of serum glucose levels and OGTT

The methods are the same as described earlier in 3.1.2. with some differences: serum glucose level measurements and OGTTs took place at weeks 7, 11 and 15.

3.2.3. Measurement of serum and pancreatic insulin levels, HOMA-IR index

The methods are the same as described earlier in 3.1.3. and 3.1.4. with some differences: blood samples were collected at weeks 7, 11 and 15. At week 15, during OGTT blood was collected at 0, 30 and 120 min for serum insulin level measurements. Moreover, pancreas insulin levels were determined at week 15.

3.2.4. Measurement of serum cholesterol levels

The methods are the same as described earlier in 3.1.5. with some differences: in order to follow up the development of hypercholesterolemia which is a risk factor of CVD, serum cholesterol levels were measured at weeks 7, 11 and 15.

3.2.5. RNA preparation and DNA microarray analysis

Total RNA was isolated from heart samples with Qiagen miRNeasy Mini Kit according to the manufacturer's protocol (Qiagen, Hilden, Germany) as described previously [53]. On-column DNase digestion was carried out with the RNase-Free DNase Set (Qiagen GmbH). RNA concentration was measured by NanoDrop 1000 Spectrophotometer (Thermo Fisher Scientific Inc., Waltham, MA, USA) and RNA integrity was determined by an Agilent 2100 Bioanalyzer System (Agilent Technologies Inc., Santa Clara, CA, USA). Samples with an RNA integrity number (RIN) above 8.0 were used for further analysis. RNA was stored at -80°C until use.

Total RNA (1000 ng) was labelled and amplified using the QuickAmp Labelling Kit according to the instructions of the manufacturer. Labelled RNA was purified and hybridized to Agilent Whole Rat Genome 4×44 K array slides, according to the manufacturer's protocol. After washing, array scanning and feature extraction was performed with default scenario by Agilent DNA Microarray Scanner and Feature Extraction Software 9.5.

3.2.6. mRNA expression profiling by qRT-PCR

In order to validate gene expression changes obtained by DNA microarray, qRT-PCR was performed with gene-specific primers. Total RNA (1 μg) was reverse transcribed using High-Capacity cDNA Reverse Transcription Kit (Thermo Fisher Scientific, Waltham, MA US). QRT-PCR was performed using TaqMan Array 96 Well Fast Plate 3×32 (Thermo Fisher Scientific, Waltham, MA US) according to the manufacturer's instructions on a 7900HT Fast Real-Time PCR System. Each well of the TaqMan Array Plate contained 5 μL of Taqman Fast Universal Master Mix (2X) no AmpErase® UNG, 1 μL cDNA (50 ng/ μL) and 4 μL distilled

water in a final reaction volume of 10 μ L per well. Then qPCR was performed with the following protocol: 50 cycles of 95 °C for 15 s and 60 °C for 1 min. The fluorescence intensity was detected after each amplification step. Melting temperature analysis was done after each reaction to check the quality of the products. Primers were designed using the online TaqMan® Assays custom plating service of the manufacturer. Relative expression ratios were calculated as normalized ratios to rat glyceraldehyde-3-phosphate dehydrogenase (*Gapdh*), hypoxanthine phosphoribosyltransferase (*Hprt*) and ribosomal protein S18 (*Rps18*) housekeeping genes. A nontemplate control sample was used for each primer to check primer-dimer formation. Normalized signal levels for each mRNA were calculated using comparative cycle threshold method (delta–delta Ct method). Fold change refers to $2^{-\Delta\Delta Ct}$ (in case of upregulated genes) and $-(1/2^{-\Delta\Delta Ct})$ (in case of downregulated genes).

3.2.7. GO analysis

By using DNA microarrays for transcriptional profiling a large number of genes can be analyzed simultaneously [52,101], however, the resulting data do not give direct information about possible biological interaction of the differentially expressed genes. GO analysis is a suitable method for integration genes with pathways and biological interaction networks to detect coordinated changes in functionally related genes [52,101]. A single gene can belong to different categories. GO analysis was performed using GO pathway analysis using the open access software DAVID bioinformatics system and database (Database for Annotation, Visualization and Integrated Discovery, <http://www.david.abcc.ncifcrf.gov> website) [52,101]. The differentially expressed genes were submitted to DAVID bioinformatics system and database to reveal significantly enriched biological functions/pathways [52,101].

3.2.8. Statistical analysis

Statistical analysis was performed by using Sigmaplot 12.0 for Windows (Systat Software Inc). All values are presented as mean \pm SEM. Repeated measures Two-Way ANOVA was used to determine the effect of T2DM and age on FBG, serum insulin and cholesterol levels as well as glucose levels during OGTT. After ANOVA, all pairwise multiple comparison procedures with HolmŠídák post hoc tests were used as multiple range tests. Two-sample t test was used to determine the effect of T2DM on OGTT AUC, pancreatic insulin concentration, body weight, heart weight, heart weight/body weight ratio (HW/BW) and CF. $P < 0.05$ was accepted as a statistically significant difference. In the microarray experiments, biological and technical replica tests were carried out to gain raw data for statistical analysis. Altogether 4 individual

parallel gene activity comparisons were done between the two groups. Both in the microarray and qRT-PCR experiments, a two-sample t test was used and the p-value was determined to find significant gene expression changes. In the microarray experiments, a corrected p-value was determined for each gene to control the false discovery rate using the Benjamini and Hochberg multiple testing correction protocol. Gene expression ratios with p-value of <0.05 and log2 ratio of <-1.00 or log2 ratio of >1.00 (~2.0-fold) were considered as repression or overexpression in gene activity, respectively.

4. RESULTS

4.1. Diet-induced prediabetes model

4.1.1. Characterization of the animal model

In the present study, male Wistar rats were fed with 60% fructose-containing chow for 24 weeks to create a model of prediabetes. In order to verify the development of the prediabetic state, FBG was measured at every 4th week and OGTT was performed at weeks 12, 16, 20, and 24. Fasting glucose levels were slightly but significantly higher in fructose-fed rats at weeks 12, 16, 20, and 24 (Figure 4a). OGTT AUC values were also significantly increased in fructose-fed rats at weeks 16, 20, and 24 (Figure 4b).

HOMA-IR, a widely used indicator of insulin resistance, was significantly higher in the fructose-fed rats at week 20 (Figure 4c), although no significant difference was detected in serum insulin levels (Figure 4d). Pancreatic insulin level was significantly higher in the fructose-fed group compared to controls (Figure 4e).

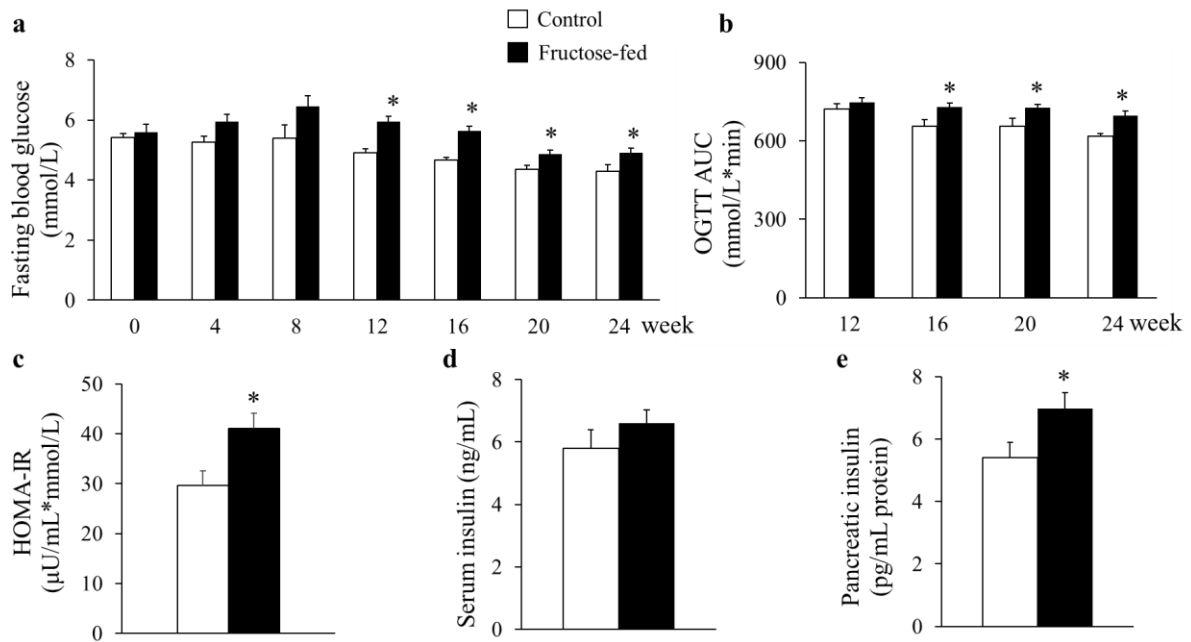


Figure 4. Confirmation of prediabetic condition. (a) fasting blood glucose levels, (b) area under the curve (AUC) values for OGTT, (c) homeostatic model assessment for insulin resistance (HOMA-IR) at week 20, (d) serum insulin level at week 20 and (e) pancreatic insulin level at week 24. Values are mean±SEM, n=7-8, *p<0.05.

Although body weight increased in both groups during the study, by the end of the 24-week feeding, the weight of the fructose-fed rats was significantly smaller compared to that of the control rats (Table 1). Weight gain during the study was decreased in fructose-fed rats (Table

1). As for the organ weights, though liver weight was not significantly different in fructose-fed rats, the liver weight to body weight ratio was increased (Table 1). Moreover, during the isolation of organs, we have observed macroscopical signs of fatty degeneration on the liver of fructose-fed animals.

Table 1. Body weights at week 0 and 24, weight gain, isolated organ weights and isolated organ weight to body weight ratios at week 24 in both control and fructose-fed rats. Values are mean \pm SEM, n=8, *p<0.05.

	control	fructose-fed	p-value
body weight at week 0 (g)	394.75 \pm 10.74	380.5 \pm 19.27	0.474
body weight at week 24 (g)	538.25 \pm 21.64	454 \pm 16.36*	0.005
body weight gain (g)	144 \pm 12	74 \pm 8*	\leq 0.001
heart weight (mg)	1726 \pm 79	1527 \pm 71	0.083
liver weight (mg)	13292 \pm 538	12262 \pm 467	0.170
pancreas weight (mg)	1093 \pm 111	1101 \pm 467	0.951
heart weight/body weight (mg/g)	3.22 \pm 0.14	3.36 \pm 0.09	0.422
liver weight/body weight (mg/g)	22.7 \pm 0.2	27.0 \pm 0.4*	\leq 0.001
pancreas weight/body weight (mg/g)	2.04 \pm 0.19	2.43 \pm 0.11	0.095

Despite these characteristic signs on the liver, neither serum lipid parameters (TGs, TC, LDL- and HDL-cholesterol) nor liver enzymes (ALAT, ASAT) were increased in fructose-fed rats (Table 2).

Table 2. Parameters measured in serum collected at week 24 in both control and fructose-fed rats. Values are mean \pm SEM, n=8.

	control	fructose-fed	p-value
serum TG (mmol/L)	0.96 \pm 0.12	0.94 \pm 0.20	0.938
serum TC (mmol/L)	1.78 \pm 0.14	1.61 \pm 0.11	0.359
LDL-cholesterol (mmol/L)	0.45 \pm 0.05	0.43 \pm 0.08	0.830
HDL-cholesterol (mmol/L)	0.86 \pm 0.08	0.76 \pm 0.07	0.335
ALAT (U/L)	38.63 \pm 3.35	35.00 \pm 4.08	0.500
ASAT (U/L)	77.88 \pm 4.05	73.29 \pm 5.74	0.517
CK (U/L)	263 \pm 46	245 \pm 45	0.776
CK-MB (U/L)	352 \pm 75	256 \pm 33	0.264
LDH (U/L)	334.86 \pm 63.77	272.50 \pm 37.36	0.437

To further characterize metabolic changes in the liver of fructose-fed rats, qRT-PCR was performed. We examined eight different genes related to DNL and experienced significant changes in case of *Acaca* and *Elovl6*; both of them increased (Figure 5c and h). Besides, a tendency of increase could be seen in *Fasn* expression (Figure 5d). As for the other five analyzed genes, we did not observe any alterations.

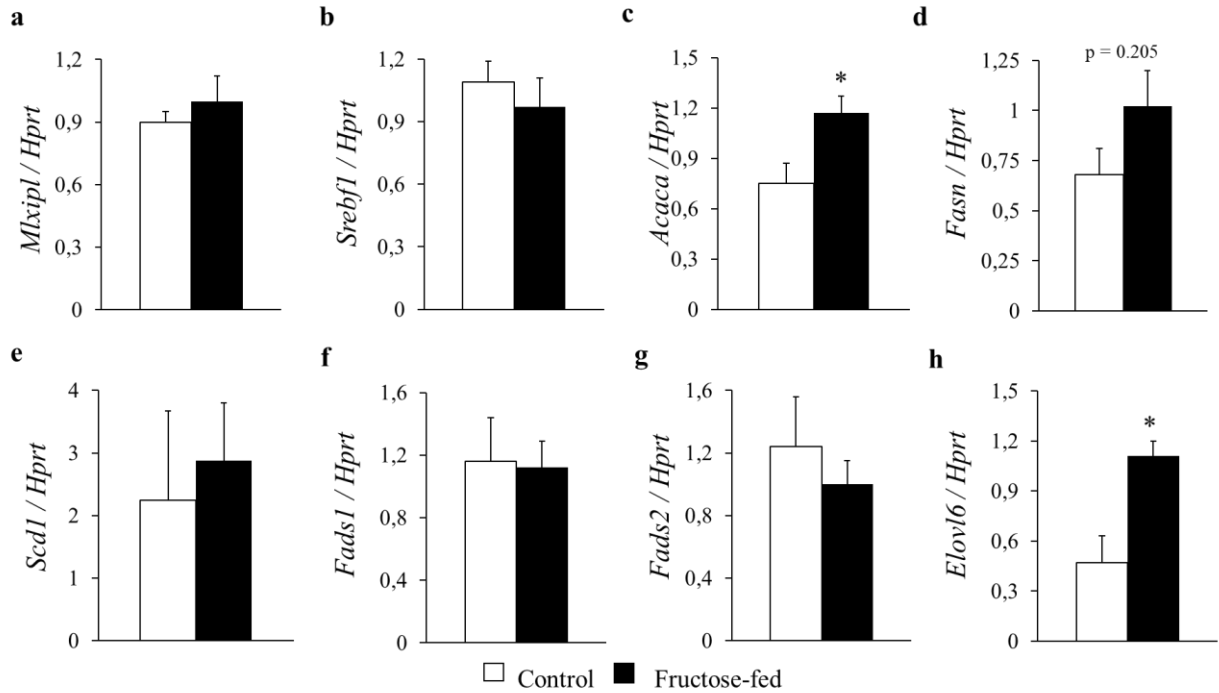


Figure 5. qRT-PCR results in the liver at week 24. Expression of (a) *Mlxipl*, (b) *Srebf1*, (c) *Acaca*, (d) *Fasn*, (e) *Scd1*, (f) *Fads1*, (g) *Fads2* and (h) *Elovl6* in the liver. Values are mean ± SEM, n=6-7, *p<0.05.

4.1.2. Heart function and morphology

To characterize prediabetes-induced cardiac changes in fructose-fed rats, transthoracic echocardiography was performed at week 24 to investigate cardiac function and morphology (data are shown in Table 3). To exclude the potential effect of variations in cardiac mass, the morphological data were given after normalization to heart weight. Wall thicknesses and ventricular diameters were not changed significantly due to fructose feeding (except for anterior wall thickness) (Table 3). Although there was no difference in HR, EF and FS, the E/A ratio was significantly smaller in fructose-fed rats indicating the impairment of diastolic filling (Table 3).

Table 3. Left ventricular morphological and functional parameters examined by echocardiography at week 24 in both control and fructose-fed rats. E/A: early/atrial; MV: mitral valve; SA: short axis; LA: long axis; MM: motion mode; 4CH: four-chamber view. Values are mean \pm SEM, n=8, *p<0.05.

Parameter (unit)	View/Mode	Control	Fructose-fed	p-value
<i>Left ventricular morphology/</i>				
<i>heart weight (mm/g)</i>				
Anterior wall thickness in systole	SA/MM	1.96 \pm 0.11	2.28 \pm 0.06*	0.02
Anterior wall thickness in diastole	SA/MM	1.27 \pm 0.07	1.32 \pm 0.06	0.60
Inferior wall thickness in systole	SA/MM	1.96 \pm 0.06	2.20 \pm 0.11	0.08
Inferior wall thickness in diastole	SA/MM	1.38 \pm 0.10	1.34 \pm 0.10	0.80
Posterior wall thickness in systole	LA/MM	1.96 \pm 0.20	2.05 \pm 0.09	0.67
Posterior wall thickness in diastole	LA/MM	1.21 \pm 0.12	1.29 \pm 0.06	0.56
Septal wall thickness in systole	LA/MM	2.28 \pm 0.14	2.34 \pm 0.11	0.74
Septal wall thickness in diastole	LA/MM	1.36 \pm 0.06	1.73 \pm 0.37	0.35
Left ventricular end diastolic diameter	LA/MM	3.86 \pm 0.23	4.56 \pm 0.27	0.07
Left ventricular end systolic diameter	LA/MM	1.81 \pm 0.10	2.26 \pm 0.20	0.08
<i>Left ventricular function</i>				
E/A	4CH	1.21 \pm 0.07	1.03 \pm 0.02*	0.02
Ejection fraction %	4CH	60.96 \pm 3.38	62.83 \pm 2.32	0.67
Fractional shortening %	SA/MM	49.57 \pm 3.82	54.00 \pm 3.60	0.41
MV E velocity (m/s)	4CH	0.81 \pm 0.05	0.73 \pm 0.06	0.36
MV A velocity (m/s)	4CH	0.71 \pm 0.07	0.82 \pm 0.06	0.26
Heart rate (1/min)	4CH	346.0 \pm 12.9	349.6 \pm 6.8	0.82

Following echocardiography, the hearts were isolated to assess cardiac performance on a working heart perfusion system. LVEDP significantly increased, while cardiac output significantly decreased in fructose-fed rats (Figure 6).

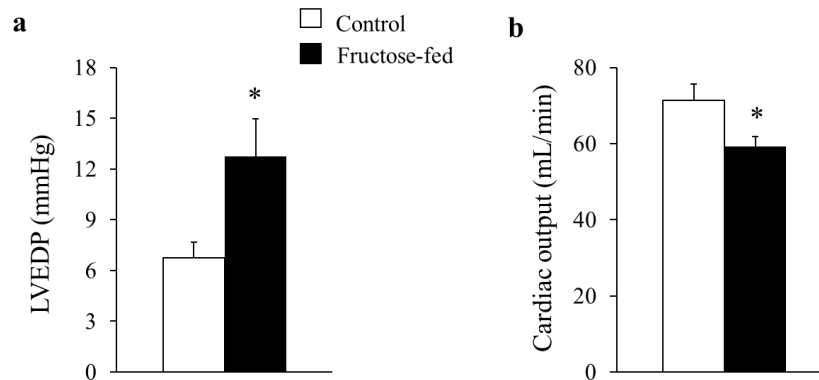


Figure 6. Cardiac function in isolated perfused hearts. (a) left ventricular end-diastolic pressure (LVEDP) and (b) cardiac output. Values are mean \pm SEM, n=7-8, *p<0.05.

Heart rate, max and min dp/dt, LVEDP, and aortic systolic and diastolic pressures were not changed between groups during working heart perfusion (Table 4).

Table 4. Parameters measured by working heart perfusion at week 24 in both control and fructose-fed rats. LVDP: left ventricular developed pressure. Values are mean \pm SEM, n=7-8.

	control	fructose-fed	p-value
aortic flow (mL)	46.6 \pm 3.7	37.4 \pm 2.4	0.065
coronary flow (mL)	24.6 \pm 1.1	21.9 \pm 1.2	0.121
max dp/dt (mmHg/s)	5975 \pm 330	6063 \pm 212	0.832
min dp/dt (mmHg/s)	-3577 \pm 222	-4090 \pm 237	0.138
aortic diastolic pressure (mmHg)	45.7 \pm 1.7	42.1 \pm 1.3	0.120
aortic systolic pressure (mmHg)	110.3 \pm 2.6	116.2 \pm 1.5	0.121
LVDP (mmHg)	137.5 \pm 6.0	139.5 \pm 4.3	0.803
Heart rate (1/min)	279 \pm 14	263 \pm 24	0.554

Since the echocardiographic examination showed significant increase of anterior wall thickness in systole in the fructose-fed group (Table 3), but the weight of the animals was significantly lower in this group (Table 1) - though the heart weight and HW/BW were not changed significantly (Table 1) -, we wanted to check the possible development of hypertrophy in the heart of the fructose-fed animals. In order to assess cardiac hypertrophy at the molecular level, mRNA expression of *Myh6* and *Myh7* was measured. We have found that cardiac *Myh6* mRNA level was increased in fructose-fed rats (Table 5). However, *Myh6/Myh7* ratio did not differ significantly.

Table 5. Estimation of cardiac hypertrophy by qRT-PCR. Values are mean \pm SEM, n=8, * p <0.05.

	control	fructose-fed	p-value
<i>Myh6/Hprt</i> ratio	0.54 \pm 0.08	0.93 \pm 0.13*	0.030
<i>Myh7/Hprt</i> ratio	0.56 \pm 0.14	0.89 \pm 0.18	0.210
<i>Myh6/Myh7</i> ratio	1.33 \pm 0.28	1.19 \pm 0.10	0.672

It is known that clinical laboratory markers of myocardial injury are increased in diabetic cardiomyopathy [102]. Therefore, we measured CK, CK-MB and LDH enzymes and found that none of them changed significantly in fructose-fed rats compared to controls (Table 2).

4.1.3. Lipidomics

To characterize and elucidate the metabolic changes in the prediabetic heart induced by chronically applied fructose-rich diet, we performed high-performance, comprehensive shotgun MS-based lipidomic analyses from LV whole membrane extracts. We have identified and quantified approximately 200 lipid molecular species encompassing 20 lipid classes. To obtain an overview, mol% of membrane lipid values was subjected to the nonsupervised multivariate statistics PCA. The clear separation of the sample sets into two nonoverlapping clusters (Figure 7) indicates complex reshaping and metabolic rewiring of the whole lipidome due to fructose

feeding. Examining these alterations in more detail and comparing the molecular species patterns for the control and fructose groups revealed 100 statistically significant differences.

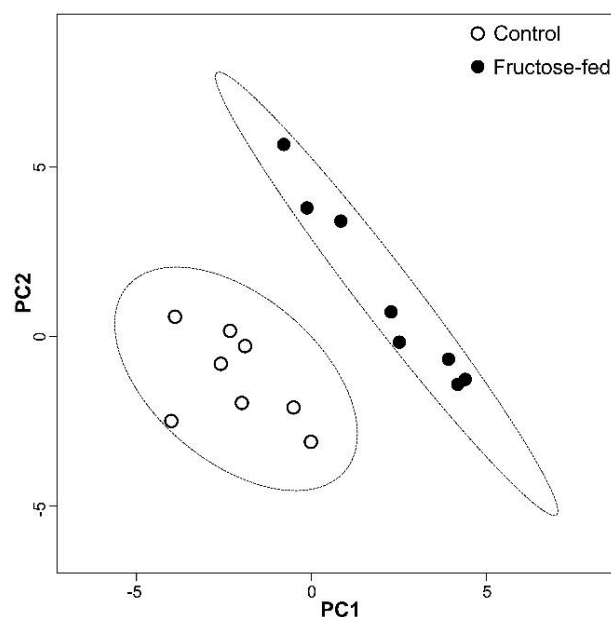


Figure 7. Principal component analysis (PCA) score plot. MS data expressed as mol% of membrane lipids were centered and normalized. Values for 8 independent experiments are shown for control and fructose-fed samples. Dashed lines display 95% confidence regions.

One of the most noteworthy changes can be connected to the CL remodeling system. The level of matured CL showed significant decrease, while monolysocardiolipin (MLCL) level increased significantly, and consequently their ratio increased markedly in the membrane (MLCL/CL, Figure 8a). Furthermore, at the molecular species level, we detected pronounced loss of the most abundant homosymmetric tetra18:2 species CL (72:8) (Figure 8b). This was the most prominent change not only in the context of membrane composition but also when considering absolute values, i.e., the protein-normalized data displayed dramatic 45% decrease for CL (72:8) (from 28.5 to 15.7 nmol/protein mg; $p < 0.05$). The loss in CL (72:8) was paralleled by elevations in practically all other asymmetric species independently on chain length and saturation for the fructose-fed animals as opposed to the normal chow diet (sum elevation from 2.82 to 4.35 mol% of membrane lipids, $p < 0.05$) (Figure 8b). This altogether resulted in a dramatic drop of the CL “symmetry” factor in the fructose group calculated as the ratio of symmetric/asymmetric species (Figure 8c).

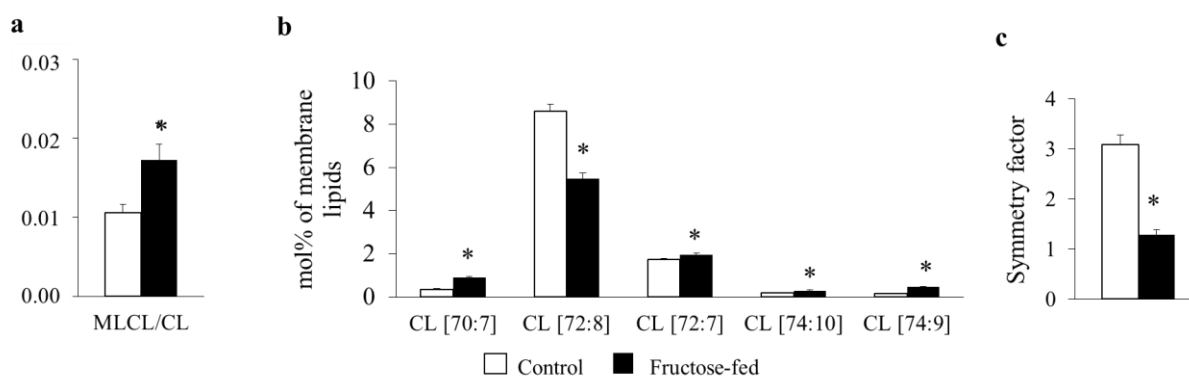


Figure 8. Defects in cardiolipin remodeling. (a) Monolysocardiolipin to cardiolipin ratio (MLCL/CL). (b) Changes in CL species due to fructose feeding. (c) CL symmetry factor calculated as the ratio of symmetric/asymmetric CL species. ESI-MS data are expressed as mol% of membrane lipids or calculated from the corresponding values and presented as means \pm SEM, $n=8$, $*p<0.05$.

It is important to note here that we could not detect oxidized lipid species either in CL or in other highly unsaturated and generally oxidation-prone lipid classes, such as plasmalogen phosphatidylethanolamine and phosphatidylserine. However, we could detect “asymmetry” defects already in the MLCL species profile; the major MLCL (54:6, tri18:2) species was found to be significantly reduced whereas the not only 18:2-containing precursors were markedly elevated.

Another important feature of the lipidome alterations was the general increase in lipid species with sum double bond (db) = 1 that could be detected in all major membrane PL classes in the fructose group as opposed the control animals (sum of db = 1: 9.3 vs. 6.9 mol% of membrane lipids, $p<0.05$). The main contributors, which contain a saturated and a monounsaturated FA leg, were collected in Figure 9a. In parallel with the elevation of species with db = 1, we detected significant depletion in species with db = 2 in fructose-fed animals (sum of db = 2: 7.1 vs. 9.7 mol% of membrane lipids, $p<0.05$); selected species are demonstrated in Figure 9b. Changes in PL molecular species with highly unsaturated acyl chains (db ≥ 4) showed fairly complex picture with several significant alterations including both elevations and decreases.

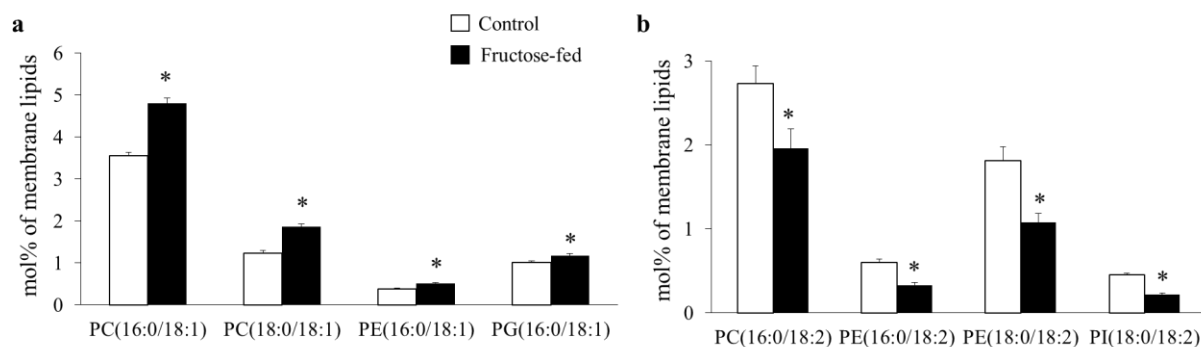


Figure 9. Changes in phospholipid (PL) molecular species with different number of double bonds. (a) Changes in PL species with 1 double bond. (b) Changes in PL species with 2 double bonds. PC: phosphatidylcholine; PE: phosphatidylethanolamine; PG: phosphatidylglycerol; PI: phosphatidylinositol. ESI-MS data are expressed as mol% of membrane lipids or mol% of the specified lipid class and presented as means \pm SEM, $n=8$, $*p<0.05$.

Since we could not detect elevation in serum TG levels due to fructose feeding, it is not surprising that the total cardiac TG content did not change significantly. However, the prominent species profile change of the TG pool is worth mentioning. The robust relative increase in species containing saturated and monounsaturated FAs, such as TG (50:1, 52:2 and 54:3), in parallel with significant reductions in more unsaturated species, e.g., TG (52:4, 54:6 and 56:8) (Figure 10a) altogether led to the decrease of the double bond index (DBI), i.e., increase in saturation for cardiac TG (Figure 10b).

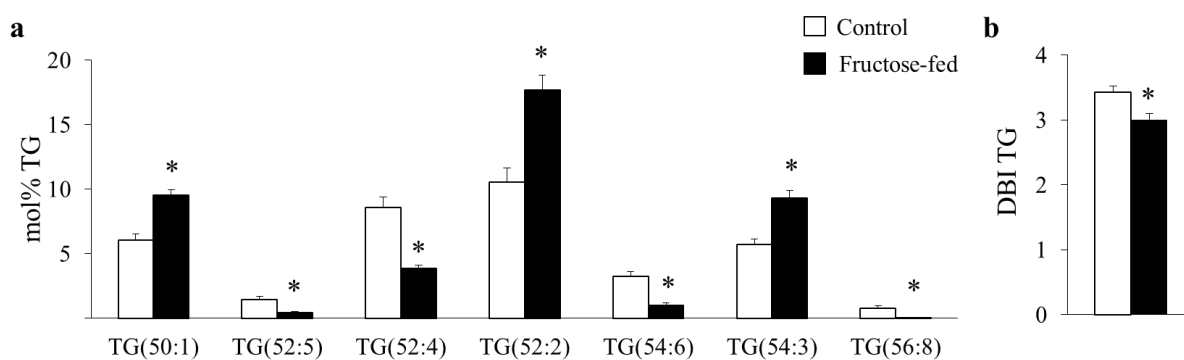


Figure 10. Remarkable species profile change of the cardiac triglyceride (TG) pool due to fructose feeding. (a) Alterations in cardiac TG species profile. (b) The double bond index (DBI) calculated for TG. ESI-MS data are expressed as mol% of membrane lipids or mol% of the specified lipid class and presented as means \pm SEM, $n=8$, $*p<0.05$.

A further interesting aspect of the complex lipidome remodeling was the reshaping of the analyzed sphingolipid (SL) pool, ceramide (Cer) and sphingomyelin (SM). We measured small but significant elevation in total cardiac Cer at membrane lipid compositional level (approximately 30%; $p<0.05$), which could be attributed almost exclusively to the increases in very long-chain Cer-24 species Cer (42:2:2, d18:1/24:1 and 42:3:2, d18:2/24:1) (Figure 11a).

Besides, the total level of SM showed only an increasing tendency in the membrane ($p=0.058$), but its species compositions changed completely (Figure 11b).

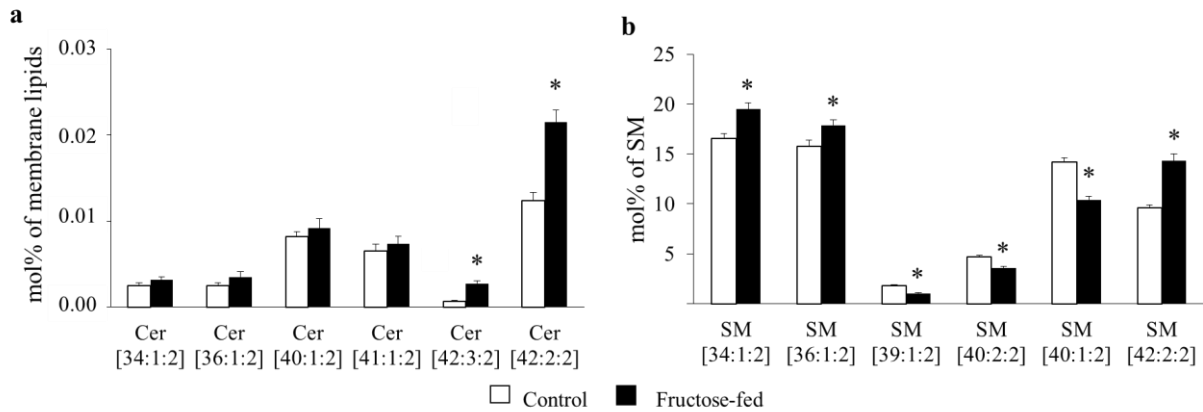


Figure 11. Modulation of the sphingolipid pool. Alterations in (a) ceramide (Cer) and (b) in sphingomyelin (SM) species profile. ESI-MS data are expressed as mol% of membrane lipids or mol% of the specified lipid class and presented as means \pm SEM, $n=8$, $*p<0.05$.

4.1.4. Oxidative stress

In our mild prediabetes model induced by fructose-enriched diet, there was no significant increase in the levels of the peroxidation product MDA in the serum or cardiac tissue, or in the cardiac level of the nitrooxidative marker 3-NT as compared to control values (Table 6).

Table 6. Oxidative stress markers measured in serum and heart tissue in both control and fructose-fed rats. MDA: malondialdehyde, 3-NT: 3-nitrotyrosine. Values are mean \pm SEM, $n=8$.

	control	fructose-fed	p-value
Serum MDA (nmol/mg protein)	4.77 \pm 0.43	4.03 \pm 0.49	0.274
Cardiac MDA (nmol/mg protein)	1.27 \pm 0.16	1.47 \pm 0.22	0.482
3-NT (nmol/mg)	190 \pm 6.0	221 \pm 20	0.164

4.1.5. Apoptosis

Since increased apoptosis often contributes to cardiac dysfunction, in our present study, we also aimed to explore the effect of prediabetes on apoptosis in the heart. We assessed the expression of pro- and antiapoptotic proteins by western blot. Prediabetes did not affect the expression of proapoptotic caspase-7 and BAX in the left ventricles, while the antiapoptotic BCL-2 was downregulated, and thereby, the BAX/BCL-2 ratio was significantly increased in the fructose-fed group (Figure 12).

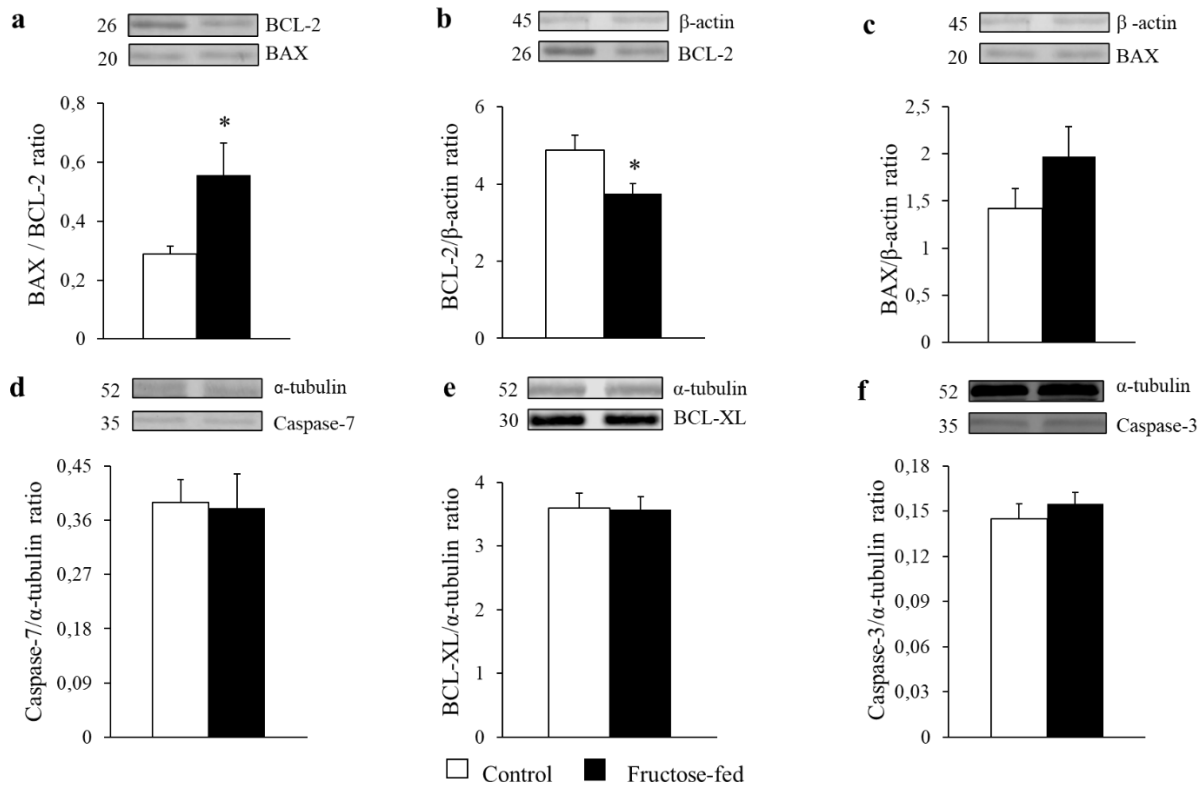


Figure 12. Western blot results at week 24. (a) BAX/BCL-2 ratio, (b) BCL-2/ β -actin ratio, (c) BAX/ β -actin ratio, (d) caspase-7/ α -tubulin ratio, (e) BCL-XL/ α -tubulin ratio and (f) caspase-3/ α -tubulin ratio. Values are means \pm SEM, $n=8$, $*p<0.05$.

4.2. Non-obese genetic model of type 2 diabetes

4.2.1. Metabolic characterization of the GK rats

In order to verify the development of T2DM in male GK rats, concentrations of several serum metabolites were measured at weeks 7, 11 and 15 (Fig. 13). GK rats showed a significantly elevated FBG level at all time points as compared to controls (Fig. 13a). At week 11 and 15, blood glucose level in GK rats was significantly lower as compared to week 7 blood glucose values (Fig. 13a). Parallel with hyperglycemia, serum insulin levels were significantly increased in GK rats compared to Wistar controls at week 7 and more profoundly at week 11 (Fig. 13b). However, there was no significant difference between serum insulin levels measured in GK and control rats at week 15, since serum insulin concentration in GK rats significantly decreased by week 15 as compared to insulin level measured at week 11 (Fig. 13b). HOMA-IR was significantly increased at weeks 7 and 11 in GK rats when compared to controls (Fig. 13c). In contrast, increase of HOMA-IR did not reach the level of statistical significance at week 15 in GK animals (Fig. 13c). Serum cholesterol levels were significantly higher in GK rats as compared to control ones throughout the study duration (Fig. 13d).

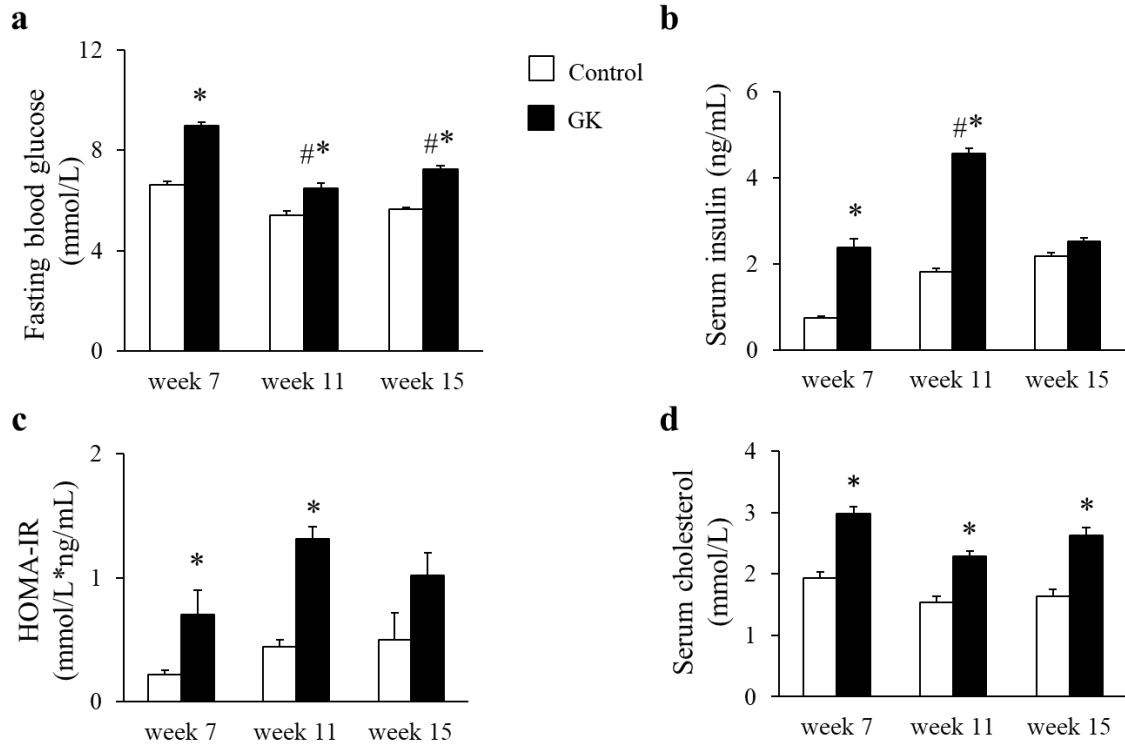


Figure 13. Basic metabolic characteristics of non-obese T2DM. (a) Fasting blood glucose, (b) serum insulin, (c) HOMA-IR index and (d) serum cholesterol levels at weeks 7, 11 and 15 in both control and GK rats. Values are mean \pm SEM, n=7–9, * p <0.05 vs. control within the same time point, # p <0.05 vs. week 7 values.

OGTT was performed at week 15 in order to verify the development of impaired glucose tolerance in GK rats. Glucose levels during OGTT were markedly increased in GK rats in every time point of blood glucose measurements (Fig. 14a). AUC of blood glucose levels during OGTT was significantly increased in GK rats representing impaired glucose tolerance (Fig. 14b). In addition, serum insulin levels in GK rats during OGTT were significantly lower 30 min after glucose loading and became markedly increased 120 min after glucose administration (Fig. 14c). Interestingly, pancreatic insulin levels were 25 % lower in GK rats compared to control ones, however, the values were not significantly different between the two groups (Fig. 14d).

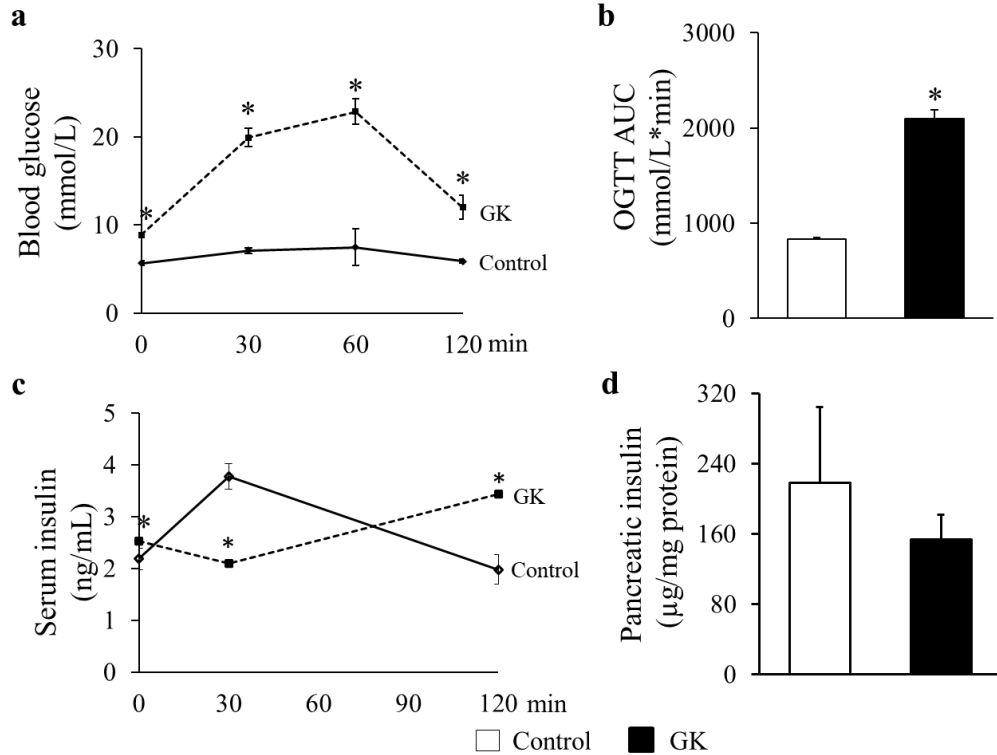


Figure 14. Impaired glucose tolerance and imperfect insulin secretion in non-obese T2DM. (a) Blood glucose levels during OGTT, (b) OGTT AUC, (c) serum insulin levels during OGTT and (d) pancreatic insulin content at week 15 in both control and GK rats. Solid line control; dashed line GK. Values are mean \pm SEM, $n=7-9$, * $p<0.05$.

4.2.2. Body weight, heart weight and CF

Body weight was significantly decreased (Fig.15a), while heart weight and HW/BW were significantly increased at week 15 in GK rats (Fig. 15b, c). Interestingly, CF was significantly increased at week 15 in GK rats as compared to control hearts (Fig. 15d).

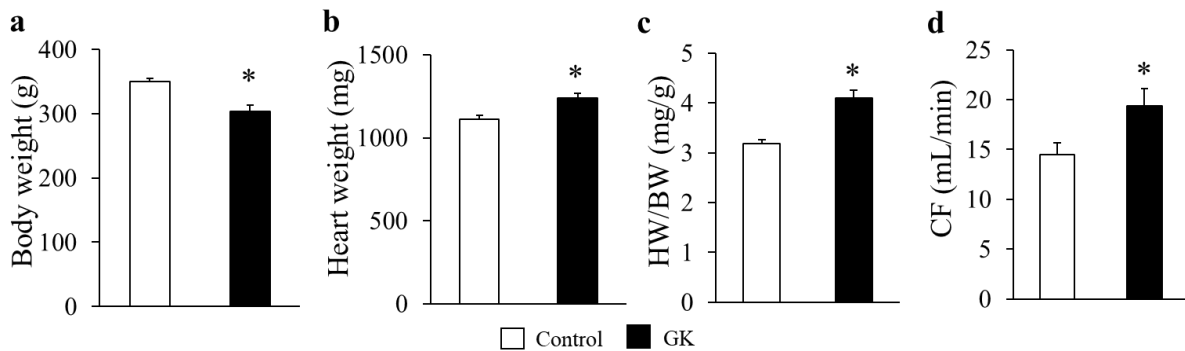


Figure 15. (a) Body weight, (b) heart weight, (c) heart weight to body weight ratio (HW/BW) and (d) coronary flow (CF) at week 15 in both control and GK rats. Values are mean \pm SEM, $n=7-9$, * $p<0.05$.

4.2.3. Cardiac gene expression profile and qRT-PCR in non-obese T2DM

Among the 41,012 genes surveyed, 507 genes whose expression was $> \sim 2.0$ -fold up- or downregulated in hearts of GK rats relative to levels of control rats showed significant change in expression. According to our results, 204 genes showed upregulation and 303 genes showed downregulation in hearts of GK rats. Moreover, 138 genes showed more than threefold change of expression in hearts of GK rats as compared to the levels of control rats. Among these 138 genes, 50 genes were significantly upregulated (Table 7) and 88 genes were significantly downregulated (Table 7) in GK rat hearts. In addition to the listed genes categorized into specific functional groups, there were several other altered genes not categorized into these groups and indicated as yet uncharacterized, predicted genes and fragments [86].

Table 7. Selected up- and downregulated genes (> 3.0 -fold up- or downregulation). In case of every altered genes, $p < 0.05$. FC: fold change.

Upregulated genes						
Gene function	Gene symbol	FC	SD	Gene symbol	FC	SD
Metabolism	<i>Abhd17c</i>	6.96	1.72	<i>Klk1c3</i>	3.79	1.07
	<i>Adh1</i>	5.38	2.78	<i>Akr1b10</i>	3.76	1.05
	<i>Retsat</i>	4.50	3.61	<i>Ampd1</i>	3.06	1.56
	<i>Dgkb</i>	4.21	0.82			
Signal transduction, regulation of transcription	<i>Pla2g7</i>	4.68	0.88	<i>Cd47</i>	3.34	0.51
	<i>Ptpn13</i>	4.38	2.18	<i>Clstn2</i>	3.09	1.41
	<i>Efna2</i>	3.41	0.60	<i>Rnf187</i>	3.06	0.63
	<i>Crym</i>	3.38	0.78			
Receptors, ion channels	<i>Kcne1</i>	6.57	4.07	<i>Chrna7</i>	3.45	0.63
	<i>Atp6v1g2</i>	5.77	2.02	<i>Atp2b2</i>	3.27	0.91
Membrane proteins	<i>Pxmp4</i>	5.73	0.74			
Cell growth and differentiation	<i>Tceal7</i>	3.63	1.88	<i>Jund</i>	3.28	0.60
Immune response	<i>RT1-T18</i>	4.95	2.21	<i>Oas1a</i>	3.94	2.50
Transport	<i>Atp2b2</i>	3.44	0.77	<i>Slc16a7</i>	3.11	0.69

Downregulated genes

Gene function	Gene symbol	FC	SD	Gene symbol	FC	SD
Metabolism	<i>Tgm1</i>	-3.93	1.87	<i>Cpox</i>	-4.98	2.06
	<i>Car6</i>	-4.08	2.61	<i>P4ha3</i>	-5.13	1.68
	<i>Pbld1</i>	-4.41	2.60			
Signal transduction, regulation of transcription	<i>Creb5</i>	-3.07	1.26	<i>Thrsp</i>	-4.86	5.18
	<i>Dyrk3</i>	-3.35	1.95	<i>Crabp2</i>	-4.98	2.42
	<i>Hic1</i>	-3.55	2.10	<i>Akap3</i>	-6.39	1.90
	<i>Arhgef5</i>	-3.89	1.45	<i>Upk1b</i>	-12.89	7.94
Receptors, ion channels	<i>Il22ra2</i>	-3.07	2.78	<i>Ptgfr</i>	-3.65	1.40
	<i>Ntrk3</i>	-3.12	1.18	<i>Slc4a1</i>	-5.23	0.94
	<i>Adra1d</i>	-3.23	1.09	<i>Sln</i>	-8.03	15.41
	<i>Lpar1</i>	-3.55	1.50	<i>Atp6ap1 I</i>	-12.06	3.25
Membrane proteins	<i>Sln</i>	-6.68	7.12			
Structural protein, cell adhesion	<i>Col5a3</i>	-3.43	1.46	<i>Myl7</i>	-10.34	20.29
	<i>Cntnap1</i>	-4.09	1.11	<i>Msln</i>	-22.03	31.18
	<i>Mybphl</i>	-7.08	8.55			
Cell growth and differentiation	<i>Ret</i>	-3.11	1.15	<i>Epyc</i>	-5.14	7.64
	<i>Esm1</i>	-4.85	1.57	<i>Ccng1</i>	-10.29	1.82
	<i>Nnat</i>	-5.06	10.47	<i>Trim16</i>	-80.63	28.07
Immune response	<i>Reg3b</i>	-3.52	5.83	<i>RGD1559482</i>	-5.83	2.19
	<i>Icoslg</i>	-3.79	1.16	<i>Cd1d1</i>	-6.21	2.67
	<i>C4a</i>	-4.77	3.07	<i>Cma1</i>	-15.40	6.26
	<i>Cxcl13</i>	-5.57	4.38			
Transport	<i>Rbp4</i>	-4.27	7.22			
Hormones	<i>Inha</i>	-3.45	1.80			

The descriptions (full names) of gene symbols can be found in the appendix.

The expression change of selected 28 genes was validated by qRT-PCR; 19 of these 28 genes have been confirmed by qRT-PCR (Table 8).

Table 8. Expressional change of selected cardiac genes confirmed by qRT-PCR in non-obese T2DM.

Gene symbol	Gene name	DNA microarray		qRT-PCR	
		AVE (log2)	Fold change	Fold change	SEM
<i>Adipoq</i>	Adiponectin, C1Q and collagen domain containing	-4.99	-31.78	-23.64	0.02
<i>Atp1b4</i>	ATPase, (Na ⁺) /K ⁺ transporting, beta 4 polypeptide	-4.21	-18.51	-4.74	0.05
<i>Car3</i>	Carbonic anhydrase 3	-3.73	-13.27	-7.88	0.03
<i>Cma1</i>	Chymase 1, mast cell	-3.11	-8.63	-5.12	0.02
<i>Arntl</i>	Aryl hydrocarbon receptor nuclear translocator-like	-2.75	-6.74	-2.95	0.03
<i>Tgm1</i>	Transglutaminase 1, K polypeptide	-1.97	-3.92	-4.88	0.03
<i>Nnat</i>	Neuronatin (Nnat), transcript variant 1	-1.87	-3.66	-4.2	0.02
<i>Ddah1</i>	Dimethylarginine dimethylaminohydrolase 1	-1.69	-3.23	-3.36	0.02
<i>Ntrk3</i>	Neurotrophic tyrosine kinase, receptor, type 3	-1.69	-3.23	-2.33	0.06
<i>Dpp4</i>	Dipeptidyl peptidase 4	-1.35	-2.55	-2.11	0.03
<i>Ephx2</i>	Epoxide hydrolase 2, cytoplasmic	-1.33	-2.51	-4.23	0.02
<i>Gpc3</i>	Glypican 3	-1.29	-2.45	-2.54	0.04
<i>Fgf18</i>	Fibroblast growth factor 18	-1.17	-2.25	-2.36	0.03
<i>Sele</i>	Selectin E	1.02	2.03	2.35	0.14
<i>Dbp</i>	D site of albumin promoter (albumin D-box) binding protein	1.06	2.08	2.39	0.17
<i>Ephx1</i>	Epoxide hydrolase 1, microsomal	1.21	2.31	2.24	0.18
<i>Nurp1</i>	Nuclear protein, transcriptional regulator, 1	1.34	2.53	3.29	0.28
<i>Slc16a7</i>	Solute carrier family 16, member 7 (monocarboxylic acid transporter 2)	1.77	3.41	3.21	0.19
<i>Atp2b2</i>	ATPase, C ⁺⁺ transporting, plasma membrane 2	1.88	3.68	3.78	0.21

4.2.4. Gene ontology analysis

In order to further determine the biological significance and functional classification of differentially expressed genes due to non-obese T2DM, GO analysis was performed [52]. Out of the 507 genes significantly altered by non-obese T2DM in our present study, 277 genes with known function were submitted to GO analysis and 115 were clustered into different categories (Table 9). The rest of the 507 genes were either unknown expressed sequence tags or unrecognized by the GO analysis database. The 115 analyzed genes were classified into five main categories such as (1) biological regulation, (2) metabolic process, (3) immune system

process, (4) biological adhesion and (5) rhythmic process. Table 9 contains only the five main GOTERM categories (BP_1), the other genes can be found in the original table [86].

Table 9. Gene ontology analysis. Five main GOTERM (GT) categories.

Category	Term	Count	%	P value	Gene symbol
GT_BP_1	GO:0065007 biological regulation	48	42	0.01	<i>Fgf18, Pdia2, Gbp1, C3, Crabp2, Trim16, Zeb2, Lpar1, Esml, Sgms1, Ccng1, Cd1d1, Aldh1a1, Atp2b2, Cd47, Npas2, Dgkb, Zfp90, Cxcr6, Jund, Per2, Tef, Chrna7, Cntnap1, Traf6, Qsox1, Ddah1, Dpp4, Dpt, Cyr61, Ret, Ncf1, Nucks1, Arhgef5, Prkab2, Loc501307, Arntl, Ptgr, Prkce, Tmem189, Stat3, Fmn1, Trps1, Klre1, Gnb3, Eif2ak2, Icoslg, Bard1</i>
GT_BP_1	GO:0008152 metabolic process	48	42	0.03	<i>Cyp2j4, Ocln, C3, Crabp2, Trim50, Trim16, Lpar1, Sgms1, Aldh1a1, Atp2b2, Ercc8, Mcm8, St6galnac3, Plod2, Zfp90, Cpox, P4ha3, Jund, Per2, Tef, Chrna7, Traf6, Qsox1, Ddah1, Dpp4, Ret, Ncf1, Prkab2, Loc501307, Arntl, Cryz, Tmem189, Lpcat2, Prkce, Wee1, Stat3, Rps7, Oxsm, Fmn1, Taf13, Slc16a7, Akr1b10, Pla2g7, Cma1, Eif2ak2, Car6, Prps2, Bard1</i>
GT_BP_1	GO:0002376 immune system process	10	9	0.05	<i>Cd47, Ncf1, C3, Rt1-T18, Klre1, Chrna7, Traf6, Cd1d1, Ddah1, Dpp4</i>
GT_BP_1	GO:0022610 biological adhesion	7	6	0.09	<i>Cd47, Sdc1, Ret, Cntnap1, Col5a3, Btbd9, Cyr61</i>
GT_BP_1	GO:0048511 rhythmic process	7	6	0.00	<i>Aldh1a1, Npas2, Jund, Per2, Tef, Chrna7, Arntl</i>

The descriptions (full names) of gene symbols can be found in the appendix.

5. DISCUSSION

DM is a metabolic disorder that is considered to be one of the most common pathological conditions in the world. It may be present within all age groups and one of its most severe consequences is heart damage. Similarly to diabetes, the preceding prediabetic state also poses a risk to the heart. It is well-known that CVD are among the most frequent causes of death in addition to cancer. Based on these information and the fact that our knowledge on diabetes and the pathological background of its cardiac complications is still insufficient, the aim of this thesis was to investigate the cardiac effects of prediabetes and non-obese T2DM, a less known but quite important type of DM.

5.1. Diet-induced prediabetes model

We used a chronic, high fructose-fed rat model in order to induce prediabetes and to investigate the effects of this pathological condition on the heart. Our goal was to examine the cardiac effects of a moderate metabolic condition, rather than exploring the consequences of a much more severe state seen for example in genetic DM models (e.g. db/db mice) [103,104].

As previously mentioned, FBG levels measured at given intervals were slightly but significantly higher in fructose-fed rats, and from week 16 the OGTT AUC values were significantly increased as well (Figure 4). Thus, we could verify the development of prediabetic condition with impaired glucose tolerance in this model. In the fructose-fed group, the significantly increased HOMA-IR and pancreatic insulin levels, and the unchanged serum insulin levels demonstrate the emergence of a mild insulin resistance (Figure 4).

In the fructose-fed group, the significantly smaller body weight by the end of the 24-week feeding and accordingly, the decreased weight gain, the increased liver weight to body weight ratio (Table 1) and the macroscopical signs of fatty degeneration on the liver can be connected and interpreted as follows. Our findings may indicate that the cause of fatty degeneration in the liver was DNL initiated by fructose feeding. As it has been demonstrated by Fakhoury-Sayegh et al., fructose may activate DNL due to its fast conversion to pyruvate bypassing the regulatory step of glycolysis [105]. High-fructose diets can affect the metabolism of skeletal muscle through metabolic stress. For example, Gatineau et al. revealed that older rats fed with fructose-containing diet lost significantly more lean body mass and maintained more adipose tissue than control rats [106]. The article also reports that in sucrose-fed rats, significantly lower diet-induced muscle protein synthesis was observed compared to starch-fed rats. Additionally, it has

been shown by Dhar et al. that excessive fructose consumption increases the production of substances like methylglyoxal in the liver, which leads to oxidative stress in the muscle [107]. Activated DNL can result in endoplasmic reticulum stress [108] and production of hepatokines that are known to negatively impact muscle energy metabolism and insulin sensitivity [109]. These results might explain the experienced body weight gain decrease in the fructose-fed rats. In spite of the macroscopic signs of fatty degeneration in the liver, the unaltered serum lipid parameters and liver enzymes suggest an early stage of hepatic consequences in the fructose-fed animals (Table 2).

For the further characterization of metabolic alterations in the liver of fructose-fed rats, qRT-PCR was performed. As mentioned earlier, out of the eight analyzed genes we found significant changes in case of two genes, *Acaca* and *Elovl6* (Figure 5). Increased expression of *Acaca* is responsible for the catalysis of the carboxylation of acetyl-CoA to malonyl-CoA, that is the rate-limiting step of FA synthesis. Besides, the expression of *Fasn*, which catalyses the remaining steps of palmitic acid synthesis, showed a tendency of increase ($p=0.205$). These findings are consistent with previous results and definitely indicate increased DNL in fructose-fed rats [110,111]. *Elovl6* enzyme - the expression of which showed significant increase in fructose-fed animals as well - catalyzes the first and rate-limiting reaction of long-chain FA elongation cycle. It has been reported that *Elovl6* plays an important role also in nonalcoholic fatty liver disease (NAFLD) and steatohepatitis [112,113].

Taken together, we successfully induced prediabetes by fructose feeding and observed impaired glucose tolerance and mild insulin resistance. Besides, based on literature data, we assume that fructose-rich diet led to DNL in the rats contributing to decreased weight gain. The presence of DNL was confirmed by investigation of genes associated with the metabolic process by qPCR technique.

To follow-up the alterations caused by prediabetes, our study was continued by the examination of the heart both functionally and morphologically. Transthoracic echocardiographic data showed only a few changes in case of the fructose-fed animals, notably the significantly increased anterior wall thickness in systole and the significantly smaller E/A ratio (Table 3). These findings might suggest a very early sign of a mild hypertrophy and diastolic dysfunction with preserved systolic function due to chronic high-fructose diet. However, the heart weight and HW/BW were not changed significantly (Table 1) in our study. Therefore, in order to assess cardiac hypertrophy at the molecular level, we measured the mRNA expression of *Myh6* and *Myh7*. We found elevated cardiac *Myh6* mRNA level along

with unchanged *Myh6/Myh7* ratio (Table 5), that indicates the lack of hypertrophy according to the literature [114–116]. As for the other examination method, working heart perfusion, we observed that LVEDP significantly increased, while cardiac output significantly decreased in fructose-fed rats (Figure 6). However, the rest of the measured parameters remained unchanged between groups, indicating the appearance of a mild diastolic dysfunction in prediabetic rats (Table 4). It is widely known that LV hypertrophy is more common in diabetic patients and that 40-75% of people suffering from T1DM or T2DM have diastolic dysfunction [117,118]. However, here we demonstrate that at this early stage of prediabetes cardiac hypertrophy has not developed yet, but the impairment of diastolic function occurs much earlier than the development of overt diabetes. These findings are consistent with recent reports showing that the development of diastolic dysfunction can precede complete diabetes [10]. Furthermore, the clinical laboratory markers of myocardial injury (CK, CK-MB and LDH) did not change significantly in fructose-fed rats compared to controls, indicating the appearance of cardiac dysfunction prior to severe structural/cellular damage. (Table 2).

Since presumably there was DNL in the liver of the fructose-fed rats, we were curious whether DNL was present in the heart of the animals as well. For this purpose, lipidomic analysis was performed from LV whole membrane extracts. The reason we investigated membrane lipid composition is that the optimal physical state of the membrane is a prerequisite for proper functioning. One of the most notable changes can be connected to the CL remodeling system. It is acknowledged that under normal circumstances, the levels of lysophospholipids (LPL) are kept low and CL remodeling requires only trace amounts of MLCL [28]. Therefore, the significantly decreased level of matured CL in parallel with the significantly increased level of MLCL, and consequently their markedly increased ratio in the membrane clearly report about an abnormal remodeling process in the fructose-fed group (Figure 8a). Another remarkable alteration occurred at the molecular species level is the pronounced loss of the most abundant homosymmetric tetra18:2 species CL (72:8) (Figure 8b). This finding is in consistence with other literature data obtained from either more severe obesity and diabetic models [119,120] or from a more similar early-stage fructose-induced T2DM study [121]. The decrease in CL (72:8) was accompanied by an increase in the other asymmetric species (Figure 8b) and these alterations altogether led to a marked drop of the CL „symmetry” factor in the prediabetic group (Figure 8c). The major contributions to the increase in asymmetry derived from species which contain one non-18:2 acyl chain, i.e., from the 16:1 FA-containing CL (70:7; 16:1_18:2_18:2_18:2) species, from the CL (74:9) species whose major component is the CL

(18:2_18:2_18:2_20:3) isobar, and from the CL (72:7) species corresponding to CL (18:1_18:2_18:2_18:2). This is in line with the result seen in a fructose-induced early T2DM rat model [121], but differs from more serious mouse models of diabetes and obesity/insulin resistance. In the latter cases, impaired cardiac CL remodeling led to the depletion of 16:1 and enrichment of the highly unsaturated docosahexaenoic acid (DHA, 22:6 n-3) [120,122], thereby considerably increasing the propensity of CL to peroxidation. As mentioned previously, it should be highlighted that although in our study there were no oxidized lipid species detected at all, we were able to detect „asymmetry” deficiencies already in the MLCL species profile.

Another notable feature of the lipidome alterations in the fructose-fed group was the general rise in lipid species with sum db=1 (Figure 9a), while PL species with db=2 showed significant depletion (Figure 9b). The latter lipids mostly contained a saturated FA in *sn1* and a linoleoyl (18:2) group in *sn2* position of the glycerol backbone; these can function as potential acyl donors for the formation of tetra 18:2 CL for the transacylation reaction catalysed by tafazzin enzyme. As for PL molecular species with highly unsaturated acyl chains (db \geq 4), several significant alterations - increases and decreases as well - were seen. According to the reports of Kiebish et al. [123], the loss of tafazzin enzymatic activity in a Barth syndrome mouse model also caused complex changes of polyunsaturated PL species. Therefore, we can suggest that the intricate imbalance in polyunsaturated PL species modifies the biophysical and signaling properties of the cardiac membrane.

As mentioned earlier, the total cardiac TG content did not show significant alteration due to fructose feeding, however, there was a great species profile change at the TG pool, namely the increase in species containing saturated and monounsaturated FAs and decrease in more unsaturated species (Figure 10a). As a consequence of these alterations, the DBI decreased (Figure 10b), i.e., cardiac TG saturation increased, which together with the monoene rise and 18:2 reduction in membrane PLs might indicate the upregulation of DNL causing a shift in FA profile towards the augmentation of monounsaturated 18:1 (and 16:1) FAs.

As the last notable aspect of the complex lipidome remodeling, we have to mention the reshaping of Cer and SM. Cer has a central role in SL metabolism as it functions as a lipid mediator of the eukaryotic stress response. Its role is mainly associated with growth inhibition; the most investigated being its function as a proapoptotic molecule [124]. Serum Cers can serve as potential biomarkers of insulin resistance, diabetes and heart disease, besides, muscle, liver and adipose tissue Cers were reported to be associated with insulin resistance [125]. In our work, a small but significant elevation occurred in total cardiac Cer at membrane lipid compositional level due to mainly the elevation in very long chain Cer-24 species (Figure 11a).

It was revealed that the length of the acyl chain in Cers affects their contribution to diseases. Long chain Cer-16 and Cer-18 often indicated greater associations with disease pathologies than very long chain Cer-24 [125]. It was showed by Marchesini et al. that in confluent Michigan Cancer Foundation-7 (MCF-7) cells C-24 Cer species influenced cell cycle arrest, but not apoptosis [126]. From these findings we assume that in our model the alterations in Cer led to the observed pathologic cardiac function by changing the membrane biophysical properties rather than triggering apoptosis. SM is considered as the major structural mammalian SL which accumulates in liquid-ordered microdomains. Its total level showed only an increasing tendency ($p=0.058$), while its species compositions changed entirely (Figure 11b). These data suggest microdomain reorganization and thus the modulation of the membrane physical state and signaling properties as a result of chronic high-fructose diet.

Reviewing our lipidomic findings, we can state that the disturbance in tafazzin action in prediabetic state is the first event leading to inaccurate CL structural uniformity and molecular symmetry. Nevertheless, there are numerous other potential contributors to be mentioned, such as the induction of phospholipase A2 [127], the upregulation of the acyl-CoA: lyso -CL-acyltransferase [128] or the downregulation of MLCL acyltransferase [129] - although these possibilities apply to more severe conditions of later stage diabetes or advanced oxidative stress induced by hyperthyroidism.

As oxidative stress has a principal role in the development of DCM [25] and oxidative stress has been linked to the impairment of cardiac function [89,130], we continued our study by the measurement of this factor. Although in a prediabetic study - in which prediabetes was induced by high-fat diet combined with a single low-dose STZ [10] - the authors reported about increased hydrogen peroxide production, increased NT formation and decreased cardiac function, in our case, there was no significant elevation in the levels of MDA and 3-NT as compared to the control values (Table 6), and we could not detect any oxidized lipid species. It is important to emphasize that in our model, we could see several significant alterations in the cardiac lipidome before the development of any changes of oxidative stress markers.

The last probable aspect we examined which might be related to cardiac dysfunction is apoptosis. Regarding our western blot results, prediabetes had no effect on the expression of proapoptotic caspase-7 and BAX, while the antiapoptotic BCL-2 was downregulated, meaning that the BAX/BCL-2 ratio was significantly elevated due to the high-fructose diet (Figure 12). Similar to our results, a moderate decrease in BCL-2 was shown in another model of prediabetes induced by a combination of high-fat diet and low-dose STZ injection [10]. Our data suggest

early dysregulation of antiapoptotic proteins in prediabetic state. However, these alterations are not remarkable enough for taking apoptosis into consideration as an essential factor in prediabetes.

5.2. Non-obese genetic model of type 2 diabetes

A further goal of this thesis was to investigate how non-obese T2DM influences cardiac gene expression pattern. The model we chose was the spontaneously diabetic GK rat, which is a recognized animal model of the disease and - as for the pathomechanism - considered to be very similar to the non-obese T2DM in humans. Our results include metabolic characterization of non-obese diabetes and the analysis of various, classified cardiac genes which had shown statistically significant changes at the transcript level compared to Wistar controls.

As it was reported by Östenson and Movassat [56,59], the abnormal glucose regulation in the GK rat develops in association with imperfect insulin secretion and also with insulin resistance. At the onset of T2DM, beta cells try to release more insulin in order to cope with insulin resistance. Unfortunately, over time this compensatory mechanism becomes insufficient to maintain normal blood glucose level and in the end leads to the functional exhaustion of the beta cells. These stages can also be traced in the GK model used in our study. Blood glucose levels were significantly higher in GK rats at each time of measurement as compared to controls and we observed significant difference in blood glucose levels in GK rats between the different time points (Figure 13a). At week 11 and 15, the blood glucose level of GK rats was significantly lower compared to the value measured at week 7 (Figure 13a). Furthermore, serum insulin level was significantly elevated at week 11 in GK animals compared to week 7 values (Figure 13b). This outstandingly high insulin value could explain the low blood glucose value found at week 11. Serum insulin levels along with HOMA-IR were significantly increased at week 7 and 11 indicating rising insulin resistance and compensative hyperinsulinemia (Figure 13 b, c). At week 15, we could not observe significant difference in serum insulin levels between GK and control rats (Figure 13b). Nevertheless, the pancreatic insulin level of GK animals was moderately decreased referring to the exhaustion of beta cells (Figure 14d). This may explain the lack of statistical significance in HOMA-IR in GK rats compared to controls at week 15 (Figure 13c). It must be noted that these findings are in accordance with literature data demonstrating that beta cell mass along with insulin production continuously decreases from birth to adulthood in GK animals as a result of defective beta cell neogenesis, chronic islet inflammation, fibrosis and angiopathy [59].

At week 15, body weight was significantly decreased in GK animals proving a non-obese phenotype of T2DM (Figure 15a). Moreover, heart weight and HW/BW were significantly elevated at week 15 in GK rats implying the development of cardiac hypertrophy due to chronic T2DM (Figure 15 b, c). As a further confirmation of increased cardiac size, we found that the CF was significantly higher in GK rats at week 15 as compared to the values measured in the control animals (Figure 15d). These findings proving the presence of cardiac hypertrophy indicate the development of DCM in the heart of GK rats.

Surprisingly, there are only a few studies where qPCR technique was performed in order to investigate the gene expression changes involved in the development of impaired cardiac morphology/function in GK rats [44,47,131]. Therefore, this study can be considered the first to characterize overall alterations in the cardiac transcriptome in male GK rats. These significantly altered genes are classified here into such categories as metabolism, signal transduction, membrane and structural proteins, immune response, etc. Besides, several other genes with unknown function in the heart were also changed in response to diabetes - the definite role of these genes in DM need to be explored in the future.

In the following part, some genes related to **DCM** showing significantly altered expression, selected from the previously classified specific clusters, will be discussed.

In our present study, we have shown altered expression of numerous genes being a factor in the structure formation of the myocardium and possibly connected with DCM, based on the previously described GO analysis. The genes with altered expression include for instance downregulation of collagen, type V, alpha 3 (*Col5a3*) and myosin, light chain 7, regulatory (*Myl7*). Extracellular matrix (ECM) component collagen V is expressed as $\alpha 1(V)2 \alpha 2(V)$ heterotrimers, which regulate collagen fibril geometry and strength in different tissues, especially regarding the pancreas and skeletal muscle. As an interesting finding reported by Huang et al. [132], skeletal muscle of *Col5a3*^{-/-} mice was defective in glucose uptake and mobilization of intracellular GLUT-4 glucose transporter to the plasma membrane in response to insulin, resulted in glucose intolerance, insulin resistance and hyperglycemia. In addition, decreased expression of the genes playing a part in contractility such as *Myl7* [133] could cause sarcomeric dysfunction and DCM.

Another group of genes - which showed altered expression due to T2DM - function as receptors and ion channels and these genes might contribute to the development of DCM. These genes are the following: e.g. downregulation of adrenoceptor alpha 1d (*Adra1d*) and sarcolipin (*Sln*). The downregulation of *Adra1d* receptor subtype has been shown earlier in connection

with cardiac hypertrophy [134] and in STZ-induced DM by our research group [53]. The increased formation of glycation end products and reactive oxygen species can contribute to the inactivation of neuronal nicotinic acetylcholine receptors, resulting in impaired synaptic transmission in sympathetic ganglia and thus autonomic failure [135]. Autonomic failure is a serious complication of DM and can result in cardiovascular aberrations. Sarcoplipin is a central regulator of SERCA and mediator of β -adrenergic responses [136]. It has been demonstrated that *Sln*^{-/-} mice are tend to develop atrial arrhythmias and interstitial fibrosis as a result of altered expression of genes encoding collagen [136]. The abnormal function of *Sln* leads to elevated SERCA activity, resulting aberrant intracellular Ca²⁺ handling and atrial remodeling with dysfunction [136,137].

A main cluster of significantly changed cardiac genes induced by non-obese T2DM was closely related to signal transduction, regulation of transcription and biological processes (for example downregulation of dipeptidyl peptidase 4 (*Dpp4*); signal transducer and activator of transcription 3 (acute-phase response factor) (*Stat3*); ret proto-oncogene transcript variant 1 (*Ret*); neurotrophic tyrosine kinase, receptor, type 3 (*Ntrk3*) and upregulation of Jun D proto-oncogene (*Jund*), etc.). Dipeptidyl peptidase 4 is an integral membrane glycoprotein. It cleaves N-terminal dipeptides from peptides, which are bioactive molecules and regulate the cardiovascular system. There are contradictory literature data about *Dpp4* inhibitors: in most of the preclinical and clinical studies in T2DM, they have been reported to be cardioprotective [138], but in other studies they are related to heart failure [139], cardiac hypertrophy, impairment of cardiac function and dysregulated expression of proteins controlling inflammation and cardiac fibrosis [140]. In our present work, we saw the downregulation of *Dpp4*, which indicates that it may not be a dominant contributor in the development of DCM in non-obese T2DM. The transcription factor *Stat3* takes part in several physiological processes such as proliferation, apoptosis and cardiac survival particularly during myocardial ischemia/reperfusion injury, although its role is contradictory in these processes [141,142]. Large number of studies have reported that cardiac *Stat3* expression was reduced in DM, potentially resulting cardiac dysfunction [143,144]. Other literature data, on the other hand, demonstrated that cardiac *Stat3* expression was increased in DM, inducing hypertrophy [145,146]. In our present work, *Stat3* was downregulated as assessed by microarray, however, qRT-PCR did not confirm this result. It is conceivable that the expression of *Stat3* depends on the duration of diabetes and the stage of DCM. Unexpectedly, downregulation of *Tef* and *Ret*, and upregulation of *Jund* has not been associated formerly with DCM. *Jund* regulates genes involved in antioxidant defense mechanisms and hydrogen peroxide production, along with

angiogenesis by controlling vascular endothelial growth factor (VEGF) transcription [147]. Another major function of *JunD* is the modulation of insulin/insulin-like growth factor 1 signaling and longevity [147]. Furthermore, the downregulation of *Ntrk3* may also have a role in the development of DCM based on literature data. As an example, mutations of *Ntrk3* gene have been proven in the development of human congenital heart diseases [148].

After discussing genes regarding DCM, there is another important group of genes to mention in which we saw significantly altered expression in response to non-obese T2DM. These cardiac genes are related to immune and antimicrobial response (e. g. downregulation of complement component 3 (*C3*); complement component 4a (*C4a*); chemokine (C-X-C motif) ligand 13 (*Cxcl13*); chymase 1, mast cell (*Cma1*) and upregulation of chemokine (C-X-C motif) receptor 6 (*Cxcr6*) and killer cell lectin-like receptor, family E, member 1 (*Klre1*), etc.). The altered expression of these genes is in line with the notorious increased susceptibility to infections in diabetes [149,150].

Finally, there were several novel genes with altered expression in this study which have not been previously related to diabetic changes in the heart (for instance downregulation of mesothelin (*Msln*) and upregulation of kallikrein 1-related peptidase C3 (*Klk1c3*), etc.). Some other altered genes were not categorized into specific functional groups or indicated as yet uncharacterized, predicted genes and fragments (e.g. upregulation of hydroxyacyl glutathione hydrolase-like and Similar to hepatic leukemia factor (*LOC690286*) or downregulation of uncharacterized *LOC102546816* and similar to protein C17orf72, etc.), which might have important roles in diabetes.

It is to be noted that due to the limited space in the dissertation, only the genes that showed more than threefold change of expression in the hearts of GK rats as compared to the levels of controls are discussed here. However, there were several genes whose expression was only 2 to 3-fold up- or downregulated, but still might have a role in the development of DCM. These altered genes include for instance ADAM metallopeptidase domain 33 (*Adam33*); troponin I type 1 (skeletal, slow) (*Tnni1*); myosin light chain kinase 2 (*Mylk2*); cholinergic receptor, nicotinic, gamma (muscle) (*Chrng*); cholinergic receptor, nicotinic, alpha 1 (muscle) (*Chrna1*); neurotrophic tyrosine kinase, receptor, type 2 (*Ntrk2*); chemokine (C-C motif) ligand 12 (*Ccl12*); chemokine (C-X-C motif) ligand 14 (*Cxcl14*) and low density lipoprotein receptor-related protein 8, apolipoprotein E receptor (*Lrp8*), which were downregulated and epsin 3 (*Epn3*) which was upregulated in our study. The function of the above mentioned genes and

their possible role in the development of DCM are discussed in the following article of our research group [86].

5.3. Conclusion

In summary, we can state that the designed comprehensive analysis of alterations in the heart caused by prediabetes and non-obese T2DM was performed successfully. In rats chronically fed a high-fructose diet we found an early stage of prediabetes that was associated with deteriorated cardiac function and the total reshaping of the myocardial lipidome - especially CL pool. It is very important to highlight that cardiac lipidomic alterations preceded the development of sizeable hypertrophy, apoptosis and oxidative stress in the heart. The most important alterations in the lipidome potentially related to impaired cardiac function are monoenoic FA enrichment, decrease in linoleic acid (18:2 FA), complex changes in heavily polyunsaturated lipids and reprofiling of SL species compositions.

In our other study, we have demonstrated for the first time that non-obese T2DM can be connected to a thorough alteration of the transcriptome in the heart of GK rats, represented by numerous up- and downregulated genes in connection with the disease. These altered genes play a role for instance in metabolism, signal transduction, cell growth and differentiation, or function as receptors and membrane or transport proteins. Nevertheless, future studies are necessary to investigate the precise role of these specific genes in the development of cardiac consequences (i.e. DCM) of non-obese T2DM.

It is crucial to emphasize that both prediabetic and non-obese type 2 diabetic states represent a high risk for developing CVD, which may lead to death in a worryingly high proportion. As for prediabetes, it is to be highlighted that there are no clinically attainable signs to clearly declare a disease as the serum parameters investigated in general do not report about hyperglycemia, lipotoxicity or cell damage. So one can say that the risk for progression of CVD and diabetes is silently present in the guise of a complex lipidome reshaping in the heart. Prediabetes can be considered reversible, thus the transition from this less severe and transient state to the more dangerous diabetic condition will not take place for sure. As our results indicate, carbohydrate-rich imbalanced diet must last for a remarkably long time to induce the transformation from the seemingly harmless prediabetes to T2DM. As for non-obese T2DM, it was previously mentioned that similarly to obese diabetes, the non-obese one also carries a high risk of CVD [45]. So both prediabetes and non-obese T2DM can be considered as insidious diseases, since it is quite difficult to recognize prediabetes and it often happens that by the time

it is recognized it had already developed into diabetes. On the other hand, most diabetic patients are obese, and the vast majority of non-obese diabetic people are suffering from T1DM, not T2DM, so similarly to prediabetes, the recognition of non-obese T2DM can be difficult in the absence of visible signs of metabolic disturbances, i.e. obesity. To be able to identify these pathological conditions sooner, one possible option would be the measurement of blood glucose level of the patients regularly. Unfortunately most people are afraid of visiting doctors, yet they could help them to diagnose diseases in time. In my opinion, general practitioners should recommend their patients to check their blood glucose levels two or three times a year by a user-friendly blood glucose meter. Although this may not be enough for a precise diagnosis on its own, it can be a good basis to discuss some further potential steps.

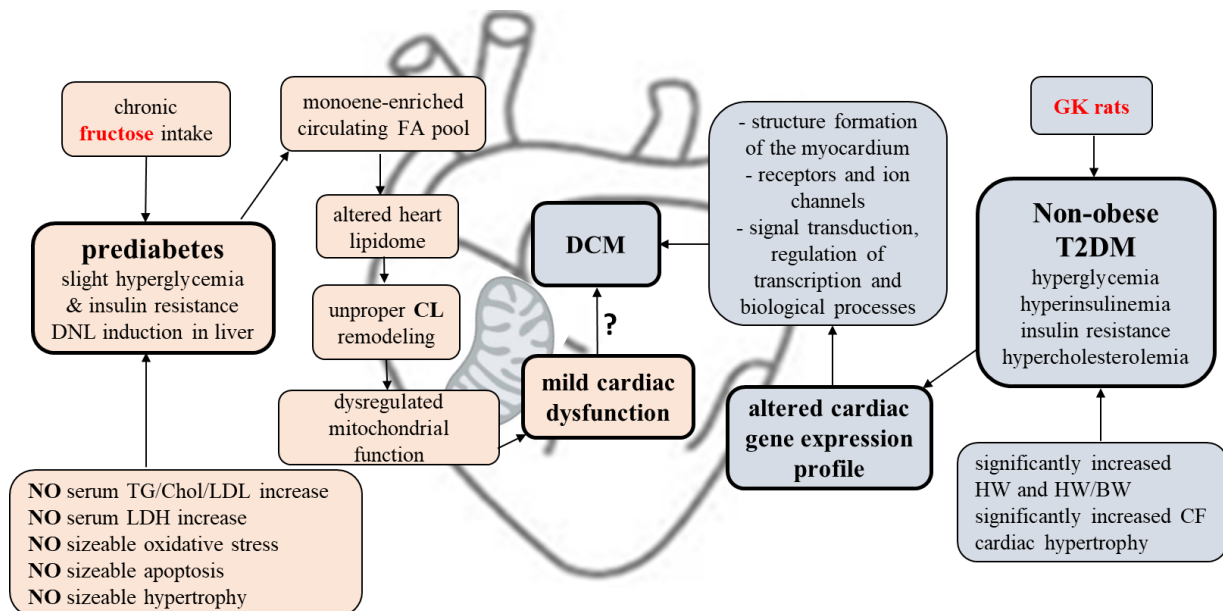


Figure 16. Summary of our findings. CL: cardiolipin, DCM: diabetic cardiomyopathy, GK: Goto-Kakizaki, T2DM: type 2 diabetes mellitus, BW: body weight, HW: heart weight, CF: coronary flow.

ACKNOWLEDGEMENTS

Our studies were supported by the grants GINOP 2.3.2-15-2016-00006, EFOP 3.6.2-16-2017-00006, OTKA-NKFIH (K115990) and 20391 3/2018/FEKUSTRAT. Furthermore, our work was also supported by the Ányos Jedlik program (MED_FOOD TECH_08-A1-2008-0275) and the Gábor Baross program (DA_TECH_07-METABBET).

First of all, I would like to thank Professor Dr. László Dux for allowing me to work at the Institute of Biochemistry.

I would like to express my gratitude to my supervisor, Dr. Tamás Csont for his helpfulness, support, enthusiasm, patience and kindness all over my studies.

I owe a debt of gratitude to all my colleagues for their help, ideas, support and encouragement.

I owe a special gratitude to my colleague in our research group, Dr. Gergő Szűcs for his enormous help and advice. I could always count on him, and I learned a lot from him.

I would like to thank our cooperation partners, Dr. Mária Péter, Dr. Gábor Balogh and Dr. László Vígh, for their great contribution to my thesis by performing lipidomic measurements and analyzing lipidomic data. Furthermore, I am grateful to Andrea Siska and Imre Földesi for their help in analysing various serum parameters.

I would like to thank to my love, Gábor Apjok for his constant support, attention, help, encouragement and love all over the years I have spent in the Institute of Biochemistry.

Last but not least, I would like to express my gratitude to my loving family and friends.

REFERENCES

- [1] Mayfield J. Diagnosis and classification of diabetes mellitus: new criteria. *Am Fam Physician* 1998;58:1355–62, 1369–70.
- [2] American Diabetes Association. Diagnosis and classification of diabetes mellitus. *Diabetes Care* 2013;36 Suppl 1:S67-74. <https://doi.org/10.2337/dc13-S067>.
- [3] Barr ELM, Zimmet PZ, Welborn TA, Jolley D, Magliano DJ, Dunstan DW, et al. Risk of cardiovascular and all-cause mortality in individuals with diabetes mellitus, impaired fasting glucose, and impaired glucose tolerance: the Australian Diabetes, Obesity, and Lifestyle Study (AusDiab). *Circulation* 2007;116:151–7. <https://doi.org/10.1161/CIRCULATIONAHA.106.685628>.
- [4] World Health Organization. Diabetes n.d. <https://www.who.int/westernpacific/health-topics/diabetes> (accessed November 29, 2021).
- [5] Gluxus Health M. Diabetes: You are NOT alone. General Diabetes Statistics. Gluxus Health - Comf 2018. <https://www.gluxus.com/jd-stats/> (accessed November 4, 2021).
- [6] American Diabetes Association. Standards of medical care in diabetes--2014. *Diabetes Care* 2014;37 Suppl 1:S14-80. <https://doi.org/10.2337/dc14-S014>.
- [7] Nichols GA, Hillier TA, Erbey JR, Brown JB. Congestive heart failure in type 2 diabetes: prevalence, incidence, and risk factors. *Diabetes Care* 2001;24:1614–9. <https://doi.org/10.2337/diacare.24.9.1614>.
- [8] Dei Cas A, Khan SS, Butler J, Mentz RJ, Bonow RO, Avogaro A, et al. Impact of diabetes on epidemiology, treatment, and outcomes of patients with heart failure. *JACC Heart Fail* 2015;3:136–45. <https://doi.org/10.1016/j.jchf.2014.08.004>.
- [9] American Diabetes Association. 2. Classification and Diagnosis of Diabetes: Standards of Medical Care in Diabetes-2019. *Diabetes Care* 2019;42:S13–28. <https://doi.org/10.2337/dc19-S002>.
- [10] Koncsos G, Varga ZV, Baranyai T, Boengler K, Rohrbach S, Li L, et al. Diastolic dysfunction in prediabetic male rats: Role of mitochondrial oxidative stress. *Am J Physiol Heart Circ Physiol* 2016;311:H927–43. <https://doi.org/10.1152/ajpheart.00049.2016>.
- [11] Tabák AG, Jokela M, Akbaraly TN, Brunner EJ, Kivimäki M, Witte DR. Trajectories of glycaemia, insulin sensitivity, and insulin secretion before diagnosis of type 2 diabetes: an analysis from the Whitehall II study. *Lancet Lond Engl* 2009;373:2215–21. [https://doi.org/10.1016/S0140-6736\(09\)60619-X](https://doi.org/10.1016/S0140-6736(09)60619-X).
- [12] Nolan CJ, Damm P, Prentki M. Type 2 diabetes across generations: from pathophysiology to prevention and management. *Lancet Lond Engl* 2011;378:169–81. [https://doi.org/10.1016/S0140-6736\(11\)60614-4](https://doi.org/10.1016/S0140-6736(11)60614-4).
- [13] Blüher M. The distinction of metabolically “healthy” from “unhealthy” obese individuals. *Curr Opin Lipidol* 2010;21:38–43. <https://doi.org/10.1097/MOL.0b013e3283346ccc>.
- [14] Diabetes Genetics Initiative of Broad Institute of Harvard and MIT, Lund University, and Novartis Institutes of BioMedical Research, Saxena R, Voight BF, Lyssenko V, Burt NP, de Bakker PIW, et al. Genome-wide association analysis identifies loci for type 2 diabetes and triglyceride levels. *Science* 2007;316:1331–6. <https://doi.org/10.1126/science.1142358>.
- [15] Huang Y, Cai X, Mai W, Li M, Hu Y. Association between prediabetes and risk of cardiovascular disease and all cause mortality: systematic review and meta-analysis. *BMJ* 2016;355:i5953. <https://doi.org/10.1136/bmj.i5953>.
- [16] Nasr G, Sliem H. Silent myocardial ischemia in prediabetics in relation to insulin resistance. *J Cardiovasc Dis Res* 2010;1:116–21. <https://doi.org/10.4103/0975-3583.70903>.
- [17] Zand A, Ibrahim K, Patham B. Prediabetes: Why Should We Care? *Methodist DeBakey Cardiovasc J* 2018;14:289–97. <https://doi.org/10.14797/mdcj-14-4-289>.
- [18] Isordia-Salas I, Galván-Plata ME, Leaños-Miranda A, Aguilar-Sosa E, Anaya-Gómez F, Majluf-Cruz A, et al. Proinflammatory and prothrombotic state in subjects with different glucose tolerance status before cardiovascular disease. *J Diabetes Res* 2014;2014:631902. <https://doi.org/10.1155/2014/631902>.

- [19] Bembde AS. A study of plasma fibrinogen level in type-2 diabetes mellitus and its relation to glycemic control. *Indian J Hematol Blood Transfus Off J Indian Soc Hematol Blood Transfus* 2012;28:105–8. <https://doi.org/10.1007/s12288-011-0116-9>.
- [20] Di Pino A, Mangiafico S, Urbano F, Scicali R, Scandura S, D'Agate V, et al. HbA1c Identifies Subjects With Prediabetes and Subclinical Left Ventricular Diastolic Dysfunction. *J Clin Endocrinol Metab* 2017;102:3756–64. <https://doi.org/10.1210/jc.2017-00954>.
- [21] Gudul NE, Karabag T, Sayin MR, Bayraktaroglu T, Aydin M. Atrial conduction times and left atrial mechanical functions and their relation with diastolic function in prediabetic patients. *Korean J Intern Med* 2017;32:286–94. <https://doi.org/10.3904/kjim.2014.380>.
- [22] Shao CH, Capek HL, Patel KP, Wang M, Tang K, DeSouza C, et al. Carbonylation contributes to SERCA2a activity loss and diastolic dysfunction in a rat model of type 1 diabetes. *Diabetes* 2011;60:947–59. <https://doi.org/10.2337/db10-1145>.
- [23] Huynh K, Kiriazis H, Du X-J, Love JE, Jandeleit-Dahm KA, Forbes JM, et al. Coenzyme Q10 attenuates diastolic dysfunction, cardiomyocyte hypertrophy and cardiac fibrosis in the db/db mouse model of type 2 diabetes. *Diabetologia* 2012;55:1544–53. <https://doi.org/10.1007/s00125-012-2495-3>.
- [24] Katare RG, Caporali A, Oikawa A, Meloni M, Emanuelli C, Madeddu P. Vitamin B1 analog benfotiamine prevents diabetes-induced diastolic dysfunction and heart failure through Akt/Pim-1-mediated survival pathway. *Circ Heart Fail* 2010;3:294–305. <https://doi.org/10.1161/CIRCHEARTFAILURE.109.903450>.
- [25] Boudina S, Abel ED. Diabetic cardiomyopathy, causes and effects. *Rev Endocr Metab Disord* 2010;11:31–9. <https://doi.org/10.1007/s11154-010-9131-7>.
- [26] Duncan JG. Mitochondrial dysfunction in diabetic cardiomyopathy. *Biochim Biophys Acta* 2011;1813:1351–9. <https://doi.org/10.1016/j.bbamcr.2011.01.014>.
- [27] Cai L, Kang YJ. Cell death and diabetic cardiomyopathy. *Cardiovasc Toxicol* 2003;3:219–28. <https://doi.org/10.1385/ct.3:3:219>.
- [28] Schlame M, Ren M. The role of cardiolipin in the structural organization of mitochondrial membranes. *Biochim Biophys Acta* 2009;1788:2080–3. <https://doi.org/10.1016/j.bbamem.2009.04.019>.
- [29] Szűcs G, Sója A, Péter M, Sárközy M, Bruszel B, Siska A, et al. Prediabetes Induced by Fructose-Enriched Diet Influences Cardiac Lipidome and Proteome and Leads to Deterioration of Cardiac Function prior to the Development of Excessive Oxidative Stress and Cell Damage. *Oxid Med Cell Longev* 2019;2019:3218275. <https://doi.org/10.1155/2019/3218275>.
- [30] Dudek J. Role of Cardiolipin in Mitochondrial Signaling Pathways. *Front Cell Dev Biol* 2017;5:90. <https://doi.org/10.3389/fcell.2017.00090>.
- [31] Axelsen LN, Lademann JB, Petersen JS, Holstein-Rathlou N-H, Ploug T, Prats C, et al. Cardiac and metabolic changes in long-term high fructose-fat fed rats with severe obesity and extensive intramyocardial lipid accumulation. *Am J Physiol Regul Integr Comp Physiol* 2010;298:R1560–1570. <https://doi.org/10.1152/ajpregu.00392.2009>.
- [32] Korkmaz-Icöz S, Lehner A, Li S, Vater A, Radovits T, Hegedűs P, et al. Mild Type 2 Diabetes Mellitus Reduces the Susceptibility of the Heart to Ischemia/Reperfusion Injury: Identification of Underlying Gene Expression Changes. *J Diabetes Res* 2015;2015:396414. <https://doi.org/10.1155/2015/396414>.
- [33] International Diabetes Federation. Facts & figures n.d. <https://www.idf.org/aboutdiabetes/what-is-diabetes/facts-figures.html> (accessed November 29, 2021).
- [34] Guthrie RA, Guthrie DW. Pathophysiology of diabetes mellitus. *Crit Care Nurs Q* 2004;27:113–25. <https://doi.org/10.1097/00002727-200404000-00003>.
- [35] Taylor SI, Accili D, Imai Y. Insulin resistance or insulin deficiency. Which is the primary cause of NIDDM? *Diabetes* 1994;43:735–40. <https://doi.org/10.2337/diab.43.6.735>.
- [36] Shaw JE, Sicree RA, Zimmet PZ. Global estimates of the prevalence of diabetes for 2010 and 2030. *Diabetes Res Clin Pract* 2010;87:4–14. <https://doi.org/10.1016/j.diabres.2009.10.007>.

- [37] Guilherme A, Virbasius JV, Puri V, Czech MP. Adipocyte dysfunctions linking obesity to insulin resistance and type 2 diabetes. *Nat Rev Mol Cell Biol* 2008;9:367–77. <https://doi.org/10.1038/nrm2391>.
- [38] Charnogursky GA, Emanuele NV, Emanuele MA. Neurologic complications of diabetes. *Curr Neurol Neurosci Rep* 2014;14:457. <https://doi.org/10.1007/s11910-014-0457-5>.
- [39] Genuth S. Insights from the diabetes control and complications trial/epidemiology of diabetes interventions and complications study on the use of intensive glycemic treatment to reduce the risk of complications of type 1 diabetes. *Endocr Pract Off J Am Coll Endocrinol Am Assoc Clin Endocrinol* 2006;12 Suppl 1:34–41. <https://doi.org/10.4158/EP.12.S1.34>.
- [40] Asrih M, Steffens S. Emerging role of epigenetics and miRNA in diabetic cardiomyopathy. *Cardiovasc Pathol Off J Soc Cardiovasc Pathol* 2013;22:117–25. <https://doi.org/10.1016/j.carpath.2012.07.004>.
- [41] Vaag A, Lund SS. Non-obese patients with type 2 diabetes and prediabetic subjects: distinct phenotypes requiring special diabetes treatment and (or) prevention? *Appl Physiol Nutr Metab Physiol Appl Nutr Metab* 2007;32:912–20. <https://doi.org/10.1139/H07-100>.
- [42] Dalton M, Cameron AJ, Zimmet PZ, Shaw JE, Jolley D, Dunstan DW, et al. Waist circumference, waist-hip ratio and body mass index and their correlation with cardiovascular disease risk factors in Australian adults. *J Intern Med* 2003;254:555–63. <https://doi.org/10.1111/j.1365-2796.2003.01229.x>.
- [43] Mohan V, Deepa R. Adipocytokines and the expanding “Asian Indian Phenotype.” *J Assoc Physicians India* 2006;54:685–6.
- [44] Devanathan S, Nemanich ST, Kovacs A, Fettig N, Gropler RJ, Shoghi KI. Genomic and metabolic disposition of non-obese type 2 diabetic rats to increased myocardial fatty acid metabolism. *PloS One* 2013;8:e78477. <https://doi.org/10.1371/journal.pone.0078477>.
- [45] Manson JE, Colditz GA, Stampfer MJ, Willett WC, Krolewski AS, Rosner B, et al. A prospective study of maturity-onset diabetes mellitus and risk of coronary heart disease and stroke in women. *Arch Intern Med* 1991;151:1141–7.
- [46] Adlerberth AM, Rosengren A, Wilhelmsen L. Diabetes and long-term risk of mortality from coronary and other causes in middle-aged Swedish men. A general population study. *Diabetes Care* 1998;21:539–45. <https://doi.org/10.2337/diacare.21.4.539>.
- [47] Chandler MP, Morgan EE, McElfresh TA, Kung TA, Rennison JH, Hoit BD, et al. Heart failure progression is accelerated following myocardial infarction in type 2 diabetic rats. *Am J Physiol Heart Circ Physiol* 2007;293:H1609–1616. <https://doi.org/10.1152/ajpheart.01338.2006>.
- [48] D’Souza A, Howarth FC, Yanni J, Dobrynski H, Boyett MR, Adeghate E, et al. Left ventricle structural remodelling in the prediabetic Goto-Kakizaki rat. *Exp Physiol* 2011;96:875–88. <https://doi.org/10.1113/expphysiol.2011.058271>.
- [49] Grönholm T, Cheng ZJ, Palojoki E, Eriksson A, Bäcklund T, Vuolteenaho O, et al. Vasoepitidase inhibition has beneficial cardiac effects in spontaneously diabetic Goto-Kakizaki rats. *Eur J Pharmacol* 2005;519:267–76. <https://doi.org/10.1016/j.ejphar.2005.07.015>.
- [50] Li X, Wu Y, Zhao J, Wang H, Tan J, Yang M, et al. Distinct cardiac energy metabolism and oxidative stress adaptations between obese and non-obese type 2 diabetes mellitus. *Theranostics* 2020;10:2675–95. <https://doi.org/10.7150/thno.40735>.
- [51] Apaijai N, Charoenphandhu N, Ittichaichareon J, Suntornsaratoon P, Krishnamra N, Aeimlapa R, et al. Estrogen deprivation aggravates cardiac hypertrophy in nonobese Type 2 diabetic Goto-Kakizaki (GK) rats. *Biosci Rep* 2017;37:BSR20170886. <https://doi.org/10.1042/BSR20170886>.
- [52] Sárközy M, Zvara A, Gyémánt N, Fekete V, Kocsis GF, Pipis J, et al. Metabolic syndrome influences cardiac gene expression pattern at the transcript level in male ZDF rats. *Cardiovasc Diabetol* 2013;12:16. <https://doi.org/10.1186/1475-2840-12-16>.
- [53] Sárközy M, Szűcs G, Pipicz M, Zvara Á, Éder K, Fekete V, et al. The effect of a preparation of minerals, vitamins and trace elements on the cardiac gene expression pattern in male diabetic rats. *Cardiovasc Diabetol* 2015;14:85. <https://doi.org/10.1186/s12933-015-0248-6>.

- [54] Al-Awar A, Kupai K, Veszélka M, Szűcs G, Attieh Z, Murlasits Z, et al. Experimental Diabetes Mellitus in Different Animal Models. *J Diabetes Res* 2016;2016:9051426. <https://doi.org/10.1155/2016/9051426>.
- [55] Lenzen S. The mechanisms of alloxan- and streptozotocin-induced diabetes. *Diabetologia* 2008;51:216–26. <https://doi.org/10.1007/s00125-007-0886-7>.
- [56] Ostenson C-G, Efendic S. Islet gene expression and function in type 2 diabetes; studies in the Goto-Kakizaki rat and humans. *Diabetes Obes Metab* 2007;9 Suppl 2:180–6. <https://doi.org/10.1111/j.1463-1326.2007.00787.x>.
- [57] Al Kury L, Smail M, Qureshi MA, Sydorenko V, Shmygol A, Oz M, et al. Calcium Signaling in the Ventricular Myocardium of the Goto-Kakizaki Type 2 Diabetic Rat. *J Diabetes Res* 2018;2018:2974304. <https://doi.org/10.1155/2018/2974304>.
- [58] Goto Y, Kakizaki M, Masaki N. Production of spontaneous diabetic rats by repetition of selective breeding. *Tohoku J Exp Med* 1976;119:85–90. <https://doi.org/10.1620/tjem.119.85>.
- [59] Movassat J, Calderari S, Fernández E, Martín MA, Escrivá F, Plachot C, et al. Type 2 diabetes - a matter of failing beta-cell neogenesis? Clues from the GK rat model. *Diabetes Obes Metab* 2007;9 Suppl 2:187–95. <https://doi.org/10.1111/j.1463-1326.2007.00786.x>.
- [60] Galli J, Li LS, Glaser A, Ostenson CG, Jiao H, Fakhrai-Rad H, et al. Genetic analysis of non-insulin dependent diabetes mellitus in the GK rat. *Nat Genet* 1996;12:31–7. <https://doi.org/10.1038/ng0196-31>.
- [61] Yu J, Yang X, Luo Y, Yang X, Yang M, Yang J, et al. Adverse effects of chronic exposure to nonylphenol on non-alcoholic fatty liver disease in male rats. *PloS One* 2017;12:e0180218. <https://doi.org/10.1371/journal.pone.0180218>.
- [62] Lozano I, Van der Werf R, Bietiger W, Seyfritz E, Peronet C, Pinget M, et al. High-fructose and high-fat diet-induced disorders in rats: impact on diabetes risk, hepatic and vascular complications. *Nutr Metab* 2016;13:15. <https://doi.org/10.1186/s12986-016-0074-1>.
- [63] Axelsen LN, Calloe K, Braunstein TH, Riemann M, Hofgaard JP, Liang B, et al. Diet-induced pre-diabetes slows cardiac conductance and promotes arrhythmogenesis. *Cardiovasc Diabetol* 2015;14:87. <https://doi.org/10.1186/s12933-015-0246-8>.
- [64] Huang D-W, Chang W-C, Yang H-J, Wu JS-B, Shen S-C. Gallic Acid Alleviates Hypertriglyceridemia and Fat Accumulation via Modulating Glycolysis and Lipolysis Pathways in Perirenal Adipose Tissues of Rats Fed a High-Fructose Diet. *Int J Mol Sci* 2018;19:E254. <https://doi.org/10.3390/ijms19010254>.
- [65] Toyoda K, Suzuki Y, Muta K, Masuyama T, Kakimoto K, Kobayashi A, et al. High fructose diet feeding accelerates diabetic nephropathy in Spontaneously Diabetic Torii (SDT) rats. *J Toxicol Sci* 2018;43:45–58. <https://doi.org/10.2131/jts.43.45>.
- [66] Alves MRP, Boia R, Campos EJ, Martins J, Nunes S, Madeira MH, et al. Subtle thinning of retinal layers without overt vascular and inflammatory alterations in a rat model of prediabetes. *Mol Vis* 2018;24:353–66.
- [67] Burgeiro A, Cerqueira MG, Varela-Rodríguez BM, Nunes S, Neto P, Pereira FC, et al. Glucose and Lipid Dysmetabolism in a Rat Model of Prediabetes Induced by a High-Sucrose Diet. *Nutrients* 2017;9:E638. <https://doi.org/10.3390/nu9060638>.
- [68] Magnone M, Leoncini G, Vigliarolo T, Emionite L, Sturla L, Zocchi E, et al. Chronic Intake of Micrograms of Absciscic Acid Improves Glycemia and Lipidemia in a Human Study and in High-Glucose Fed Mice. *Nutrients* 2018;10:E1495. <https://doi.org/10.3390/nu10101495>.
- [69] Jurado-Ruiz E, Álvarez-Amor L, Varela LM, Berná G, Parra-Camacho MS, Oliveras-Lopez MJ, et al. Extra virgin olive oil diet intervention improves insulin resistance and islet performance in diet-induced diabetes in mice. *Sci Rep* 2019;9:11311. <https://doi.org/10.1038/s41598-019-47904-z>.
- [70] Howell GE, Mulligan C, Meek E, Chambers JE. Effect of chronic p,p'-dichlorodiphenyldichloroethylene (DDE) exposure on high fat diet-induced alterations in glucose and lipid metabolism in male C57BL/6H mice. *Toxicology* 2015;328:112–22. <https://doi.org/10.1016/j.tox.2014.12.017>.

- [71] Deol P, Evans JR, Dhahbi J, Chellappa K, Han DS, Spindler S, et al. Soybean Oil Is More Obesogenic and Diabetogenic than Coconut Oil and Fructose in Mouse: Potential Role for the Liver. *PloS One* 2015;10:e0132672. <https://doi.org/10.1371/journal.pone.0132672>.
- [72] Kale OE, Akinpelu OB, Bakare AA, Yusuf FO, Gomba R, Araka DC, et al. Five traditional Nigerian Polyherbal remedies protect against high fructose fed, Streptozotocin-induced type 2 diabetes in male Wistar rats. *BMC Complement Altern Med* 2018;18:160. <https://doi.org/10.1186/s12906-018-2225-6>.
- [73] Aslam M, Aggarwal S, Sharma KK, Galav V, Madhu SV. Postprandial Hypertriglyceridemia Predicts Development of Insulin Resistance Glucose Intolerance and Type 2 Diabetes. *PloS One* 2016;11:e0145730. <https://doi.org/10.1371/journal.pone.0145730>.
- [74] Coppey L, Davidson E, Shevalye H, Obrosova A, Yorek M. Effect of Early and Late Interventions with Dietary Oils on Vascular and Neural Complications in a Type 2 Diabetic Rat Model. *J Diabetes Res* 2019;2019:5020465. <https://doi.org/10.1155/2019/5020465>.
- [75] Shao Q, Meng L, Lee S, Tse G, Gong M, Zhang Z, et al. Empagliflozin, a sodium glucose co-transporter-2 inhibitor, alleviates atrial remodeling and improves mitochondrial function in high-fat diet/streptozotocin-induced diabetic rats. *Cardiovasc Diabetol* 2019;18:165. <https://doi.org/10.1186/s12933-019-0964-4>.
- [76] Kanuri G, Bergheim I. In vitro and in vivo models of non-alcoholic fatty liver disease (NAFLD). *Int J Mol Sci* 2013;14:11963–80. <https://doi.org/10.3390/ijms140611963>.
- [77] Chung M, Ma J, Patel K, Berger S, Lau J, Lichtenstein AH. Fructose, high-fructose corn syrup, sucrose, and nonalcoholic fatty liver disease or indexes of liver health: a systematic review and meta-analysis. *Am J Clin Nutr* 2014;100:833–49. <https://doi.org/10.3945/ajcn.114.086314>.
- [78] Skovsø S. Modeling type 2 diabetes in rats using high fat diet and streptozotocin. *J Diabetes Investig* 2014;5:349–58. <https://doi.org/10.1111/jdi.12235>.
- [79] Ghanaat-Pour H, Huang Z, Lehtihet M, Sjöholm A. Global expression profiling of glucose-regulated genes in pancreatic islets of spontaneously diabetic Goto-Kakizaki rats. *J Mol Endocrinol* 2007;39:135–50. <https://doi.org/10.1677/JME-07-0002>.
- [80] Homo-Delarche F, Calderari S, Irminger J-C, Gangnerau M-N, Coulaud J, Rickenbach K, et al. Islet inflammation and fibrosis in a spontaneous model of type 2 diabetes, the GK rat. *Diabetes* 2006;55:1625–33. <https://doi.org/10.2337/db05-1526>.
- [81] Zhou H, Saito S, Piao G, Liu Z-P, Wang J, Horimoto K, et al. Network screening of Goto-Kakizaki rat liver microarray data during diabetic progression. *BMC Syst Biol* 2011;5 Suppl 1:S16. <https://doi.org/10.1186/1752-0509-5-S1-S16>.
- [82] Nie J, Xue B, Sukumaran S, Jusko WJ, Dubois DC, Almon RR. Differential muscle gene expression as a function of disease progression in Goto-Kakizaki diabetic rats. *Mol Cell Endocrinol* 2011;338:10–7. <https://doi.org/10.1016/j.mce.2011.02.016>.
- [83] Herrera BM, Lockstone HE, Taylor JM, Ria M, Barrett A, Collins S, et al. Global microRNA expression profiles in insulin target tissues in a spontaneous rat model of type 2 diabetes. *Diabetologia* 2010;53:1099–109. <https://doi.org/10.1007/s00125-010-1667-2>.
- [84] Abdul-Rahman O, Sasvari-Szekely M, Ver A, Rosta K, Szasz BK, Kereszturi E, et al. Altered gene expression profiles in the hippocampus and prefrontal cortex of type 2 diabetic rats. *BMC Genomics* 2012;13:81. <https://doi.org/10.1186/1471-2164-13-81>.
- [85] Sárközy M, Fekete V, Szűcs G, Török S, Szűcs C, Bárkányi J, et al. Anti-diabetic effect of a preparation of vitamins, minerals and trace elements in diabetic rats: a gender difference. *BMC Endocr Disord* 2014;14:72. <https://doi.org/10.1186/1472-6823-14-72>.
- [86] Sárközy M, Szűcs G, Fekete V, Pipicz M, Éder K, Gáspár R, et al. Transcriptomic alterations in the heart of non-obese type 2 diabetic Goto-Kakizaki rats. *Cardiovasc Diabetol* 2016;15:110. <https://doi.org/10.1186/s12933-016-0424-3>.
- [87] Gayoso-Diz P, Otero-Gonzalez A, Rodriguez-Alvarez MX, Gude F, Cadarso-Suarez C, García F, et al. Insulin resistance index (HOMA-IR) levels in a general adult population: curves percentile by gender and age. The EPIRCE study. *Diabetes Res Clin Pract* 2011;94:146–55. <https://doi.org/10.1016/j.diabres.2011.07.015>.

- [88] Barr ELM, Cameron AJ, Balkau B, Zimmet PZ, Welborn TA, Tonkin AM, et al. HOMA insulin sensitivity index and the risk of all-cause mortality and cardiovascular disease events in the general population: the Australian Diabetes, Obesity and Lifestyle Study (AusDiab) study. *Diabetologia* 2010;53:79–88. <https://doi.org/10.1007/s00125-009-1588-0>.
- [89] Csont T, Bereczki E, Bencsik P, Fodor G, Görbe A, Zvara A, et al. Hypercholesterolemia increases myocardial oxidative and nitrosative stress thereby leading to cardiac dysfunction in apoB-100 transgenic mice. *Cardiovasc Res* 2007;76:100–9. <https://doi.org/10.1016/j.cardiores.2007.06.006>.
- [90] Kocsis GF, Sárközy M, Bencsik P, Pipicz M, Varga ZV, Pálóczi J, et al. Preconditioning protects the heart in a prolonged uremic condition. *Am J Physiol Heart Circ Physiol* 2012;303:H1229–1236. <https://doi.org/10.1152/ajpheart.00379.2012>.
- [91] Kiscsatári L, Sárközy M, Kővári B, Varga Z, Gömöri K, Morvay N, et al. High-dose Radiation Induced Heart Damage in a Rat Model. *Vivo Athens Greece* 2016;30:623–31.
- [92] Sárközy M, Gáspár R, Zvara Á, Siska A, Kővári B, Szűcs G, et al. Chronic kidney disease induces left ventricular overexpression of the pro-hypertrophic microRNA-212. *Sci Rep* 2019;9:1302. <https://doi.org/10.1038/s41598-018-37690-5>.
- [93] Csont T, Viappiani S, Sawicka J, Slee S, Altarejos JY, Batinić-Haberle I, et al. The involvement of superoxide and iNOS-derived NO in cardiac dysfunction induced by pro-inflammatory cytokines. *J Mol Cell Cardiol* 2005;39:833–40. <https://doi.org/10.1016/j.yjmcc.2005.07.010>.
- [94] Pipicz M, Kocsis GF, Sárváry-Arantes L, Bencsik P, Varga ZV, Ferdinandy P, et al. Low-Dose Endotoxin Induces Late Preconditioning, Increases Peroxynitrite Formation, and Activates STAT3 in the Rat Heart. *Mol Basel Switz* 2017;22:E433. <https://doi.org/10.3390/molecules22030433>.
- [95] Csont T, Csonka C, Onody A, Görbe A, Dux L, Schulz R, et al. Nitrate tolerance does not increase production of peroxynitrite in the heart. *Am J Physiol Heart Circ Physiol* 2002;283:H69–76. <https://doi.org/10.1152/ajpheart.00817.2001>.
- [96] Csont T, Csonka C, Kovács P, Jancsó G, Ferdinandy P. Capsaicin-sensitive sensory neurons regulate myocardial nitric oxide and cGMP signaling. *Eur J Pharmacol* 2003;476:107–13. [https://doi.org/10.1016/s0014-2999\(03\)02117-4](https://doi.org/10.1016/s0014-2999(03)02117-4).
- [97] Peksel B, Gombos I, Péter M, Vigh L, Tizslavicz Á, Brameshuber M, et al. Mild heat induces a distinct “eustress” response in Chinese Hamster Ovary cells but does not induce heat shock protein synthesis. *Sci Rep* 2017;7:15643. <https://doi.org/10.1038/s41598-017-15821-8>.
- [98] Buege JA, Aust SD. Microsomal lipid peroxidation. *Methods Enzymol* 1978;52:302–10. [https://doi.org/10.1016/s0076-6879\(78\)52032-6](https://doi.org/10.1016/s0076-6879(78)52032-6).
- [99] Storey JD, Tibshirani R. Statistical significance for genomewide studies. *Proc Natl Acad Sci U S A* 2003;100:9440–5. <https://doi.org/10.1073/pnas.1530509100>.
- [100] Xia J, Wishart DS. Web-based inference of biological patterns, functions and pathways from metabolomic data using MetaboAnalyst. *Nat Protoc* 2011;6:743–60. <https://doi.org/10.1038/nprot.2011.319>.
- [101] Skov V, Thomassen M, Riley CH, Jensen MK, Bjerrum OW, Kruse TA, et al. Gene expression profiling with principal component analysis depicts the biological continuum from essential thrombocythemia over polycythemia vera to myelofibrosis. *Exp Hematol* 2012;40:771–780.e19. <https://doi.org/10.1016/j.exphem.2012.05.011>.
- [102] Althunibat OY, Al Hroob AM, Abukhalil MH, Germoush MO, Bin-Jumah M, Mahmoud AM. Fisetin ameliorates oxidative stress, inflammation and apoptosis in diabetic cardiomyopathy. *Life Sci* 2019;221:83–92. <https://doi.org/10.1016/j.lfs.2019.02.017>.
- [103] Hsueh W, Abel ED, Breslow JL, Maeda N, Davis RC, Fisher EA, et al. Recipes for creating animal models of diabetic cardiovascular disease. *Circ Res* 2007;100:1415–27. <https://doi.org/10.1161/01.RES.0000266449.37396.1f>.
- [104] Russell JC, Proctor SD. Small animal models of cardiovascular disease: tools for the study of the roles of metabolic syndrome, dyslipidemia, and atherosclerosis. *Cardiovasc Pathol Off J Soc Cardiovasc Pathol* 2006;15:318–30. <https://doi.org/10.1016/j.carpath.2006.09.001>.

- [105] Fakhoury-Sayegh N, Trak-Smayra V, Khazzaka A, Esseily F, Obeid O, Lahoud-Zouein M, et al. Characteristics of nonalcoholic fatty liver disease induced in wistar rats following four different diets. *Nutr Res Pract* 2015;9:350–7. <https://doi.org/10.4162/nrp.2015.9.4.350>.
- [106] Gatineau E, Savary-Auzeloux I, Migné C, Polakof S, Dardevet D, Mosoni L. Chronic Intake of Sucrose Accelerates Sarcopenia in Older Male Rats through Alterations in Insulin Sensitivity and Muscle Protein Synthesis. *J Nutr* 2015;145:923–30. <https://doi.org/10.3945/jn.114.205583>.
- [107] Dhar I, Dhar A, Wu L, Desai KM. Increased methylglyoxal formation with upregulation of renin angiotensin system in fructose fed Sprague Dawley rats. *PLoS One* 2013;8:e74212. <https://doi.org/10.1371/journal.pone.0074212>.
- [108] Malhi H, Kaufman RJ. Endoplasmic reticulum stress in liver disease. *J Hepatol* 2011;54:795–809. <https://doi.org/10.1016/j.jhep.2010.11.005>.
- [109] Stefan N, Häring H-U. The role of hepatokines in metabolism. *Nat Rev Endocrinol* 2013;9:144–52. <https://doi.org/10.1038/nrendo.2012.258>.
- [110] Yang F, Dai Y, Min C, Li X. Neonatal overfeeding induced glucocorticoid overexposure accelerates hepatic lipogenesis in male rats. *Nutr Metab* 2018;15:30. <https://doi.org/10.1186/s12986-018-0272-0>.
- [111] Baena M, Sangüesa G, Hutter N, Sánchez RM, Roglans N, Laguna JC, et al. Fructose supplementation impairs rat liver autophagy through mTORC activation without inducing endoplasmic reticulum stress. *Biochim Biophys Acta* 2015;1851:107–16. <https://doi.org/10.1016/j.bbailip.2014.11.003>.
- [112] Softic S, Cohen DE, Kahn CR. Role of Dietary Fructose and Hepatic De Novo Lipogenesis in Fatty Liver Disease. *Dig Dis Sci* 2016;61:1282–93. <https://doi.org/10.1007/s10620-016-4054-0>.
- [113] Matsuzaka T, Atsumi A, Matsumori R, Nie T, Shinozaki H, Suzuki-Kemuriyama N, et al. Elovl6 promotes nonalcoholic steatohepatitis. *Hepatology* 2012;56:2199–208. <https://doi.org/10.1002/hep.25932>.
- [114] Pandya K, Kim H-S, Smithies O. Fibrosis, not cell size, delineates beta-myosin heavy chain reexpression during cardiac hypertrophy and normal aging in vivo. *Proc Natl Acad Sci U S A* 2006;103:16864–9. <https://doi.org/10.1073/pnas.0607700103>.
- [115] Nakao K, Minobe W, Roden R, Bristow MR, Leinwand LA. Myosin heavy chain gene expression in human heart failure. *J Clin Invest* 1997;100:2362–70. <https://doi.org/10.1172/JCI119776>.
- [116] Pandya K, Smithies O. β -MyHC and cardiac hypertrophy: size does matter. *Circ Res* 2011;109:609–10. <https://doi.org/10.1161/CIRCRESAHA.111.252619>.
- [117] Brooks BA, Franjic B, Ban CR, Swaraj K, Yue DK, Celermajer DS, et al. Diastolic dysfunction and abnormalities of the microcirculation in type 2 diabetes. *Diabetes Obes Metab* 2008;10:739–46. <https://doi.org/10.1111/j.1463-1326.2007.00803.x>.
- [118] Shivalkar B, Dhondt D, Goovaerts I, Van Gaal L, Bartunek J, Van Crombrugge P, et al. Flow mediated dilatation and cardiac function in type 1 diabetes mellitus. *Am J Cardiol* 2006;97:77–82. <https://doi.org/10.1016/j.amjcard.2005.07.111>.
- [119] Han X, Yang J, Cheng H, Yang K, Abendschein DR, Gross RW. Shotgun lipidomics identifies cardiolipin depletion in diabetic myocardium linking altered substrate utilization with mitochondrial dysfunction. *Biochemistry* 2005;44:16684–94. <https://doi.org/10.1021/bi051908a>.
- [120] Han X, Yang J, Yang K, Zhao Z, Abendschein DR, Gross RW. Alterations in myocardial cardiolipin content and composition occur at the very earliest stages of diabetes: a shotgun lipidomics study. *Biochemistry* 2007;46:6417–28. <https://doi.org/10.1021/bi7004015>.
- [121] Lou P-H, Lucchinetti E, Scott KY, Huang Y, Gandhi M, Hersberger M, et al. Alterations in fatty acid metabolism and sirtuin signaling characterize early type-2 diabetic hearts of fructose-fed rats. *Physiol Rep* 2017;5:e13388. <https://doi.org/10.14814/phy2.13388>.
- [122] Shi Y. Emerging roles of cardiolipin remodeling in mitochondrial dysfunction associated with diabetes, obesity, and cardiovascular diseases. *J Biomed Res* 2010;24:6–15. [https://doi.org/10.1016/S1674-8301\(10\)60003-6](https://doi.org/10.1016/S1674-8301(10)60003-6).

- [123] Kiebish MA, Yang K, Liu X, Mancuso DJ, Guan S, Zhao Z, et al. Dysfunctional cardiac mitochondrial bioenergetic, lipidomic, and signaling in a murine model of Barth syndrome. *J Lipid Res* 2013;54:1312–25. <https://doi.org/10.1194/jlr.M034728>.
- [124] Taha TA, Mullen TD, Obeid LM. A house divided: ceramide, sphingosine, and sphingosine-1-phosphate in programmed cell death. *Biochim Biophys Acta* 2006;1758:2027–36. <https://doi.org/10.1016/j.bbamem.2006.10.018>.
- [125] Holland WL, Summers SA. Strong Heart, Low Ceramides. *Diabetes* 2018;67:1457–60. <https://doi.org/10.2337/dbi18-0018>.
- [126] Marchesini N, Osta W, Bielawski J, Luberto C, Obeid LM, Hannun YA. Role for mammalian neutral sphingomyelinase 2 in confluence-induced growth arrest of MCF7 cells. *J Biol Chem* 2004;279:25101–11. <https://doi.org/10.1074/jbc.M313662200>.
- [127] Su X, Han X, Mancuso DJ, Abendschein DR, Gross RW. Accumulation of long-chain acylcarnitine and 3-hydroxy acylcarnitine molecular species in diabetic myocardium: identification of alterations in mitochondrial fatty acid processing in diabetic myocardium by shotgun lipidomics. *Biochemistry* 2005;44:5234–45. <https://doi.org/10.1021/bi047773a>.
- [128] Peng SY, Norman J, Curtin G, Corrier D, McDaniel HR, Busbee D. Decreased mortality of Norman murine sarcoma in mice treated with the immunomodulator, Acemannan. *Mol Biother* 1991;3:79–87.
- [129] Mutter T, Dolinsky VW, Ma BJ, Taylor WA, Hatch GM. Thyroxine regulation of monolysocardiolipin acyltransferase activity in rat heart. *Biochem J* 2000;346 Pt 2:403–6.
- [130] Varga ZV, Kupai K, Szűcs G, Gáspár R, Pálóczi J, Faragó N, et al. MicroRNA-25-dependent up-regulation of NADPH oxidase 4 (NOX4) mediates hypercholesterolemia-induced oxidative/nitrative stress and subsequent dysfunction in the heart. *J Mol Cell Cardiol* 2013;62:111–21. <https://doi.org/10.1016/j.yjmcc.2013.05.009>.
- [131] Salem KA, Qureshi MA, Sydorenko V, Parekh K, Jayaprakash P, Iqbal T, et al. Effects of exercise training on excitation-contraction coupling and related mRNA expression in hearts of Goto-Kakizaki type 2 diabetic rats. *Mol Cell Biochem* 2013;380:83–96. <https://doi.org/10.1007/s11010-013-1662-2>.
- [132] Huang G, Ge G, Wang D, Gopalakrishnan B, Butz DH, Colman RJ, et al. $\alpha 3(V)$ collagen is critical for glucose homeostasis in mice due to effects in pancreatic islets and peripheral tissues. *J Clin Invest* 2011;121:769–83. <https://doi.org/10.1172/JCI45096>.
- [133] Liu X, Takeda N, Dhalla NS. Myosin light-chain phosphorylation in diabetic cardiomyopathy in rats. *Metabolism* 1997;46:71–5. [https://doi.org/10.1016/s0026-0495\(97\)90171-2](https://doi.org/10.1016/s0026-0495(97)90171-2).
- [134] Rokosh DG, Stewart AF, Chang KC, Bailey BA, Karliner JS, Camacho SA, et al. Alpha1-adrenergic receptor subtype mRNAs are differentially regulated by alpha1-adrenergic and other hypertrophic stimuli in cardiac myocytes in culture and in vivo. Repression of alpha1B and alpha1D but induction of alpha1C. *J Biol Chem* 1996;271:5839–43. <https://doi.org/10.1074/jbc.271.10.5839>.
- [135] Chandna AR, Nair M, Chang C, Pennington PR, Yamamoto Y, Mousseau DD, et al. RAGE mediates the inactivation of nAChRs in sympathetic neurons under high glucose conditions. *Eur J Neurosci* 2015;41:341–51. <https://doi.org/10.1111/ejn.12795>.
- [136] Xie L-H, Shanmugam M, Park JY, Zhao Z, Wen H, Tian B, et al. Ablation of sarcolipin results in atrial remodeling. *Am J Physiol Cell Physiol* 2012;302:C1762–1771. <https://doi.org/10.1152/ajpcell.00425.2011>.
- [137] Shanmugam M, Li D, Gao S, Fefelova N, Shah V, Voit A, et al. Cardiac specific expression of threonine 5 to alanine mutant sarcolipin results in structural remodeling and diastolic dysfunction. *PloS One* 2015;10:e0115822. <https://doi.org/10.1371/journal.pone.0115822>.
- [138] Bando YK, Murohara T. Heart Failure as a Comorbidity of Diabetes: Role of Dipeptidyl Peptidase 4. *J Atheroscler Thromb* 2016;23:147–54. <https://doi.org/10.5551/jat.33225>.
- [139] Son JW, Kim S. Dipeptidyl Peptidase 4 Inhibitors and the Risk of Cardiovascular Disease in Patients with Type 2 Diabetes: A Tale of Three Studies. *Diabetes Metab J* 2015;39:373–83. <https://doi.org/10.4093/dmj.2015.39.5.373>.

- [140] Mulvihill EE, Varin EM, Ussher JR, Campbell JE, Bang KWA, Abdullah T, et al. Inhibition of Dipeptidyl Peptidase-4 Impairs Ventricular Function and Promotes Cardiac Fibrosis in High Fat-Fed Diabetic Mice. *Diabetes* 2016;65:742–54. <https://doi.org/10.2337/db15-1224>.
- [141] Hilfiker-Kleiner D, Hilfiker A, Fuchs M, Kaminski K, Schaefer A, Schieffer B, et al. Signal transducer and activator of transcription 3 is required for myocardial capillary growth, control of interstitial matrix deposition, and heart protection from ischemic injury. *Circ Res* 2004;95:187–95. <https://doi.org/10.1161/01.RES.0000134921.50377.61>.
- [142] Pipicz M, Demján V, Sárközy M, Csont T. Effects of Cardiovascular Risk Factors on Cardiac STAT3. *Int J Mol Sci* 2018;19:E3572. <https://doi.org/10.3390/ijms19113572>.
- [143] Xu J, Lei S, Liu Y, Gao X, Irwin MG, Xia Z-Y, et al. Antioxidant N-acetylcysteine attenuates the reduction of Brg1 protein expression in the myocardium of type 1 diabetic rats. *J Diabetes Res* 2013;2013:716219. <https://doi.org/10.1155/2013/716219>.
- [144] Wang T, Qiao S, Lei S, Liu Y, Ng KFJ, Xu A, et al. N-acetylcysteine and allopurinol synergistically enhance cardiac adiponectin content and reduce myocardial reperfusion injury in diabetic rats. *PLoS One* 2011;6:e23967. <https://doi.org/10.1371/journal.pone.0023967>.
- [145] Sun X, Chen R, Yang Z, Sun G, Wang M, Ma X, et al. Taxifolin prevents diabetic cardiomyopathy in vivo and in vitro by inhibition of oxidative stress and cell apoptosis. *Food Chem Toxicol Int J Publ Br Ind Biol Res Assoc* 2014;63:221–32. <https://doi.org/10.1016/j.fct.2013.11.013>.
- [146] Wang L, Li J, Li D. Losartan reduces myocardial interstitial fibrosis in diabetic cardiomyopathy rats by inhibiting JAK/STAT signaling pathway. *Int J Clin Exp Pathol* 2015;8:466–73.
- [147] Meixner A, Karreth F, Kenner L, Penninger JM, Wagner EF. Jun and JunD-dependent functions in cell proliferation and stress response. *Cell Death Differ* 2010;17:1409–19. <https://doi.org/10.1038/cdd.2010.22>.
- [148] Werner P, Paluru P, Simpson AM, Latney B, Iyer R, Brodeur GM, et al. Mutations in NTRK3 suggest a novel signaling pathway in human congenital heart disease. *Hum Mutat* 2014;35:1459–68. <https://doi.org/10.1002/humu.22688>.
- [149] Lappas M. Lower circulating levels of complement split proteins C3a and C4a in maternal plasma of women with gestational diabetes mellitus. *Diabet Med J Br Diabet Assoc* 2011;28:906–11. <https://doi.org/10.1111/j.1464-5491.2011.03336.x>.
- [150] Berrou J, Fougeray S, Venot M, Chardiny V, Gautier J-F, Dulphy N, et al. Natural killer cell function, an important target for infection and tumor protection, is impaired in type 2 diabetes. *PLoS One* 2013;8:e62418. <https://doi.org/10.1371/journal.pone.0062418>.

I.

ORIGINAL INVESTIGATION

Open Access



Transcriptomic alterations in the heart of non-obese type 2 diabetic Goto-Kakizaki rats

Márta Sárközy¹, Gergő Szűcs^{1,2}, Veronika Fekete¹, Márton Pipicz¹, Katalin Éder³, Renáta Gáspár¹, Andrea Sója¹, Judit Pipis⁴, Péter Ferdinandy^{4,5}, Csaba Csonka¹ and Tamás Csont^{1*}

Abstract

Background: There is a spectacular rise in the global prevalence of type 2 diabetes mellitus (T2DM) due to the worldwide obesity epidemic. However, a significant proportion of T2DM patients are non-obese and they also have an increased risk of cardiovascular diseases. As the Goto-Kakizaki (GK) rat is a well-known model of non-obese T2DM, the goal of this study was to investigate the effect of non-obese T2DM on cardiac alterations of the transcriptome in GK rats.

Methods: Fasting blood glucose, serum insulin and cholesterol levels were measured at 7, 11, and 15 weeks of age in male GK and control rats. Oral glucose tolerance test and pancreatic insulin level measurements were performed at 11 weeks of age. At week 15, total RNA was isolated from the myocardium and assayed by rat oligonucleotide microarray for 41,012 genes, and then expression of selected genes was confirmed by qRT-PCR. Gene ontology and protein–protein network analyses were performed to demonstrate potentially characteristic gene alterations and key genes in non-obese T2DM.

Results: Fasting blood glucose, serum insulin and cholesterol levels were significantly increased, glucose tolerance and insulin sensitivity were significantly impaired in GK rats as compared to controls. In hearts of GK rats, 204 genes showed significant up-regulation and 303 genes showed down-regulation as compared to controls according to microarray analysis. Genes with significantly altered expression in the heart due to non-obese T2DM includes functional clusters of metabolism (e.g. *Cyp2e1*, *Akr1b10*), signal transduction (e.g. *Dpp4*, *Stat3*), receptors and ion channels (e.g. *Sln*, *Chrn*), membrane and structural proteins (e.g. *Tnni1*, *Mylk2*, *Col8a1*, *Adam33*), cell growth and differentiation (e.g. *Gpc3*, *Jund*), immune response (e.g. *C3*, *C4a*), and others (e.g. *Lrp8*, *Msln*, *Klkc1*, *Epn3*). Gene ontology analysis revealed several significantly enriched functional inter-relationships between genes influenced by non-obese T2DM. Protein–protein interaction analysis demonstrated that Stat is a potential key gene influenced by non-obese T2DM.

Conclusions: Non-obese T2DM alters cardiac gene expression profile. The altered genes may be involved in the development of cardiac pathologies and could be potential therapeutic targets in non-obese T2DM.

Keywords: Spontaneous diabetes mellitus, Inherited diabetes mellitus, Non-obese type 2 diabetes mellitus, Myocardium, DNA microarray, GO, String, Insulin resistance

Background

Diabetes mellitus is a heterogeneous chronic metabolic disorder characterized by hyperglycemia as a common feature resulting from impaired insulin secretion, insulin resistance, or both [1]. In 2014, the global prevalence of

diabetes mellitus (DM) was estimated to be 9 % among adults according to WHO data [2]. The total number of people suffering from DM is projected to almost triple from 190 million to 552 million by 2030 [3, 4]. T2DM accounts for more than 90 % of all diabetes cases and its incidence is continuously rising worldwide [1, 5, 6]. The major cause for this phenomenon is the so-called obesity epidemic due to physical inactivity and increased consumption of energy-rich food [7]. Nevertheless, it is often

*Correspondence: csont.tamas@med.u-szeged.hu

¹ Department of Biochemistry, Faculty of Medicine, University of Szeged, Dóm tér 9, Szeged 6720, Hungary

Full list of author information is available at the end of the article

neglected that around 20 % of T2DM patients are non-obese in Europe and Asia [7–10]. The non-obese T2DM phenotype is characterized by a more pronounced reduction in insulin secretion and less severe insulin resistance as compared to obese T2DM patients [7]. The risk of T2DM in non-obese individuals is considered to be mostly influenced by polygenic inheritance and prenatal environment [7].

It is well known that diabetic patients have an increased risk of developing a number of co-morbidities including cardiovascular diseases (CVD). It has been reported that T2DM patients have a two to four-fold increased risk of CVD in general [7, 11, 12]. Obesity is recognized as an independent risk factor for both T2DM and CVD [7, 13]. Interestingly, it has been reported that non-obese T2DM patients also have a high risk of CVD similarly to that of obese T2DM patients [7, 11, 14]. Indeed, CVD are estimated to be responsible for more than 50 % of deaths among T2DM population [15].

One of the major pathologies of the aforementioned CVD is diabetic cardiomyopathy (DCM) [15, 16]. DCM is defined as left ventricular (LV) diastolic and/or systolic dysfunction with hypertrophy and fibrosis in the absence of preceding hypertension, coronary artery disease and valvular or congenital heart disease [15–17]. Although DCM is a distinct clinical entity, it is also a part of the diabetic atherosclerosis process [18]. DCM might be independent of the coexistence of arterial hypertension, coronary artery disease or other macrovascular complications [18]. DCM is characterized by the development of myocardial damage, reactive hypertrophy and fibrosis, structural and functional changes of the small coronary vessels, and cardiac autonomic neuropathy [18]. These alterations make the diabetic heart more susceptible to ischemia and subsequent remodeling [18–20].

We have previously shown that cardiac gene expression pattern is significantly altered in obese ZDF rats, a model of T2DM and metabolic syndrome [21], and in streptozotocin-induced T1DM rats [22] at the transcript level. The effect of non-obese T2DM on gene expression pattern in various tissue types has been investigated in a few studies. Pancreatic islets [23, 24], liver [25], skeletal muscle [26], adipose tissue [27], hippocampus and prefrontal cortex [28] obtained from the well-known non-obese T2DM model Goto-Kakizaki (GK) rat showed altered gene expression pattern as compared to controls. Surprisingly, whole transcriptomic analysis in the heart of GK rats has not been performed previously. Therefore, in the present study, our aim was to investigate the effect of non-obese T2DM on cardiac alterations of the transcriptome in GK rats.

Methods

Ethics approval

This investigation conforms to the National Institutes of Health Guide for the Care and Use of Laboratory Animals (NIH Pub. No. 85–23, Revised 1996) and was approved by the Animal Research Ethics Committee of the University of Szeged.

Animal model of non-obese T2DM

Male Goto-Kakizaki rats and their age-matched male Wistar controls were obtained from Charles River Laboratories at the age of 6 weeks and were housed at 22 ± 2 °C with a 12:12-h light–dark cycle. The rats received standard rat chow and water ad libitum for 9 weeks after their arrival. The GK rat is a recognized model of inherited type 2 diabetes mellitus [29]. This spontaneously diabetic rat strain was developed by selective breeding of Wistar rats with the highest normal blood glucose levels in response to oral glucose tolerance test [30, 31]. GK rats develop a non-obese and mild hyperglycemic phenotype at week 4–5 accompanied by a metabolic state of glucose intolerance and later peripheral insulin resistance [29, 32] which develops to a hyperglycemic insulin-deficient state with aging [29, 32–34]. The metabolic features manifested in this animal model are in many ways similar to the pathogenesis of inherited spontaneous T2DM in humans [29, 32]. However, hyperglycemia and glucose intolerance developed in GK rats are not associated with the development of obesity or hypertension [1]. The adult GK rat of T2DM has been shown to develop cardiovascular complications including left ventricular hypertrophy, fibrosis, as well as diastolic and/or systolic dysfunction [1, 20, 35, 36]. Therefore, the GK rat is an applicable model for investigation of the consequences of non-obese T2DM in the heart.

Experimental setup

Body weight, serum glucose, insulin, cholesterol levels and homeostasis model assessment-estimated insulin resistance (HOMA-IR) were determined at 7, 11 and 15 weeks of age in order to monitor the basic parameters of glucose and lipid metabolism and insulin resistance in GK and control rats (Figs. 1, 2, 3). Oral glucose tolerance test (OGTT) was performed at week 15 to further characterize glucose homeostasis of GK and control rats (Fig. 2). At 15 weeks of age, rats were anaesthetized using pentobarbital sodium (Euthasol, 50 mg/kg, Produlab Pharma b.v., Raamsdonksveer, The Netherlands). Hearts and pancreata were isolated, and then hearts were perfused according to Langendorff as described earlier [21, 37]. After 5 min perfusion ventricular tissue was frozen and stored at -80 °C until gene expression analysis by DNA microarray and qRT-PCR techniques.

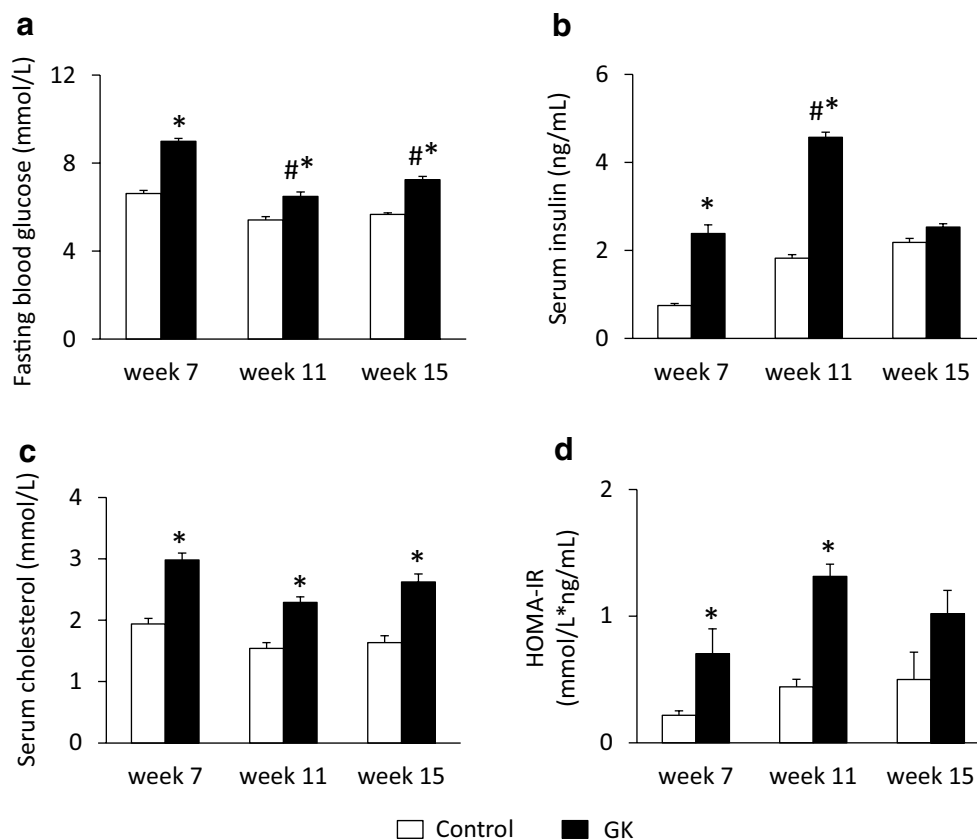


Fig. 1 Fasting blood glucose, serum insulin and cholesterol levels. Fasting blood glucose (a), serum insulin (b) and cholesterol (c) levels as well as HOMA-IR index (d) at weeks 7, 11 and 15 in both control and GK rats. Values are mean \pm SEM, $n = 7-9$, * $p < 0.05$ vs. control within the same time point, # $p < 0.05$ vs. week 7 values

Serum glucose level measurements and OGTT

As described previously, rats were fasted overnight (12 h) prior to serum glucose level measurements and OGTTs (weeks 7, 11 and 15) to verify the development of hyperglycemia and glucose-intolerance as diagnostic criteria of diabetes mellitus [21, 22, 36]. Blood samples were collected from the saphenous vein. Blood glucose levels were measured using AccuCheck blood glucose monitoring systems (Roche Diagnostics Corporation, USA, Indianapolis) [21, 22, 38]. In case of OGTT, after the measurement of baseline glucose concentrations, 1.5 g/kg body weight glucose was administered per os via gavage and blood glucose levels were checked 30, 60 and 120 min later [21, 22, 38]. Area under the curve values for OGTT was also calculated.

Measurement of serum and pancreatic insulin levels

Serum and pancreatic insulin levels were measured by an enzyme-linked immunosorbent assay (Merckodia, Ultrasensitive Rat Insulin ELISA) as described

previously [21, 22, 38]. Blood samples were collected from the saphenous vein at weeks 7, 11 and 15. At week 15, during OGTT blood was collected at 0, 30 and 120 min for serum insulin level measurements. Blood samples were centrifuged (4500 rpm for 10 min at 4 °C) and kept at -20°C until the assay was performed. At week 15, pancreata were removed, trimmed free of adipose tissue and weighed. Pancreata were homogenized in 6 mL cold acidified-ethanol (0.7 M HCl: ethanol, 1:3 v/v) with an Ultraturrax homogenizer and were kept at 4 °C for 24 h. Then pancreas homogenates were centrifuged (900g for 15 min at 4 °C), and the supernatants were stored at 4 °C. The pellet was extracted again with 3 mL acidified ethanol for 24 h at 4 °C. The supernatant obtained after centrifugation was pooled with the previous one and kept at -20°C until assayed. Insulin ELISA was carried out according to the instructions of the manufacturer from either sera or homogenized pancreatic tissue samples of GK and control rats.

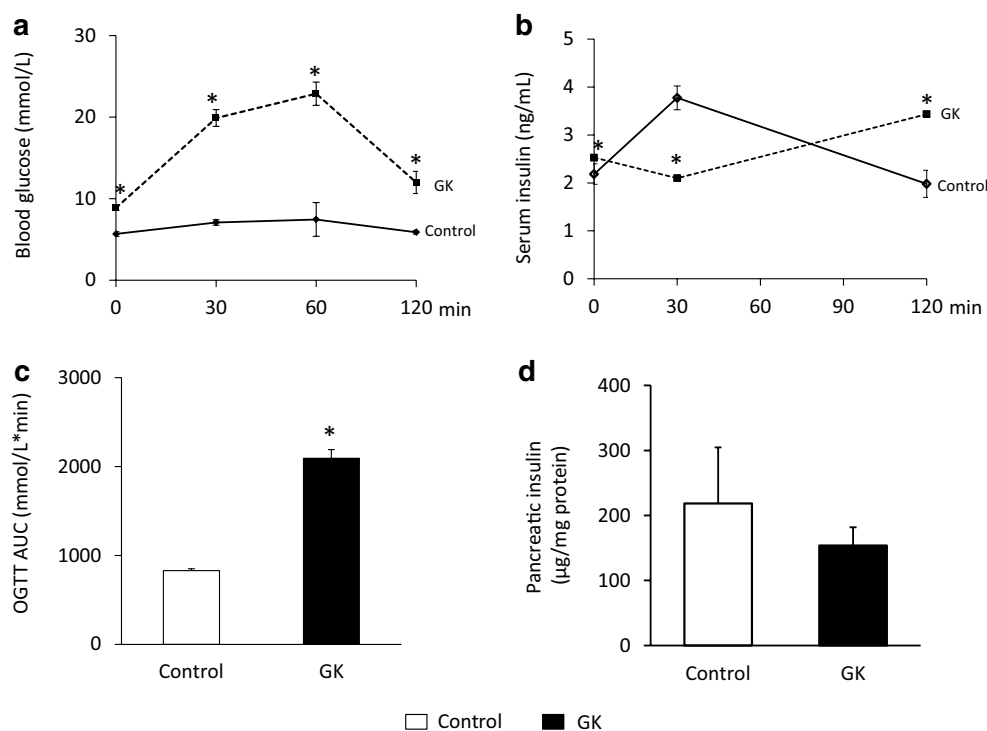


Fig. 2 Blood glucose and insulin levels during OGTT and pancreatic insulin content. Blood glucose (**a**) and serum insulin (**b**) levels during OGTT, OGTT AUC (**c**) and pancreatic insulin (**d**) content at week 15 in both control and GK rats. Solid line control; dashed line GK. Values are mean \pm SEM, $n = 7-9$, * $p < 0.05$

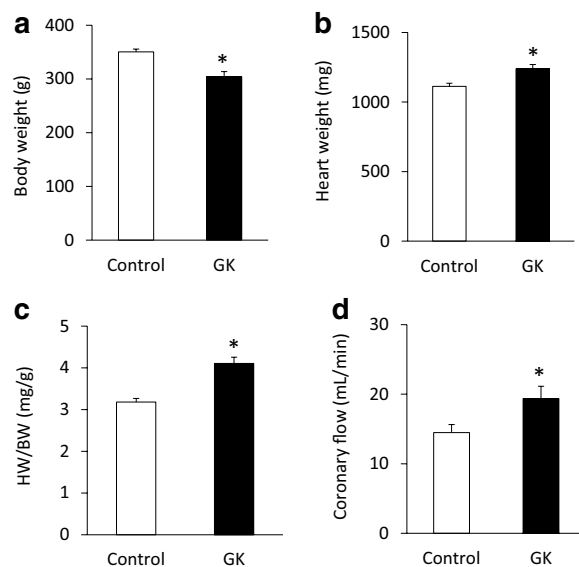


Fig. 3 Body weight, heart weight and coronary flow. Body weight (**a**), heart weight (**b**), heart weight to body weight ratio (**c**) and coronary flow (**d**) at week 15 in both control and GK rats. Values are mean \pm SEM, $n = 7-9$, * $p < 0.05$

HOMA-IR index

To estimate insulin resistance in GK or control rats the widely used HOMA-IR index was calculated [21, 39] by multiplying fasting serum insulin ($\mu\text{g/mL}$) with fasting blood glucose (mmol/L), then dividing by the constant 22.5, i.e. $\text{HOMA-IR} = (\text{fasting serum insulin concentration} \times \text{fasting blood glucose concentration})/22.5$.

Measurement of serum cholesterol levels

In order to follow up the development of hypercholesterolemia which is a risk factor of cardiovascular diseases, serum cholesterol levels were measured at weeks 7, 11 and 15 using a test kit (Diagnosticum Zrt., Budapest, Hungary) as described previously [21, 40, 41].

RNA preparation and DNA microarray analysis

Total RNA was isolated from heart samples with Qia-gen miRNeasy Mini Kit according to the manufacturer's protocol (Qiagen, Hilden, Germany) as described previously [22]. On-column DNase digestion was carried out with the RNase-Free DNase Set (Qiagen GmbH). RNA concentration was measured by NanoDrop 1000

Spectrophotometer (Thermo Fisher Scientific Inc., Waltham, MA, USA) and RNA integrity was determined by an Agilent 2100 Bioanalyzer System (Agilent Technologies Inc., Santa Clara, CA, USA). Samples with an RNA integrity number (RIN) above 8.0 were used for further analysis. RNA was stored at -80°C until use.

Total RNA (1000 ng) was labelled and amplified using the QuickAmp Labelling Kit according to the instructions of the manufacturer. Labelled RNA was purified and hybridized to Agilent Whole Rat Genome 4×44 K array slides, according to the manufacturer's protocol. After washing, array scanning and feature extraction was performed with default scenario by Agilent DNA Microarray Scanner and Feature Extraction Software 9.5.

Messenger RNA (mRNA) expression profiling by qRT-PCR

In order to validate gene expression changes obtained by DNA microarray, qRT-PCR was performed with gene-specific primers. Total RNA (1 μg) was reverse transcribed using High-Capacity cDNA Reverse Transcription Kit (Thermo Fisher Scientific, Waltham, MA US). Quantitative RT-PCR was performed using TaqMan Array 96 Well Fast Plate 3×32 (Thermo Fisher Scientific, Waltham, MA US) according to the manufacturer's instructions on a 7900HT Fast Real-Time PCR System. Each well of the TaqMan Array Plate contained 5 μL of Taqman Fast Universal Master Mix (2X) no AmpErase[®] UNG, 1 μL cDNA (50 ng/ μL) and 4 μL distilled water in a final reaction volume of 10 μL per well. Then qPCR was performed with the following protocol: 50 cycles of 95°C for 15 s and 60°C for 1 min. The fluorescence intensity was detected after each amplification step. Melting temperature analysis was done after each reaction to check the quality of the products. Primers were designed using the online TaqMan[®] Assays custom plating service of the manufacturer. Relative expression ratios were calculated as normalized ratios to rat glyceraldehyde-3-phosphate dehydrogenase (GAPDH), hypoxanthine phosphoribosyltransferase (HPRT) and ribosomal protein S18 (RPS18) housekeeping genes. A non-template control sample was used for each primer to check primer-dimer formation. Normalized signal levels for each mRNA were calculated using comparative cycle threshold method (delta-delta Ct method). Fold change refers to $2^{-\Delta\Delta\text{Ct}}$ (in the case of up-regulated genes) and $-(1/2^{-\Delta\Delta\text{Ct}})$ (in the case of down-regulated genes).

Gene ontology (GO) analysis

By using DNA microarrays for transcriptional profiling a large number of genes can be analyzed simultaneously [21, 42], however, the resulting data do not give direct information about possible biological interaction of the differentially expressed genes. GO analysis is a suitable

method for integration genes with pathways and biological interaction networks to detect coordinated changes in functionally related genes [21, 42]. GO analysis was performed using GO pathway analysis using the open access software DAVID bioinformatics system and database (Database for Annotation, Visualization and Integrated Discovery, <http://www.david.abcc.ncifcrf.gov> website) [21, 42]. The differentially expressed genes were submitted to DAVID bioinformatics system and database to reveal significantly enriched biological functions/pathways [21, 42].

Protein-protein interaction analysis

Gene expression networks are of great biological interest since co-expressed genes could be (1) controlled by the same transcriptional regulatory program, (2) functionally related, or (3) members of the same pathway or protein complex [43]. In order to further characterize the connections of significantly altered genes obtained by DNA microarray, protein-protein network analysis was performed by STRING10 based on two types of evidence: experimental (protein-protein interaction databases) and text-mining (abstracts of scientific literature). STRING (<http://www.string-db.org/>), is an online accessible database of known and predicted protein-protein interactions. Protein-protein interactions from STRING 10 were collected for the construction of differential protein interaction network among the genes whose expressions were significantly different in hearts of GK rats. The differently expressed genes were mapped to the String database and then known and predicted associations were scored and integrated. Combined-score > 0.4 was the threshold. Differently expressed genes were visualized after KMEANS clustering. Finally, interaction network was constructed by integrating these relationships.

Statistical analysis

Statistical analysis was performed by using Sigmaplot 12.0 for Windows (Systat Software Inc). All values are presented as mean \pm SEM. Repeated measures Two-Way ANOVA was used to determine the effect of T2DM and the age on FBG, serum insulin and cholesterol levels as well as glucose levels during OGTT. After ANOVA, all pairwise multiple comparison procedures with Holm-Šidák post hoc tests were used as multiple range tests. Two sample t test was used to determine the effect of T2DM on OGTT AUC, pancreatic insulin concentration, body weight, heart weight, heart weight/body weight ratio and coronary flow. $P < 0.05$ was accepted as a statistically significant difference. In the microarray experiments, biological and technical replica tests were carried out to gain raw data for statistical analysis. Altogether 4 individual parallel gene activity comparisons were done

between the two groups. Both in the microarray and qRT-PCR experiments, a two-sample t test was used and the p value was determined to find significant gene expression changes. In the microarray experiments, a corrected p value was determined for each gene to control the false discovery rate using the Benjamini and Hochberg multiple testing correction protocol. Gene expression ratios with p value of <0.05 and \log_2 ratio of < -1.00 or \log_2 ratio of >1.00 (~2.0-fold) were considered as repression or overexpression respectively in gene activity.

Results

Metabolic characterization of non-obese T2DM

In order to verify the development of T2DM in male GK rats, concentrations of several serum metabolites were measured at weeks 7, 11 and 15 (Fig. 1). GK rats showed a significantly elevated FBG level at all time points as compared to controls (Fig. 1a). Interestingly, blood glucose level in GK rats were significantly lower at week 11 as compared to week 7 or week 15 blood glucose values (Fig. 1a). Parallel with hyperglycemia, serum insulin levels were significantly increased in GK rats compared to Wistar controls at week 7 and more profoundly at week 11 showing the presence of hyperinsulinemia in GK animals (Fig. 1b). However, there was no significant difference between serum insulin levels measured in GK and control rats at week 15, since serum insulin concentration in GK rats significantly decreased by week 15 as compared to insulin level measured at week 11 indicating beta-cell damage in GK rats (Fig. 1b). HOMA-IR was significantly increased at weeks 7 and 11 in GK rats when compared to controls showing insulin resistance in GK animals (Fig. 1d). In contrast, increase of HOMA-IR did not reach the level of statistical significance at week 15 in GK animals (Fig. 1d). Serum cholesterol levels were significantly higher in GK rats as compared to control ones throughout the study duration representing hypercholesterolemia (Fig. 1c). OGTT was performed at week 15 in order to verify the development of impaired glucose tolerance in GK rats. Glucose levels during OGTT were markedly increased in GK rats in every time point of blood glucose measurements (Fig. 2a). Area under the curve (AUC) of blood glucose levels during OGTT was significantly increased in GK rats representing impaired glucose tolerance (Fig. 2c). In addition, serum insulin level in GK rats during OGTT was significantly lower 30 min after glucose loading and became markedly increased 120 min after glucose administration indicating impaired insulin secretion (Fig. 2b). Interestingly, pancreatic insulin levels were 25 % lower in GK rats compared to control ones, however, the values were not significantly different between the two groups (Fig. 2d).

Body weight, heart weight and coronary flow

Body weight was significantly decreased at week 15 in GK rats proving a non-obese phenotype of T2DM in GK rats (Fig. 3a). Heart weight and heart weight to body weight ratio were significantly increased at week 15 in GK rats suggesting the development of cardiac hypertrophy in response to chronic T2DM (Fig. 3b, c). Interestingly, coronary flow was significantly increased at week 15 in GK rats as compared to control hearts (Fig. 3d).

Gene expression profile and qRT-PCR

Among the 41,012 genes surveyed (Additional file 1: Table S1), 507 genes whose expression was > ~2.0-fold up- or down-regulated in hearts of GK rats relative to levels of control rats showed significant change in expression. According to our results, 204 genes showed up-regulation (Additional file 2: Table S2) and 303 genes showed down-regulation in hearts of GK rats (Additional file 2: Table S3). Moreover, 138 genes showed more than threefold change of expression in hearts of GK rats as compared to the levels of control rats. Among these 138 genes, 50 genes were significantly up-regulated (Table 1) and 88 genes were significantly down-regulated (Table 2) in GK rat hearts. The expression change of selected 28 genes was validated by qRT-PCR (Table 3), 19 of these 28 genes have been confirmed by qRT-PCR (Table 3).

Gene ontology analysis

In order to further determine the biological significance and functional classification of differentially expressed genes due to non-obese T2DM, GO analysis was performed (Table 4) [21]. GO analysis is suitable for identifying significantly enriched GO terms related to multiple genes and for discovering enriched functionally related gene groups. A single gene can belong to different categories. Out of the 507 genes significantly altered by non-obese T2DM in our present study, 277 genes with known function were submitted to GO analysis and 115 were clustered into different categories. The rest of the 507 genes were either unknown expressed sequence tags or unrecognized by the GO analysis database (Table 4). The 115 analyzed genes were classified into five main categories such as (1) biological regulation, (2) metabolic process, (3) immune system process, (4) biological adhesion, and (5) rhythmic process (Table 4).

Protein–protein interaction analysis

To better understand the relationships between the functionally related gene groups analyzed by GO, we examined protein–protein interactions between protein products of all 507 genes showing significant difference in gene expression (Fig. 4). Here, Stat3 seems to have a major networking group affecting multiple top GO

Table 1 Up-regulated genes (>3.0-fold up-regulation)

Gene function	Description (gene symbol)	Acc. no.	AVE log2	SD (LOG)	P value (Corr)	Fold change	SD
Metabolism	Abhydrolase domain containing 17C (Abhd17c)	NM_001100736	2.79	0.39	0.00	6.96	1.72
	Alcohol dehydrogenase 1 (class I) (Adh1)	NM_019286	2.43	0.99	0.00	5.38	2.78
	Retinol saturase (all trans retinol 13,14 reductase) (Retsat)	NM_145084	2.17	1.14	0.01	4.50	3.61
	Diacylglycerol kinase, beta (Dgkb)	NM_019304	2.07	0.34	0.00	4.21	0.82
	Kallikrein 1-related peptidase C3 (Klk1c3)	NM_001271315	1.92	0.45	0.00	3.79	1.07
	Aldo-keto reductase family 1, member B10 (aldose reductase) (Akr1b10)	NM_001013084	1.91	0.44	0.00	3.76	1.05
	Adenosine monophosphate deaminase 1 (Ampd1)	NM_138876	1.61	0.71	0.00	3.06	1.56
Signal transduction, regulation of transcription	Phospholipase A2, group VII (platelet-activating factor acetylhydrolase, plasma) (Pla2g7)	NM_001009353	2.23	0.29	0.00	4.68	0.88
	Protein tyrosine phosphatase, non-receptor type 13 (Ptpn13)	NM_001100789	2.13	1.06	0.00	4.38	2.18
	Ephrin A2 (Efna2)	NM_001168670	1.77	0.31	0.00	3.41	0.60
	Crystallin, mu (Crym)	NM_053955	1.76	0.39	0.00	3.38	0.78
	Cd47 molecule (Cd47)	NM_019195	1.74	0.26	0.00	3.34	0.51
	Calsyntenin 2 (Clstn2)	NM_134377	1.63	0.65	0.00	3.09	1.41
	Ring finger protein 187 (Rnf187)	NM_001164264	1.61	0.34	0.00	3.06	0.63
Receptors, ion channels	Potassium voltage-gated channel, Isk-related family, member 1 (Kcne1)	NM_012973	2.72	0.82	0.00	6.57	4.07
	ATPase, H ⁺ transporting, lysosomal V1 subunit G2 (Atp6v1g2)	NM_212490	2.53	0.60	0.00	5.77	2.02
	Cholinergic receptor, nicotinic, alpha 7 (neuronal) (Chrna7)	S53987	1.79	0.31	0.00	3.45	0.63
	ATPase, Ca ⁺⁺ transporting, plasma membrane 2 (Atp2b2)	NM_012508	1.71	0.50	0.00	3.27	0.91
Membrane proteins	Peroxisomal membrane protein 4 (Pxmp4)	NM_172223	2.52	0.21	0.00	5.73	0.74
Cell growth and differentiation	Transcription elongation factor A (SII)-like 7 (Tceal7)	NM_001109401	1.86	0.84	0.00	3.63	1.88
	Jun D proto-oncogene (Jund)	NM_138875	1.71	0.29	0.00	3.28	0.60
Immune response	RT1 class Ib, locus T18 (RT1-T18)	NM_001002821	2.31	0.77	0.00	4.95	2.21
	2'-5' oligoadenylate synthetase 1A (Oas1a)	NM_138913	1.98	0.86	0.00	3.94	2.50
Transport	ATPase, Ca ⁺⁺ transporting, plasma membrane 2 (Atp2b2)	NM_012508	1.78	0.41	0.00	3.44	0.77
	Solute carrier family 16 (monocarboxylate transporter), member 7 (Slc16a7)	NM_017302	1.64	0.38	0.00	3.11	0.69
Others	Guanylate binding protein 1, interferon-inducible (gbp1)	XM_006224278	4.80	0.49	0.00	27.84	8.96
	Uncharacterized LOC102549588	XR_362031	4.69	0.54	0.00	25.85	8.31
	Twin-arginine translocation pathway signal		4.52	0.58	0.00	23.01	9.81
	TL0ADA29YA08 mRNA sequence	FQ222105	3.27	0.42	0.00	9.64	2.34
	Similar to ribosomal protein L6 (LOC366145)	XM_345411	2.94	0.59	0.00	7.70	3.03

Table 1 continued

Gene function	Description (gene symbol)	Acc. no.	AVE log2	SD (LOG)	P value (Corr)	Fold change	SD
	Mitochondrial ribosomal protein S10 (Mrps10)	NM_001008859	2.86	1.24	0.00	7.28	4.07
	Cd300 molecule-like family member G (Cd300lg)	XM_003750936	2.61	0.68	0.00	6.10	2.99
	MRNA decapping enzyme		2.32	0.35	0.00	4.99	1.11
	Transmembrane emp24 domain-containing protein 5 precursor		2.14	0.28	0.00	4.41	0.72
	Macrophage activation 2 like (Mpa2 l)	XM_006221662	2.10	1.05	0.00	4.30	3.00
	Similar to interferon-inducible GTPase (RGD1309362)	NM_001024884	2.02	0.84	0.00	4.06	2.65
	Myc-like oncogene, s-myc protein (Mycs)	NM_021837	2.00	0.80	0.00	4.00	1.64
	Uncharacterized LOC102556738	XR_340771	1.96	0.44	0.00	3.89	1.10
	Nuclear casein kinase and cyclin-dependent kinase substrate 1 (Nucks1)	XM_006249797	1.96	0.34	0.00	3.89	0.74
	Transducin-like enhancer of split 6 (E(sp1) homolog, Drosophila) (Tle6)	XM_006241027	1.95	0.43	0.00	3.87	1.10
	Transmembrane protein 132C (Tmem132c)	XM_002724836	1.91	0.45	0.00	3.75	1.09
	CWC25 spliceosome-associated protein homolog (<i>S. cerevisiae</i>) (Cwc25)	NM_001108295	1.82	0.76	0.00	3.52	1.65
	Contactin associated protein-like 2 (Cntnap2)	XM_006236412	1.79	0.39	0.00	3.47	0.84
	Anaphase promoting complex subunit 10 (Anapc10)	XM_006255406	1.77	1.29	0.03	3.41	4.41
	Deoxycytidine triphosphate deaminase		1.73	0.35	0.00	3.32	0.74
	Hypothetical protein LOC500028	NM_001047954	1.65	0.38	0.00	3.13	0.66
	RNA binding motif protein 44 (Rbm44)	XM_001066845	1.64	0.46	0.00	3.12	0.87
	Trichorhinophalangeal syndrome I (Trps1)	XM_006241626	1.62	0.39	0.00	3.08	0.69
	Excision repair cross-complementing rodent repair deficiency, complementation group 8 (Ercc8)	NM_001107650	1.60	0.27	0.00	3.03	0.49
	Uncharacterized LOC100912569	XR_348427	1.59	0.82	0.01	3.02	1.80

pathways in non-obese T2DM. Moreover, there are proteins interconnected with each other in smaller networking groups including networks of (1) Sdc1; (2) Cyp2e1 and (3) Tef proteins (Fig. 4) affecting the top GO pathways as well (Table 4).

Discussion

In the present study, our aim was to investigate how cardiac gene expression pattern is influenced by non-obese T2DM. Here we show several characteristics of non-obese T2DM in 15 weeks old male GK rats including decreased body weight, fasting hyperglycemia, hypercholesterolemia, insulin resistance, and impaired glucose

tolerance. Moreover, we show increased heart weight and heart weight/body weight ratio in GK rats indicating cardiac hypertrophy. We also demonstrate that non-obese T2DM influences cardiac gene expression pattern by altering transcript levels of several genes. We identified 507 genes which were differentially expressed in the myocardium of GK rats compared to Wistar controls.

The spontaneously diabetic GK rat is a well characterized and recognized model of non-obese type 2 diabetes mellitus. The abnormal glucose regulation in the GK rat develops in association both with impaired insulin secretion and with insulin resistance as reviewed by Östenson and Movassat [29, 32]. At the onset of T2DM, there is a

Table 2 Down-regulated genes (>3.0-fold down-regulation)

Gene function	Description (gene symbol)	Acc. no.	AVE log2	SD (LOG)	P value (Corr)	Fold change	SD
Metabolism	Transglutaminase 1 (Tgm1)	NM_031659	-1.98	0.55	0.0002	-3.93	1.87
	CARBONIC anhydrase 6 (Car6)	NM_001134841	-2.03	0.76	0.0002	-4.08	2.61
	Phenazine biosynthesis-like protein domain containing 1 (Pbld1)	NM_138530	-2.14	0.68	0.0001	-4.41	2.60
	Coproporphyrinogen oxidase (Cpox)	NM_001037095	-2.32	0.45	0.0001	-4.98	2.06
	Prolyl 4-hydroxylase, alpha polypeptide III (P4ha3)	XM_006229769	-2.36	0.38	0.0001	-5.13	1.68
Signal transduction, regulation of transcription	cAMP responsive element binding protein 5 (Creb5)	XM_006236505	-1.62	0.52	0.0001	-3.07	1.26
	Dual-specificity tyrosine-(Y)-phosphorylation regulated kinase 3 (Dyrk3)	NM_001024767	-1.74	0.65	0.0006	-3.35	1.95
	Hypermethylated in cancer 1 (Hic1)	NM_001107021	-1.83	0.70	0.0019	-3.55	2.10
	Rho guanine nucleotide exchange factor (GEF) 5 (Arhgef5)	XM_006224892	-1.96	0.47	0.0001	-3.89	1.45
	Thyroid hormone responsive (Thrsp)	NM_012703	-2.28	0.98	0.0020	-4.86	5.18
	Cellular retinoic acid binding protein 2 (Crabp2)	NM_017244	-2.32	0.50	0.0001	-4.98	2.42
	A kinase (PRKA) anchor protein 3 (Akap3)	NM_001005557	-2.68	0.35	0.0000	-6.39	1.90
Receptors, ion channels	Uroplakin 1B (Upk1b)	NM_001024253	-3.69	0.69	0.0001	-12.89	7.94
	Interleukin 22 receptor, alpha 2 (Il22ra2)	NM_001003404	-1.62	0.93	0.0064	-3.07	2.78
	Neurotrophic tyrosine kinase, receptor, type 3 (Ntrk3), transcript variant 3	NM_019248	-1.64	0.45	0.0005	-3.12	1.18
	Adrenoceptor alpha 1D (Adra1d)	NM_024483	-1.69	0.37	0.0007	-3.23	1.09
	Lysophosphatidic acid receptor 1 (Lpar1)	NM_053936	-1.83	0.51	0.0000	-3.55	1.50
	Prostaglandin F receptor (Ptgfr)	NM_013115	-1.87	0.44	0.0000	-3.65	1.40
	Solute carrier family 4 (anion exchanger), member 1 (Slc4a1)	NM_012651	-2.39	0.22	0.0000	-5.23	0.94
	Sarcolipin (Slip)	NM_001013247	-3.00	1.41	0.0028	-8.03	15.41
	ATPase, H + transporting, lysosomal accessory protein 1-like (Atp6ap1 l)	NM_001191843	-3.59	0.31	0.0000	-12.06	3.25
	Sarcolipin (Slip)	CK841541	-2.51	1.08	0.0019	-5.68	7.12
Membrane proteins	Collagen, type V, alpha 3 (Col5a3)	NM_021760	-1.78	0.59	0.0001	-3.43	1.46
Structural protein, cell adhesion	Contactin associated protein 1 (Cntnap1)	NM_032061	-2.03	0.34	0.0000	-4.09	1.11
	Myosin binding protein H-like (Mybphl)	NM_001014042	-2.82	1.17	0.0011	-7.08	8.55
	Myosin, light chain 7, regulatory (Myl7)	NM_001106017	-3.37	1.66	0.0030	-10.34	20.29
	Mesothelin (Msln)	NM_031658	-4.46	1.44	0.0010	-22.03	31.18
	Ret proto-oncogene (Ret), transcript variant 1	NM_012643	-1.64	0.44	0.0000	-3.11	1.15
Cell growth and differentiation	Endothelial cell-specific molecule 1 (Esm1)	NM_022604	-2.28	0.39	0.0000	-4.85	1.57
	Neuronatin (Nnat), transcript variant 1	NM_053601	-2.34	1.34	0.0119	-5.06	10.47
	Endothelial cell-specific molecule 1 (Esm1)	NM_022604	-2.36	0.40	0.0000	-5.13	1.64
	Epiphycan (Epyc)	NM_001108088	-2.36	1.37	0.0083	-5.14	7.64
	Cyclin G1 (Ccng1)	NM_012923	-3.36	0.21	0.0000	-10.29	1.82
	Tripartite motif-containing 16 (Trim16)	NM_001135033	-6.33	0.41	0.0000	-80.63	28.07
	Regenerating islet-derived 3 beta (Reg3b)	NM_053289	-1.81	1.34	0.0300	-3.52	5.83
Immune response	Inducible T-cell co-stimulator ligand (Icoslg)	XM_006223832	-1.92	0.37	0.0000	-3.79	1.16
	Complement component 4A (Rodgers blood group) (C4a)	NM_031504	-2.25	0.75	0.0002	-4.77	3.07
	Chemokine (C-X-C motif) ligand 13 (Cxcl13)	NM_001017496	-2.48	0.78	0.0003	-5.57	4.38
	Similar to immunoglobulin superfamily, member 7 (RGD1559482),	NM_001168285	-2.54	0.43	0.0000	-5.83	2.19
	CD1d1 molecule (Cd1d1)	NM_017079	-2.64	0.53	0.0000	-6.21	2.67
	Chymase 1, mast cell (Cma1)	NM_013092	-3.95	0.45	0.0000	-15.40	6.26

Table 2 continued

Gene function	Description (gene symbol)	Acc. no.	AVE log2	SD (LOG)	P value (Corr)	Fold change	SD
Transport	Retinol binding protein 4, plasma (Rbp4)	NM_013162	-2.09	1.20	0.0131	-4.27	7.22
Hormones	Inhibin alpha (Inha)	NM_012590	-1.79	0.56	0.0020	-3.45	1.80
Others	Protein Arhgef5 (Source:UniProtKB/ TrEMBL;Acc:E9PT59)	XM_006224892	-1.62	0.54	0.0002	-3.07	1.33
	Hypothetical protein LOC100302372 (LOC100302372)	NM_001162897	-1.63	0.57	0.0004	-3.10	1.69
	(F344/Crj)rearranged mRNA for T-cell receptor gamma chain (1483 bp)	Z27087	-1.65	0.71	0.0045	-3.13	1.94
	Similar to RIKEN cDNA 1700001E04 (LOC367428), mRNA (XM_346135)	XM_346135	-1.65	0.25	0.0000	-3.14	0.68
	BTB (POZ) domain containing 9 (Btb9)	XM_006256185	-1.66	0.30	0.0000	-3.15	0.73
	Q99NG8_RAT (Q99NG8) T:G mismatch thy- mine glycosylase		-1.67	0.44	0.0001	-3.17	1.24
	Hypothetical protein LOC689316 (LOC689316)	XR_086061	-1.68	0.39	0.0000	-3.21	1.02
	Uroplakin 3B-like (Upk3bl)	NM_001109020	-1.69	0.37	0.0013	-3.22	1.04
	NEUU_MOUSE (Q9QXK8) Neuromedin U-23 precursor (NmU-23)		-1.71	0.43	0.0000	-3.28	1.10
	Ripply transcriptional repressor 2 (Ripply2)	XM_001064780	-1.73	0.44	0.0000	-3.31	1.22
	Uncharacterized LOC100912446 (LOC100912446)	FQ221838	-1.73	0.64	0.0005	-3.33	1.76
	Similar to TP53-regulating kinase (p53-related protein kinase) (Nori-2) (LOC685619)	XM_002729250	-1.75	0.32	0.0000	-3.37	0.84
	Erythrocyte membrane protein band 4.1-like 3 (Epb41l3)	NM_053927	-1.77	0.90	0.0057	-3.41	2.69
	Uncharacterized LOC102556259 (LOC102556259)	XR_355327	-1.77	0.38	0.0001	-3.42	1.22
	EF-hand domain family, member D1 (Efhd1)	NM_001109310	-1.81	0.46	0.0000	-3.50	1.45
	Zinc finger and BTB domain containing 20 (Zbtb20)	XM_006248302	-1.87	0.48	0.0000	-3.67	1.69
	Suppressor of glucose, autophagy associated 1 (Soga1)	XM_001067659	-1.89	0.66	0.0001	-3.72	2.23
	Protein RGD1562667	XM_221091	-1.91	0.45	0.0000	-3.75	1.49
	Uncharacterized protein (Source:UniProtKB/ TrEMBL;Acc:F1LSJ2) (ENSRNOT00000035259)	XM_001061015	-1.93	0.61	0.0001	-3.80	2.07
	Uncharacterized LOC102546664 (LOC102546664)	XR_342060	-1.95	0.18	0.0000	-3.87	0.58
	Protein Rsf1 (Source:UniProtKB/ TrEMBL;Acc:D3ZGQ8)	XM_218939	-1.95	1.05	0.0109	-3.87	2.89
	Nucleosome assembly protein 1-like 5 (Nap1l5)	NM_001044293	-1.97	1.04	0.0039	-3.92	3.86
	Methyltransferase like 2B (Mettl2b)	NM_001108839	-2.07	0.40	0.0000	-4.20	1.36
	Similar to immunoreceptor Ly49si3 (LOC690097)	XM_003753951	-2.19	0.50	0.0001	-4.55	2.20
	Neuronal PAS domain protein 2 (Npas2)	NM_001108214	-2.23	0.47	0.0000	-4.69	1.73
	FM089532 etnofat cDNA clone etno- fatP0014D18 5', mRNA sequence	FM089532	-2.40	0.36	0.0001	-5.28	1.54
	Chordin-like 1 (Chrdl1)	NM_199502	-2.46	0.27	0.0000	-5.51	1.30
	Uncharacterized LOC102557390 (LOC102557390)	XR_348511	-2.54	0.48	0.0000	-5.82	2.30
	Q7TQ12_RAT (Q7TQ12) Aa1114		-2.62	0.32	0.0000	-6.14	1.69
	TL0ACA45YL24 mRNA sequence	FQ215947	-2.65	0.48	0.0000	-6.27	2.81
	Aryl hydrocarbon receptor nuclear transloca- tor-like (Arntl)	NM_024362	-2.75	0.54	0.0000	-6.75	2.85
	Similar to RIKEN cDNA 1500015O10 (RGD1305645)	NM_001271051	-2.84	0.88	0.0003	-7.17	7.06

Table 2 continued

Gene function	Description (gene symbol)	Acc. no.	AVE log2	SD (LOG)	P value (Corr)	Fold change	SD
	Uncharacterized LOC100911508 (LOC100911508)	XR_145872	-2.86	0.30	0.0000	-7.25	1.86
	TLOACA40YB18 mRNA sequence.	FQ216879	-2.99	1.21	0.0012	-7.94	9.21
	Family with sequence similarity 216, member B (Fam216b)	XM_003751515	-3.04	0.89	0.0002	-8.25	6.41
	SARCO_MOUSE (Q9CQD6) Sarcolipin, complete (TC628765)	AW918768	-3.06	1.35	0.0020	-8.33	14.57
	Endogenous retrovirus mRNA	AY212271	-3.51	1.47	0.0015	-11.38	17.10
	Uncharacterized LOC102552170 (LOC102552170)	XM_006224493	-4.01	0.40	0.0000	-16.09	5.74
	O89816_9GAMR (O89816) Envelope glycoprotein		-4.04	0.99	0.0001	-16.49	15.56
	Rat PRRHIS8 mRNA for ribosomal protein S8. (X56846)	X56846	-4.14	0.73	0.0000	-17.63	12.05
	Elongator protein 3/MiaB/NifB		-4.21	0.37	0.0000	-18.51	5.56
	Endogenous retrovirus mRNA	AY212271	-4.21	1.48	0.0006	-18.52	28.67
	Similar to 60S ribosomal protein L19 (LOC316856)	XM_229366	-4.46	0.84	0.0000	-22.05	16.63
	Uncharacterized LOC102554872 (LOC102554872)	XR_348916	-4.86	0.35	0.0000	-29.02	8.07
	WDNM1 homolog (LOC360228)	NM_001003706	-5.14	1.80	0.0013	-35.24	76.86

compensatory attempt of the beta cells to release more insulin to defeat insulin resistance. Later this mechanism is insufficient to maintain blood glucose level within a physiological range and finally leads to the functional exhaustion of the surviving beta cells. These stages in the GK model could be also observed in our present study. Blood glucose levels were significantly increased in GK rats at weeks 7, 11 and 15 as compared to controls and there was a statistically significant difference in blood glucose levels in GK rats between the different time points. Blood glucose level in GK rats were significantly lower at week 11 as compared to week 7 or week 15 blood glucose values. Moreover, serum insulin level was significantly increased at week 11 in GK rats as compared to week 7 values. The significantly higher serum insulin level at week 11 could explain the lower blood glucose level at week 11 as compared to week 7 blood glucose values. Serum insulin levels and HOMA-IR were significantly increased at week 7 and 11 showing increasing insulin resistance and compensatory hyperinsulinemia. At week 15, there was no significant difference in serum insulin level between GK and control animals. However, pancreatic insulin content of GK rats was slightly decreased suggesting the functional exhaustion of pancreatic beta cells. Probably this is the reason why HOMA-IR failed to reach the level of statistical significance in GK rats compared to controls at this time point. Nevertheless, this is not a sign of spontaneous improvement of insulin resistance in GK rats in our present study. These results

are in accordance with literature data showing that beta cell mass and insulin production continuously decreases from birth to adulthood in GK rats due to chronic islet inflammation, angiopathy, fibrosis and defective beta cell neogenesis [32].

Surprisingly, only a few studies were performed previously using the qPCR technique to investigate the gene expression changes playing a role in the development of left ventricular hypertrophy and structural remodeling [20, 35, 44], excitation–contraction coupling [45, 46], and lipotoxicity [10] in the hearts of GK rats. Thus, our study is the first to describe overall alterations in the cardiac transcriptome in male GK rats. In our present study, the significantly altered genes can be classified into different clusters (e.g. metabolism, stress response, signal transduction, regulation of transcription, receptors, ion channels, membrane and structural proteins, cell growth and differentiation, immune response, transport, hormones, etc.). Moreover, some other genes without any definite function in the myocardium were also changed in response to DM. The majority of these genes have not been related to non-obese T2DM yet, and therefore, characterization of the functional effects of these genes on the heart in non-obese T2DM is suggested in future mechanistic studies.

Genes related to metabolic alterations in T2DM

In our present study, several genes related to metabolism were found to be affected in the hearts of GK rats as compared to controls. A group of these altered genes

Table 3 Confirmation by qRT-PCR

Gene symbol	Gene name	Acc. nr.	DNA microarray		qRT-PCR		Confirmed
			AVE (log2)	Fold change	Fold change	SEM	
Adipoq	Adiponectin, C1Q and collagen domain containing	Rn00595250_m1	-4.99	-31.78	-23.64	0.02	Yes
Retn	Resistin	Rn00595224_m1	-4.74	-26.72	31.08	14.46	No
Atp1b4	ATPase, (Na ⁺)/K ⁺ transporting, beta 4 polypeptide	Rn00584523_m1	-4.21	-18.51	-4.74	0.05	Yes
Car3	Carbonic anhydrase 3	Rn01461970_m1	-3.73	-13.27	-7.88	0.03	Yes
Cma1	Chymase 1, mast cell	Rn00565319_m1	-3.11	-8.63	-5.12	0.02	Yes
Arntl	Aryl hydrocarbon receptor nuclear translocator-like	Rn00577590_m1	-2.75	-6.74	-2.95	0.03	Yes
Tgm1	Transglutaminase 1, K polypeptide	Rn00581408_m1	-1.97	-3.92	-4.88	0.03	Yes
Nnat	Neuronatin (Nnat), transcript variant 1	Rn00440480_m1	-1.87	-3.66	-4.2	0.02	Yes
Ddah1	Dimethylarginine dimethylaminohydrolase 1	Rn00574200_m1	-1.69	-3.23	-3.36	0.02	Yes
Ntrk3	Neurotrophic tyrosine kinase, receptor, type 3	Rn00570389_m1	-1.69	-3.23	-2.33	0.06	Yes
Stat3	Signal transducer and activator of transcription 3	Rn00562562_m1	-1.49	-2.81	1.36	0.08	No
Dpp4	Dipeptidylpeptidase 4	Rn00562910_m1	-1.35	-2.55	-2.11	0.03	Yes
Ephx2	Epoxide hydrolase 2, cytoplasmic	Rn00576023_m1	-1.33	-2.51	-4.23	0.02	Yes
Gpc3	Glypican 3	Rn00516722_m1	-1.29	-2.45	-2.54	0.04	Yes
Fgf18	Fibroblast growth factor 18	Rn00433286_m1	-1.17	-2.25	-2.36	0.03	Yes
Tfpi	Tissue factor pathway inhibitor (lipoprotein-associated coagulation inhibitor)	Rn00567935_m1	-1.10	-2.14	1.12	0.06	No
Gckr	Glucokinase (hexokinase 4) regulator	Rn00565467_m1	-0.98	-1.97	-2.09	0.05	N/A
Cdkn1a	Cyclin-dependent kinase inhibitor 1A	Rn00589996_m1	-0.93	-1.91	-1.34	0.04	N/A
Bat5	HLA-B associated transcript 5	Rn01525709_g1	0.96	1.95	-1.3	0.06	N/A
Sele	Selectin E	Rn00594072_m1	1.02	2.03	2.35	0.14	Yes
Dbp	D site of albumin promoter (albumin D-box) binding protein	Rn00497539_m1	1.06	2.08	2.39	0.17	Yes
Abcg1	ATP-binding cassette, subfamily G (WHITE), member 1	Rn00585262_m1	1.08	2.11	1.99	0.14	No
Cyr61	Cysteine-rich, angiogenic inducer, 61	Rn00580055_m1	1.14	2.20	1.58	0.12	No
Ephx1	Epoxide hydrolase 1, microsomal	Rn00563349_m1	1.21	2.31	2.24	0.18	Yes
Prkce	Protein kinase C, epsilon	Rn01769089_m1	1.28	2.43	1.09	0.08	No
Nurp1	Nuclear protein, transcriptional regulator, 1	Rn00586046_m1	1.34	2.53	3.29	0.28	Yes
Slc16a7	Solute carrier family 16, member 7 (monocarboxylic acid transporter 2)	Rn00568872_m1	1.77	3.41	3.21	0.19	Yes
Atp2b2	ATPase, C ⁺⁺ transporting, plasma membrane 2	Rn01425460_m1	1.88	3.68	3.78	0.21	Yes

is involved in cellular ketone metabolic process according to GO and STRING protein–protein interaction analyses (e.g. down-regulation of cytochrome P450 2E1, (*Cyp2e1*); cytochrome P450 2J4, (*Cyp2j4*); and up-regulation of aldehyde dehydrogenase 1 family, member A1, (*Aldh1a1*); alcohol dehydrogenase 1, (*Adh1c*); aldo–keto reductase family 1, member B10, (*Akr1b10*); aldo–keto reductase family 1, member, *C12*, (*Akr1c12*); etc.) (Fig. 4; Table 4). It has been shown that 60 day old GK rats developed increased ketone body production [47], however, there is no literature data available about ketone body metabolism in the heart of GK rats. The ketone body acetone can be converted in vivo to glucose via acetol and pyruvate, and the initial conversion to acetol is catalyzed by *Cyp2e1* [48]. It has been shown that

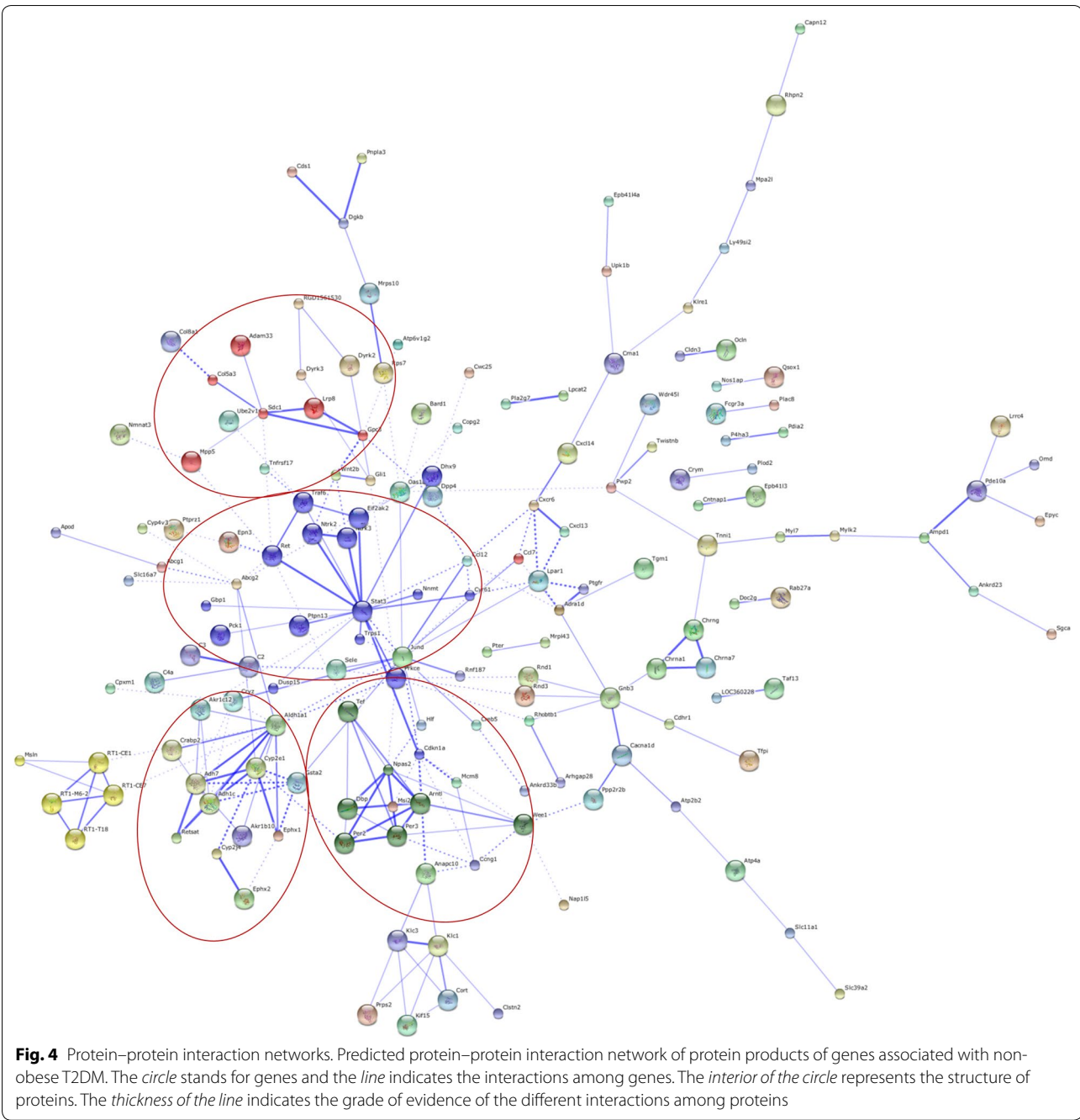
Cyp2e1 knockout mice subjected to starvation to induce ketogenesis develop blood acetone levels much higher than those observed in wild-type mice [48]. In our present study, the down-regulation of *Cyp2e1* might be a possible cause of increased ketone body level in the myocardium, however, up-regulation of other genes involved in ketone metabolic process including *Aldh1a1*; *Adh1c*; *Akr1b10*; and *Akr1c12* may be an adaptive response in the myocardium to antagonize elevated ketone body levels. Moreover, *Akr1b10* has been shown to be inducible by hyperglycemia in peripheral blood mononuclear cells obtained from patients with diabetic nephropathy. It also could have potential downstream effect of reducing cellular retinoic acid level, which is a key molecule during organogenesis as well as the development of diabetic

Table 4 Gene ontology analysis

Category	Term	Count	%	P value	Gene symbol
GOTERM_BP_1	GO:0065007 ~ biological regulation	48	41.74	0.01	FGF18, PDIA2, GPBP1, C3, CRABP2, TRIM16, ZEB2, LPAR1, ESM1, SGMS1, CCNG1, CD1D1, ALDH1A1, ATP2B2, CD47, NPAS2, DGKB, ZFP90, CXCR6, JUND, PER2, TEF, CHRNA7, CNTNAP1, TRAF6, QSOX1, DDAH1, DPP4, DPT, CYR61, RET, NCF1, NUCKS1, ARHGEF5, PRKAB2, LOC501307, ARNTL, PTGFR, PRKCE, TMEM189, STAT3, FMN1, TRPS1, KLRE1, GNB3, EIF2AK2, ICOSLG, BARD1
GOTERM_BP_2	GO:0006950 ~ response to stress	16	13.91	0.04	NCF1, PDIA2, C3, SGMS1, CD1D1, STAT3, ALDH1A1, ERCC8, SDC1, PLOD2, CHRNA7, TRAF6, EIF2AK2, DDAH1, DPP4, BARD1
GOTERM_BP_2	GO:0050789 ~ regulation of biological process	45	39.13	0.02	FGF18, PDIA2, GPBP1, C3, TRIM16, ZEB2, LPAR1, ESM1, SGMS1, CD1D1, ALDH1A1, ATP2B2, CD47, NPAS2, DGKB, ZFP90, CXCR6, JUND, PER2, TEF, CHRNA7, CNTNAP1, TRAF6, QSOX1, DDAH1, DPP4, DPT, CYR61, RET, NCF1, NUCKS1, ARHGEF5, PRKAB2, ARNTL, PTGFR, PRKCE, TMEM189, STAT3, FMN1, TRPS1, KLRE1, GNB3, EIF2AK2, ICOSLG, BARD1
GOTERM_BP_2	GO:0048518 ~ positive regulation of biological process	24	20.87	0.00	FGF18, C3, GPBP1, ZEB2, TRIM16, ARNTL, LPAR1, CD1D1, STAT3, FMN1, ALDH1A1, ATP2B2, CD47, NPAS2, JUND, KLRE1, TEF, CHRNA7, EIF2AK2, TRAF6, DDAH1, ICOSLG, CYR61, BARD1
GOTERM_BP_2	GO:0048646 ~ anatomical structure formation involved in morphogenesis	9	7.83	0.00	ALDH1A1, ATP2B2, FGF18, RET, RIPPLY2, ZEB2, TRAF6, DDAH1, CYR61
GOTERM_BP_2	GO:0009653 ~ anatomical structure morphogenesis	14	12.17	0.03	FMN1, ALDH1A1, ATP2B2, FGF18, SDC1, RET, EFNA2, CRABP2, RIPPLY2, ZEB2, TRAF6, DDAH1, STAT3, CYR61
GOTERM_BP_1	GO:0008152 ~ metabolic process	48	41.74	0.03	CYP2J4, OCLN, C3, CRABP2, TRIM50, TRIM16, LPAR1, SGMS1, ALDH1A1, ATP2B2, ERCC8, MCM8, ST6GALNAC3, PLOD2, ZFP90, CPOX, P4HA3, JUND, PER2, TEF, CHRNA7, TRAF6, QSOX1, DDAH1, DPP4, RET, NCF1, PRKAB2, LOC501307, ARNTL, CRYZ, TMEM189, LPCAT2, PRKCE, WEE1, STAT3, RPS7, OXSM, FMN1, TAF13, SLC16A7, AKR1B10, PLA2G7, CMA1, EIF2AK2, CAR6, PRPS2, BARD1
GOTERM_BP_2	GO:0044237 ~ cellular metabolic process	39	33.91	0.09	CYP2J4, OCLN, CRABP2, TRIM50, TRIM16, LPAR1, SGMS1, ALDH1A1, ATP2B2, ERCC8, MCM8, ST6GALNAC3, ZFP90, CPOX, JUND, PER2, TEF, CHRNA7, TRAF6, QSOX1, DDAH1, RET, NCF1, PRKAB2, LOC501307, ARNTL, TMEM189, PRKCE, LPCAT2, WEE1, STAT3, RPS7, OXSM, TAF13, SLC16A7, EIF2AK2, CAR6, PRPS2, BARD1
GOTERM_BP_3	GO:0034641 ~ cellular nitrogen compound metabolic process	19	16.52	0.09	OCLN, LOC501307, ARNTL, LPCAT2, STAT3, RPS7, ERCC8, ATP2B2, MCM8, TAF13, ZFP90, CPOX, JUND, TEF, PER2, CHRNA7, DDAH1, PRPS2, BARD1
GOTERM_BP_4	GO:0006575 ~ cellular amino acid derivative metabolic process	4	3.48	0.10	ATP2B2, OCLN, CHRNA7, LPCAT2
GOTERM_BP_3	GO:0010033 ~ response to organic substance	11	9.57	0.09	ALDH1A1, CYP2J4, SDC1, JUND, TRIM16, CHRNA7, GNB3, EIF2AK2, DDAH1, STAT3, CYR61
GOTERM_BP_4	GO:0014070 ~ response to organic cyclic substance	5	4.35	0.05	ALDH1A1, CYP2J4, JUND, CHRNA7, STAT3
GOTERM_BP_3	GO:0006629 ~ lipid metabolic process	9	7.83	0.08	ALDH1A1, CYP2J4, NCF1, CRABP2, PRKAB2, PLA2G7, SGMS1, LPCAT2, OXSM
GOTERM_BP_4	GO:0006720 ~ isoprenoid metabolic process	3	2.61	0.06	ALDH1A1, CYP2J4, CRABP2
GOTERM_BP_5	GO:0006720 ~ isoprenoid metabolic process	3	2.61	0.05	ALDH1A1, CYP2J4, CRABP2

Table 4 continued

Category	Term	Count	%	P value	Gene symbol
GOTERM_BP_5	GO:0001523 ~ retinoid metabolic process	3	2.61	0.02	ALDH1A1, CYP2J4, CRABP2
GOTERM_BP_4	GO:0042573 ~ retinoic acid metabolic process	2	1.74	0.10	ALDH1A1, CRABP2
GOTERM_BP_3	GO:0044255 ~ cellular lipid metabolic process	8	6.96	0.04	ALDH1A1, CYP2J4, NCF1, CRABP2, PRKAB2, SGMS1, LPCAT2, OXSM
GOTERM_BP_4	GO:0044255 ~ cellular lipid metabolic process	8	6.96	0.04	ALDH1A1, CYP2J4, NCF1, CRABP2, PRKAB2, SGMS1, LPCAT2, OXSM
GOTERM_BP_3	GO:0006082 ~ organic acid metabolic process	8	6.96	0.06	ALDH1A1, CYP2J4, SLC16A7, NCF1, CRABP2, PRKAB2, DDAH1, OXSM
GOTERM_BP_4	GO:0043436 ~ oxoacid metabolic process	8	6.96	0.06	ALDH1A1, CYP2J4, SLC16A7, NCF1, CRABP2, PRKAB2, DDAH1, OXSM
GOTERM_BP_5	GO:0019752 ~ carboxylic acid metabolic process	8	6.96	0.05	ALDH1A1, CYP2J4, SLC16A7, NCF1, CRABP2, PRKAB2, DDAH1, OXSM
GOTERM_BP_3	GO:0042180 ~ cellular ketone metabolic process	8	6.96	0.07	ALDH1A1, CYP2J4, SLC16A7, NCF1, CRABP2, PRKAB2, DDAH1, OXSM
GOTERM_BP_3	GO:0006721 ~ terpenoid metabolic process	3	2.61	0.02	ALDH1A1, CYP2J4, CRABP2
GOTERM_BP_4	GO:0016101 ~ diterpenoid metabolic process	3	2.61	0.02	ALDH1A1, CYP2J4, CRABP2
GOTERM_BP_5	GO:0006721 ~ terpenoid metabolic process	3	2.61	0.02	ALDH1A1, CYP2J4, CRABP2
GOTERM_BP_1	GO:0002376 ~ immune system process	10	8.70	0.05	CD47, NCF1, C3, RT1-T18, KLRE1, CHRNA7, TRAF6, CD1D1, DDAH1, DPP4
GOTERM_BP_2	GO:0045321 ~ leukocyte activation	5	4.35	0.06	KLRE1, CHRNA7, TRAF6, CD1D1, DPP4
GOTERM_BP_3	GO:0045321 ~ leukocyte activation	5	4.35	0.05	KLRE1, CHRNA7, TRAF6, CD1D1, DPP4
GOTERM_BP_4	GO:0046649 ~ lymphocyte activation	4	3.48	0.10	KLRE1, CHRNA7, CD1D1, DPP4
GOTERM_BP_2	GO:0006955 ~ immune response	7	6.09	0.06	CD47, NCF1, C3, RT1-T18, TRAF6, CD1D1, DDAH1
GOTERM_BP_2	GO:0002682 ~ regulation of immune system process	7	6.09	0.04	CD47, C3, KLRE1, TRAF6, CD1D1, DDAH1, DPP4
GOTERM_BP_3	GO:0050776 ~ regulation of immune response	6	5.22	0.02	C3, KLRE1, TRAF6, CD1D1, DDAH1, DPP4
GOTERM_BP_4	GO:0050776 ~ regulation of immune response	6	5.22	0.01	C3, KLRE1, TRAF6, CD1D1, DDAH1, DPP4
GOTERM_BP_5	GO:0002253 ~ activation of immune response	4	3.48	0.02	C3, KLRE1, TRAF6, DDAH1
GOTERM_BP_4	GO:0002697 ~ regulation of immune effector process	5	4.35	0.01	C3, KLRE1, TRAF6, CD1D1, DPP4
GOTERM_BP_5	GO:0002697 ~ regulation of immune effector process	5	4.35	0.00	C3, KLRE1, TRAF6, CD1D1, DPP4
GOTERM_BP_5	GO:0002706 ~ regulation of lymphocyte mediated immunity	5	4.35	0.00	C3, KLRE1, TRAF6, CD1D1, DPP4
GOTERM_BP_5	GO:0002703 ~ regulation of leukocyte mediated immunity	5	4.35	0.00	C3, KLRE1, TRAF6, CD1D1, DPP4
GOTERM_BP_4	GO:0002819 ~ regulation of adaptive immune response	4	3.48	0.01	C3, TRAF6, CD1D1, DPP4
GOTERM_BP_3	GO:0002682 ~ regulation of immune system process	7	6.09	0.04	CD47, C3, KLRE1, TRAF6, CD1D1, DDAH1, DPP4
GOTERM_BP_4	GO:0002684 ~ positive regulation of immune system process	6	5.22	0.02	CD47, C3, KLRE1, TRAF6, CD1D1, DDAH1
GOTERM_BP_2	GO:0002252 ~ immune effector process	4	3.48	0.05	CD47, NCF1, C3, DDAH1
GOTERM_BP_3	GO:0002252 ~ immune effector process	4	3.48	0.05	CD47, NCF1, C3, DDAH1
GOTERM_BP_4	GO:0006968 ~ cellular defense response	2	1.74	0.05	NCF1, DDAH1
GOTERM_BP_1	GO:0022610 ~ biological adhesion	7	6.09	0.09	CD47, SDC1, RET, CNTNAP1, COL5A3, BTBD9, CYR61
GOTERM_BP_2	GO:0007155 ~ cell adhesion	7	6.09	0.09	CD47, SDC1, RET, CNTNAP1, COL5A3, BTBD9, CYR61
GOTERM_BP_1	GO:0048511 ~ rhythmic process	7	6.09	0.00	ALDH1A1, NPAS2, JUND, PER2, TEF, CHRNA7, ARNTL
GOTERM_BP_2	GO:0007623 ~ circadian rhythm	4	3.48	0.01	NPAS2, JUND, PER2, ARNTL



nephropathy [49]. In our present study, non-obese T2DM also influenced expression of genes related to epoxide metabolism (down-regulation of Epoxide hydrolase 2, cytoplasmic, (*Ephx2*); glutathione S-transferase alpha 2, (*Gsta2*) and up-regulation of Epoxide hydrolase 1, microsomal, (xenobiotic) (*Ephx1*) (Fig. 3). Epoxides are possible products of Cyp450 catalyzed oxidation of aromatic compounds which can lead to toxic, mutagenic or carcinogenic effects [50]. One possibility for their inactivation

is the metabolism by epoxide hydrolases. In addition, glutathione-S-transferase catalyzed nucleophilic attack by glutathione may also lead to the inactivation of epoxides [50]. In our present study, *Cyp2e1*, *Cyp2j4*, *Ephx2* and *Gsta2* were down-regulated, showing decreased activity of epoxide metabolism. Moreover, glutathione S-transferase is a well-known enzyme catalyzing the conjugation of reduced glutathione on a wide variety of substrates including reactive oxygen and nitrogen species

[51, 52]. Our results suggest that down-regulation of the anti-oxidative gene *Gsta2* may contribute to elevated myocardial oxidative/nitrative stress, a phenomenon that has been demonstrated in T2DM by several studies [53, 54]. Interestingly, we have found overexpression of glutathione S-transferase in the heart in streptozotocin-induced DM in neonatal rats [22], metabolic syndrome [21] and cholesterol diet-induced hyperlipidaemia [55] in our previous studies. Moreover, polymorphism of *Ephx2* has been shown to be a possible risk factor for developing insulin resistance and T2DM [56]. In addition, polymorphisms of another gene, the cellular retinoic acid binding protein 2 (*Crapb2*, down-regulated in our present study) has been reported to be a genetic marker of metabolic syndrome [57] and hypercholesterolemia [58].

Genes related to diabetic cardiomyopathy

One of the major cardiovascular complications of DM is diabetic cardiomyopathy [59, 60], which is defined as left ventricular dysfunction with hypertrophy and fibrosis in the absence of hypertension, coronary artery disease and valvular or congenital heart disease [61]. The complex underlying molecular mechanisms of the above-mentioned functional and morphologic changes are not yet clear despite intensive investigations [59–61].

Structure elements

In our present study, we have shown altered expression of several genes playing a role in myocardial structure formation and potentially related to diabetic cardiomyopathy based on GO and STRING protein–protein interaction analyses. These altered genes include e.g. down-regulation of ADAM metalloproteinase domain 33 (*Adam33*); collagen, type V, alpha 3, (*Col5a3*); syndecan 1, (*Sdc1*); glypican 3 (*Gpc3*); troponin I type 1 (skeletal, slow) (*Tnni1*); myosin, light chain 7, regulatory (*Myl7*); myosin light chain kinase 2 (*Mylk2*) and up-regulation of collagen, type VIII, alpha 1, (*Col8a1*); etc. (Fig. 4; Table 4). Adam33 is a member of the ADAM protein family encoding a disintegrin and metalloprotease (ADAM) domain 33. It plays a role in cell–cell and cell–matrix interactions, including muscle development and neurogenesis and its polymorphism is associated with the development of T1DM [62]. Moreover, elevated type VIII collagen deposition in human diabetic nephropathy was demonstrated leading to the accumulation of extracellular matrix and periglomerular and interstitial fibrosis. Another ECM component, collagen V, is expressed as $\alpha 1(V)2 \alpha 2(V)$ heterotrimers, which regulate collagen fibril geometry and strength in several tissues including the pancreas and skeletal muscle. Interestingly, skeletal muscle of *Col5a3*^{−/−} mice was defective in glucose uptake and mobilization of intracellular GLUT4 glucose

transporter to the plasma membrane in response to insulin thereby leading to a glucose intolerant, insulin-resistant, and hyperglycemic phenotype [63]. Membrane proteoglycans Gpc3 and Sdc1 have not yet been demonstrated to play a role in the development of diabetic cardiomyopathy, however, increased expression of the heparan sulfate proteoglycans Gpc1 and Sdc4 has been shown to lead to diastolic dysfunction in streptozotocin-induced diabetic rats [64]. In addition, decreased expression of the genes playing a role in contractility including troponin I [65, 66], myosin light chain 7 [67] and myosin light chain kinase 2 [67] could lead to sarcomeric dysfunction and diabetic cardiomyopathy.

Receptors and ion channels

In our present study, several genes with receptor and/or ion channel function were found to be affected by non-obese T2DM and these genes might play a role in the development of diabetic cardiomyopathy. These genes include e.g. down-regulation of adrenoceptor alpha 1d (*Adra1d*); cholinergic receptor, nicotinic, gamma (muscle) (*Chrng*); cholinergic receptor, nicotinic, alpha 1 (muscle) (*Chrna1*); sarcolipin (*Sln*) and up-regulation of cholinergic receptor, nicotinic, alpha 7 (neuronal) (*Chrna7*); etc. Down-regulation of *Adra1d* receptor subtype has been previously shown in cardiac hypertrophy [68] and in STZ-induced DM by our research group [22]. Autonomic dysfunction is a serious complication of diabetes and can lead to cardiovascular abnormalities. It could be triggered by advanced glycation end products and reactive oxygen species mediated inactivation of neuronal nicotinic acetylcholine receptors, impairing synaptic transmission in sympathetic ganglia and resulting in autonomic failure [69]. Myocardial down-regulation of *Chrng* and *Chrna1* demonstrated in our present study might be another factor of cardiac autonomic dysfunction in diabetes. Moreover, it has been demonstrated that nicotinic cholinergic receptor alpha 7 (*Chrna7*) null mice showed decreased baroreflex-mediated tachycardia [70]. Sarcolipin (*Sln*) is a key regulator of sarcoplasmic reticulum Ca^{2+} -ATPase (SERCA) and mediator of β -adrenergic responses [71]. It has been shown that *Sln*^{−/−} mice are susceptible to develop atrial arrhythmias and interstitial fibrosis due to altered expression of genes encoding collagen [71]. Ablation or mutation of *Sln* results in increased SERCA activity and Ca^{2+} load, causing abnormal intracellular Ca^{2+} handling and atrial remodeling with dysfunction [71, 72].

Signal transduction, regulation of transcription and biological processes

A major cluster of significantly altered cardiac genes in response to non-obese T2DM was associated with signal

transduction, regulation of transcription and biological processes based on GO and STRING protein–protein interaction analyses (e.g. down-regulation of dipeptidyl-peptidase 4 (*Dpp4*); signal transducer and activator of transcription 3 (acute-phase response factor) (*Stat3*); ret proto-oncogene transcript variant 1 (*Ret*); neurotrophic tyrosine kinase, receptor, type 2 (*Ntrk2*); neurotrophic tyrosine kinase, receptor, type 3 (*Ntrk3*) and up-regulation of Jun D proto-oncogene (*Jund*); etc.) (Fig. 4; Table 4). Dipeptidyl peptidase-4 is an integral membrane glycoprotein which cleaves N-terminal dipeptides from peptide molecules. The cleaved dipeptides are bioactive molecules regulating the cardiovascular system as well. Dpp4 inhibitors have been reported to be cardioprotective in most of the preclinical and clinical studies in T2DM [73]. In contrast, some cardiovascular outcome studies revealed increased hospitalization rates for heart failure among a subset of DPP4 inhibitor-treated diabetic subjects [74]. Recently a preclinical study has reported that diabetic mice treated with Dpp4 inhibitor exhibited modest cardiac hypertrophy, impairment of cardiac function, and dysregulated expression of genes and proteins controlling inflammation and cardiac fibrosis [75]. In our present study, *Dpp4* was down-regulated; therefore it does not seem to be a major and/or necessary regulator in the development of diabetic cardiomyopathy in non-obese T2DM. The transcription factor *Stat3* participates in a wide variety of physiological processes including proliferation, apoptosis, and cardiac survival especially during myocardial ischemia/reperfusion injury, however, its role is contradictory in these aforementioned processes [76]. Several studies have reported that cardiac *Stat3* and *phospho-Stat3* expression were reduced in diabetes, which can lead to cardiac dysfunction [76–78]. However, other studies reported that cardiac *Stat3* and *phospho-Stat3* expression were increased in diabetes leading to hypertrophy [79, 80]. Furthermore, it has been also reported that *Stat3* deficient mice developed dilated cardiomyopathy [76] and patients with dilated cardiomyopathy had severely decreased myocardial *Stat3* expression [81]. In the present study, *Stat3* was down-regulated as assessed by microarray, however, qRT-PCR did not confirm these results in our hands. Expression of *Stat3* might depend on the duration of DM and the stage of diabetic cardiomyopathy or heart failure. Moreover, there is no literature data available about *Stat3* expression in hearts of GK rats; therefore we could not compare our results to others. Surprisingly, down-regulation of *Tef* and *Ret* as well as up-regulation of *Jund* has not been shown previously to play a role in the development of diabetic cardiomyopathy. It has been reported that *Ret*-deficient mice exhibited a reduced volume of cardiac ganglia and cholinergic innervation of the ventricular conduction

system [82]. JunD regulates genes involved in antioxidant defense and hydrogen peroxide (H_2O_2) production, as well as angiogenesis by controlling VEGF transcription [83]. Furthermore, an important function for JunD is to modulate insulin/insulin-like-growth factor 1 signaling and longevity [83]. Moreover, down-regulation of *Ntrk2* and *Ntrk3* genes might also play a role in the development of diabetic cardiomyopathy. Interestingly, it has been reported that mice with disrupted *Ntrk2* gene lacked a significant proportion of their intramyocardial blood vessels indicating that activation of the *Ntrk2* gene was crucial for normal vascularization of the developing heart [84]. In addition, mutations of *Ntrk3* gene have been shown in the development of human congenital heart diseases [85].

Genes related to immune and antimicrobial response

A major cluster of significantly altered cardiac genes in response to non-obese T2DM in GK rats was associated with immune and antimicrobial response based on GO and STRING protein–protein interaction analyses (e.g. complement component 3 (C3); *complement component 4a* (*C4a*); chemokine (C–C motif) ligand 12 (*Ccl12*); chemokine (C–X–C motif) ligand 13 (*Cxcl13*); chemokine (C–X–C motif) ligand 14 (*Cxcl14*); chymase 1, mast cell (*Cma1*) and up-regulation of chemokine (C–X–C motif) receptor 6 (*Cxcr6*); killer cell lectin-like receptor, family E, member 1 (*Klre1*); etc.) which is in line with the well-known increased susceptibility to infections in DM [86, 87].

Novel genes previously not related to diabetic alterations in the heart

Many of the genes showing altered expression in diabetic hearts in the present study have not yet been related to any diabetic alterations in the heart (e.g. down-regulation of low density lipoprotein receptor-related protein 8, apolipoprotein E receptor (*Lrp8*) and mesothelin (*Msln*) and up-regulation of kallikrein 1-related peptidase C3 (*Klk1c3*) and Epsin 3 (*Epn3*); etc.) (Table 4). Some other altered genes were not classified into specific functional clusters or indicated as yet uncharacterized, predicted genes and fragments (e.g. up-regulation of hydroxyacyl glutathione hydrolase-like and Similar to hepatic leukemia factor (*LOC690286*) or down-regulation of *uncharacterized LOC102546816* and similar to protein C17orf72; etc.) (Table 4), the relevance of which should not be ignored.

Limitations

Our study is not without limitations. Insulin resistance was estimated in our study by determining HOMA-IR rather than the gold standard hyperinsulinemic

euglycemic clamp technique. Nevertheless, the presence of insulin resistance in GK rats has been confirmed in several studies [88–91]. Although detailed morphological or histological analysis of GK hearts is lacking, our data including increased heart weight, heart weight to body weight ratio and coronary flow together with literature data suggest the development of LV hypertrophy in our model. Although our study does not specify which cell type (i.e. cardiomyocyte, fibroblast, smooth muscle cell, etc.) may be responsible for the observed alterations of cardiac gene expression due to DM, the contribution of cardiomyocytes is likely the most significant [92, 93]. In addition, it is unclear whether significantly altered gene expression changes at the mRNA level are further translated to changes in protein levels and if gene expression changes are causes or consequences of the development of diabetic cardiomyopathy, therefore, additional in-depth mechanistic studies should be carried out.

Conclusions

In summary, we have found that 15 week old male GK rats develop non-obese T2DM and we have demonstrated for the first time that non-obese T2DM is associated with a profound modification of the cardiac transcriptome. Some of the genes showing altered expression in the hearts of GK rats have been implicated in non-obese T2DM previously by other techniques. Some of the genes showing altered expression in our present study in non-obese T2DM have been reported to be associated with cardiac alterations in obese T2DM or T1DM models. Many of the genes showing significant expressional alterations in GK rat hearts in the present study have not been associated with non-obese T2DM previously. We conclude that non-obese T2DM alters the gene expression pattern of the myocardium. These altered genes may be involved in the development of cardiac pathologies in the state of non-obese type 2 diabetes mellitus. Based on our exploratory results, future studies should be carried out to investigate the precise role of specific genes in the development of cardiac consequences of non-obese T2DM to obtain deeper mechanistic insight.

Additional files

Additional file 1. Raw data of the DNA microarray.

Additional file 2. Additional Tables.

Abbreviations

Adra1d: adrenoceptor alpha 1d; Adam33: a disintegrin and metalloprotease domain 33; Adh1c: alcohol dehydrogenase 1; Akr1b10: aldo-keto reductase family 1, member B10; Akr1c12: aldo-keto reductase family 1, member, C12; Aldh1a1: aldehyde dehydrogenase 1 family, member A1; ANOVA: analysis of variance; AUC: area under the curve; C3: complement component 3; C4a: complement component 4a; Ccl12: chemokine (C–C motif) ligand 12; cDNA:

complementary deoxyribonucleic acid; Chrna1: cholinergic receptor, nicotinic, alpha 1 (muscle); Chrna7: cholinergic receptor, nicotinic, alpha 7 (neuronal); Chrng: cholinergic receptor, nicotinic, gamma (muscle); Cma1: chymase 1, mast cell; Col5a3: collagen, type V, alpha 3; Col8a1: collagen, type VIII, alpha 1; Crapb2: cellular retinoic acid binding protein 2; Cxcl13: chemokine (C–X–C motif) ligand 13; Cxcr6: chemokine (C–X–C motif) receptor 6; Cyp2e1: cytochrome P450 2E1; Cyp2j4: cytochrome P450 2J4; DAVID: Database for Annotation, Visualization and Integrated Discovery; DCM: diabetic cardiomyopathy; DNA: deoxyribonucleic acid; Dpp4: dipeptidylpeptidase 4; ELISA: enzyme linked immunosorbent assay; Ephx1: epoxide hydrolase 1, microsomal, (xenobiotic); Ephx2: epoxide hydrolase 2, cytoplasmic; Epn3: epsin 3; GAPDH: glyceraldehyde-3-phosphate dehydrogenase; GK rat: Goto-Kakizaki rat; GLUT4: glucose transporter 4; GO: gene ontology; Gpc3: glypican 3; Gsta2: glutathione S-transferase alpha 2; HOMA-IR: homeostasis model assessment-estimated insulin resistance; HPRT: hypoxanthine phosphoribosyl transferase; Jund: Jun D proto-oncogene; Klk1c3: kallikrein 1-related peptidase C3; Klr1: killer cell lectin-like receptor, family E, member 1; Lrp6: low density lipoprotein receptor-related protein 8, apolipoprotein E receptor; LV: left ventricular; mRNA: messenger ribonucleic acid; Msln: mesothelin; Myl7: myosin, light chain 7, regulatory; Mylk2: myosin light chain kinase 2; Ntrk: neurotrophic tyrosine kinase, receptor; OGTT: oral glucose tolerance test; qRT-PCR: quantitative real-time polymerase chain reaction; Ret: ret proto-oncogene transcript variant 1; RNA: ribonucleic acid; RPS18: ribosomal protein S18; Sdc1: syndecan 1; SEM: standard error of mean; SERCA: sarcoplasmic reticulum Ca²⁺-ATPase; Sln: sarcoplipin; Stat3: signal transducer and activator of transcription 3; STZ: streptozotocin; T1DM: type 1 diabetes mellitus; T2DM: type 2 diabetes mellitus; Tnni1: troponin I type 1 (skeletal, slow); ZDF rat: Zucker Diabetic Fatty rat.

Author contributions and consent for publication

PF, CC and TC conception and design of research; MS, GS, VF, MP, KE, RG, AS, JP and CC performed experiments; MS, GS, VF, MP, KE, RG, AS, AZ, CC, and TC analysed data; MS, GS, VF, MP, KE, RG, AS, AZ, CC, and TC interpreted results of experiments; MS, SA, and MP prepared figures and tables; MS and TC drafted manuscript; MS, PF, CC, and TC edited and revised manuscript; MS, GS, VF, MP, KE, RG, AS, JP, AZ, PF, CC, and TC approved final version of manuscript. All authors read and approved the final manuscript.

Author details

¹ Department of Biochemistry, Faculty of Medicine, University of Szeged, Dóm tér 9, Szeged 6720, Hungary. ² Department of Physiology, Anatomy and Neuroscience, Faculty of Science and Informatics, University of Szeged, Szeged, Hungary. ³ Department of Genetics, Cell- and Immunobiology, Semmelweis University, Budapest, Hungary. ⁴ Pharmahungary Group, Szeged, Hungary. ⁵ Department of Pharmacology and Pharmacotherapy, Semmelweis University, Budapest, Hungary.

Acknowledgements

We acknowledge the excellent technical support of Szilvia Török and Anikó Pósa for blood sampling and insulin assays, of Ágnes Semsei for performing qRT-PCR measurements, Ágnes Zvara for advices in protein–protein interaction analysis and Jeremy Parrott language editor for proofreading the manuscript.

Availability of data and materials

The conclusions of the manuscript are based on relevant data sets available in the manuscript and in Additional file tables.

Competing interests

Béres Pharmaceuticals Ltd., Pharmahungary Group and University of Szeged had a consortial grant funded by the National Development Agency (MED_FOOD TECH_08-A1-2008-0275). P.F. is the founder and CEO and T.C. and C.C. were involved in the management of Pharmahungary Group, a pharmaceutical/biotechnological company partially financing the current study.

Sources of funding

Ányos Jedlik program (MED_FOOD TECH_08-A1-2008-0275), Gábor Baross program (DA_TECH_07-METABET), the Hungarian Scientific Research Fund (OTKA K115990), CC holds a “Bolyai Fellowship” from the Hungarian Academy of Sciences. G.S. is financed by the MTA Postdoctoral Fellowship Programme. This article was supported by GINOP-2.3.2-15-2016-00006 financed by the Hungarian Government and co-financed by the European Structural Fund.

Received: 11 April 2016 Accepted: 14 July 2016

Published online: 05 August 2016

References

- Korkmaz-Icöz S, Lehner A, Li S, Vater A, Radovits T, Hegedűs P, et al. Mild Type 2 diabetes mellitus reduces the susceptibility of the heart to ischemia/reperfusion injury: identification of underlying gene expression changes. *J Diabetes Res*. 2015;2015:396414.
- Global status report on noncommunicable diseases 2014. Geneva: WHO; 2014. <http://www.who.int/global-coordination-mechanism/publications/global-status-report-ncds-2014-eng.pdf>. Accessed 29 Mar 2016.
- Danaei G, Finucane MM, Lu Y, Singh GM, Cowan MJ, Paciorek CJ, et al. National, regional, and global trends in fasting plasma glucose and diabetes prevalence since 1980: systematic analysis of health examination surveys and epidemiological studies with 370 country-years and 2.7 million participants. *Lancet*. 2011;378:31–40.
- Whiting DR, Guariguata L, Weil C, Shaw J. IDF diabetes atlas: global estimates of the prevalence of diabetes for 2011 and 2030. *Diabetes Res Clin Pract*. 2011;94:311–2.
- Wild S, Roglic G, Green A, Sicree R, King H. Global prevalence of diabetes: estimates for the year 2000 and projections for 2030. *Diabetes Care*. 2004;27:1047–53.
- Zimmet P, Alberti KG, Shaw J. Global and societal implications of the diabetes epidemic. *Nature*. 2001;414:782–7.
- Vaag A, Lund SS. Non-obese patients with type 2 diabetes and prediabetic subjects: distinct phenotypes requiring special diabetes treatment and (or) prevention? *Appl Physiol Nutr Metab*. 2007;32:912–20.
- Dalton M, Cameron AJ, Zimmet PZ, Shaw JE, Jolley D, Dunstan DW, et al. Waist circumference, waist-hip ratio and body mass index and their correlation with cardiovascular disease risk factors in Australian adults. *J Intern Med*. 2003;254:555–63.
- Mohan V, Deepa R. Adipocytokines and the expanding 'Asian Indian Phenotype'. *J Assoc Physicians India*. 2006;54:685–6.
- Devanathan S, Nemanich ST, Kovacs A, Fettig N, Gropler RJ, Shoghi KI. Genomic and metabolic disposition of non-obese type 2 diabetic rats to increased myocardial fatty acid metabolism. *PLoS ONE*. 2013;8:e78477.
- Manson JE, Colditz GA, Stampfer MJ, Willett WC, Krolevski AS, Rosner B, et al. A prospective study of maturity-onset diabetes mellitus and risk of coronary heart disease and stroke in women. *Arch Intern Med*. 1991;151:1141–7.
- Wilson PW. Diabetes mellitus and coronary heart disease. *Endocrinol Metab Clin North Am*. 2001;30:857–81.
- Willett WC, Dietz WH, Colditz GA. Guidelines for healthy weight. *N Engl J Med*. 1999;341:427–34.
- Adlerberth AM, Rosengren A, Wilhelmsen L. Diabetes and long-term risk of mortality from coronary and other causes in middle-aged Swedish men. A general population study. *Diabetes Care*. 1998;21:539–45.
- Asrih M, Steffens S. Emerging role of epigenetics and miRNA in diabetic cardiomyopathy. *Cardiovasc Pathol*. 2013;22(2):117–25.
- Wang J, Song Y, Wang Q, Kralik PM, Epstein PN. Causes and characteristics of diabetic cardiomyopathy. *Rev Diabet Stud*. 2006;3:108–17.
- Rubler S, Dlugash J, Yuceoglu YZ, Kumral T, Branwood AW, Grishman A. New type of cardiomyopathy associated with diabetic glomerulosclerosis. *Am J Cardiol*. 1972;30:595–602.
- Voulgari C, Papadogiannis D, Tentolouris N. Diabetic cardiomyopathy: from the pathophysiology of the cardiac myocytes to current diagnosis and management strategies. *Vasc Health Risk Manag*. 2010;6:883–903.
- Solomon SD, St John Sutton M, Lamas GA, Plappert T, Rouleau JL, Skali H, et al. Ventricular remodeling does not accompany the development of heart failure in diabetic patients after myocardial infarction. *Circulation*. 2002;106:1251–5.
- Chandler MP, Morgan EE, McElfresh TA, Kung TA, Rennison JH, Hoit BD, et al. Heart failure progression is accelerated following myocardial infarction in type 2 diabetic rats. *Am J Physiol Heart Circ Physiol*. 2007;293:H1609–16.
- Sárközy M, Zvara A, Gyémánt N, Fekete V, Kocsis GF, Pipis J, et al. Metabolic syndrome influences cardiac gene expression pattern at the transcript level in male ZDF rats. *Cardiovasc Diabetol*. 2013;12:16.
- Sárközy M, Szűcs G, Pipicz M, Zvara Á, Éder K, Fekete V, et al. The effect of a preparation of minerals, vitamins and trace elements on the cardiac gene expression pattern in male diabetic rats. *Cardiovasc Diabetol*. 2015;14:85.
- Ghanaat-Pour H, Huang Z, Lehtihet M, Sjöholm A. Global expression profiling of glucose-regulated genes in pancreatic islets of spontaneously diabetic Goto-Kakizaki rats. *J Mol Endocrinol*. 2007;39:135–50.
- Homo-Delarche F, Calderari S, Irminger JC, Gangnerau MN, Coulaud J, Rickenbach K, et al. Islet inflammation and fibrosis in a spontaneous model of type 2 diabetes, the GK rat. *Diabetes*. 2006;55:1625–33. Erratum in: *Diabetes*. 2006; 55:2665.
- Zhou H, Saito S, Piao G, Liu ZP, Wang J, Horimoto K, et al. Network screening of Goto-Kakizaki rat liver microarray data during diabetic progression. *BMC Syst Biol*. 2011;5(Suppl 1):S16.
- Nie J, Xue B, Sukumaran S, Jusko WJ, Dubois DC, Almon RR. Differential muscle gene expression as a function of disease progression in Goto-Kakizaki diabetic rats. *Mol Cell Endocrinol*. 2011;338:10–7.
- Herrera BM, Lockstone HE, Taylor JM, Ria M, Barrett A, Collins S, et al. Global microRNA expression profiles in insulin target tissues in a spontaneous rat model of type 2 diabetes. *Diabetologia*. 2010;53:1099–109.
- Abdul-Rahman O, Sasvari-Szekely M, Ver A, Rosta K, Szasz BK, Kereszturi E, et al. Altered gene expression profiles in the hippocampus and prefrontal cortex of type 2 diabetic rats. *BMC Genom*. 2012;13:81.
- Ostenson CG, Efendic S. Islet gene expression and function in type 2 diabetes; studies in the Goto-Kakizaki rat and humans. *Diabetes Obes Metab*. 2007;9(Suppl 2):180–6.
- Goto Y, Kakizaki M, Masaki N. Production of spontaneous diabetic rats by repetition of selective breeding. *Tohoku J Exp Med*. 1976;119:85–90.
- Goto Y, Suzuki K, Ono T, Sasaki M, Toyota T. Development of diabetes in the non-obese NIDDM rat (GK rat). *Adv Exp Med Biol*. 1988;246:29–31.
- Movassat J, Calderari S, Fernández E, Martín MA, Escrivá F, Plachot C, et al. Type 2 diabetes—a matter of failing beta-cell neogenesis? Clues from the GK rat model. *Diabetes Obes Metab*. 2007;9(Suppl 2):187–95.
- Galli J, Li LS, Glaser A, Ostenson CG, Jiao H, Fakhrai-Rad H, et al. Genetic analysis of non-insulin dependent diabetes mellitus in the GK rat. *Nat Genet*. 1996;12:31–7.
- Ostenson CG. The pathophysiology of type 2 diabetes mellitus: an overview. *Acta Physiol Scand*. 2001;171:241–7.
- D'Souza A, Howarth FC, Yanni J, Dobryznski H, Boyett MR, Adeghate E, Bidasee KR, Singh J. Left ventricle structural remodelling in the prediabetic Goto-Kakizaki rat. *Exp Physiol*. 2011;96:875–88.
- Grönholm T, Cheng ZJ, Palojoki E, Eriksson A, Bäcklund T, Vuolteenaho O, Finckenberg P, Laine M, Mervaala E, Tikkanen I. Vasopeptidase inhibition has beneficial cardiac effects in spontaneously diabetic Goto-Kakizaki rats. *Eur J Pharmacol*. 2005;519:267–76.
- Kocsis GF, Sárközy M, Bencsik P, Pipicz M, Varga ZV, Pálóczi J, et al. Pre-conditioning protects the heart in a prolonged uremic condition. *Am J Physiol Heart Circ Physiol*. 2012;303:H1229–36.
- Sárközy M, Fekete V, Szűcs G, Török S, Szűcs C, Bárkányi J, et al. Anti-diabetic effect of a preparation of vitamins, minerals and trace elements in diabetic rats: a gender difference. *BMC Endocr Disord*. 2014;14:72.
- Barr EL, Cameron AJ, Balkau B, Zimmet PZ, Welborn TA, Tonkin AM, et al. HOMA insulin sensitivity index and the risk of all-cause mortality and cardiovascular disease events in the general population: the Australian Diabetes, Obesity and Lifestyle Study (AusDiab) study. *Diabetologia*. 2010;53:79–88.
- Csont T, Bereczki E, Bencsik P, Fodor G, Görbe A, Zvara A, et al. Hypercholesterolemia increases myocardial oxidative and nitrosative stress thereby leading to cardiac dysfunction in apoB-100 transgenic mice. *Cardiovasc Res*. 2007;76:100–9.
- Csont T, Sárközy M, Szűcs G, Szűcs C, Bárkányi J, Bencsik P, et al. Effect of a multivitamin preparation supplemented with phytosterol on serum lipids and infarct size in rats fed with normal and high cholesterol diet. *Lipids Health Dis*. 2013;12:138.
- Skov V, Thomassen M, Riley CH, Jensen MK, Bjerrum OW, Kruse TA, et al. Gene expression profiling with principal component analysis depicts the biological continuum from essential thrombocythemia over polycythemia vera to myelofibrosis. *Exp Hematol*. 2012;40(771–780):e19.
- Weirauch MT. Gene coexpression networks for the analysis of DNA microarray data. *Applied statistics for network biology: methods in systems biology*. 2011; doi:10.1002/9783527638079.ch11.

44. D'Souza A, Howarth FC, Yanni J, Dobrzynski H, Boyett MR, Adeghate E, Bidasee KR, Singh J. Chronic effects of mild hyperglycaemia on left ventricle transcriptional profile and structural remodelling in the spontaneously type 2 diabetic Goto-Kakizaki rat. *Heart Fail Rev*. 2014;19:65–74.
45. Salem KA, Qureshi MA, Sydorenko V, Parekh K, Jayaprakash P, Iqbal T, Singh J, Oz M, Adrian TE, Howarth FC. Effects of exercise training on excitation-contraction coupling and related mRNA expression in hearts of Goto-Kakizaki type 2 diabetic rats. *Mol Cell Biochem*. 2013;380:83–96.
46. Gaber EM, Jayaprakash P, Qureshi MA, Parekh K, Oz M, Adrian TE, Howarth FC. Effects of a sucrose-enriched diet on the pattern of gene expression, contraction and Ca^{2+} transport in Goto-Kakizaki type 2 diabetic rat heart. *Exp Physiol*. 2014;99:881–93.
47. Zhao LC, Zhang XD, Liao SX, Gao HC, Wang HY, Lin DH. A metabonomic comparison of urinary changes in Zucker and GK rats. *J Biomed Biotechnol*. 2010;2010:431894.
48. Palmer M. Combination treatment of epilepsy with ketogenic diet and concurrent pharmacological inhibition of cytochrome P450 2E1. *Med Hypotheses*. 2013;80:481–5.
49. Shaw N, Yang B, Millward A, Demaine A, Hodgkinson A. AKR1B10 is induced by hyperglycaemia and lipopolysaccharide in patients with diabetic nephropathy. *Cell Stress Chaperones*. 2014;19:281–7.
50. Schladt L, Wörner W, Setiabudi F, Oesch F. Distribution and inducibility of cytosolic epoxide hydrolase in male Sprague-Dawley rats. *Biochem Pharmacol*. 1986;35:3309–16.
51. Douglas KT. Mechanism of action of glutathione-dependent enzymes. *Adv Enzymol Relat Areas Mol Biol*. 1987;59:103–67.
52. L'Ecuyer T, Allebban Z, Thomas R, Vander Heide R. Glutathione S-transferase overexpression protects against anthracycline-induced H9C2 cell death. *Am J Physiol Heart Circ Physiol*. 2004;286:H2057–64.
53. Bhatt NM, Aon MA, Tocchetti CG, Shen X, Dey S, Ramirez-Correa G, et al. Restoring redox balance enhances contractility in heart trabeculae from type 2 diabetic rats exposed to high glucose. *Am J Physiol Heart Circ Physiol*. 2015;308:H291–302.
54. Mandavia CH, Aroor AR, Demarco VG, Sowers JR. Molecular and metabolic mechanisms of cardiac dysfunction in diabetes. *Life Sci*. 2013;92:601–8.
55. Puskas LG, Nagy ZB, Giricz Z, Onody A, Csonka C, Kitajka K, et al. Cholesterol diet-induced hyperlipidemia influences gene expression pattern of rat hearts: a DNA microarray study. *FEBS Lett*. 2004;562:99–104.
56. Ghattas MH, Amer MA. Possible role of microsomal epoxide hydrolase gene polymorphism as a risk factor for developing insulin resistance and type 2 diabetes mellitus. *Endocrine*. 2012;42:577–83.
57. Salazar J, Ferré R, Vallvé JC, Pocoví M, Cabezas MC, Masana L, et al. Two novel single nucleotide polymorphisms in the promoter of the cellular retinoic acid binding protein II gene (CRABP-II). *Mol Cell Probes*. 2003;17:21–3.
58. Salazar J, Guardiola M, Ferré R, Coll B, Alonso-Villaverde C, Winkhofer-Roob BM, et al. Association of a polymorphism in the promoter of the cellular retinoic acid-binding protein II gene (CRABP2) with increased circulating low-density lipoprotein cholesterol. *Clin Chem Lab Med*. 2007;45:615–20.
59. Bugger H, Abel ED. Molecular mechanisms of DCM. *Diabetologia*. 2014;57:660–71.
60. Dhalla NS, Takeda N, Rodriguez-Leyva D, Elimban V. Mechanisms of subcellular remodeling in heart failure due to diabetes. *Heart Fail Rev*. 2014;19:87–99.
61. Wang J, Song Y, Wang Q, Kralik PM, Epstein PN. Causes and characteristics of DCM. *Rev Diabet Stud*. 2006;3:108–17.
62. Smyth DJ, Howson JM, Payne F, Maier LM, Bailey R, Holland K, et al. Analysis of polymorphisms in 16 genes in type 1 diabetes that have been associated with other immune-mediated diseases. *BMC Med Genet*. 2006;7:20.
63. Huang G, Ge G, Wang D, Gopalakrishnan B, Butz DH, Colman RJ, et al. $\alpha 3(\text{V})$ collagen is critical for glucose homeostasis in mice due to effects in pancreatic islets and peripheral tissues. *J Clin Invest*. 2011;121:769–83.
64. Strunz CM, Matsuda M, Salemi VM, Nogueira A, Mansur AP, Cestari IN, et al. Changes in cardiac heparan sulfate proteoglycan expression and streptozotocin-induced diastolic dysfunction in rats. *Cardiovasc Diabetol*. 2011;10:35.
65. Aydemir-Koksoy A, Bilginoglu A, Sariahmetoglu M, Schulz R, Turan B. Antioxidant treatment protects diabetic rats from cardiac dysfunction by preserving contractile protein targets of oxidative stress. *J Nutr Biochem*. 2010;21:827–33.
66. Dhalla N, Takeda N, Rodriguez-Leyva D, Elimban V. Mechanisms of subcellular remodeling in heart failure due to diabetes. *Heart Fail Rev*. 2014;19:87–99.
67. Liu X, Takeda N, Dhalla NS. Myosin light-chain phosphorylation in diabetic cardiomyopathy in rats. *Metabolism*. 1997;46:71–5.
68. Rokosh DG, Stewart AF, Chang KC, Bailey BA, Karliner JS, Camacho SA, et al. Alpha1-adrenergic receptor subtype mRNAs are differentially regulated by alpha1-adrenergic and other hypertrophic stimuli in cardiac myocytes in culture and in vivo. Repression of alpha1B and alpha1D but induction of alpha1C. *J Biol Chem*. 1996;271:5839–43.
69. Chandna AR, Nair M, Chang C, Pennington PR, Yamamoto Y, Mousseau DD, et al. RAGE mediates the inactivation of nAChRs in sympathetic neurons under high glucose conditions. *Eur J Neurosci*. 2015;41:341–51.
70. Franceschini D, Orr-Urtreger A, Yu W, Mackey LY, Bond RA, Armstrong D, et al. Altered baroreflex responses in alpha7 deficient mice. *Behav Brain Res*. 2000;113:3–10.
71. Xie LH, Shanmugam M, Park JY, Zhao Z, Wen H, Tian B, et al. Ablation of sarcolipin results in atrial remodeling. *Am J Physiol Cell Physiol*. 2012;302:C1762–71.
72. Shanmugam M, Li D, Gao S, Fefelova N, Shah V, Voit A, et al. Cardiac specific expression of threonine 5 to alanine mutant sarcolipin results in structural remodeling and diastolic dysfunction. *PLoS ONE*. 2015;10:e0115822.
73. Bando YK, Murohara T. Heart Failure as a Comorbidity of Diabetes: role of Dipeptidyl Peptidase 4. *J Atheroscler Thromb*. 2016;23:147–54.
74. Son JW, Kim S. Dipeptidyl Peptidase 4 Inhibitors and the Risk of Cardiovascular Disease in Patients with Type 2 Diabetes: a Tale of Three Studies. *Diabetes Metab J*. 2015;39:373–83.
75. Mulvihill EE, Varin EM, Ussher JR, Campbell JE, Bang KW, Abdullah T, et al. Inhibition of Dipeptidyl Peptidase-4 impairs ventricular function and promotes cardiac fibrosis in high fat-fed diabetic mice. *Diabetes*. 2016;65:742–54.
76. Hilfiker-Kleiner D, Hilfiker A, Fuchs M, Kaminski K, Schaefer A, Schieffer B, et al. Signal transducer and activator of transcription 3 is required for myocardial capillary growth, control of interstitial matrix deposition, and heart protection from ischemic injury. *Circ Res*. 2004;95:187–95.
77. Xu J, Lei S, Liu Y, Gao X, Irwin MG, Xia ZY, et al. Antioxidant N-acetylcysteine attenuates the reduction of Brg1 protein expression in the myocardium of type 1 diabetic rats. *J Diabetes Res*. 2013;2013:716219.
78. Wang T, Qiao S, Lei S, Liu Y, Ng KF, Xu A, et al. N-acetylcysteine and allopurinol synergistically enhance cardiac adiponectin content and reduce myocardial reperfusion injury in diabetic rats. *PLoS ONE*. 2011;6:e23967.
79. Sun X, Chen RC, Yang ZH, Sun GB, Wang M, Ma XJ, et al. Taxifolin prevents diabetic cardiomyopathy in vivo and in vitro by inhibition of oxidative stress and cell apoptosis. *Food Chem Toxicol*. 2014;63:221–32.
80. Wang L, Li J, Li D. Losartan reduces myocardial interstitial fibrosis in diabetic cardiomyopathy rats by inhibiting JAK/STAT signaling pathway. *Int J Clin Exp Pathol*. 2015;8:466–73.
81. Podewski EK, Hilfiker-Kleiner D, Hilfiker A, Morawietz H, Lichtenberg A, Wollert KC, et al. Alterations in Janus kinase (JAK)-signal transducers and activators of transcription (STAT) signaling in patients with end-stage dilated cardiomyopathy. *Circulation*. 2003;107:798–802.
82. Hiltunen JO, Laurikainen A, Airaksinen MS, Saarna M. GDNF family receptors in the embryonic and postnatal rat heart and reduced cholinergic innervation in mice hearts lacking ret or GFRalpha2. *Dev Dyn*. 2000;219:28–39.
83. Meixner A, Karreth F, Kenner L, Penninger JM, Wagner EF. Jun and JunD-dependent functions in cell proliferation and stress response. *Cell Death Differ*. 2010;17:1409–19.
84. Wagner N, Wagner KD, Theres H, Englert C, Schedl A, Scholz H. Coronary vessel development requires activation of the TrkB neurotrophin receptor by the Wilms' tumor transcription factor Wt1. *Genes Dev*. 2005;19:2631–42.
85. Werner P, Paluru P, Simpson AM, Latney B, Iyer R, Brodeur GM, et al. Mutations in NTRK3 suggest a novel signaling pathway in human congenital heart disease. *Hum Mutat*. 2014;35:1459–68.
86. Lappas M. Lower circulating levels of complement split proteins C3a and C4a in maternal plasma of women with gestational diabetes mellitus. *Diabet Med*. 2011;28:906–11.

87. Berrou J, Fougeray S, Venot M, Chardiny V, Gautier JF, Dulphy N, et al. Natural killer cell function, an important target for infection and tumor protection, is impaired in type 2 diabetes. *PLoS ONE*. 2013;8:e62418.
88. Ishizaki N, Okushi N, Yano T, Yamamura Y. Improvement in glucose tolerance as a result of enhanced insulin sensitivity during electroacupuncture in spontaneously diabetic Goto-Kakizaki rats. *Metabolism*. 2009;58:1372–8.
89. Iizuka Y, Ueda Y, Yagi Y, Sakurai E. Significant improvement of insulin resistance of GK rats by treatment with sodium selenate. *Biol Trace Elem Res*. 2010;138:265–71.
90. O'Rourke CM, Davis JA, Saltiel AR, Cornicelli JA. Metabolic effects of troglitazone in the Goto-Kakizaki rat, a non-obese and normolipidemic rodent model of non-insulin-dependent diabetes mellitus. *Metabolism*. 1997;46:192–8.
91. Muniyappa R, Lee S, Chen H, Quon MJ. Current approaches for assessing insulin sensitivity and resistance in vivo: advantages, limitations, and appropriate usage. *Am J Physiol Endocrinol Metab*. 2008;294:E15–26.
92. Bell RM, Yellon DM. Conditioning the whole heart—not just the cardiomyocyte. *J Mol Cell Cardiol*. 2012;53:24–32.
93. Cury DP, Dias FJ, Sosthenes MC, Dos Santos Haemmerle CA, Ogawa K, et al. Morphometric, quantitative, and three-dimensional analysis of the heart muscle fibers of old rats: transmission electron microscopy and high-resolution scanning electron microscopy methods. *Microsc Res Tech*. 2013;76:184–95.

Submit your next manuscript to BioMed Central and we will help you at every step:

- We accept pre-submission inquiries
- Our selector tool helps you to find the most relevant journal
- We provide round the clock customer support
- Convenient online submission
- Thorough peer review
- Inclusion in PubMed and all major indexing services
- Maximum visibility for your research




Submit your manuscript at
www.biomedcentral.com/submit



II.

Research Article

Prediabetes Induced by Fructose-Enriched Diet Influences Cardiac Lipidome and Proteome and Leads to Deterioration of Cardiac Function prior to the Development of Excessive Oxidative Stress and Cell Damage

Gergő Szűcs^{1,2} , **Andrea Sója**^{1,2}, **Mária Péter**³, **Márta Sárközy**^{1,2} , **Bella Bruszel**^{2,4}, **Andrea Siska**⁵, **Imre Földesi**⁵, **Zoltán Szabó**^{2,4}, **Tamás Janáky**^{2,4}, **László Vigh**³, **Gábor Balogh**³ and **Tamás Csont**^{1,2} 

¹Metabolic Diseases and Cell Signaling Group, Department of Biochemistry, Faculty of Medicine, University of Szeged, Szeged H-6720, Hungary

²Interdisciplinary Centre of Excellence, University of Szeged, Szeged H-6720, Hungary

³Institute of Biochemistry, Biological Research Center of the Hungarian Academy of Sciences, Szeged H-6726, Hungary

⁴Institute of Medical Chemistry, Faculty of Medicine, University of Szeged, Szeged H-6720, Hungary

⁵Department of Laboratory Medicine, Faculty of Medicine, University of Szeged, Szeged H-6720, Hungary

Correspondence should be addressed to Gergő Szűcs; szucs.gergo@med.u-szeged.hu and Tamás Csont; csont.tamas@med.u-szeged.hu

Received 21 June 2019; Revised 3 October 2019; Accepted 16 October 2019; Published 9 December 2019

Guest Editor: Konstantin Lyamzaev

Copyright © 2019 Gergő Szűcs et al. This is an open access article distributed under the Creative Commons Attribution License, which permits unrestricted use, distribution, and reproduction in any medium, provided the original work is properly cited.

Prediabetes is a condition affecting more than 35% of the population. In some forms, excessive carbohydrate intake (primarily refined sugar) plays a prominent role. Prediabetes is a symptomless, mostly unrecognized disease which increases cardiovascular risk. In our work, we examined the effect of a fructose-enriched diet on cardiac function and lipidome as well as proteome of cardiac muscle. Male Wistar rats were divided into two groups. The control group received a normal diet while the fructose-fed group received 60% fructose-supplemented chow for 24 weeks. Fasting blood glucose measurement and oral glucose tolerance test (OGTT) showed slightly but significantly elevated values due to fructose feeding indicating development of a prediabetic condition. Both echocardiography and isolated working heart perfusion performed at the end of the feeding protocol demonstrated diastolic cardiac dysfunction in the fructose-fed group. Mass spectrometry-based, high-performance lipidomic and proteomic analyses were executed from cardiac tissue. The lipidomic analysis revealed complex rearrangement of the whole lipidome with special emphasis on defects in cardiolipin remodeling. The proteomic analysis showed significant changes in 75 cardiac proteins due to fructose feeding including mitochondria-, apoptosis-, and oxidative stress-related proteins. Nevertheless, just very weak or no signs of apoptosis induction and oxidative stress were detected in the hearts of fructose-fed rats. Our results suggest that fructose feeding induces marked alterations in the cardiac lipidome, especially in cardiolipin remodeling, which leads to mitochondrial dysfunction and impaired cardiac function. However, at the same time, several adaptive responses are induced at the proteome level in order to maintain a homeostatic balance. These findings demonstrate that even very early stages of prediabetes can impair cardiac function and can result in significant changes in the lipidome and proteome of the heart prior to the development of excessive oxidative stress and cell damage.

1. Introduction

Diabetes mellitus is a heterogeneous chronic metabolic disorder characterized by hyperglycemia [1]. The number of people suffering from diabetes increased from 108 million in 1980 to 422 million by 2014, and global prevalence almost doubled since 1980, from 4.7% to 8.5% [2]. According to the International Diabetes Federation, the number of people with diabetes may rise to 629 million by 2045 [3]. Prediabetes—in which glucose levels do not meet the criteria for diabetes but are too high to be considered normal—usually precedes diabetes mellitus and may remain symptomless for several years [4]. Prediabetes affects more than 35% of the population, and it is known that even nondiabetic levels of hyperglycemia and impaired glucose tolerance may be associated with an elevated risk of cardiovascular disease [5]. It has been recently shown that a mild diastolic dysfunction occurs even in prediabetic rats [6].

Type 2 diabetes is associated with myocardial lipotoxicity [7], which can cause impaired mitochondrial function [8]. Impaired mitochondrial function enhances oxidative stress, activates apoptosis, and thus contributes to cardiac dysfunction [7, 9, 10]. Although the role of lipotoxicity, oxidative stress, and apoptosis in diabetes has been well studied, the role of these mechanisms in prediabetes has not yet been well described. Saccharose and high-fructose corn syrup (isoglucose) are often used as sweeteners in the food and drink industry, and the consumption of these fructose-rich foods or beverages has an adverse effect on both animals [11] and humans [12]. A high-fructose diet is often used as a model of prediabetes or impaired glucose tolerance. After absorption, fructose is rapidly and uncontrollably absorbed in the liver, where its metabolism increases *de novo* lipogenesis (DNL). Induction of DNL has the capacity to alter the circulating nonesterified fatty acid (FA) profile, which, in turn, might affect cardiac lipid composition [13].

Proper cardiac lipid composition is strongly correlated with cardiac function and largely relies on proper cardiolipin (CL) content and species profile [14]. CL is the hallmark phospholipid (PL) of mitochondria that plays a role in many mitochondrial processes, including respiration and energy conversion. The heart is full of mitochondria, and CL accounts for about 10–15 mol% of all membrane lipids. Changes in the CL pool due to either oxidation or pathological remodeling cause mitochondrial dysfunctions and trigger retrograde signaling pathways that are associated with a large number of cardiac diseases including diabetes [15]. It is widely accepted that the symmetric tetralinoleoyl (18:2) CL species, which constitutes up to 80% of mammalian cardiac CL, is required for mitochondria to work optimally in metabolically active tissues [16]. After its initial biosynthesis, premature CL undergoes intensive remodeling processes to produce matured CL (Supplementary Lipid Figure 1) [14, 15, 17–19]. In the first step of maturation, the removal of a single acyl chain is executed by a calcium-independent phospholipase A_2 to produce monolysocardiolipin (MLCL). Reacylation can be carried out by CoA-dependent acyltransferases or a CoA-independent reversible PL-lysoPL (LPL) transacylase called

tafazzin. Tafazzin itself lacks acyl chain preference; still, it is believed to be the major enzyme involved in CL remodeling to produce homo-acylated CL [16]. Mutations in tafazzin cause abnormal molecular species of CL and the clinical phenotype of Barth syndrome, a rare and often fatal x-linked genetic disorder characterized by dilated cardiomyopathy, skeletal myopathy, and neutropenia [20].

Although CL is known to be relatively resistant to dietary manipulations, by “appropriate” interventions, the linoleoyl chain can be replaced [21]. Fructose feeding might represent such an intervention due to its highly lipogenic nature. Therefore, our study is aimed at examining the effects of fructose-enriched diet on the interplay of cardiac function, cardiac lipidome and proteome, and oxidative stress and apoptosis in a rat prediabetes model. To achieve this goal, several methods and techniques were applied including conventional blood tests, detailed serum analysis, enzymatic assays, protein expression analyses, transthoracic echocardiography, and high-performance mass spectrometry- (MS-) based proteomics and lipidomics.

2. Materials and Methods

This investigation conformed to the National Institutes of Health *Guide for the Care and Use of Laboratory Animals* (NIH Publication No. 85-23, Revised 1996) and was approved by the Animal Research Ethics Committee of University of Szeged.

2.1. Experimental Design. Male Wistar rats (310–450 g, $n = 16$ in the entire study) were kept under controlled temperature with 12/12 h light/dark cycles. Animals were divided into two groups and were fed with the following diets for 24 weeks: the control group ($n = 8$) was fed with a standard laboratory chow, while the fructose-fed group ($n = 8$) received a chow containing 60% fructose. Fasting blood glucose was measured every 4 weeks, while at weeks 12, 16, 20, and 24 oral glucose tolerance tests (OGTT) were performed. At week 20 and week 24, blood samples were taken to measure serum parameters. At the end of the feeding protocol, cardiac function was assessed by both *in vivo* echocardiography and *ex vivo* working heart perfusions (Figure 1). Following the perfusions, myocardial tissue was harvested for biochemical analysis.

2.2. Transthoracic Echocardiography. Cardiac morphology and function were assessed by transthoracic echocardiography at week 24 as described previously [22–24]. Briefly, rats were anesthetized with sodium pentobarbital (Euthasol, 40 mg/kg body weight *i.p.*). Then, the chest was shaved, and the rat was placed in a supine position onto a heating pad. Two-dimensional, M-mode, and Doppler echocardiographic examinations were performed by the criteria of the American Society of Echocardiography with a Vivid IQ ultrasound system (General Electric Medical Systems) using a phased array 5.0–11 MHz transducer (GE 12S-RS probe). Data of three consecutive heart cycles were analyzed (EchoPac Dimension software; General Electric Medical Systems) by an experienced investigator in a blinded

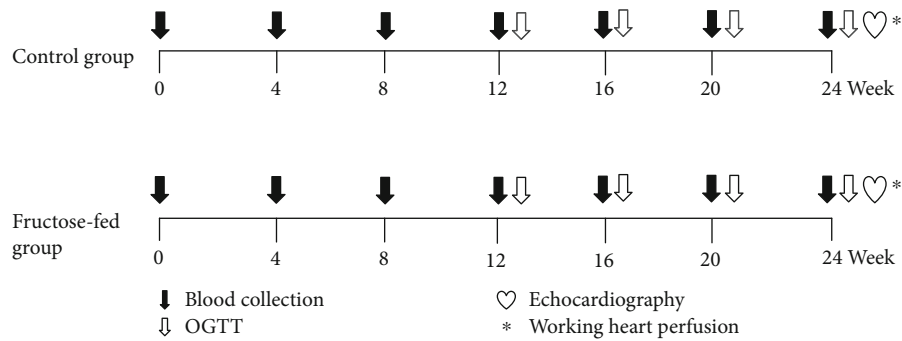


FIGURE 1: Experimental protocol. Male Wistar rats were divided into control ($n = 8$) and fructose-fed ($n = 8$) groups receiving either a standard chow or a chow supplemented with 60% fructose, respectively, for 24 weeks. Fasting blood glucose measurement or oral glucose tolerance test (OGTT) was performed every four weeks to monitor the development of prediabetic condition. At week 24, transthoracic echocardiography was performed to monitor cardiac function and morphology. Then, the hearts of the animals were isolated and mounted on a working heart perfusion system to measure hemodynamic and pressure parameters. After the perfusions, hearts were frozen for measurement of biochemical parameters.

manner. Systolic and diastolic wall thickness parameters were obtained from parasternal short-axis view at the level of the papillary muscles (anterior and inferior walls) and long-axis view at the level of the mitral valve (septal and posterior walls). The left ventricular diameters were measured by means of M-mode echocardiography from long-axis views between the endocardial borders. Fractional shortening (FS) was used as a measure of cardiac contractility ($FS = (LVEDD - LVESD) / LVEDD \times 100$). Functional parameters including left ventricular end-diastolic volume (LVEDV) and left ventricular end-systolic volume (LVESV) were calculated on four-chamber view images delineating the endocardial borders in diastole and systole. The stroke volume was calculated as the difference of LVEDV and LVESV. The ejection fraction (EF) was calculated according to the formula $(LVEDV - LVESV) / LVEDV \times 100$. Diastolic function was assessed using pulse-wave Doppler across the mitral valve from the apical four-chamber view. Early (E) and atrial (A) flow velocities provide an indication of diastolic function. Heart rate was also calculated using pulse-wave Doppler images during the measurement of transvalvular flow velocity profiles according to the length of 3 consecutive heart cycles measured between the start points of the E waves. The mean values of three measurements were calculated and used for statistical evaluation.

2.3. Working Heart Perfusion. Immediately after the echocardiography, cardiac performance was assessed in isolated working rat hearts, as described earlier [25–27]. Anesthetized rats were given $500 \text{ U} \cdot \text{kg}^{-1}$ heparin intravenously. Hearts were then isolated, and the aorta was cannulated and initially perfused in Langendorff mode (at a constant pressure of 73 mmHg, 37°C) with Krebs-Henseleit buffer containing NaCl 118 mM, NaHCO_3 25 mM, KCl 4.3 mM, CaCl_2 2.4 mM, KH_2PO_4 1.2 mM, MgSO_4 1.2 mM, and glucose 11 mM, gassed with 95% O_2 and 5% CO_2 [22, 28]. Then, the perfusion system was switched to working mode according to Neely with recirculating buffer [28, 29]. Hydrostatic preload and afterload were kept constant at 13 mmHg and

73 mmHg, respectively, throughout the experiments. Hearts were subjected to 10 min equilibration period before measurement ($n = 7 - 8$). Cardiac functional parameters including heart rate, coronary flow, aortic flow, cardiac output, left ventricular developed pressure (LVDP) and its first derivatives (dp/dt max and dp/dt min), and left ventricular end-diastolic pressure (LVEDP) were measured. At the end of the perfusion, the hearts were weighed, and the left and right ventricles were separated. The right and left ventricles were snap frozen in liquid nitrogen and stored at -80°C until they were used for biochemical assays.

2.4. Measurement of Malondialdehyde Levels. In order to measure the level of systemic and cardiac lipid peroxidation, serum malondialdehyde and left ventricular tissue malondialdehyde were assayed spectrophotometrically at 535 nm as described previously [27, 30]. Results are expressed as nmol/mL serum and nmol/mg protein.

2.5. mRNA Expression Profiling by qRT-PCR. Quantitative RT-PCR was performed with gene-specific primers to monitor mRNA expression as described previously [24]. To assess de novo lipid synthesis, expression of sterol regulatory element-binding transcription factor 1 (Srebf1), stearoyl-CoA desaturase 1 (Scd1), stearoyl-CoA desaturase 2 (SCD2), fatty acid synthase (Fasn), acetyl-CoA carboxylase 1 (Acaca), carbohydrate-responsive element-binding protein (Mlxip1), elongation of very-long-chain fatty acids protein 6 (ELOVL6), fatty acid desaturase 1 (Fads1), and fatty acid desaturase 2 (Fads2) were measured from liver samples. To assess cardiac hypertrophy, expression of myosin heavy chain α isoform (MYH6) and myosin heavy chain β isoform (MYH7) was measured. RNA was isolated using Qiagen RNeasy Fibrous Tissue Mini Kit (Qiagen, #74704) from the liver and heart tissues. Briefly, $4 \mu\text{g}$ and $2.2 \mu\text{g}$ of total RNA from liver and heart samples, respectively, were reverse transcribed using iScript™ Advanced cDNA Synthesis kit (Bio-Rad, 1725038), and specific primers and SsoAdvanced™ Universal SYBR® Green Supermix (Bio-Rad) were

used according to the manufacturer's instructions. Hypoxanthine phosphoribosyltransferase 1 (Hprt1) was used as control for normalization.

2.6. Lipidomics. Approximately 20 mg of the powdered left ventricle was directly extracted by adding 1 mL of methanol containing 0.001% butylated hydroxytoluene as an antioxidant and 60 μ g di20:0 phosphatidylcholine as extraction standard. After a 5 min sonication in a water bath sonicator, the mixture was shaken for 5 min and centrifuged at $10000 \times g$ for 5 min. The supernatant was transferred into a new Eppendorf tube and stored at -20°C until mass spectrometry (MS) analysis.

The solvents used for extraction and MS analyses were of Optima LCMS grade from Thermo Fisher Scientific (Bremen, Germany) and liquid chromatographic grade from Merck (Darmstadt, Germany). Lipid standards were purchased from Avanti Polar Lipids (Alabaster, AL). All other chemicals were from Sigma-Aldrich (Steinheim, Germany) and were of the best available grade.

Mass spectrometric analyses were performed on an LTQ-Orbitrap Elite instrument (Thermo Fisher Scientific, Bremen, Germany) equipped with a robotic nanoflow ion source (TriVersa NanoMate; Advion BioSciences; Ithaca, NY, USA) as described in [31]. Further details of MS measurements and lipid species annotation are given in the Supplementary Methods.

2.7. Proteomics. Approximately 30 mg of powdered left ventricle tissue samples was homogenized in lysate buffer (containing 2% SDS and 0.1 M DTT in 0.1 Tris solution). The homogenized samples were incubated at 98°C for 5 min. Proteins were precipitated by the addition of methanol/chloroform mixture (4:1) and were resuspended in 8 M urea. The total protein contents were determined using BCA (Thermo) protocol. 20 μ g protein was digested by trypsin (Thermo) using RapiGest (Waters) detergent to enhance the digestion. In-gel fractionation was performed for pooled sample. In-gel fractionated samples were also digested by trypsin.

1D gel samples and pooled samples were measured in DDA (data-dependent acquisition) using a 90 min gradient on a Waters nanoAcquity-Thermo Q Exactive Plus LC-MS system to build a spectrum library of detectable peptides. The individual samples were measured in DIA (Data Independent Acquisition) mode for protein quantification with the same LC gradient using the spectrum library. The acquired data were analyzed with Encyclopedia [32] and statistically evaluated using Perseus [33] software. Enrichment of significantly changing proteins according to subcellular localization was carried out by Gene Ontology analysis (<https://www.ebi.ac.uk/QuickGO/>). Pathway assignment analysis of significantly altered proteins was performed with Reactome (<https://www.reactome.org>) after assignment to human genes, for higher annotation coverage. Further details of proteomic analysis are given in the Supplementary Methods.

2.8. Measurement of Serum and Pancreatic Insulin Levels. Serum and pancreatic insulin levels were measured by an

enzyme immunoassay (Mercodia, Ultrasensitive Rat Insulin ELISA) in order to verify the development of hyperinsulinemia and decreased pancreatic insulin content as a consequence of beta cell damage in impaired glucose tolerance. Insulin ELISA was carried out according to the instructions of the manufacturer from either sera or homogenized pancreatic tissue samples of fructose-fed and control rats. Sera were centrifuged (2000 g for 10 min at 4°C) and kept at -20°C until further investigation. Pancreata were removed, trimmed free of adipose tissue, and weighed. Pancreata were homogenized in 6 mL cold acidified ethanol (0.7 M HCl:ethanol (1:3 v/v)) with an Ultra Turrax homogenizer and were kept at 4°C for 24 h. Then, pancreas homogenates were centrifuged (900 g for 15 min at 4°C), and the supernatants were stored at 4°C . The pellet was extracted again with 3 mL acidified ethanol for 24 h at 4°C . The supernatant obtained after centrifugation was pooled with the previous one and kept at -20°C until assayed [34, 35].

2.9. HOMA-IR Index. To estimate insulin resistance in fructose-fed or control rats, the widely used HOMA-IR index was calculated [34, 36, 37] by multiplying fasting serum insulin ($\mu\text{U/mL}$) with fasting serum glucose (mmol/L) then dividing by the constant 22.5, i.e., $\text{HOMA-IR} = (\text{fasting serum insulin concentration} \times \text{fasting serum glucose concentration})/22.5$.

2.10. Measurement of Serum Lipid Levels. Serum cholesterol, triglyceride, LDL, and HDL levels were measured at week 24 using a test kit supplied by Diagnosticum Zrt. (Budapest, Hungary) as described previously [27].

2.11. 3-NT ELISA. A double-antibody sandwich ELISA kit specific for 3-nitrotyrosine measurement was purchased from Genasiabio (Shanghai, China). Left ventricles were homogenized (Heilscher UP100H Ultrasonic Processor) in Phosphate Buffer Saline (PBS) (pH 7.2–7.4) and then centrifuged at 3000 rpm for 20 min at 4°C . Nitrotyrosine was measured according to the manufacturer's instructions and protocols, and optical densities (OD) were determined at 450 nm. Results were expressed as nmol/mg protein.

2.12. Measurement of Serum Laboratory Parameters. Urea and creatinine levels in serum were quantified by kinetic UV method using urease and glutamate dehydrogenase enzymes and Jaffe method, respectively. The reagents and the platform analyzers were from Roche Diagnostics. Serum sodium, potassium, and chloride levels were determined by indirect potentiometry using ion-selective electrodes at week 24. All reagents and instruments were from Roche Diagnostics. Alanine aminotransferase (ALAT), aspartate aminotransferase (ASAT), creatine kinase (CK), and lactate dehydrogenase (LDH) enzyme activities were measured with Roche UV assays standardized according to the recommendations of IFCC (International Federation of Clinical Chemistry). Creatine kinase MB enzyme activities were determined using an immunological UV assay of Roche.

2.13. Western Blot. To investigate changes of apoptotic proteins, the standard western blot technique was used in case

of Bax, Bcl-2, Bcl-xL, caspase-7, and caspase-3 with actin or tubulin loading background. Left ventricular samples ($n = 8$) were homogenized with an ultrasonicator (UP100H Hielscher, Teltow, Germany) in Radio-Immunoprecipitation Assay (RIPA) buffer (50 mM Tris-HCl (pH 8.0)), 150 mM NaCl, 0.5% sodium deoxycholate, 5 mM ethylenediamine tetra-acetic acid (EDTA), 0.1% sodium dodecyl sulfate, 1% NP-40 (Cell Signaling, Carlsbad, CA, USA) supplemented with phenylmethanesulfonyl fluoride (PMSF). The crude homogenates were centrifuged at $15000 \times g$ for 30 min at 4°C . After quantification of protein concentrations of the supernatants using the BCA Protein Assay Kit (Pierce, Rockford, IL, USA), 25 μg of reduced and denatured protein was loaded. Then, sodium dodecyl-sulfate polyacrylamide gel electrophoresis (SDS-PAGE) was performed (10% gel, 50 V, 4 h) followed by the transfer of proteins onto a nitrocellulose membrane (20% methanol, 35 V, 1.5 h). The efficacy of transfer was checked using Ponceau staining. The membranes were cut horizontally into parts corresponding to the molecular weights of Bax, Bcl-2, Bcl-xL, caspase-7, caspase-3, actin, and tubulin. Membranes were blocked for 1 h in 5% (w/v) bovine serum albumin (BSA) and were incubated with primary antibodies in the concentrations of 1:1000 against Bax (#2772), Bcl-2 (#3498), Bcl-xL (#2764), caspase-7 (#12827), caspase-3 (#14220), α -tubulin (#2144), and β -actin (#4970) overnight at 4°C in 5% BSA. Then, the membranes were incubated with IRDye® 800CW Goat Anti-Rabbit secondary antibody (Li-Cor) for 1 h at room temperature in 5% BSA. Fluorescent signals were detected by Odyssey CLx, and digital images were analyzed and evaluated by Quantity One Software.

2.14. Statistical Analysis. Proteomic data are presented as mean intensities \pm CV, fold change, and p value. For proteomic data, the statistical significance was tested using unpaired Welch test. $p < 0.05$ and a fold change > 1.5 were accepted as a statistically significant difference. Lipidomic data are presented as mean \pm SEM; statistical significance was determined according to Storey and Tibshirani [38] and was accepted for $p < 0.05$ corresponding to a false discovery rate < 0.05 . PCA analyses were performed using MetaboAnalyst [39]. All other parameters are presented as mean \pm SEM, and significance between groups was determined with two sample t -test or Mann-Whitney Rank Sum Test.

3. Results and Discussion

3.1. Prediabetes and Characterization of the Animal Model. In the present study, male Wistar rats were fed with 60% fructose-containing chow for 24 weeks to create a model of prediabetes. We have chosen this model in order to examine the effect of a moderate metabolic condition on the heart, rather than looking at the effects of severely disturbed glucose and lipid homeostasis seen for instance in genetically modified diabetes models (e.g., db/db or ob/ob mice) [40, 41]. In order to verify the development of the prediabetic state, fasting blood glucose was measured at every 4th week, and OGTT was performed at weeks 12, 16, 20, and 24. Fasting

glucose levels were slightly but significantly higher in fructose-fed rats at weeks 12, 16, 20, and 24 (Figure 2(a)). OGTT area under the curve values were also significantly increased in fructose-fed rats at weeks 16, 20, and 24 (Figure 2(b)). These results demonstrate the development of prediabetes with impaired glucose tolerance in the present model. HOMA-IR, a widely used indicator of insulin resistance, was significantly higher in the fructose-fed rats at week 20, although no significant difference was detected in serum insulin levels (Figure 2(c)). Pancreatic insulin level was significantly higher in the fructose-fed group compared to controls (Figure 2(e)). These data demonstrate the appearance of a mild insulin resistance in our present model.

Although body weight increased in both groups during the course of the study, by the end of 24-week feeding, the weight of the fructose-fed rats was significantly smaller compared to that of the control rats (Figure 3(a)). Weight gain during the study was decreased in fructose-fed rats (Figure 3(b)). Although liver weight was not significantly different in fructose-fed rats, the liver weight to body weight ratio was increased (Table 1). Moreover, during the isolation of organs, we have observed macroscopical signs of fatty degeneration on the liver of fructose-fed animals. These findings may indicate fatty degeneration in the liver due to DNL initiated by fructose feeding. In fact, it has been demonstrated that fructose may activate DNL due to its rapid conversion to pyruvate bypassing the regulatory step of glycolysis catalyzed by the phosphofructokinase-1 enzyme [42]. Compared to the effects of fat-supplemented diet which leads to fat deposits both in the liver and adipose tissue (liver as well as body weight gain), dietary fructose preferably increases lipid accumulation only in the liver [42]. Fructose feeding may affect the metabolism of skeletal muscle through metabolic stress. For instance, Gatieneau et al. showed that older rats fed with fructose-containing diet lost significantly more lean body mass and maintained more adipose tissue than control rats [43]. In sucrose-fed rats, significantly lower diet-induced muscle protein synthesis was observed compared to starch-fed rats [43]. Additionally, excessive fructose consumption was shown in the liver to increase production of substances such as methylglyoxal, which leads to oxidative stress in the muscle [44]. Activated DNL leads to endoplasmic reticulum stress [45] and production of hepatokines, such as fetuin-A [46], known to adversely affect muscle energy metabolism and insulin sensitivity [47]. These findings might explain decreased body weight gain in fructose-fed rats in our present study. Despite the macroscopic signs of fatty degeneration in the liver, neither serum lipid parameters (triglycerides, total cholesterol, and LDL and HDL cholesterol) nor liver enzymes (ALAT, ASAT) were increased in fructose-fed rats (Table 2) indicating an early stage of hepatic consequences.

To further characterize metabolic changes in the liver of fructose-fed rats, we performed qRT-PCR. We examined Srebf1 and Mlxipl transcription factors which regulate fatty acid metabolism related genes. No difference was found between control and fructose-fed group. We also examined Acaca and Fasn. Acaca catalyzes the carboxylation of

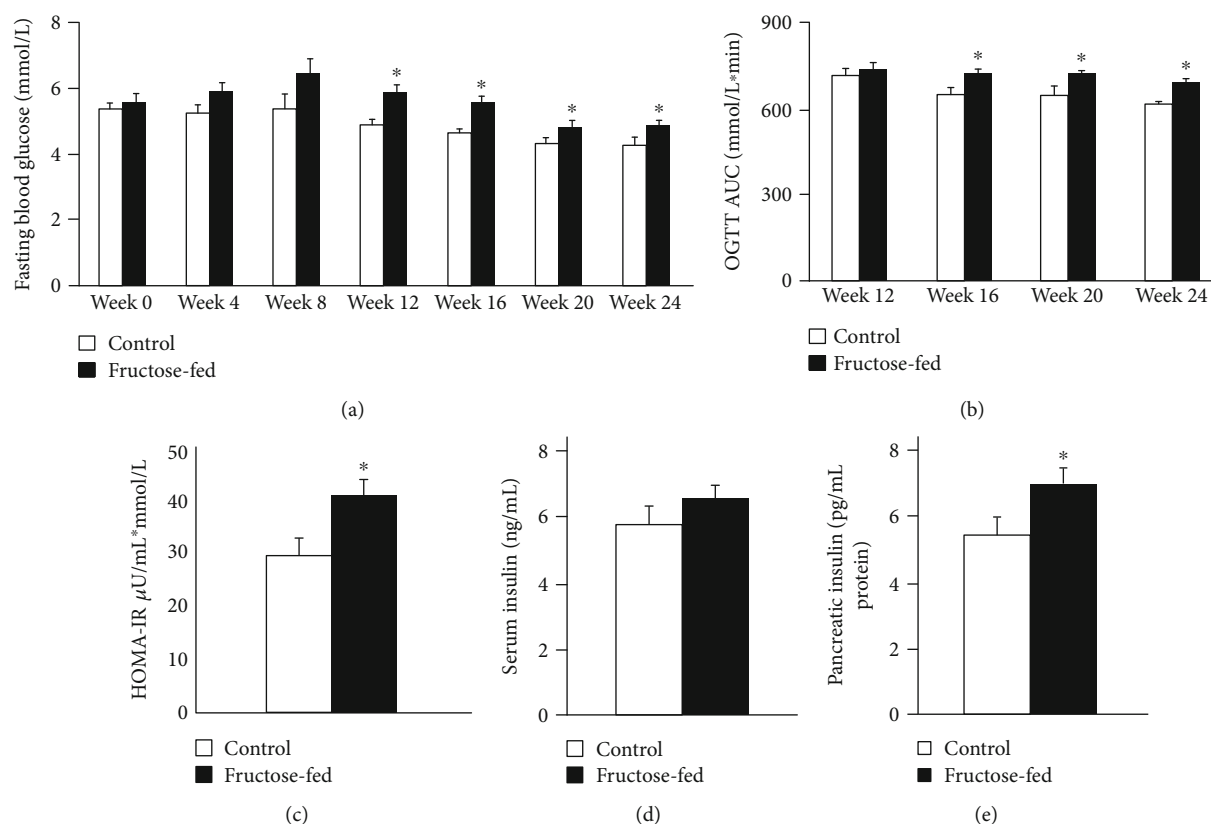


FIGURE 2: Prediabetic condition: (a) fasting blood glucose levels, (b) area under the curve (AUC) values for OGTT, (c) HOMA-IR index at week 20, (d) serum insulin level at week 20, and (e) pancreatic insulin level at week 24. Values are mean \pm SEM ($n = 7-8$), * $p < 0.05$.

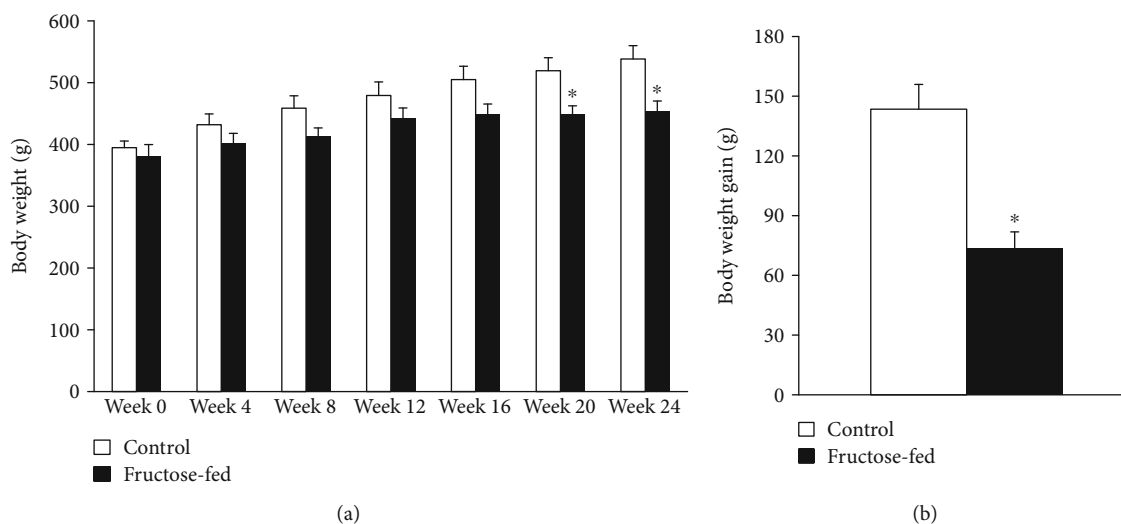


FIGURE 3: Body weight and weight gain of control and fructose-fed rats. Values are mean \pm SEM ($n = 8$), * $p < 0.05$.

acetyl-CoA to malonyl-CoA, the rate-limiting step of fatty acid synthesis. Fasn catalyzes the remaining steps of palmitic acid synthesis. Fasn expression showed a tendency of increase, while Acaca expression significantly increased in fructose-fed rats (Figure 4(c)). These findings are consistent with previous results and clearly indicate increased de novo

lipid synthesis in fructose-fed rats [48, 49]. ELOVL6 enzyme, which catalyzes the first and rate-limiting reaction of long-chain fatty acid elongation cycle, was also significantly increased in fructose-fed rats. ELOVL6 enzyme is also known to play an important role in nonalcoholic fatty liver disease and steatohepatitis [50, 51] (Figure 4(h)).

TABLE 1: Isolated organ weights and isolated organ weight to body weight ratios at week 24 in both control and fructose-fed rats. Values are mean \pm SEM ($n = 8$), * $p < 0.05$.

	Control	Fructose-fed	p value
Heart weight (mg)	1726 \pm 79	1527 \pm 71	0.083
Liver weight (mg)	13292 \pm 538	12262 \pm 467	0.170
Pancreas weight (mg)	1093 \pm 111	1101 \pm 467	0.951
Heart (mg)/body weight (g)	3.22 \pm 0.14	3.36 \pm 0.09	0.422
Liver (mg)/body weight (g)	22.7 \pm 0.2	27.0 \pm 0.4*	≤ 0.001
Pancreas (mg)/body weight (g)	2.04 \pm 0.19	2.43 \pm 0.11	0.095

TABLE 2: Parameters measured in serum collected at week 24 in both control and fructose-fed rats. Values are mean \pm SEM ($n = 8$), * $p < 0.05$.

	Control	Fructose-fed	p value
Serum triglyceride (mmol/L)	0.96 \pm 0.12	0.94 \pm 0.20	0.938
Serum cholesterol (mmol/L)	1.78 \pm 0.14	1.61 \pm 0.11	0.359
LDL (mmol/L)	0.45 \pm 0.05	0.43 \pm 0.08	0.830
HDL (mmol/L)	0.86 \pm 0.08	0.76 \pm 0.07	0.335
ALAT (U/L)	38.63 \pm 3.35	35.00 \pm 4.08	0.500
ASAT (U/L)	77.88 \pm 4.05	73.29 \pm 5.74	0.517
CK (U/L)	263 \pm 46	245 \pm 45	0.776
CKMB (U/L)	352 \pm 75	256 \pm 33	0.264
LDH (U/L)	334.86 \pm 63.77	272.50 \pm 37.36	0.437
Cl (mmol/L)	102.50 \pm 0.78	102.63 \pm 0.82	0.914
K (mmol/L)	6.33 \pm 0.36	5.95 \pm 0.57	0.588
Na (mmol/L)	141.63 \pm 0.60	141.38 \pm 0.78	0.802

3.2. Heart Function and Morphology. To characterize prediabetes-induced cardiac changes in fructose-fed rats, transthoracic echocardiography was performed at week 24 to investigate cardiac function. Although the weight of the animals was significantly lower in the fructose-fed group, the heart weight and heart weight to body weight ratio were not changed significantly (Table 1).

Echocardiographic parameters of morphology and function are shown in Table 3. To exclude the potential effect of variations in cardiac mass, the morphological data were also given after normalization to heart weight (Table 3). Wall thicknesses and ventricular diameters were not changed significantly due to fructose feeding (except for anterior wall thickness) (Table 3). Although there was no difference in heart rate, ejection fraction, and fractional shortening, the E/A ratio was significantly smaller in fructose-fed rats indicating the impairment of diastolic filling (Table 3). These findings may suggest a very early manifestation of a mild hypertrophy and diastolic dysfunction with preserved systolic function in prediabetic rats.

Following echocardiography, the hearts were isolated to assess cardiac performance on a working heart perfusion system. Left ventricular end-diastolic pressure significantly increased, while cardiac output significantly decreased in fructose-fed rats (Figure 5). However, HR, max and min

dp/dt, LVDP, and aortic systolic and diastolic pressures were not changed between groups during working heart perfusion (Table 4). These results demonstrate the appearance of a mild diastolic dysfunction in prediabetic rats. It is well known that left ventricular hypertrophy is more common in diabetic patients and that 40-75% of patients with type 1 or type 2 diabetes have diastolic dysfunction [52, 53]. However, here we show that the deterioration of diastolic function occurs much earlier than the development of overt diabetes. These results are consistent with recent reports showing that the development of diastolic dysfunction can precede complete diabetes [6].

In order to assess cardiac hypertrophy at the molecular level, mRNA expression of myosin heavy chain α isoform (MYH6) and myosin heavy chain β isoform (MYH7) was measured. We have found that cardiac MYH6 mRNA level, consistent with myosin 6 protein level measured by proteomics (Table 5), was increased in fructose-fed rats (Figure 6). However, MYH6/MYH7 ratio did not differ significantly. According to the literature [54–56], these data do not support cardiac hypertrophy in our fructose-fed rats.

It is known that clinical laboratory markers of myocardial injury are increased in diabetic cardiomyopathy [57] and serum ion parameters, especially potassium, can affect heart function. Therefore, we measured serum ions (potassium,

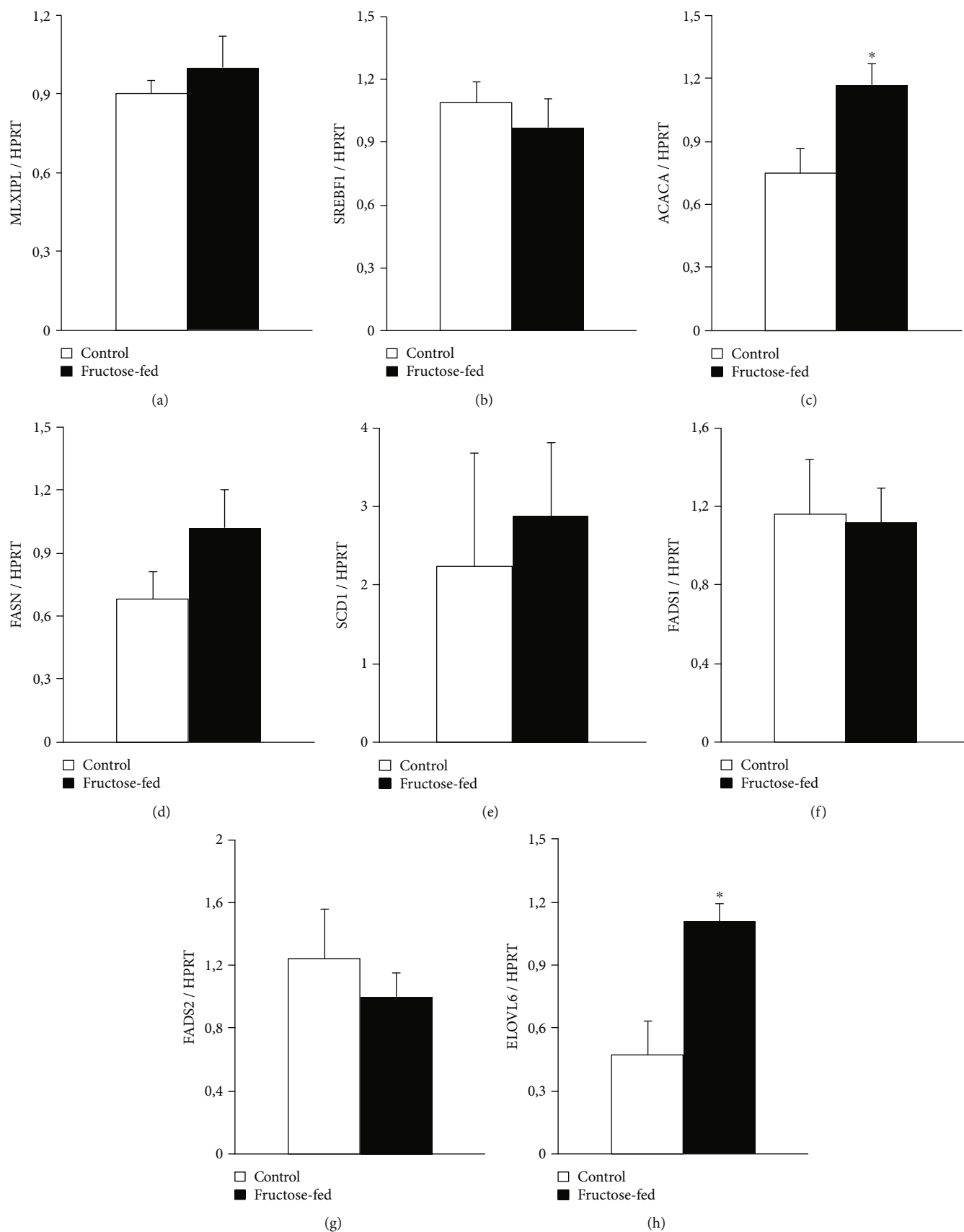


FIGURE 4: qRT-PCR results at week 24. Liver (a) *Mlxipl* expression, (b) *Srebf1* expression, (c) *Acaca* expression, (d) *Fasn* expression, (e) *Scd1* expression, (f) *Fads1* expression, (g) *Fads2* expression, and (h) *Elovl6* expression. Values are mean \pm SEM ($n = 6-7$), * $p < 0.05$.

TABLE 3: Left ventricular morphological and functional parameters examined by echocardiography at week 24 in both control and fructose-fed rats. Values are mean \pm SEM ($n = 8$), * $p < 0.05$.

Parameter (unit)	View/mode	Control	Fructose-fed	p value
Left ventricle morphology				
Anterior wall thickness in systole (mm)	Short axis/MM	3.59 ± 0.14	3.47 ± 0.12	0.506
Anterior wall thickness in diastole (mm)	Short axis/MM	2.35 ± 0.04	$2.00 \pm 0.10^*$	0.012
Inferior wall thickness in systole (mm)	Short axis/MM	3.38 ± 0.18	3.41 ± 0.07	0.871
Inferior wall thickness in diastole (mm)	Short axis/MM	2.20 ± 0.11	2.01 ± 0.08	0.167
Posterior wall thickness in systole (mm)	Long axis/MM	3.33 ± 0.30	3.13 ± 0.19	0.596
Posterior wall thickness in diastole (mm)	Long axis/MM	2.22 ± 0.14	1.96 ± 0.11	0.155
Septal wall thickness in systole (mm)	Long axis/MM	3.88 ± 0.18	3.55 ± 0.20	0.239
Septal wall thickness in diastole (mm)	Long axis/MM	2.33 ± 0.10	2.05 ± 0.17	0.169
Left ventricular end-diastolic diameter (mm)	Long axis/MM	6.85 ± 0.24	6.85 ± 0.21	0.996
Left ventricular end-systolic diameter (mm)	Long axis/MM	3.07 ± 0.16	3.37 ± 0.20	0.270
Left ventricular end-diastolic volume (μ L)	4CH	100.3 ± 20.6	90.3 ± 11.7	0.681
Left ventricular end-systolic volume (μ L)	4CH	39.23 ± 9.04	36.23 ± 6.03	0.787
Left ventricular morphology/heart weight				
Anterior wall thickness in systole (mm/g)	Short axis/MM	1.96 ± 0.11	$2.28 \pm 0.06^*$	0.021
Anterior wall thickness in diastole (mm/g)	Short axis/MM	1.27 ± 0.07	1.32 ± 0.06	0.596
Inferior wall thickness in systole (mm/g)	Short axis/MM	1.96 ± 0.06	2.20 ± 0.11	0.079
Inferior wall thickness in diastole (mm/g)	Short axis/MM	1.38 ± 0.10	1.34 ± 0.10	0.795
Posterior wall thickness in systole (mm/g)	Long axis/MM	1.96 ± 0.20	2.05 ± 0.09	0.665
Posterior wall thickness in diastole (mm/g)	Long axis/MM	1.21 ± 0.12	1.29 ± 0.06	0.559
Septal wall thickness in systole (mm/g)	Long axis/MM	2.28 ± 0.14	2.34 ± 0.11	0.735
Septal wall thickness in diastole (mm/g)	Long axis/MM	1.36 ± 0.06	1.73 ± 0.37	0.348
Left ventricular end-diastolic diameter (mm/g)	Long axis/MM	3.86 ± 0.23	4.56 ± 0.27	0.067
Left ventricular end-systolic diameter (mm/g)	Long axis/MM	1.81 ± 0.10	2.26 ± 0.20	0.082
Left ventricle function				
E/A	4CH	1.21 ± 0.07	$1.03 \pm 0.02^*$	0.015
Ejection fraction (%)	4CH	60.96 ± 3.38	62.83 ± 2.32	0.666
Fractional shortening (%)	Short axis/MM	49.57 ± 3.82	54.00 ± 3.60	0.414
MV E velocity (m/s)	4CH	0.81 ± 0.05	0.73 ± 0.06	0.358
MV A velocity (m/s)	4CH	0.71 ± 0.07	0.82 ± 0.06	0.260
Heart rate (1/min)	4CH	346.0 ± 12.9	349.6 ± 6.8	0.819

sodium, and chloride) and enzyme markers of myocardial injury (creatine kinase (CK), creatine kinase-MB (CK-MB), and lactate dehydrogenase (LDH)). Neither serum ion parameters nor markers of myocardial injury were changed significantly in fructose-fed rats compared to controls (Table 2).

3.3. Lipidomics. To characterize and elucidate the metabolic changes in the prediabetic heart induced by chronically applied fructose-rich diet, we performed high-performance, comprehensive shotgun MS-based lipidomic analyses from left ventricular whole membrane extracts. We have identified and quantified approximately 200 lipid molecular species encompassing 20 lipid classes (lipidomic data are summa-

rized in Supplementary Lipid Table expressed either as lipid/protein or as mol% of membrane lipids or mol% of a given lipid class). Because the optimal physical state of the membrane is a prerequisite for proper functioning, in the following, we focus on membrane lipid compositional data. To obtain an overview, mol% of membrane lipid values was subjected to the nonsupervised multivariate statistics principal component analysis (PCA). The clear separation of the sample sets into two nonoverlapping clusters (Figure 7) indicates complex reshaping and metabolic rewiring of the whole lipodome due to fructose feeding. Examining these alterations in more detail and comparing the molecular species patterns for the control and fructose groups revealed 100 statistically significant differences (Supplementary Lipid Table).

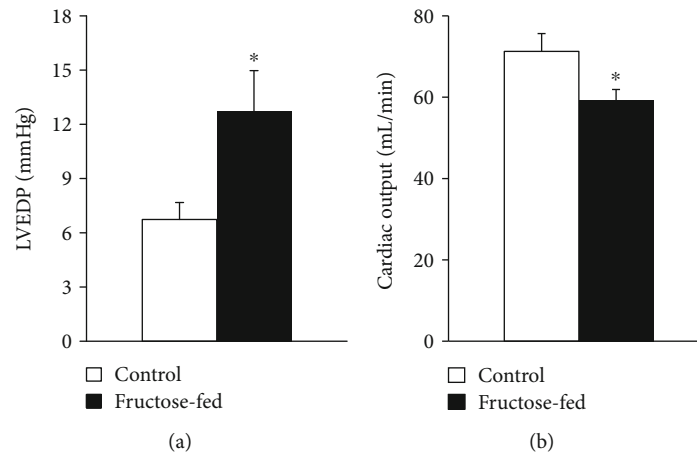


FIGURE 5: Cardiac function in isolated perfused hearts: (a) left ventricular end-diastolic pressure (LVEDP) and (b) cardiac output. Values are mean \pm SEM ($n = 7-8$), * $p < 0.05$.

TABLE 4: Parameters measured by working heart perfusion at week 24 in both control and fructose-fed rats. Values are mean \pm SEM ($n = 7-8$).

	Control	Fructose-fed	<i>p</i> value
Aortic flow (mL)	46.6 \pm 3.7	37.4 \pm 2.4	0.065
Coronary flow (mL)	24.6 \pm 1.1	21.9 \pm 1.2	0.121
Max dp/dt (mmHg/s)	5975 \pm 330	6063 \pm 212	0.832
Min dp/dt (mmHg/s)	-3577 \pm 222	-4090 \pm 237	0.138
Aortic diastolic pressure (mmHg)	45.7 \pm 1.7	42.1 \pm 1.3	0.120
Aortic systolic pressure (mmHg)	110.3 \pm 2.6	116.2 \pm 1.5	0.121
LVDP (mmHg)	137.5 \pm 6.0	139.5 \pm 4.3	0.803
Heart rate (1/min)	279 \pm 14	263 \pm 24	0.554

TABLE 5: Alteration of selected cardiac proteins in fructose-fed rats by proteomic analysis. Values are expressed as fold change and *p* value.

Protein names	Gene names	Fold change	<i>p</i> value
Alpha B crystallin	Cryab	5.56	0.047
3-ketoacyl-CoA thiolase (mitochondrial)	Acaa2	4.56	0.005
Alpha-aminoacidic semialdehyde dehydrogenase	Aldh7a1	4.34	≤ 0.001
60 kDa heat shock protein (mitochondrial)	Hspd1	3.37	0.010
Myosin 6	MYH6	3.06	0.003
Peroxiredoxin-6	Prdx6	2.87	0.001
Superoxide dismutase [Mn] (mitochondrial)	Sod2	-1.82	0.033
Protein disulfide-isomerase	P4hb	-3.40	0.001

One of the most noteworthy changes can be connected to the CL remodeling system. It is known that under normal conditions, the levels of LPLs are kept low in general, and CL remodeling requires only trace amounts of MLCL [14]. Therefore, the significantly lowered level of matured CL in parallel with the significantly increased amount of MLCL (Supplementary Lipid Table), and consequently their markedly increased ratio in the membrane (MLCL/CL, Figure 8(a)), obviously report about an aberrant remodeling

process in the fructose-fed group as compared to the controls. The ratio of MLCL/CL was found to be a more sensitive indicator than the level changes of CL and MLCL in Barth patients [58]. Furthermore, at the molecular species level, we detected pronounced loss of the most abundant homo-symmetric tetra18:2 species CL(72:8) (Figure 8(b)).

This was the most prominent change not only in the context of membrane composition but also when considering absolute values, i.e., the protein-normalized data displayed

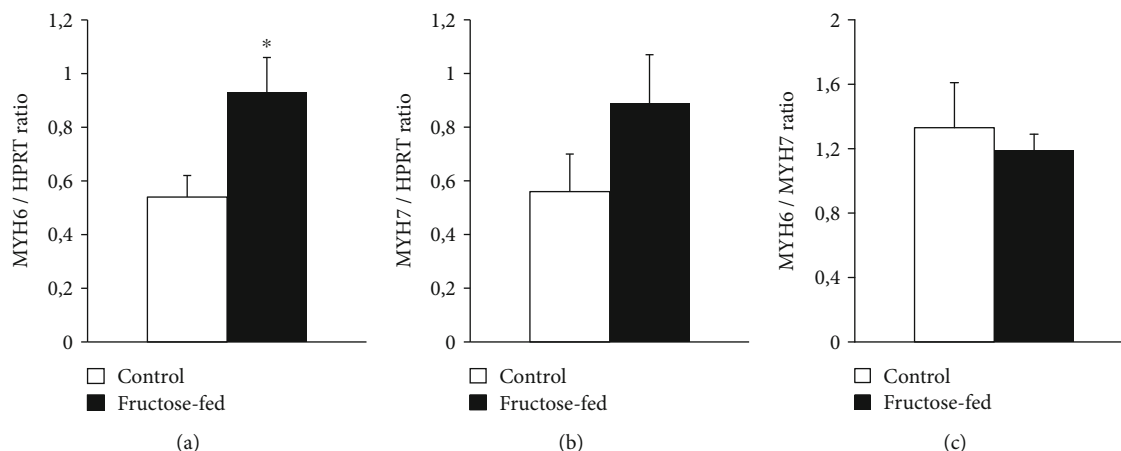


FIGURE 6: qRT-PCR results at week 24. Heart (a) MYH6 expression, (b) MYH7 expression, and (c) MYH6/MYH7 ratio. Values are means \pm SEM ($n = 8$), * $p < 0.05$.

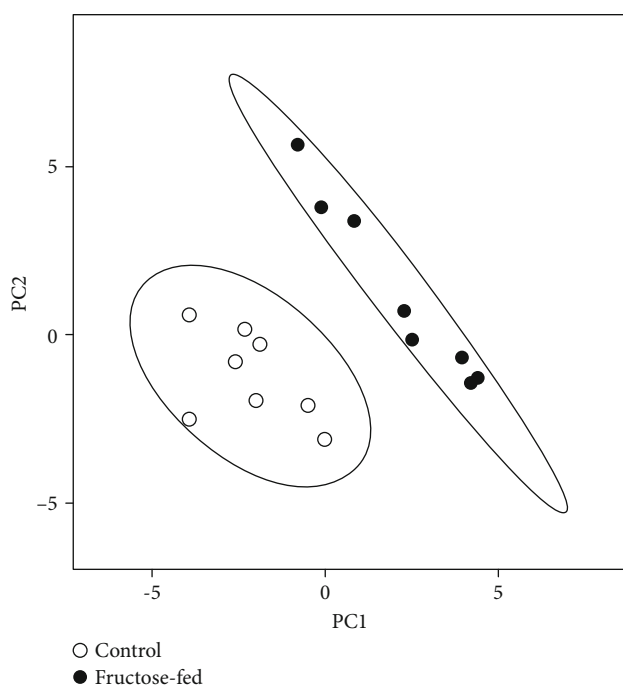


FIGURE 7: Principal component analysis (PCA) score plot. MS data expressed as mol% of membrane lipids were centered and normalized. Values for 8 independent experiments are shown for control and fructose-fed samples. Dashed lines display 95% confidence regions.

dramatic 45% decrease for CL(72:8) (from 28.5 to 15.7 nmol/protein mg; $p < 0.05$; Supplementary Lipid Table). This observation is in full agreement with other literature data obtained for either more severe diabetic and obesity models [59, 60] or recorded in a more similar early-stage fructose-induced type 2 diabetes study [61]. The loss in CL(72:8) was paralleled by elevations in practically all other asymmetric species independently on chain length and saturation for the fructose-fed animals as opposed to the normal chow diet (sum elevation from 2.82 to 4.35 mol% of membrane lipids, $p < 0.05$) (Figure 8(b)). This altogether resulted

in a dramatic drop of the CL “symmetry” factor in the fructose group calculated as the ratio of symmetric/asymmetric species (Figure 8(c)). The major contributions to the increase in asymmetry derived from species which contain one non-18:2 acyl chain, i.e., from the 16:1 FA-containing CL(70:7; 16:1_18:2_18:2_18:2) species, from the CL(74:9) species whose major component is the CL(18:2_18:2_18:2_20:3) isobar, and from the CL(72:7) species corresponding to CL(18:1_18:2_18:2_18:2). This is in correspondence with the result observed in a fructose-induced early type 2 diabetic rat model [61] but differs from more severe mouse models of diabetes and insulin resistance/obesity. In the latter cases, defective cardiac CL remodeling resulted in depletion of 16:1 and enrichment of the highly unsaturated docosahexaenoic acid (DHA, 22:6 n-3) [17, 60], thereby essentially increasing the propensity of CL to peroxidation. In our study, the double bond index (DBI) of CL, a measure of unsaturation, did not change significantly (Supplementary Lipid Table). It can be partially due to the prediabetic nature of the model but also due to the sizeable difference in cardiac CL species composition between mouse and rat. Mouse cardiac CL contains essentially more DHA [61–63]. Therefore, it is more prone to ROS attack and peroxidation than that of the rat CL. Nevertheless, we have to mention that regarding fold increases of the individual CL species in the fructose-fed animals compared to the controls, the highest, ca. 10-fold elevations, was registered for DHA-containing CL species (78:12, 18:0_18:2-20:4_22:6 (major)) and (78:13, 18:1_18:2_20:4_22:6), although their levels barely reached the 0.1 mol% of total CL value even in the fructose group (Supplementary Lipid Table). It is important to note here that we could not detect oxidized lipid species either in CL or in other highly unsaturated and generally oxidation-prone lipid classes, such as plasmalogen phosphatidylethanolamine and phosphatidylserine. However, we could detect “asymmetry” defects already in the MLCL species profile; the major MLCL(54:6, tri18:2) species was found to be significantly reduced whereas the not only 18:2-containing precursors were markedly elevated (Supplementary Lipid Figure 2).

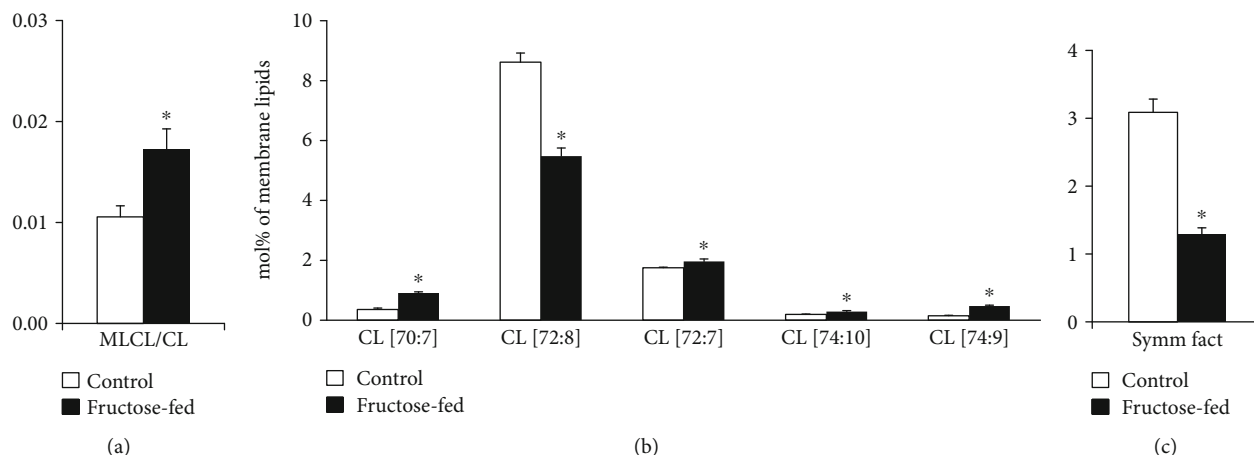


FIGURE 8: Defects in cardiolipin remodeling. (a) Monolysocardiolipin to cardiolipin ratio (MLCL/CL). (b) Changes in CL species due to fructose feeding. (c) CL symmetry factor calculated as the ratio of symmetric/asymmetric CL species. ESI-MS data are expressed as mol% of membrane lipids or calculated from the corresponding values and presented as means \pm SEM ($n = 8$), $*p < 0.05$.

Another important feature of the lipidome alterations was the general increase in lipid species with sum double bond (db) = 1 that could be detected in all major membrane PL classes in the fructose group as opposed the control animals (sum of db = 19.3 vs. 6.9 mol% of membrane lipids, $p < 0.05$; Supplementary Lipid Table). The main contributors, which contain a saturated and a monounsaturated FA leg, were collected in Figure 9(a). PL species with db = 2 predominantly contained a saturated FA in *sn*1 and a linoleoyl (18:2) group in *sn*2 position of the glycerol backbone; these can serve as potential acyl donors for the formation of tetra18:2 CL for the tafazzin-catalyzed transacylation. In parallel with the elevation of species with db = 1, we detected significant depletion in species with db = 2 in fructose-fed animals (sum of db = 27.1 vs. 9.7 mol% of membrane lipids, $p < 0.05$; Supplementary Lipid Table); selected species are demonstrated in Figure 9(b).

Changes in PL molecular species with highly unsaturated acyl chains (db ≥ 4) showed fairly complex picture with several significant alterations including both elevations and decreases (Supplementary Lipid Table). It was reported that the loss of tafazzin enzymatic activity in a Barth syndrome mouse model also resulted in complex alterations of polyunsaturated PL species [64]. Therefore, it is conceivable to suggest that the intricate imbalance in polyunsaturated PL species alters the biophysical and signaling properties of the cardiac membrane.

Since we could not detect the elevation in serum triglyceride levels due to fructose feeding, it is not surprising that neither the total cardiac TG content changed significantly (Supplementary Lipid Table). However, the prominent species profile change of the TG pool is worth mentioning. The robust relative increase in species containing saturated and monounsaturated FAs, such as TG(50:1, 52:2, and 54:3), in parallel with significant reductions in more unsaturated species, e.g., TG(52:4, 54:6, and 56:8) (Figure 9(c)) altogether led to the decrease of the double bond index (DBI), i.e., increase in saturation for cardiac TG (Figure 9(d)). Cardiac TG saturation together with the monoene increase and

18:2 decrease in membrane PLs may indicate the upregulation of DNL leading to a shift in FA profile towards the augmentation of monounsaturated 18:1 (and 16:1) FAs.

A further interesting aspect of the complex lipidome remodeling was the reshaping of the analyzed sphingolipid (SL) pool, ceramide (Cer) and sphingomyelin (SM). Cer has a central role in SL metabolism as well as it is known as a lipid mediator of the eukaryotic stress response. Its role is mostly associated with growth inhibition; the most studied being its function as a proapoptotic molecule [65]. Serum Cers have emerged as potential biomarkers of insulin resistance, diabetes, and heart disease, but also, muscle, liver, or adipose tissue Cers were shown to be associated with insulin resistance [66]. In our study, we measured small but significant elevation in total cardiac Cer at membrane lipid compositional level (approximately 30%; $p < 0.05$, Supplementary Lipid Table), which could be attributed almost exclusively to the increases in very-long-chain Cer-24 species Cer(42:2:2, d18:1/24:1 and 42:3:2, d18:2/24:1) (Figure 10(a)). It was reported that the nature of the acyl chain in Cers influences their contribution to the disease. Long-chain Cer-16 and Cer-18 often showed stronger associations with disease pathologies than very-long-chain Cer-24 [66]. Marchesini et al. reported that in confluent MCF-7 cells cell cycle arrest but not apoptosis was mediated by C24-Cer species [67]. It seems, therefore, that the alterations in Cer in our model might contribute to the observed cardiac dysfunction through changing the membrane biophysical properties rather than inducing sizeable apoptotic signaling. SM is the major structural mammalian SL which accumulates in liquid-ordered microdomains. Its total level showed only an increasing tendency in the membrane ($p = 0.058$), but its species compositions changed completely (Figure 10(b) and Supplementary Lipid Table). This may point to microdomain reorganization and hence, again, to the modulation of the membrane physical state and signaling properties due to fructose-rich diet.

Schlame et al. proposed that the acyl specificity of tafazzin arises from the physical properties of the lipid environment and is born out of a transacylation equilibrium in

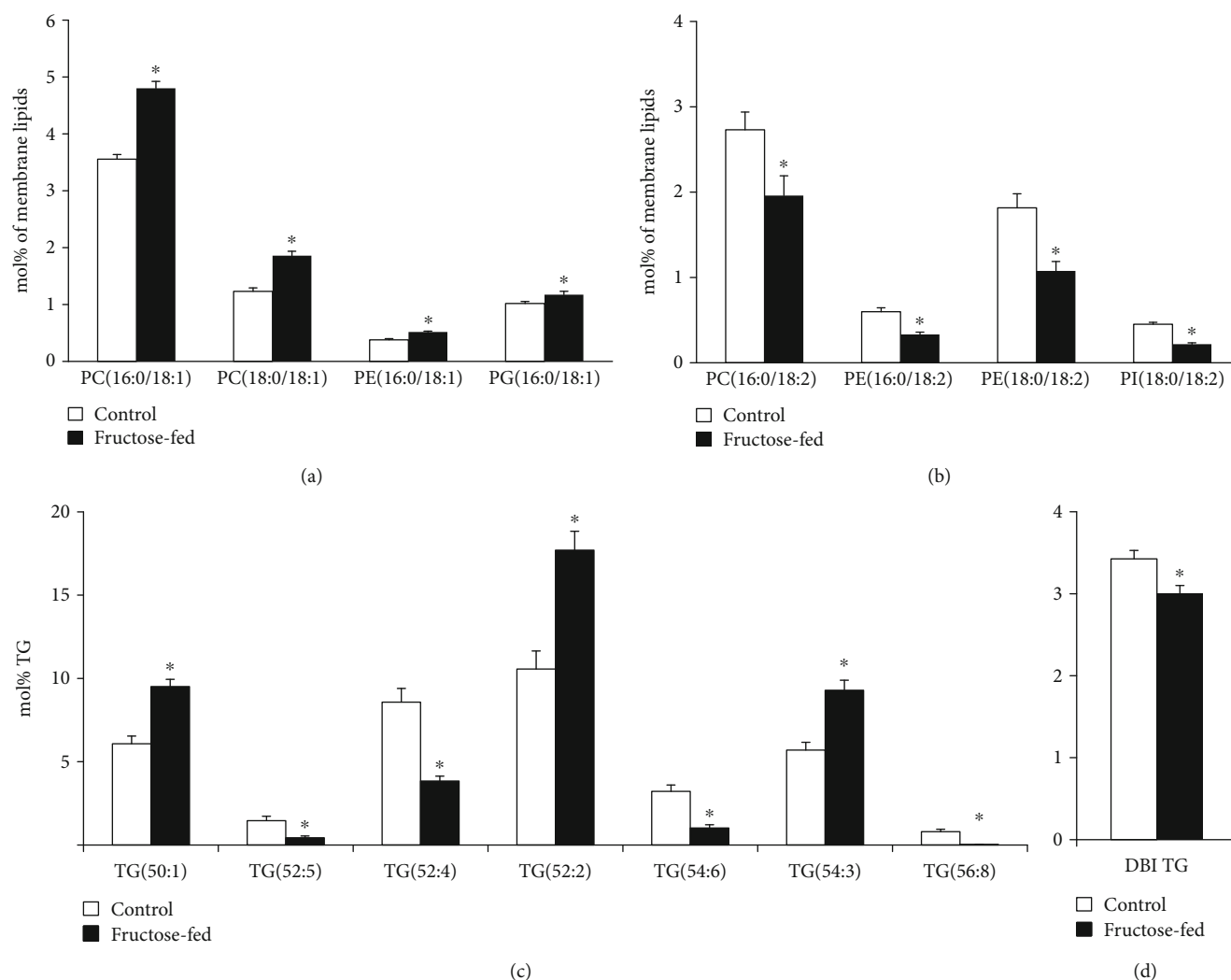


FIGURE 9: Early signs of de novo lipogenesis induction. (a) Changes in phospholipid species with 1 double bond. (b) Changes in phospholipid species with 2 double bonds. (c) Alterations in cardiac triglyceride (TG) species profile due to fructose feeding. (d) The double bond index calculated for TG. PC: phosphatidylcholine; PE: phosphatidylethanolamine; PG: phosphatidylglycerol; PI: phosphatidylinositol. ESI-MS data are expressed as mol% of membrane lipids or mol% of the specified lipid class and presented as means \pm SEM ($n = 8$), * $p < 0.05$.

which the tissue-specific availability of FAs and the specific packing conditions of lipids are manifested [18]. In line with this proposal, our lipidomic data fully support the disturbance in tafazzin action in the prediabetic state as the very first event leading to defective CL structural uniformity and molecular symmetry. Nevertheless, several other options may contribute to the observed changes. These include the induction of phospholipase A₂, which should increase the level of LPLs. It is known to happen in the diabetic state [68], and the registered increases in the relative levels of cardiac MLCL and LPE (Supplementary Lipid Table) in our prediabetic model might also reflect such an upregulation. In addition, the upregulation of the acyl-CoA:lyso-CL-acyltransferase that lacks preference for the linoleoyl group [69] as well as the downregulation of MLCL acyltransferase that specifically catalyzes the synthesis of tetra18:2 CL [70] also might play a role. However, these possibilities were reported for harsher conditions of later stage diabetes or well-developed oxidative stress induced by hyperthyroidism.

3.4. Proteomics. The complex changes in the heart detected by lipidomics at the metabolite level in the prediabetic state induced by chronic fructose feeding can be further mapped and complemented by alterations that occur at the protein level. Therefore, we performed comprehensive LC-MS-based proteomic analysis from left ventricular extracts.

Altogether, 1406 proteins were identified with at least two validate peptides from 1D-GE bands of pooled left ventricular samples. Using a spectral library built from those identifications, 802 proteins could be repeatedly quantified in individual samples. Seventy-five different proteins were significantly changed ($p \leq 0.05$ and a minimum of 1.5-fold change) in fructose-fed rats compared to control animals. Out of these proteins, 49 were upregulated and 26 were downregulated. Gene ontology analysis based on subcellular localization revealed enrichments of proteins with significant changes in different cell compartments including mitochondria ($n = 27$), cytoplasm ($n = 32$), nucleus ($n = 10$), extracellular space ($n = 8$), lysosome ($n = 3$), and Golgi apparatus

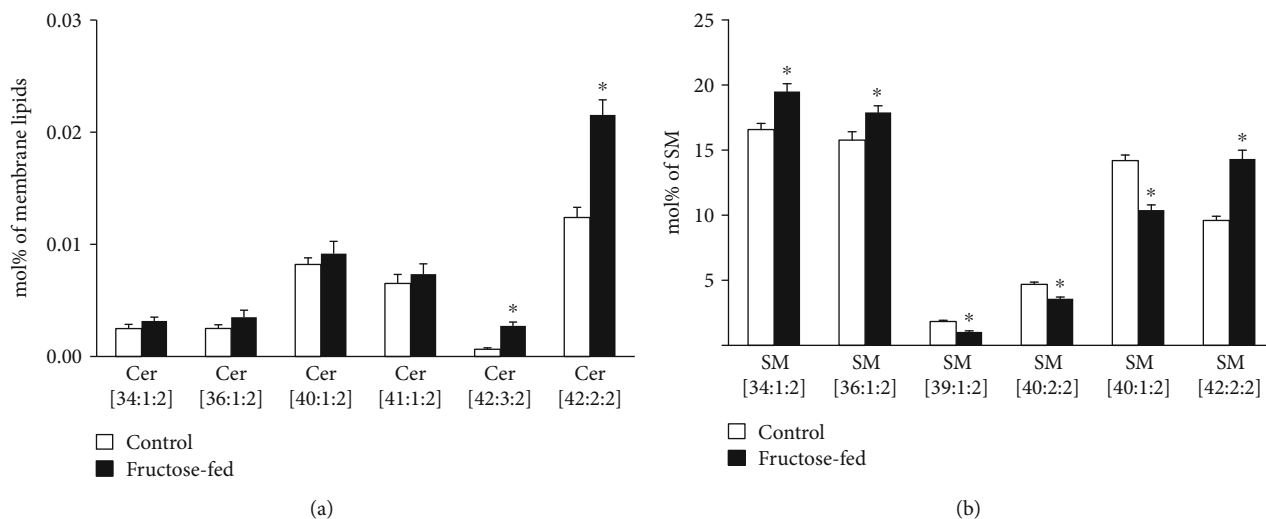


FIGURE 10: Modulation of the sphingolipid pool. (a) Alterations in ceramide (Cer) species. (b) Changes in the sphingomyelin (SM) species profile. ESI-MS data are expressed as mol% of membrane lipids or mol% of the specified lipid class and presented as means \pm SEM ($n = 8$), $*p < 0.05$.

($n = 3$) (Proteomic Table in the Supplementary Material). The relation of these proteins to different biochemical pathways was further analyzed in Reactome (<https://www.reactome.org>). The pathway analysis showed that most of the significantly altered proteins are related to metabolism (30 in pathways plus 9 interacting with some pathway proteins). Several metabolic pathways are affected, including the citric acid (TCA) cycle and respiratory electron transport ($n = 10 + 3$), metabolism of proteins ($n = 9 + 11$), lipids ($n = 5 + 3$), amino acids ($n = 8$), and carbohydrates ($n = 6 + 1$) (for a complete list, see the Supplementary Proteomic Table). Significantly altered proteins related to mitochondria, extracellular matrix, histones, oxidative stress, or apoptosis will be discussed in the following chapters.

3.5. Mitochondria. The proteomic analysis revealed changes in several proteins associated to various mitochondrial metabolic pathways due to fructose feeding (Table 6). These altered proteins can be coupled to the pyruvate dehydrogenase complex, electron transport chain, transport processes, and various metabolic pathways, such as the beta oxidation, tricarboxylic acid cycle, or amino acid metabolism. Pyruvate dehydrogenase complex plays a central role in the utilization of glucose as an energy source. Pyruvate dehydrogenase complex-related genes significantly decreased measured by proteomic analysis. In contrast, some beta oxidation-related proteins were increased. The first common point in the breakdown of glucose and fatty acids, citrate synthase, was also increased measured by proteomic analysis. These findings may suggest a shift to fatty acid utilization in cardiac tissue. We have also found both increased and decreased proteins related to the electron transport chain and amino acid metabolism.

3.6. Extracellular Matrix. We have found three extracellular matrix-related proteins to be significantly increased and another one to be decreased in the hearts of fructose-fed rats

as assessed by proteomic analysis (Table 7). The increased proteins (prolargin, biglycan, and cathepsin D) may play a role in coping mechanism of the heart to prevent severe impairment. Prolargin was shown to be increased in a porcine model of ischemia/reperfusion injury [71]. Our group had previously shown that biglycan protects cardiomyocytes against hypoxia/reoxygenation injury [72, 73] and increases the expression of several proteins related to cardioprotection [74]. It has been also reported that myocardial cathepsin D upregulation induced by myocardial infarction protects against cardiac remodeling in mice [75]. Interestingly, galectin-1, known to have a protective role in cardiac homeostasis and postinfarction remodeling, is decreased in fructose-fed rats [76]. These results support the activation of adaptive mechanisms in the hearts of prediabetic rats.

3.7. Histones. Interestingly, expression of two histone proteins (core histone macro-H2A.1 and histone H1.5) was significantly increased in the hearts of fructose-fed rats. Histones are involved in packing the DNA in the nucleus, and mis-regulated histone expression is thought to lead to aberrant gene transcription by altering the chromatin structure [77].

3.8. Oxidative Stress and Apoptosis. Oxidative stress has a major role in the development of diabetic cardiomyopathy [7], and oxidative stress has been linked to the development of cardiac dysfunction [27, 78]. Moreover, elevated hydrogen peroxide production, elevated nitrotyrosine formation, and decreased cardiac function were observed in a prediabetes model induced by high-fat chow combined with a single low-dose STZ [6]. In our mild prediabetes model induced by fructose-enriched diet, there was no significant increase in the levels of the peroxidation product malondialdehyde in the serum or left ventricular tissue or in the cardiac level of the nitrooxidative marker 3-nitrotyrosine as compared to control values (Table 8).

TABLE 6: Alteration of selected mitochondrial proteins in fructose-fed rats by proteomic analysis. Values are expressed as fold change and *p* value.

Protein names	Gene names	Fold change	<i>p</i> value
Pyruvate dehydrogenase complex			
Dihydrolipoyllysine-residue acetyltransferase component of pyruvate dehydrogenase complex (mitochondrial)	Dlat	-3.47	0.022
Dihydrolipoamide acetyltransferase component of pyruvate dehydrogenase complex	Dbt	-9.53	0.039
Electron transport chain			
ETF-ubiquinone oxidoreductase (mitochondrial)	Etfdh	3.13	0.004
NADH dehydrogenase [ubiquinone] 1 alpha subcomplex subunit 2	Ndufa2	2.06	0.047
NADH-ubiquinone oxidoreductase chain 4	Mt-Nd4	1.59	0.007
Cytochrome c, testis-specific	Cyct	1.56	0.011
Cytochrome b-c1 complex subunit Rieske (mitochondrial)	Uqcrrs1	-1.95	0.001
NADH dehydrogenase [ubiquinone] 1 alpha subcomplex subunit 10 (mitochondrial)	Ndufa10	-3.15	0.038
Amino acid metabolism			
3-Hydroxyisobutyryl-CoA hydrolase (mitochondrial)	Hibch	5.44	0.042
Isovaleryl-CoA dehydrogenase (mitochondrial)	Ivd	-1.90	0.004
Methylcrotonoyl-CoA carboxylase beta chain (mitochondrial)	Mccc2	-2.18	0.046
Transport function			
ADP/ATP translocase 1	Slc25a4	2.47	0.005
Voltage-dependent anion-selective channel protein 3	Vdac3	2.17	0.018
MICOS complex subunit Mic60	Immt	1.58	0.003
Beta oxidation			
Enoyl CoA hydratase domain-containing 2	Echdc2	1.50	0.018
Electron transfer flavoprotein subunit alpha (mitochondrial)	Etfalpha	-1.94	0.001
Other			
Malic enzyme	Me3	4.27	0.022
Citrate synthase	Cs	3.14	≤0.001
Enoyl-[acyl-carrier-protein] reductase (mitochondrial)	Mecr	-1.61	0.029
Prohibitin-2	Phb2	-1.65	0.001

TABLE 7: Alteration of selected extracellular matrix proteins in fructose-fed rats by proteomic analysis. Values are expressed as fold change and *p* value.

Protein names	Gene names	Fold change	<i>p</i> value
Extracellular matrix			
Prolargin	Prep	5.23	0.001
Biglycan	Bgn	1.91	0.018
Cathepsin D	Ctsd	1.52	0.001
Galectin-1	Lgals1	-3.23	0.005

However, we have detected by proteomics the increase of some oxidative stress-related enzymes from cardiac tissue, which may suggest an initial stage of oxidative stress that seems to be controlled by adaptive responses. We have found that alpha-aminoadipic semialdehyde dehydrogenase was increased in the hearts of fructose-fed rats (Table 5). Alpha-aminoadipic semialdehyde dehydrogenase protects cells from oxidative stress by metabolizing a number of lipid peroxidation-derived aldehydes [79, 80]. We have found that peroxiredoxin-6 was also increased in the fructose-fed group

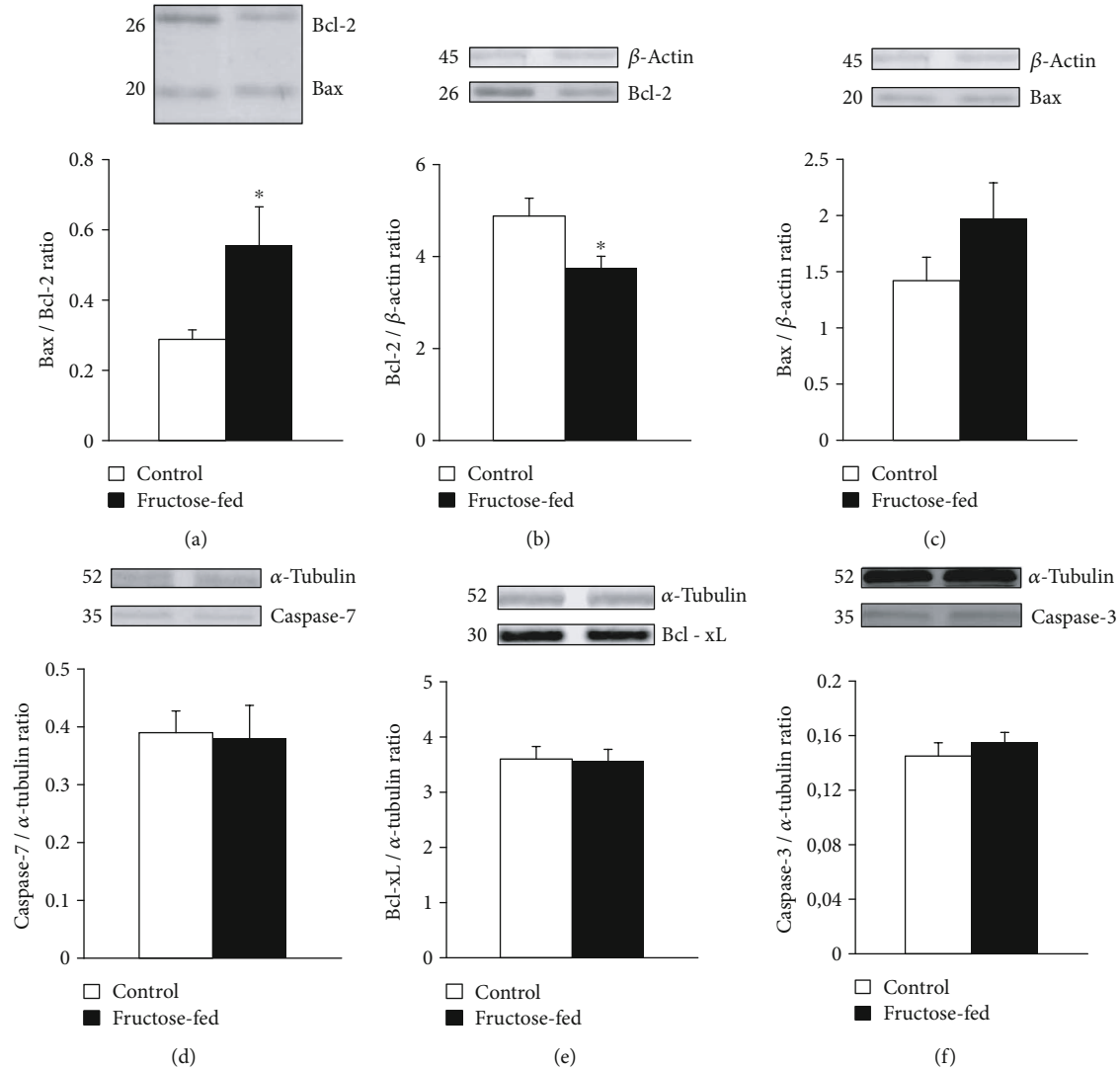
(Table 5). This enzyme catalyzes the reduction of hydrogen peroxide, short chain organic, fatty acid, and phospholipid hydroperoxides. It also has phospholipase activity and can therefore either reduce the oxidized sn2 fatty acyl group of phospholipids (peroxidase activity) or hydrolyze the sn2 ester bond of phospholipids (phospholipase activity). It plays a role in phospholipid homeostasis and in cell protection against oxidative stress by detoxifying peroxides [81]. Mitochondrial superoxide dismutase decreased in fructose-fed rats, and this result is consistent with the findings of Lappalainen et al. showing that SOD2 decreased in the kidney of STZ-induced diabetic rats [82].

Since increased apoptosis often contributes to cardiac dysfunction, in our present study, we also aimed to explore the effect of prediabetes on apoptosis in the heart. We assessed the expression of pro- and antiapoptotic proteins by western blot. Prediabetes did not affect the expression of proapoptotic caspase-7 and Bax in the left ventricles, while the antiapoptotic Bcl-2 was downregulated, and thereby, the Bax/Bcl-2 ratio was significantly increased in the fructose-fed group (Figure 11).

Similar to our results, a modest decrease in Bcl-2 has been shown recently in another model of prediabetes induced by a combination of high-fat diet and low-dose

TABLE 8: Oxidative stress markers measured in serum and heart tissue in both control and fructose-fed rats. Values are mean \pm SEM ($n = 8$).

	Control	Fructose-fed	<i>p</i> value
Serum malondialdehyde (nmol/mg protein)	4.77 \pm 0.43	4.03 \pm 0.49	0.274
Cardiac malondialdehyde (nmol/mg protein)	1.27 \pm 0.16	1.47 \pm 0.22	0.482
3-Nitrotyrosine (nmol/mg)	190 \pm 6.0	221 \pm 20	0.164

FIGURE 11: Western blot results at week 24: (a) Bax/Bcl-2 ratio, (b) Bcl-2/ β -actin ratio, (c) Bax/ β -actin ratio, (d) caspase-7/ α -tubulin ratio, (e) Bcl-xL/ α -tubulin ratio, and (f) caspase-3/ α -tubulin ratio. Values are means \pm SEM ($n = 8$), * $p < 0.05$.

STZ injection [6]. In our present study, we also found in the proteomic results an increase in the antiapoptotic mitochondrial 3-ketoacyl-CoA thiolase in the hearts of fructose-fed rats (Table 5). We think that this alteration is part of the coping mechanism which protects the cardiomyocytes against apoptosis. Indeed, it is known that 3-ketoacyl-CoA thiolase abolishes BNIP3-mediated apoptosis and mitochondrial damage [83]. It was shown that 3-ketoacyl-CoA thiolase increased in the heart of STZ-induced diabetic mice [84]. The -3.4-fold decrease in the disulfide-isomerase protein level may also contribute to

the suppression of apoptosis (Table 5) [85]. The upregulation of proapoptotic proteins and the downregulation of antiapoptotic proteins have already been described in a diabetic model in rodents [86, 87]. Our data suggest early dysregulation of pro- and antiapoptotic proteins in prediabetes; however, they do not show high induction of apoptosis. Furthermore, it is generally accepted that in type 1 and type 2 diabetes, the low levels of certain heat stress proteins (e.g., Hsp70 and Hsp27) and their impaired response to stress may contribute to the etiology of the disease [88]. It is important to note that in the prediabetic

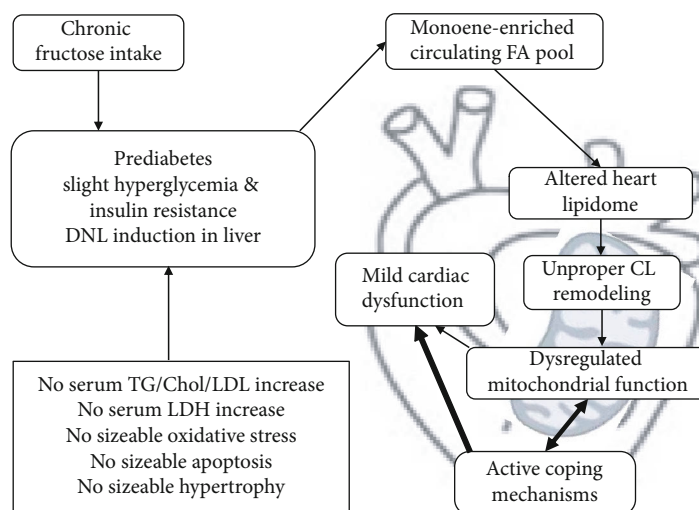


FIGURE 12: Summary of our findings.

state, we could not detect any disruption of Hsps. Instead, the Hsp60 and alphaB-Crystallin levels were markedly elevated by 3.3- and 5.6-fold, respectively (Table 5).

4. Conclusion

This is the first comprehensive analysis of the effect of prediabetes on the lipidome and proteome of the heart and its relationship to impaired diastolic function in a nongenetic rodent model. In our present study, chronically applied fructose intake led to the development of a prediabetic condition characterized by slight hyperglycemia, glucose intolerance, and insulin resistance (Figure 12).

This prediabetic state likely caused slight DNL induction in the liver. DNL induction has the capacity to alter the circulating accessible fatty acid (FA) pool for lipid biosynthesis in other organs. Consequently, the cardiac lipidome has been altered. The change was found to be comprehensive, deep, and characteristic with main features of monoenoic FA enrichment, decrease in linoleic acid (18:2 FA), complex changes in highly polyunsaturated lipids, and reprofiling of sphingolipid species compositions. Recent large-scale findings highlighted that the lower risk of type 2 diabetes was strongly associated with higher 18:2 FA biomarker levels [89, 90]. Linoleic acid was able to alleviate the STZ-induced diabetic phenotype in mice by normalizing FA metabolism and desaturation and correcting glucose and insulin levels [91].

It is conceivable that the observed lipidomic changes ultimately altered the biophysical properties of membrane lipids, which, together with restricted substrate availability, led to unproper CL remodeling in cardiac mitochondria. Dysregulation of CL remodeling possibly contributed to the impairment of several mitochondrial processes, as it was assessed by proteomic analysis, and finally could result in mild cardiac dysfunction. As mentioned previously, Barth syndrome shares biochemical features, like increased CL molecular species heterogeneity and increased MLCL/CL ratio, with ischemia,

hypothyroidism, heart failure, and aging [19, 92, 93]. Moreover, drastic CL remodeling was observed at early stages in type 1 and type 2 diabetic hearts [19]. Evidences from prospective cohort studies and randomized trials have demonstrated that high n-6 polyunsaturated FA (predominantly linoleic acid) intake plays an important role in the dietary prevention of cardiovascular diseases [94]. Altogether, it is well-established that the loss and defective remodeling of CL alone can provoke cardiac dysfunction but it is not sufficient to induce diabetes [95]. However, the deprivation of 18:2 caused by the fructose-induced overproduction of nonessential FAs can be an important contributor to the development of the disease. Moreover, as a consequence of the mitochondrial dysfunction, a vicious cycle can be initiated by ROS-induced damage to mitochondrial components [96] at the transition from the prediabetic to the diabetic stage.

Our data show that at this very early stage of prediabetes there was no sizeable oxidative stress or apoptosis in the heart. Instead, several active coping mechanisms were activated against the harmful consequences of fructose feeding including the upregulation of enzymes responsible for the removal of lipid peroxidation products and upregulation of mitochondrial Hsp60.

Taken together, our study evidences that at the prediabetic stage there are no clinically accessible signs to declare a disease because the generally investigated serum parameters do not report about lipotoxicity, cell damage, or substantial hyperglycemia. Nevertheless, the results presented here clearly demonstrate that the risk for progression of diabetes and cardiovascular disease is silently present in the guise of a complex cardiac lipid metabolic imbalance and altered proteomic pattern. Prediabetes might represent a transient, reversible, “decision-making” state in that process. The nature of our nongenetic model implies that improper food intake must persist chronically; the longer you apply the higher the risk. Therefore, early intervention is important to prevent the transition from prediabetes to more severe disease stages.

Data Availability

All data used to support the findings of this study are included within the article or the supplementary information file.

Conflicts of Interest

The authors declare that there is no conflict of interest regarding the publication of this paper.

Authors' Contributions

Gergő Szűcs, Andrea Sója, and Mária Péter contributed equally. Gábor Balogh and Tamás Csont are equal senior contributors.

Acknowledgments

We acknowledge the outstanding technical support of Flóra Diána Gausz and Alexandra Fejes for blood sampling, oral glucose tolerance test, organ weight measurement, and frozen tissue sample preparation and of Ilona Ungi for anaesthetizing and shaving the animals for echocardiography and of Ferenc Péntek in the sample preparation for proteomics studies. This article was supported by the grants GINOP 2.3.2-15-2016-00006, EFOP 3.6.2-16-2017-00006, OTKA-NKFIH (K115990), and 20391 3/2018/FEKUSTRAT. Márta Sárközy was supported by the János Bolyai Research Scholarship of the Hungarian Academy of Sciences and the New National Excellence Program of the Ministry of Human Capacities (UNKP-18-4-SZTE-63).

Supplementary Materials

Supplementary methods for more detailed descriptions of the methodologies of lipidomics and proteomics. Supplementary Figure 1: cardiolipin (CL) maturation. Supplementary Figure 2: alterations in monolysocardiolipin (MLCL) species composition due to fructose-rich diet. Then, the Supplementary Tables are given to provide detailed data related to lipidomic and proteomic analyses. The Supplementary Tables include the following: lipid compositional data (mol% of membrane lipids), species composition of individual lipid classes (mol% of individual classes), lipid/protein values (nmol/mg), double bonds (db) and double bond index (DBI), protein quantification, and Reactome pathway analysis. (*Supplementary Materials*)

References

- [1] M. Sárközy, G. Szűcs, M. Pipicz et al., "The effect of a preparation of minerals, vitamins and trace elements on the cardiac gene expression pattern in male diabetic rats," *Cardiovascular Diabetology*, vol. 14, no. 1, article 248, 2015.
- [2] World Health Organization, *Global Report on Diabetes*, World Health Organization, 2016.
- [3] International Diabetes Federation, *IDF Diabetes Atlas*, International Diabetes Federation, Brussels, 8th edition, 2017.
- [4] American Diabetes Association, "2. Classification and diagnosis of diabetes: *standards of medical care in diabetes—2019*," *Diabetes Care*, vol. 42, Supplement 1, pp. S13–S28, 2019.
- [5] E. L. M. Barr, P. Z. Zimmet, T. A. Welborn et al., "Risk of cardiovascular and all-cause mortality in individuals with diabetes mellitus, impaired fasting glucose, and impaired glucose tolerance: the Australian Diabetes, Obesity, and Lifestyle Study (AusDiab)," *Circulation*, vol. 116, no. 2, pp. 151–157, 2007.
- [6] G. Koncsos, Z. V. Varga, T. Baranyai et al., "Diastolic dysfunction in prediabetic male rats: role of mitochondrial oxidative stress," *American Journal of Physiology-Heart and Circulatory Physiology*, vol. 311, no. 4, pp. H927–H943, 2016.
- [7] S. Boudina and E. D. Abel, "Diabetic cardiomyopathy, causes and effects," *Reviews in Endocrine & Metabolic Disorders*, vol. 11, no. 1, article 9131, pp. 31–39, 2010.
- [8] J. G. Duncan, "Mitochondrial dysfunction in diabetic cardiomyopathy," *Biochimica et Biophysica Acta (BBA) - Molecular Cell Research*, vol. 1813, no. 7, pp. 1351–1359, 2011.
- [9] L. Cai and Y. J. Kang, "Cell death and diabetic cardiomyopathy," *Cardiovascular Toxicology*, vol. 3, no. 3, pp. 219–228, 2003.
- [10] J. S. Bhatti, G. K. Bhatti, and P. H. Reddy, "Mitochondrial dysfunction and oxidative stress in metabolic disorders – A step towards mitochondria based therapeutic strategies," *Biochimica et Biophysica Acta (BBA) - Molecular Basis of Disease*, vol. 1863, no. 5, pp. 1066–1077, 2017.
- [11] G. Kanuri and I. Bergheim, "In vitro and in vivo models of non-alcoholic fatty liver disease (NAFLD)," *International Journal of Molecular Sciences*, vol. 14, no. 6, pp. 11963–11980, 2013.
- [12] M. Chung, J. Ma, K. Patel, S. Berger, J. Lau, and A. H. Lichtenstein, "Fructose, high-fructose corn syrup, sucrose, and nonalcoholic fatty liver disease or indexes of liver health: a systematic review and meta-analysis," *The American Journal of Clinical Nutrition*, vol. 100, no. 3, pp. 833–849, 2014.
- [13] L. N. Axelsen, J. B. Lademann, J. S. Petersen et al., "Cardiac and metabolic changes in long-term high fructose-fat fed rats with severe obesity and extensive intramyocardial lipid accumulation," *American Journal of Physiology-Regulatory, Integrative and Comparative Physiology*, vol. 298, no. 6, pp. R1560–R1570, 2010.
- [14] M. Schlame and M. Ren, "The role of cardiolipin in the structural organization of mitochondrial membranes," *Biochimica et Biophysica Acta (BBA) - Biomembranes*, vol. 1788, no. 10, pp. 2080–2083, 2009.
- [15] J. Dudek, "Role of cardiolipin in mitochondrial signaling pathways," *Frontiers in Cell and Development Biology*, vol. 5, p. 90, 2017.
- [16] J. J. Maguire, Y. Y. Tyurina, D. Mohammadyani et al., "Known unknowns of cardiolipin signaling: the best is yet to come," *Biochimica et Biophysica Acta (BBA) - Molecular and Cell Biology of Lipids*, vol. 1862, no. 1, pp. 8–24, 2017.
- [17] Y. Shi, "Emerging roles of cardiolipin remodeling in mitochondrial dysfunction associated with diabetes, obesity, and cardiovascular diseases," *Journal of Biomedical Research*, vol. 24, no. 1, pp. 6–15, 2010.
- [18] M. Schlame, Y. Xu, and M. Ren, "The basis for acyl specificity in the tafazzin reaction," *The Journal of Biological Chemistry*, vol. 292, no. 13, pp. 5499–5506, 2017.
- [19] Q. He and X. Han, "Cardiolipin remodeling in diabetic heart," *Chemistry and Physics of Lipids*, vol. 179, pp. 75–81, 2014.

- [20] P. G. Barth, F. Valianpour, V. M. Bowen et al., "X-linked cardioskeletal myopathy and neutropenia (Barth syndrome): an update," *American Journal of Medical Genetics. Part A*, vol. 126A, no. 4, pp. 349–354, 2004.
- [21] M. Schlame, D. Rua, and M. L. Greenberg, "The biosynthesis and functional role of cardiolipin," *Progress in Lipid Research*, vol. 39, no. 3, pp. 257–288, 2000.
- [22] G. F. Kocsis, M. Sárközy, P. Bencsik et al., "Preconditioning protects the heart in a prolonged uremic condition," *American Journal of Physiology—Heart and Circulatory Physiology*, vol. 303, no. 10, pp. H1229–H1236, 2012.
- [23] L. Kiscsatári, M. Sárközy, B. Kövári et al., "High-dose radiation induced heart damage in a rat model," *In Vivo*, vol. 30, no. 5, pp. 623–631, 2016.
- [24] M. Sárközy, R. Gáspár, Á. Zvara et al., "Chronic kidney disease induces left ventricular overexpression of the pro-hypertrophic microRNA-212," *Scientific Reports*, vol. 9, no. 1, p. 1302, 2019.
- [25] T. Csont, S. Viappiania, J. Sawickaa et al., "The involvement of superoxide and iNOS-derived NO in cardiac dysfunction induced by pro-inflammatory cytokines," *Journal of Molecular and Cellular Cardiology*, vol. 39, no. 5, pp. 833–840, 2005.
- [26] M. Pipicz, G. Kocsis, L. Sárváry-Arantes et al., "Low-dose endotoxin induces late preconditioning, increases peroxynitrite formation, and activates STAT3 in the rat heart," *Molecules*, vol. 22, no. 3, p. 433, 2017.
- [27] T. Csont, E. Bereczki, P. Bencsik et al., "Hypercholesterolemia increases myocardial oxidative and nitrosative stress thereby leading to cardiac dysfunction in apoB-100 transgenic mice," *Cardiovascular Research*, vol. 76, no. 1, pp. 100–109, 2007.
- [28] T. Csont, C. Csonka, A. Ónody et al., "Nitrate tolerance does not increase production of peroxynitrite in the heart," *American Journal of Physiology—Heart and Circulatory Physiology*, vol. 283, no. 1, pp. H69–H76, 2002.
- [29] T. Csont, C. Csonka, P. Kovács, G. Jancsó, and P. Ferdinandy, "Capsaicin-sensitive sensory neurons regulate myocardial nitric oxide and cGMP signaling," *European Journal of Pharmacology*, vol. 476, no. 1–2, pp. 107–113, 2003.
- [30] A. Ónody, C. Csonka, Z. Giricz, and P. Ferdinandy, "Hyperlipidemia induced by a cholesterol-rich diet leads to enhanced peroxynitrite formation in rat hearts," *Cardiovascular Research*, vol. 58, no. 3, pp. 663–670, 2003.
- [31] B. Peksel, I. Gombos, M. Péter et al., "Mild heat induces a distinct "eustress" response in Chinese Hamster Ovary cells but does not induce heat shock protein synthesis," *Scientific Reports*, vol. 7, no. 1, article 15643, 2017.
- [32] B. C. Searle, L. K. Pino, J. D. Egertson et al., "Chromatogram libraries improve peptide detection and quantification by data independent acquisition mass spectrometry," *Nature Communications*, vol. 9, no. 1, p. 5128, 2018.
- [33] S. Tyanova, T. Temu, P. Sinitcyn et al., "The Perseus computational platform for comprehensive analysis of (prote)omics data," *Nature Methods*, vol. 13, no. 9, pp. 731–740, 2016.
- [34] M. Sárközy, Á. Zvara, N. Gyémánt et al., "Metabolic syndrome influences cardiac gene expression pattern at the transcript level in male ZDF rats," *Cardiovascular Diabetology*, vol. 12, no. 1, p. 16, 2013.
- [35] M. Sárközy, G. Szűcs, V. Fekete et al., "Transcriptomic alterations in the heart of non-obese type 2 diabetic Goto-Kakizaki rats," *Cardiovascular Diabetology*, vol. 15, no. 1, p. 110, 2016.
- [36] P. Gayoso-Diz, A. Otero-Gonzalez, M. X. Rodriguez-Alvarez et al., "Insulin resistance index (HOMA-IR) levels in a general adult population: curves percentile by gender and age. The EPIRCE study," *Diabetes Research and Clinical Practice*, vol. 94, no. 1, pp. 146–155, 2011.
- [37] E. L. M. Barr, A. J. Cameron, B. Balkau et al., "HOMA insulin sensitivity index and the risk of all-cause mortality and cardiovascular disease events in the general population: the Australian Diabetes, Obesity and Lifestyle Study (AusDiab) study," *Diabetologia*, vol. 53, no. 1, pp. 79–88, 2010.
- [38] J. D. Storey and R. Tibshirani, "Statistical significance for genome-wide studies," *Proceedings of the National Academy of Sciences of the United States of America*, vol. 100, no. 16, pp. 9440–9445, 2003.
- [39] J. Xia and D. S. Wishart, "Web-based inference of biological patterns, functions and pathways from metabolomic data using MetaboAnalyst," *Nature Protocols*, vol. 6, no. 6, pp. 743–760, 2011.
- [40] W. Hsueh, E. D. Abel, J. L. Breslow et al., "Recipes for creating animal models of diabetic cardiovascular disease," *Circulation Research*, vol. 100, no. 10, pp. 1415–1427, 2007.
- [41] J. C. Russell and S. D. Proctor, "Small animal models of cardiovascular disease: tools for the study of the roles of metabolic syndrome, dyslipidemia, and atherosclerosis," *Cardiovascular Pathology*, vol. 15, no. 6, pp. 318–330, 2006.
- [42] N. Fakhoury-Sayegh, V. Trak-Smayra, A. Khazzaka et al., "Characteristics of nonalcoholic fatty liver disease induced in wistar rats following four different diets," *Nutrition Research and Practice*, vol. 9, no. 4, pp. 350–357, 2015.
- [43] E. Gatineau, I. Savary-Auzeloux, C. Migné, S. Polakof, D. Dardevet, and L. Mosoni, "Chronic intake of sucrose accelerates sarcopenia in older male rats through alterations in insulin sensitivity and muscle protein synthesis," *The Journal of Nutrition*, vol. 145, no. 5, pp. 923–930, 2015.
- [44] I. Dhar, A. Dhar, L. Wu, and K. M. Desai, "Increased methylglyoxal formation with upregulation of renin angiotensin system in fructose fed Sprague Dawley rats," *PLoS One*, vol. 8, no. 9, article e74212, 2013.
- [45] H. Malhi and R. J. Kaufman, "Endoplasmic reticulum stress in liver disease," *Journal of Hepatology*, vol. 54, no. 4, pp. 795–809, 2011.
- [46] H.-Y. Ou, H.-T. Wu, H.-C. Hung, Y.-C. Yang, J.-S. Wu, and C.-J. Chang, "Multiple mechanisms of GW-9508, a selective G protein-coupled receptor 40 agonist, in the regulation of glucose homeostasis and insulin sensitivity," *American Journal of Physiology—Endocrinology and Metabolism*, vol. 304, no. 6, pp. E668–E676, 2013.
- [47] N. Stefan and H. U. Häring, "The role of hepatokines in metabolism," *Nature Reviews Endocrinology*, vol. 9, no. 3, pp. 144–152, 2013.
- [48] F. Yang, Y. Dai, C. Min, and X. Li, "Neonatal overfeeding induced glucocorticoid overexposure accelerates hepatic lipogenesis in male rats," *Nutrition & Metabolism*, vol. 15, no. 1, 2018.
- [49] M. Baena, G. Sangüesa, N. Hutter et al., "Fructose supplementation impairs rat liver autophagy through mTORC activation without inducing endoplasmic reticulum stress," *Biochimica et Biophysica Acta (BBA) - Molecular and Cell Biology of Lipids*, vol. 1851, no. 2, pp. 107–116, 2015.

- [50] S. Softic, D. E. Cohen, and C. R. Kahn, "Role of dietary fructose and hepatic de novo lipogenesis in fatty liver disease," *Digestive Diseases and Sciences*, vol. 61, no. 5, pp. 1282–1293, 2016.
- [51] T. Matsuzaka, A. Atsumi, R. Matsumori et al., "Elovl6 promotes nonalcoholic steatohepatitis," *Hepatology*, vol. 56, no. 6, pp. 2199–2208, 2012.
- [52] B. A. Brooks, B. Franjic, C. R. Ban et al., "Diastolic dysfunction and abnormalities of the microcirculation in type 2 diabetes," *Diabetes, Obesity and Metabolism*, vol. 10, no. 9, pp. 739–746, 2008.
- [53] B. Shivalkar, D. Dhondt, I. Goovaerts et al., "Flow mediated dilatation and cardiac function in type 1 diabetes mellitus," *The American Journal of Cardiology*, vol. 97, no. 1, pp. 77–82, 2006.
- [54] K. Pandya, H.-S. Kim, and O. Smithies, "Fibrosis, not cell size, delineates β -myosin heavy chain reexpression during cardiac hypertrophy and normal aging *in vivo*," *Proceedings of the National Academy of Sciences of the United States of America*, vol. 103, no. 45, pp. 16864–16869, 2006.
- [55] K. Nakao, W. Minobe, R. Roden, M. R. Bristow, and L. A. Leinwand, "Myosin heavy chain gene expression in human heart failure," *The Journal of Clinical Investigation*, vol. 100, no. 9, pp. 2362–2370, 1997.
- [56] K. Pandya and O. Smithies, " β -MyHC and cardiac hypertrophy: size does matter," *Circulation Research*, vol. 109, no. 6, pp. 609–610, 2011.
- [57] O. Y. Althunibat, A. M. Al Hroob, M. H. Abukhalil, M. O. Germoush, M. Bin-Jumah, and A. M. Mahmoud, "Fisetin ameliorates oxidative stress, inflammation and apoptosis in diabetic cardiomyopathy," *Life Sciences*, vol. 221, pp. 83–92, 2019.
- [58] W. Kulik, H. van Lenthe, F. S. Stet et al., "Bloodspot assay using HPLC-tandem mass spectrometry for detection of Barth syndrome," *Clinical Chemistry*, vol. 54, no. 2, pp. 371–378, 2008.
- [59] X. Han, J. Yang, H. Cheng, K. Yang, D. R. Abendschein, and R. W. Gross, "Shotgun lipidomics identifies cardiolipin depletion in diabetic myocardium linking altered substrate utilization with mitochondrial dysfunction," *Biochemistry*, vol. 44, no. 50, pp. 16684–16694, 2005.
- [60] X. Han, J. Yang, K. Yang, Z. Zhao, D. R. Abendschein, and R. W. Gross, "Alterations in myocardial cardiolipin content and composition occur at the very earliest stages of diabetes: a shotgun lipidomics study," *Biochemistry*, vol. 46, no. 21, pp. 6417–6428, 2007.
- [61] P. H. Lou, E. Lucchinetti, K. Y. Scott et al., "Alterations in fatty acid metabolism and sirtuin signaling characterize early type-2 diabetic hearts of fructose-fed rats," *Physiological Reports*, vol. 5, no. 16, article e13388, 2017.
- [62] X. Han, K. Yang, J. Yang, H. Cheng, and R. W. Gross, "Shotgun lipidomics of cardiolipin molecular species in lipid extracts of biological samples," *Journal of Lipid Research*, vol. 47, no. 4, pp. 864–879, 2006.
- [63] F. Novák, E. Tvrzická, B. Hamplová, F. Kolář, and O. Nováková, "Postnatal development of phospholipids and their fatty acid profile in rat heart," *Molecular and Cellular Biochemistry*, vol. 293, no. 1–2, pp. 23–33, 2006.
- [64] M. A. Kiebish, K. Yang, X. Liu et al., "Dysfunctional cardiac mitochondrial bioenergetic, lipidomic, and signaling in a murine model of Barth syndrome," *Journal of Lipid Research*, vol. 54, no. 5, pp. 1312–1325, 2013.
- [65] T. A. Taha, T. D. Mullen, and L. M. Obeid, "A house divided: ceramide, sphingosine, and sphingosine-1-phosphate in programmed cell death," *Biochimica et Biophysica Acta (BBA) - Biomembranes*, vol. 1758, no. 12, pp. 2027–2036, 2006.
- [66] W. L. Holland and S. A. Summers, "Strong heart, low ceramides," *Diabetes*, vol. 67, no. 8, pp. 1457–1460, 2018.
- [67] N. Marchesini, W. Osta, J. Bielawski, C. Luberto, L. M. Obeid, and Y. A. Hannun, "Role for mammalian neutral sphingomyelinase 2 in confluence-induced growth arrest of MCF7 cells," *The Journal of Biological Chemistry*, vol. 279, no. 24, pp. 25101–25111, 2004.
- [68] X. Su, X. Han, D. J. Mancuso, D. R. Abendschein, and R. W. Gross, "Accumulation of long-chain acylcarnitine and 3-hydroxy acylcarnitine molecular species in diabetic myocardium: identification of alterations in mitochondrial fatty acid processing in diabetic myocardium by shotgun lipidomics," *Biochemistry*, vol. 44, no. 13, pp. 5234–5245, 2005.
- [69] J. Cao, W. Shen, Z. Chang, and Y. Shi, "ALCAT1 is a polyglycerophospholipid acyltransferase potentially regulated by adenine nucleotide and thyroid status," *American Journal of Physiology-Endocrinology and Metabolism*, vol. 296, no. 4, pp. E647–E653, 2009.
- [70] T. Mutter, V. W. Dolinsky, B. J. Ma, W. A. Taylor, and G. M. Hatch, "Thyroxine regulation of monolysocardiolipin acyltransferase activity in rat heart," *The Biochemical Journal*, vol. 346, no. 2, Part 2, pp. 403–406, 2000.
- [71] T. Martin-Rojas, L. Mourino-Alvarez, S. Alonso-Orgaz et al., "iTRAQ proteomic analysis of extracellular matrix remodeling in aortic valve disease," *Scientific Reports*, vol. 5, article 17290, 2015.
- [72] T. Csont, A. Görbe, E. Bereczki et al., "Biglycan protects cardiomyocytes against hypoxia/reoxygenation injury: role of nitric oxide," *Journal of Molecular and Cellular Cardiology*, vol. 48, no. 4, pp. 649–652, 2010.
- [73] R. Gáspár, M. Pipicz, F. Hawchar et al., "The cytoprotective effect of biglycan core protein involves Toll-like receptor 4 signaling in cardiomyocytes," *Journal of Molecular and Cellular Cardiology*, vol. 99, pp. 138–150, 2016.
- [74] E. Bereczki, S. Gonda, T. Csont et al., "Overexpression of biglycan in the heart of transgenic mice: an antibody microarray study," *Journal of Proteome Research*, vol. 6, no. 2, pp. 854–861, 2007.
- [75] P. Wu, X. Yuan, F. Li et al., "Myocardial upregulation of cathepsin D by ischemic heart disease promotes autophagic flux and protects against cardiac remodeling and heart failure," *Circulation. Heart Failure*, vol. 10, no. 7, 2017.
- [76] I. M. Seropian, J. P. Cerliani, S. Toldo et al., "Galectin-1 controls cardiac inflammation and ventricular remodeling during acute myocardial infarction," *The American Journal of Pathology*, vol. 182, no. 1, pp. 29–40, 2013.
- [77] Q. Mei, J. Huang, W. Chen et al., "Regulation of DNA replication-coupled histone gene expression," *Oncotarget*, vol. 8, no. 55, pp. 95005–95022, 2017.
- [78] Z. V. Varga, K. Kupai, G. Szűcs et al., "MicroRNA-25-dependent up-regulation of NADPH oxidase 4 (NOX4) mediates hypercholesterolemia-induced oxidative/nitrative stress and subsequent dysfunction in the heart," *Journal of Molecular and Cellular Cardiology*, vol. 62, pp. 111–121, 2013.
- [79] T. Xu, L. Zheng, L. Xu et al., "Protective effects of dioscin against alcohol-induced liver injury," *Archives of Toxicology*, vol. 88, no. 3, pp. 739–753, 2014.

- [80] C. Brocker, N. Lassen, T. Estey et al., "Aldehyde dehydrogenase 7A1 (ALDH7A1) is a novel enzyme involved in cellular defense against hyperosmotic stress," *The Journal of Biological Chemistry*, vol. 285, no. 24, pp. 18452–18463, 2010.
- [81] E. V. Karaduleva, E. K. Mubarakshina, M. G. Sharapov et al., "Cardioprotective effect of modified peroxiredoxins in retrograde perfusion of isolated rat heart under conditions of oxidative stress," *Bulletin of Experimental Biology and Medicine*, vol. 160, no. 5, pp. 639–642, 2016.
- [82] J. Lappalainen, N. K. J. Oksala, D. E. Laaksonen et al., "Suppressed heat shock protein response in the kidney of exercise-trained diabetic rats," *Scandinavian Journal of Medicine & Science in Sports*, vol. 28, no. 7, pp. 1808–1817, 2018.
- [83] W. Cao, N. Liu, S. Tang et al., "Acetyl-coenzyme A acyltransferase 2 attenuates the apoptotic effects of BNIP3 in two human cell lines," *Biochimica et Biophysica Acta (BBA) - General Subjects*, vol. 1780, no. 6, pp. 873–880, 2008.
- [84] W. Li, M. Yao, R. Wang et al., "Profile of cardiac lipid metabolism in STZ-induced diabetic mice," *Lipids in Health and Disease*, vol. 17, no. 1, p. 231, 2018.
- [85] B. G. Hoffstrom, A. Kaplan, R. Letso et al., "Inhibitors of protein disulfide isomerase suppress apoptosis induced by misfolded proteins," *Nature Chemical Biology*, vol. 6, no. 12, pp. 900–906, 2010.
- [86] A. H. Amin, M. A. El-Missiry, and A. I. Othman, "Melatonin ameliorates metabolic risk factors, modulates apoptotic proteins, and protects the rat heart against diabetes-induced apoptosis," *European Journal of Pharmacology*, vol. 747, pp. 166–173, 2015.
- [87] W. Yu, W. Zha, S. Guo, H. Cheng, J. Wu, and C. Liu, "Flos puerariae extract prevents myocardial apoptosis via attenuation oxidative stress in streptozotocin-induced diabetic mice," *PLoS One*, vol. 9, no. 5, article e98044, 2014.
- [88] P. L. Hooper, G. Balogh, E. Rivas, K. Kavanagh, and L. Vigh, "The importance of the cellular stress response in the pathogenesis and treatment of type 2 diabetes," *Cell Stress & Chaperones*, vol. 19, no. 4, pp. 447–464, 2014.
- [89] J. H. Y. Wu, M. Marklund, F. Imamura et al., "Omega-6 fatty acid biomarkers and incident type 2 diabetes: pooled analysis of individual-level data for 39 740 adults from 20 prospective cohort studies," *The Lancet Diabetes and Endocrinology*, vol. 5, no. 12, pp. 965–974, 2017.
- [90] N. G. Forouhi, F. Imamura, S. J. Sharp et al., "Association of plasma phospholipid n-3 and n-6 polyunsaturated fatty acids with type 2 diabetes: the EPIC-InterAct case-cohort study," *PLoS Medicine*, vol. 13, no. 7, article e1002094, 2016.
- [91] L. Canetti, H. Werner, and A. Leikin-Frenkel, "Linoleic and alpha linolenic acids ameliorate streptozotocin-induced diabetes in mice," *Archives of Physiology and Biochemistry*, vol. 120, no. 1, pp. 34–39, 2014.
- [92] N. Ikon and R. O. Ryan, "Barth syndrome: connecting cardiolipin to cardiomyopathy," *Lipids*, vol. 52, no. 2, pp. 99–108, 2017.
- [93] A. J. Chicco and G. C. Sparagna, "Role of cardiolipin alterations in mitochondrial dysfunction and disease," *American Journal of Physiology-Cell Physiology*, vol. 292, no. 1, pp. C33–C44, 2007.
- [94] D. D. Wang, "Dietary n-6 polyunsaturated fatty acids and cardiovascular disease: epidemiologic evidence," *Prostaglandins, Leukotrienes, and Essential Fatty Acids*, vol. 135, pp. 5–9, 2018.
- [95] W. T. Cade, C. T. Spencer, D. N. Reeds et al., "Substrate metabolism during basal and hyperinsulinemic conditions in adolescents and young-adults with Barth syndrome," *Journal of Inherited Metabolic Disease*, vol. 36, no. 1, pp. 91–101, 2013.
- [96] T. K. Silzer and N. R. Phillips, "Etiology of type 2 diabetes and Alzheimer's disease: Exploring the mitochondria," *Mitochondrion*, vol. 43, pp. 16–24, 2018.



APPENDIX

Abbreviations for Table 7 and Table 9

- Abhd17c*: Abhydrolase domain containing 17C
- Adh1*: Alcohol dehydrogenase 1 (class I)
- Adra1d*: Adrenoceptor alpha 1D
- Akap3*: A kinase (PRKA) anchor protein 3
- Akr1b10*: Aldo–keto reductase family 1, member B10 (aldose reductase)
- Aldh1a1*: Aldehyde Dehydrogenase 1 Family Member A1
- Ampd1*: Adenosine monophosphate deaminase 1
- Arhgef5*: Rho guanine nucleotide exchange factor (GEF) 5
- Arntl*: Aryl Hydrocarbon Receptor Nuclear Translocator Like
- Atp2b2*: ATPase, Ca⁺⁺ transporting, plasma membrane 2
- Atp6ap1 l*: ATPase, H⁺ transporting, lysosomal accessory protein 1-like
- Atp6v1g*: ATPase, H⁺ transporting, lysosomal V1 subunit G2
- Bard1*: BRCA1 Associated RING Domain 1
- Btbd9*: BTB Domain Containing 9
- C3*: Complement C3
- C4a*: Complement component 4A (Rodgers blood group)
- Car6*: CARBONIC anhydrase 6
- Ccng1*: Cyclin G1
- Cd1d1*: CD1d1 molecule
- Cd47*: Cd47 molecule
- Chrna7*: Cholinergic receptor, nicotinic, alpha 7 (neuronal)
- Clstn2*: Calsyntenin 2
- Cma1*: Chymase 1, mast cell
- Cntnap1*: Contactin associated protein 1
- Col5a3*: Collagen, type V, alpha 3
- Cpox*: Coproporphyrinogen oxidase

Crabp2: Cellular retinoic acid binding protein 2

Creb5: cAMP responsive element binding protein 5

Crym: Crystallin, mu

Cryz: Crystallin Zeta

Cxcl13: Chemokine (C-X-C motif) ligand 13

Cxcr6: C-X-C Motif Chemokine Receptor 6

Cyp2j4: Cytochrome P450, family 2, subfamily J, polypeptide 4

Cyr61: Cysteine-rich angiogenic inducer 61

Ddah1: Dimethylarginine Dimethylaminohydrolase 1

Dgkb: Diacylglycerol kinase, beta

Dpp4: Dipeptidyl Peptidase 4

Dpt: Dermatotontin

Dyrk3: Dual-specificity tyrosine-(Y)-phosphorylation regulated kinase 3

Efna2: Ephrin A2

Eif2ak2: Eukaryotic Translation Initiation Factor 2 Alpha Kinase 2

Epyc: Epiphycan

Ercc8: ERCC Excision Repair 8, CSA Ubiquitin Ligase Complex Subunit

Esm1: Endothelial cell-specific molecule 1

Fgf18: Fibroblast Growth Factor 18

Fmn1: Formin 1

Gnb3: G Protein Subunit Beta 3

Gpbp1: GC-Rich Promoter Binding Protein 1

Hic1: Hypermethylated in cancer 1

Icoslg: Inducible T-cell co-stimulator ligand

Il22ra2: Interleukin 22 receptor, alpha 2

Inha: Inhibin alpha

Jund: Jun D proto-oncogene

Kcne1: Potassium voltage-gated channel, Isk-related family, member 1

Klk1c3: Kallikrein 1-related peptidase C3

Klre1: Killer cell lectin-like receptor subfamily E member 1

Loc501307: Similar to spermatogenesis associated glutamate (E)-rich protein 4d

Lpar1: Lysophosphatidic acid receptor 1

Lpcat2: Lysophosphatidylcholine Acyltransferase 2

Mcm8: Minichromosome Maintenance 8 Homologous Recombination Repair Factor

Msln: Mesothelin

Mybphl: Myosin binding protein H-like

Myl7: Myosin, light chain 7, regulatory

Ncf1: Neutrophil Cytosolic Factor 1

Nnat: Neuronatin, transcript variant 1

Npas2: Neuronal PAS Domain Protein 2

Ntrk3: Neurotrophic tyrosine kinase, receptor, type 3, transcript variant 3

Nucks1: Nuclear Casein Kinase And Cyclin Dependent Kinase Substrate 1

Oas1a: 2'-5' oligoadenylate synthetase 1A

Ocln: Occludin

Oxsm: 3-Oxoacyl-ACP Synthase, Mitochondrial

P4ha3: Prolyl 4-hydroxylase, alpha polypeptide III

Pbld1: Phenazine biosynthesis-like protein domain containing 1

Pdia2: Protein Disulfide Isomerase Family A Member 2

Per2: Period Circadian Regulator 2

Pla2g7: Phospholipase A2, group VII (platelet-activating factor acetylhydrolase, plasma)

Plod2: Procollagen-Lysine,2-Oxoglutarate 5-Dioxygenase 2

Prkab2: Protein Kinase AMP-Activated Non-Catalytic Subunit Beta 2

Prkce: Protein Kinase C Epsilon

Prps2: Phosphoribosyl Pyrophosphate Synthetase 2

Ptgfr: Prostaglandin F receptor

Ptpn13: Protein tyrosine phosphatase, non-receptor type 13

Pxmp4: Peroxisomal membrane protein 4

Qsox1: Quiescin Sulfhydryl Oxidase 1

Rbp4: Retinol binding protein 4, plasma

Reg3b: Regenerating islet-derived 3 beta

Ret: Ret proto-oncogene, transcript variant 1

Retsat: Retinol saturase (all trans retinol 13,14 reductase)

RGD1559482: Similar to immunoglobulin superfamily, member 7

Rnf187: Ring finger protein 187

Rps7: Ribosomal Protein S7

RT1-T18: RT1 class Ib, locus T18

Sdc1: Syndecan 1

Sgms1: Sphingomyelin Synthase 1

Slc16a7: Solute carrier family 16 (onocarboxylate transporter), member 7

Slc4a1: Solute carrier family 4 (anion exchanger), member 1

Sln: Sarcolipin

St6galnac3: ST6 N-Acetylgalactosaminide Alpha-2,6-Sialyltransferase 3

Stat3: Signal Transducer And Activator Of Transcription 3

Taf13: TATA-Box Binding Protein Associated Factor 13

Tceal7: Transcription elongation factor A (SII)-like 7

Tef: TEF Transcription Factor, PAR BZIP Family Member

Tgm1: Transglutaminase 1

Thrsp: Thyroid hormone responsive

Tmem189: Transmembrane protein 189

Traf6: TNF Receptor Associated Factor 6

Trim16: Tripartite motif-containing 16

Trim50: Tripartite Motif Containing 50

Trps1: Transcriptional Repressor GATA Binding 1

Upk1b: Uroplakin 1B

Wee1: WEE1 G2 Checkpoint Kinase

Zeb2: Zinc Finger E-Box Binding Homeobox 2

Zfp90: ZFP90 Zinc Finger Protein

Társszerzői lemondó nyilatkozat

Alulírott Dr. Szűcs Gergő (megosztott elsőszerző) kijelentem, hogy Sója Andrea (jelölt) PhD értekezésének tézispontjaiban bemutatott - közösen publikált - tudományos eredmények elérésében a pályázónak meghatározó szerepe volt, ezért ezeket a téziseket más a PhD fokozat megszerzését célzó minősítési eljárásban nem használta fel, illetve nem kívánja felhasználni.

2021.10.26

dátum



szerző

A pályázó tézispontjaiban érintett, közösen publikált közlemények:

Szűcs G, Sója A, Péter M, Sárközy M, Bruszel B, Siska A, Földesi I, Szabó Z, Janáky T, Vígh L, Balogh G, Csont T.

Prediabetes Induced by Fructose-Enriched Diet Influences Cardiac Lipidome and Proteome and Leads to Deterioration of Cardiac Function prior to the Development of Excessive Oxidative Stress and Cell Damage

Oxidative Medicine and Cellular Longevity 2019:3218275

Társszerzői lemondó nyilatkozat

Alulírott Dr. Péter Mária (megosztott elsőszerző) kijelentem, hogy Sója Andrea (jelölt) PhD értekezésének tézispontjaiban bemutatott - közösen publikált - tudományos eredmények elérésében a pályázónak meghatározó szerepe volt, ezért ezeket a téziseket más a PhD fokozat megszerzését célzó minősítési eljárásban nem használta fel, illetve nem kívánja felhasználni.

Szeged, 2021. 10. 27.

dátum

Peter Maria

szerző

A pályázó tézispontjaiban érintett, közösen publikált közlemények:

Szűcs G, Sója A, Péter M, Sárközy M, Bruszel B, Siska A, Földesi I, Szabó Z, Janáky T, Vigh L, Balogh G, Csont T.

Prediabetes Induced by Fructose-Enriched Diet Influences Cardiac Lipidome and Proteome and Leads to Deterioration of Cardiac Function prior to the Development of Excessive Oxidative Stress and Cell Damage

Oxidative Medicine and Cellular Longevity 2019:3218275

Társszerzői lemondó nyilatkozat

Alulírott Dr. Sárközy Márta (elsőszerző) kijelentem, hogy Sója Andrea (jelölt) PhD értekezésének tézispontjaiban bemutatott - közösen publikált - tudományos eredmények elérésében a pályázónak meghatározó szerepe volt, ezért ezeket a téziseket más a PhD fokozat megszerzését célzó minősítési eljárásban nem használta fel, illetve nem kívánja felhasználni.

.....2021.10.26.....

dátum

Dr. Sárközy Márta

szerző

A pályázó tézispontjaiban érintett, közösen publikált közlemények:

Sárközy M., Szűcs G, Fekete V, Pipicz M, Éder K, Gáspár R, **Sója A.**, Pipis J, Ferdinandy P, Csonka C, Csont T.

Transcriptomic alterations in the heart of non-obese type 2 diabetic Goto-Kakizaki rats
Cardiovascular Diabetology (2016) 15:110